DISTRIBUTION, CLEARANCE, AND CONTROLLED RELEASE OF MOLECULES AND PARTICLES AFTER MICRONEEDLE INJECTION INTO THE SUPRACHOROIDAL SPACE

A Dissertation
Presented to
The Academic Faculty

by

Bryce Chiang

In Partial Fulfillment
of the Requirements for the Degree
Doctor of Philosophy in the
Wallace H. Counter Department of Biomedical Engineering

Georgia Institute of Technology
August 2016

DISTRIBUTION, CLEARANCE, AND CONTROLLED RELEASE OF MOLECULES AND PARTICLES AFTER MICRONEEDLE INJECTION INTO THE SUPRACHOROIDAL SPACE

Approved by:

Dr. Mark R. Prausnitz, Advisor School of Chemical & Biomolecular Engineering Georgia Institute of Technology	Dr. Timothy W. Olsen Department of Ophthalmology Emory University
Dr. Michael E. Davis Wallace H. Coulter Department of Biomedical Engineering Georgia Institute of Technology	Dr. Steven P. Schwendeman College of Pharmacy University of Michigan
Dr. C. Ross Ethier Wallace H. Coulter Department of Biomedical Engineering Georgia Institute of Technology	

Date Approved: April 29, 2016

To my wife Pauline Che and son Nathan Chiang

ACKNOWLEDGEMENTS

I wish to thank my advisor Dr. Prausnitz for providing me the opportunity, resources, and encouragement in bringing this thesis to fruition. Dr. Prausnitz has been incredibly helpful in my development as a scientist. His suggestions and advice pushed me to think critically and, perhaps more importantly, determine what was important and what was not. Some times that meant I needed to perform experiments that I had never thought of; other times, it meant I needed to resist jumping down the rabbit hole. He has also helped me become a better writer and speaker. I have learned that the value of being a good storyteller – to lead the audience on by providing sufficient detail so they can follow, and to not bombard them with every little detail and every tangent.

I also want to thank my committee members for their help, comments, and advice, especially in reigning in my thesis so it was not even more amorphous. I would like to thank Dr. Davis for being an advocate in keeping my eye on the prize; Dr. Ethier for providing resources and facilitated *in vivo* pressure measurements; Dr. Olsen for helping to interpret data, and serving as a role model of a successful clinician-scientist in ophthalmology; and Dr. Schwendeman for providing drug-loaded microspheres and his expertise on controlled release polymeric systems. I am thankful for the advice and guidance of Dr. Edelhauser. Though he did not live to see this completion of this work, he was instrumental in guiding experimental design, data analysis, and data interpretation. Each conversation with Dr. Edelhauser left me feeling extremely motivated and excited about my work. The ophthalmic drug delivery community is diminished by his loss.

I am also thankful for the help and advice of my lab mates in the Laboratory for Drug Delivery both past and present. In particular, I am thankful for the assistance Donna Bondy has provided. Without her organizational skills in keeping the lab running smoothly and orderly, I would never have been able to finish in <4 yrs. I would like to thank Yoo Chun Kim for teaching me the basics of suprachoroidal drug delivery; Samir Patel for helpful discussions; and Jaehwan Jung and Brandon Gerberich for helping me finish my experiments, as well as making sure some of my ideas and findings are progressing. I would also like to thank Pradnya Samant, Jessica Joyce, Andrew Tadros, Stefany Holguin, and others for providing sanity checks and suggestions. I will always remember our “Sunday dinner parties.” My time in the Drug Delivery Lab has been fun and exciting due to the people in it.

I am also thankful for the help of others from Georgia Tech, Emory University, and elsewhere. Dr. O’Farrell, Kim, Andrea, Altair, Ogeda, and the other Physiological Research Laboratory staff have been extremely helpful and cheerful. Dr. Grossniklaus and the histology core have helped process ocular tissue and explained ocular pathology. Amy Doty and Kari Nieto developed and optimized the polymeric microspheres used in the pharmacodynamic studies. Drs. Pardue, Nickerson, and Iuvone have also helped me shape my experimental plan, as well as making sense of my data. Cathy Payne was very generous in responding to my cold call for specimens and providing them. Sha’Aqua Asberry also helped with histological technique. Mary Horton, Dr. Chuck Parkos, and Dr. Kerry Ressler have provided helpful advice as I develop into a clinician scientist. I appreciate the help provided by undergraduate researchers: Nitin Venugopal, Taeyoung Lee, and Yeong Won Kim.

I’d like to thank my previous advisor and mentor Dr. Charley Della Santina, as well as Dr. Gene Fridman. They instilled in me a love for the development of novel therapies to treat human disease, and setting me down the path of becoming a clinician scientist.

I am of course thankful for my parents Pen Pong and Yiwen Chiang for raising me, believing in me, and teaching me the value of using my skills and abilities for good. I thank my brother Eric Chiang for our philosophical discussions, for always playing devil’s advocate, and for my inferiority complex.

Finally, I wish to thank my wife Pauline Che and son Nathan Chiang. Pauline has believed in me even when I did not. She has provided me organization to my mess, spontaneity to my strict rules, a second pair of eyes, reminders to be more empathetic, and most importantly, unconditional love. Pauline has pushed me to become better and do more than I ever thought possible, sometimes through coaxing and sometimes through the reward of a hug. Although Nathan is new to this world, he has shifted my perspective and reminded me of the importance of family. And I wish to instill in him an appreciation for the world and the desire to improve it.

TABLE OF CONTENTS

Page
ACKNOWLEDGEMENTS iv

LIST OF TABLES xi

LIST OF FIGURES xii

LIST OF SYMBOLS AND ABBREVIATIONS xvii

SUMMARY xviii

CHAPTER

1 INTRODUCTION 1
- 1.1 Anatomy and Physiology of the Eye 1
  - 1.1.1 Anterior segment of the ocular globe 3
  - 1.1.2 Posterior segment of the ocular globe 6
  - 1.1.3 Extra-ocular structures 9
- 1.2 Ocular Pathology 10
  - 1.2.1 Primary open angle glaucoma 10
  - 1.2.2 Posterior segment diseases 12
- 1.3 Ophthalmic Imaging Modalities 14
  - 1.3.1 *Post mortem* imaging techniques 14
  - 1.3.2 *In vivo* imaging techniques 15
- 1.4 General Overview of Ophthalmic Drug Delivery 18
  - 1.4.1 Ocular barriers of the eye 18
  - 1.4.2 Traditional ophthalmic drug delivery techniques 22
- 1.5 Microneedle Injections to Access Suprachoroidal Space 26
  - 1.5.1 Microneedles 26
- 1.6 Suprachoroidal Delivery using Microneedles 27
- 1.7 Aims 31
  - 1.7.1 Aim 1: Identify anatomical barriers that limit spread in the SCS 32
  - 1.7.2 Aim 2: Study the distribution of particles and molecules in the SCS 32
  - 1.7.3 Aim 3: Investigate kinetics of the SCS thickness 33
  - 1.7.4 Aim 4: Determine the relative contribution of clearance routes and study the clearance kinetics of molecules from the SCS 33
  - 1.7.5 Aim 5: Develop controlled-release brimonidine microspheres in the SCS for the treatment of glaucoma 34

2 CIRCUMFERENTIAL FLOW OF PARTICLES IN THE SUPRACHOROIDAL SPACE IS IMPEDED BY THE POSTERIOR CILIARY ARTERIES 35
- 2.1 Summary 35
- 2.2 Introduction 36
- 2.3 Methods 37
  - 2.3.1 Microneedle injection and tissue processing 37
  - 2.3.2 *In vivo* injection into the SCS of rabbits 40
  - 2.3.3 Dissection of ocular globe of rabbits and humans 41
  - 2.3.4 Effect of injection site on spread in the SCS of cadaver eyes 41

2.3.5 Image acquisition and analysis, and statistics 42
2.4 Results 43
2.4.1 Effect of injection site on spread in SCS of rabbits 43
2.4.2 Effect of IOP, injection volume, and particle size on spread in SCS 46
2.4.3 Effect of bevel orientation on spread in SCS 48
2.4.4 *In vivo* injection into SCS 48
2.4.5 Dissections of *ex vivo* rabbit eyes and human eyes 50
2.4.6 Microneedle injection into human cadaver eyes 52
2.5 Discussion 53

3 DISTRIBUTION OF PARTICLES AND MOLECULES IN THE SUPRACHOROIDAL SPACE AFTER MICRONEEDLE INJECTION 57
3.1 Summary 57
3.2 Introduction 58
3.3 Materials and Methods 60
3.3.1 *Ex vivo* injection procedure 60
3.3.2 Flat mount to characterize 2D circumferential spread 61
3.3.3 3D cryo-reconstruction to determine 3D distribution of particles and fluorescein 62
3.3.4 Fluorescent tagging of excipient formulation 63
3.3.5 *In vivo* SCS injections and image acquisition 64
3.3.6 Statistical analysis 65
3.4 Results 66
3.4.1 Distribution of particles and molecules immediately after injection into the SCS 66
3.4.2 Distribution of particles and molecules over time after injection into the SCS *in vivo* 70
3.4.3 Effect of particle size on particle distribution over time after injection into the SCS *in vivo* 77
3.5 Discussion 78
3.5.1 Distribution of particles and molecules injected into the SCS 79
3.5.2 Distribution of particles relative to molecules 79
3.5.3 Effect of formulation on distribution of particles 80
3.5.4 Effect of particle size on distribution of particles 80
3.5.5 Study limitations 81
3.5.6 Conclusion 82

4 THICKNESS AND CLOSURE KINETICS OF THE SUPRACHOROIDAL SPACE FOLLOWING MICRONEEDLE INJECTION OF LIQUID FORMULATIONS 83
4.1 Summary 83
4.2 Introduction 84
4.3 Materials and Methods 86
4.3.1 *Ex vivo* injection procedure 86
4.3.2 Ultrasound imaging to determine SCS thickness 87
4.3.3 3D cryo-reconstruction to determine 3D distribution of particles and fluorescein 87
4.3.4 Mechanical testing of sclera-choroid attachments 90
4.3.5 SCS collapse rate with different liquid formulations 91

4.3.6 Determination of SCS clearance kinetics by fundus imaging 92
4.4 Results 93
4.4.1 Effect of injection volume on SCS thickness: cryo-reconstruction measurement 93
4.4.2 Effect of injection volume on SCS thickness: ultrasound B-scan measurement 97
4.4.3 Measurement of force of adhesion between sclera and choroid 99
4.4.4 Effect of liquid formulation on SCS thickness and collapse time 101
4.4.5 Effect of liquid formulation on clearance of fluorescent molecules from the SCS 106
4.5 Discussion 107
4.5.1 SCS thickness is independent of injection volume 107
4.5.2 SCS thickness depends strongly on injection liquid formulation 109
4.5.3 SCS thickness controlled by balance between viscous forces of the liquid formulation and biomechanical forces of the tissue 109
4.5.4 Additional comments 112
4.6 Conclusions 114

5 CLEARANCE KINETICS AND CLEARANCE ROUTES OF MOLECULES FROM THE SUPRACHOROIDAL SPACE AFTER MICRONEEDLE INJECTION 116
5.1 Summary 116
5.2 Introduction 117
5.3 Methods 119
5.3.1 Microneedle injection 120
5.3.2 Determination of SCS collapse rate by ultrasonography 120
5.3.3 Fluorescent labeling of monoclonal antibody 121
5.3.4 Determination of SCS clearance kinetics by fundus imaging 121
5.3.5 Intraocular pressure measurements 122
5.3.6 Collection of fluorescein by different clearance routes 123
5.3.7 Data and Statistical Analysis 126
5.4 Results 126
5.4.1 SCS collapse rate as a measure of fluid clearance rate from the SCS 126
5.4.2 Clearance rate of fluorescent molecules from the SCS 128
5.4.3 Route of clearance after SCS injection 133
5.5 Discussion 136
5.5.1 Modeling clearance from the SCS 137
5.5.2 Effect of molecular size on residence time 150
5.5.3 Implications for drug delivery 151
5.5.4 Limitations 152
5.5.5 Conclusions 153

6 SUSTAINED REDUCTION OF INTRAOCULAR PRESSURE BY SUPRACILIARY DELIVERY OF BRIMONIDINE-LOADED POLY(LACTIC ACID) MICROSPHERES FOR THE TREATMENT OF GLAUCOMA 154
6.1 Summary 154
6.2 Introduction 155
6.2.1 The need for improved patient adherence with administration of IOP-lowering drugs 156

6.2.2 Injections targeting the supraciliary spacing using microneedles 157
6.3 Materials and Methods 158
6.3.1 Materials 158
6.3.2 Removal of low molecular weight acids from PLA 159
6.3.3 Microsphere preparation 159
6.3.4 Scanning electron microscopy 159
6.3.5 Determination of brimonidine loading and encapsulation efficiency 160
6.3.6 In vitro release kinetics of brimonidine 160
6.3.7 Brimonidine quantification 160
6.3.8 Microneedle fabrication 161
6.3.9 *In vivo* experimental treatment groups 161
6.3.10 Intraocular pressure monitoring 164
6.3.11 Histology 164
6.3.12 Statistical analysis 165
6.4 Results 165
6.4.1 Characterization of brimonidine-loaded microspheres 165
6.4.2 Targeted injection localized to the supraciliary space 167
6.4.3 Effect of supraciliary delivery of brimonidine-loaded microspheres on intraocular pressure 169
6.4.4 Effect of fluid carrier on intraocular pressure 172
6.4.5 Integrated pharmacodynamic response of treatment groups 173
6.4.6 Initial safety assessment 175
6.5 Discussion 177

7 CONCLUSION 154
7.1 Kinetics of Suprachoroidal Space Delivery using Microneedles 183
7.1.1 Distribution in the suprachoroidal space 183
7.1.2 Clearance from the suprachoroidal space 186
7.1.3 Controlled release systems within the suprachoroidal space 187
7.2 Role of Formulation on Kinetics 188
7.2.1 Liquid formulation 188
7.2.2 Polymeric microparticles 189
7.3 Limitations of the Studies 189
7.4 Final Note 190

8 FUTURE DIRECTIONS 191
8.1 SCS Thickness can be Modulated with Liquid Formulation 191
8.2 Strategies for Controlled Release Treatments of Posterior Segment Diseases 193
8.3 Visualization of SCS Injections in Human Subjects 193
8.4 Future Outlook of Suprachoroidal Delivery 194

REFERENCES 196

VITA 208

LIST OF TABLES

Table 1.1 – Summary of medications used to treat glaucoma 11

Table 1.2 – Selected posterior segment diseases and their distribution............................ 12

Table 5.1 - Characteristic times of transport phenomena in the eye............................... 144

Table 6.1 – Microsphere formulation parameters.. 159

Table 6.2 – Summary of in vivo experimental treatment groups 162

Table 6.3 – Characterization of brimonidine encapsulation in microspheres................ 167

LIST OF FIGURES

Figure 1.1 – Diagram of the human eye. 2

Figure 1.2 – Single slice of ex vivo rabbit eye acquired with Bruker Pharmascan 7T MRI imager after microneedle injection of contrast agent.. 16

Figure 1.3 – Single slice of ex vivo rabbit eye acquired with Scanco µCT 40 scanner after microneedle injection of contrast agent 17

Figure 1.4 – Diagram of the ocular barriers in eye. 19

Figure 1.5 – Diagram of the human eye demonstrating the common ophthalmic drug delivery routes.. 23

Figure 1.6 – Three types of microneedles that can be used to penetrate the body's superficial barrier (e.g., epidermis) and deliver drugs 27

Figure 1.7 – Hollow Metal Microneedle.. 28

Figure 1.8 – SCS separation caused by microneedle injection. 28

Figure 2.1 – SCS injections at different injection sites, shown in the right eyes ex vivo. 44

Figure 2.2 – Percentage of particles above versus below LPCA. 45

Figure 2.3 – Effect of IOP (A), injection volume (B), and particle size (C) on LPCA barrier function.. 47

Figure 2.4 – Distribution of particles in SCS after injection into rabbit eyes in vivo. 49

Figure 2.5 – Image of rabbit sclera showing LPCA perforations through sclera. 50

Figure 2.6 – Images of the posterior pole of a representative human cadaver eye showing LPCA and SPCAs. 51

Figure 2.7 – Images of human cadaver eye after microneedle injection (A) 2 mm from the optic nerve (ON), and (B) 8 mm from the ON. 53

Figure 3.1 – Percentage area of SCS containing injected particles and fluorescein molecules, as determined by flat-mount measurement method. 67

Figure 3.2 – Percentage area of SCS containing injected particles and fluorescein molecules, as determined by 3D cryo-reconstruction method. 68

Figure 3.3 – Parity plot comparing area calculated from flat mount and cryo-reconstruction methods. 69

Figure 3.4 – Spread of particles and fluorescein molecules in the SCS after injection of HBSS formulation in vivo. 73

Figure 3.5 – Spread of particles and fluorescein molecules in the SCS after injection in FITC-CMC formulation in vivo. 74

Figure 3.6 – Spread of particles and fluorescein molecules in the SCS after injection in FITC-Discovisc formulation in vivo. 75

Figure 3.7 – Plot of transport time (mean±SEM) vs. formulation viscosity. 76

Figure 3.8 – Plot of SCS area coverage (mean±SEM) vs. formulation viscosity. 77

Figure 5 – Quantification of area covered (mean±SEM, N=3-4) after SCS injection with (A) 2 nm red- and 200 nm green-fluorescent particles in HBSS, (B) 200 nm red- and 200 nm green-fluorescent particles in HBSS, (C) 200 nm red- and 2 µm green- fluorescent particles in HBSS, and (D) 20 nm red- and 2 µm green-fluorescent particles in Discovisc over time in vivo. 78

Figure 4.1 – Diagram of 3D cryo-reconstruction methods. 89

Figure 4.2 – Calculation of SCS thickness in ultrasound B scans. 92

Figure 4.3 – Distribution of SCS thickness after injection of particles suspended in HBSS into the SCS of the rabbit eye ex vivo. 95

Figure 4.4 – Area of SCS coverage with increasing injection volume. 96

Figure 4.5 – SCS thickness measured with ultrasound B-scan in the rabbit eye ex vivo. 98

Figure 4.6 – Modified ATSM 1876 peel test performed on scleral/chorioretinal (Sc-Ch-Re) strips from eyes that had either received (gray bar) or not received (black bar) a 100 µL SCS injection of HBSS ex vivo. 99

Figure 4.7 – Representative histological images showing SCS fibrils. 100

Figure 4.8 – Quantification of median SCS thickness after injection of different liquid formulations as a function of time. 102

Figure 4.9 – Representative ultrasound B-scan images of the SCS after 50 µL injection of (A) HBSS and (B) 5% CMC solution. 103

Figure 4.10 – Time course of SCS thickness following microneedle injection of (A) 50 µL Discovisc and (B) 50 µL 5% carboxymethyl cellulose in HBSS. 105

Figure 4.11 – The total clearance time of fluorescein from the SCS after injection in HBSS or 5% CMC solution. 107

Figure 4.12 – Schematic of SCS expansion after injection of fluid............................... 112

Figure 5.1 – SCS thickness over time determined by ultrasound B-scan images acquired during supranasal injection of 50 µL HBSS into the SCS of the live rabbit. 127

Figure 5.2 – Representative brightfield and fluorescent fundus images of the live rabbit eye before, 3 min post- and 14 days post-injection of 50 µL of fluorescein, 2 MDa FITC-dextran, or 20 nm polystyrene particles. 130

Figure 5.3 – Analysis of rates of clearance from the SCS after 50 µL SCS injection with molecules ranging from 1 – 60 nm in diameter and a 20 nm polystyrene particle. 131

Figure 5.4 – Pressure measurement in vivo and postmortem after SCS injection of 50 µL HBSS.. 133

Figure 5.5 – Fluorescein collected from four routes out of the SCS after 50 µL SCS injection of fluorescein in HBSS. 135

Figure 5.6 - Results from 2D model of molecule transport in the SCS. 142

Figure 5.7 – Sensitivity analysis of parameters used in two-dimensional model of molecule transport from the SCS. 148

Figure 6.1 – Graphical description of rationale to target ciliary body. Higher bioavailability achievable with supraciliary injection of briomindine-loaded microspheres compared with topical eye drops. 155

Figure 6.2 – Representative SEM images of four microsphere formulations................ 166

Figure 6.3 – Hollow microneedle measuring 750 µm in length 168

Figure 6.4 – Representative histological image of a section from the rabbit eye showing brimonidine-loaded microspheres... 168

Figure 6.5 – Representative fluorescence image showing localization of red-fluorescent microspheres to the supraciliary space. 169

Figure 6.6 – Effect of brimonidine delivery on IOP in the rabbit eye. 171

Figure 6.7 – Integrated pharmacodynamic response of treatment groups. 174

Figure 6.8 – Representative images of the rabbit eye 5 min (A) and 1 day (B) after microneedle injection... 175

Figure 6.9 – Representative histological images after microneedle injection of HBSS only (SC-HBSS, A) 88 days post-injection; blank microspheres (SC-blank, B) 46 days

post-injection; and brimonidine-loaded microspheres (SC-low dose, C) 69 days post-injection... 176

LIST OF SYMBOLS AND ABBREVIATIONS

AMD	Age-related macular degeneration
ANOVA	Analysis of variance
C	Conjunctiva
Ch	Choroid
CMC	Carboxymethyl cellulose
HBSS	Hank’s balanced salt solution
ID	Inner diameter
IOP	Intraocular pressure
IVT	Intravitreal
kDa	Kilodalton
LPCA	Long posterior ciliary artery
MDa	Megadalton
MN	Microneedle
OD	Outer diamer
ON	Optic nerve
PD	Pharmacodynamic
PLA	Poly (lactic acid)
PLGA	Poly(lactic-co-glycolic acid)
PK	Pharmacokinetic
Re	Retina
Sc	Sclera
SCS	Suprachoroidal space
SPCA	Short posterior ciliary artery
U/S	Ultrasound
VH	Vitreous humor

SUMMARY

Blindness and visual impairment due to eye disease results in significant loss in patient quality of life. Although therapeutics to treat these diseases may exist, specific targeting of diseased ocular tissue, while sparing other tissues, is difficult with traditional ophthalmic routes of administration. The suprachoroidal space (SCS, a potential space bordered by the choroid and sclera) is being explored as a site for drug delivery since high bioavailability and targeting can be achieved at the retina, choroid, and ciliary body. A hollow microneedle sized to pierce the sclera, while preventing penetration through the chorioretina, enables injections into the SCS in a reliable and efficient manner. The safety and efficacy of microneedle injections into the SCS is being investigated for posterior segment indications in ongoing clinical trials.

One goal of this thesis was to investigate the distribution and clearance kinetics of formulations injected into the SCS using a microneedle. Specifically, we identified anatomical barriers in the SCS that impeded circumferential spread of particles. We next looked for other factors that could influence particle and molecule spread. We found that increasing injection volume resulted in increased particle and molecule coverage, with molecules occupying a larger area than particles. Increasing formulation viscosity reduced this discrepancy in area coverage. We next studied the SCS thickness, and found that injection volume had a minor effect and formulation injected had a major effect on it. We investigated the kinetics and routes of clearance of fluid and molecules injected into the SCS. We found that molecules exited the SCS via reflux, pressure-mediated trans-scleral transport, and diffusion-mediated clearance by the choroid. We also showed greatly prolonged residence time in the SCS was possible with very large macromolecules.

A second goal was to develop a controlled release system for use in the SCS. We demonstrated 1-month efficacy of a controlled-release microparticle system injected into the SCS to treat glaucoma in a rabbit model. Dose sparing was achieved compared with conventional therapy.

This work advances our understanding of the SCS as an emerging route of administration in treating ophthalmic disease.

1 INTRODUCTION

Visual perception is a complex sensation that allows humans to identify objects, navigate the world, awaken in the morning, and appreciate a smile. Visual perception begins with visible light (~400-700 nm in wavelength) that is transmitted, reflected, refracted, or absorbed by an object[1]. The eyes are a pair of organs located in the head that detect this visible light, and process and transmit signals to the brain that subsequently become vision.

Unfortunately, ocular diseases can cause vision loss, robbing an individual of arguably the most important of the senses. Drugs can be used to treat or cure these diseases, however, targeting drugs within the eye can be challenging. This work further examines the use of microneedle injections to specifically target regions of the SCS to treat ocular diseases.

1.1 Anatomy and Physiology of the Eye

The human eye is a spherical organ composed of three concentric layers surrounding fluid (Figure 1.1). The outermost fibrous layer consists of the cornea anteriorly and sclera posteriorly; the intermediate layer consists of the uvea, which can be sub-classified as iris, ciliary body, and choroid; and the innermost layer is the neurosensory retina[1]. The retina is a thin sheet of light-sensitive neurons that detects and processes light. Within these three layers is the watery aqueous humor in the anterior segment and the jelly-like vitreous humor in the posterior segment. The eye weighs ~7.3 g, and occupies a volume of 6.2 to 7.2 mL[1]. The ocular globe has dimensions of 24.2 mm (transverse), 23.7 mm (sagittal), and 22.0 to 24.8 mm (axial)[2].

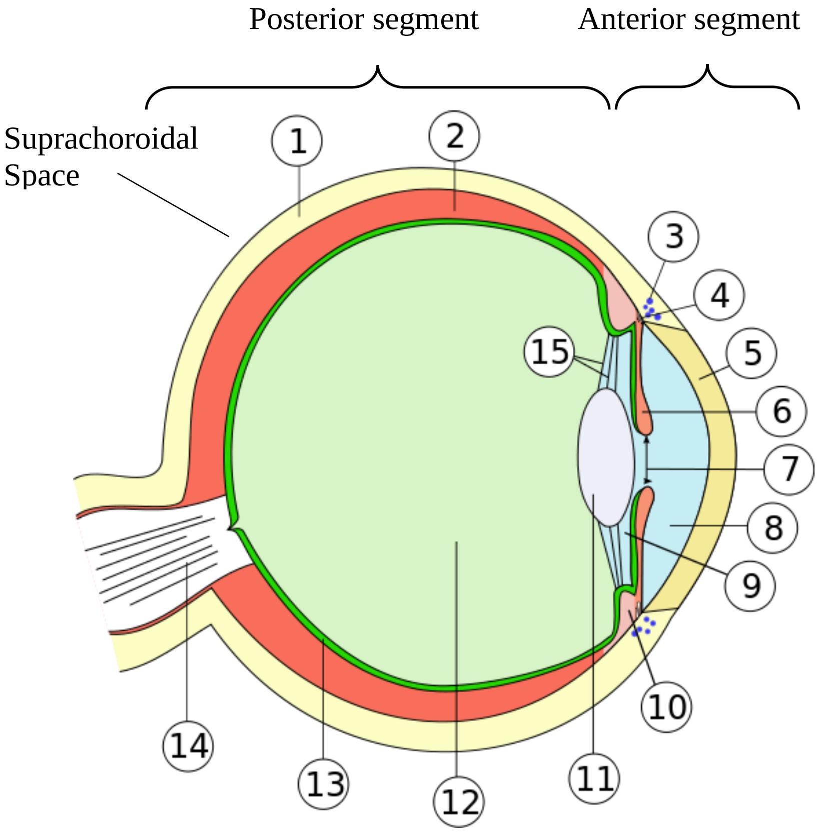

Figure 1.1 – Diagram of the human eye. Suprachoroidal space is potential space between sclera and choroid.(1) sclera, (2) choroid, (5) cornea, (6) iris, (7) pupil, (8) aqueous humor, (10) ciliary body, (11) lens, (12) vitreous humor, (13) retina, (14) optic nerve, (15) zonules. Credit: Talos, colorized by Jakov (https://commons.wikimedia.org/wiki/Human_eye#/media/File:Eye_scheme_mulitlingual.svg)

As light enters the eye, the cornea and lens refract light so as to focus it on the retina. The iris dynamically controls the amount of light reaching the retina by changing the size of the pupil. The lens can dynamically change shape to adjust its own refractive power, allowing fine adjustments in the focal plane of the eye. The aqueous and vitreous humor maintain the shape and rigidity of the eye so the focal plane of the light does not shift away from the retina. The retina detects light, processes the signal, and transmits electrical impulses (i.e., action potentials) along the optic nerve to the visual cortex of the brain. The visual cortex and other regions of the brain further process these signals to produce vision.

1.1.1 Anterior segment of the ocular globe

The anterior segment of the eye is generally responsible for focusing light on the retina, controlling light intensity, and controlling intraocular pressure (IOP)[1]. The anterior segment consists of the cornea, ciliary body, iris, lens, and aqueous humor.

1.1.1.1 Cornea

The cornea (5 in Figure 1.1) is the transparent fibrous layer in the anterior segment of the eye. It is comprised of five layers, from anterior to posterior: corneal epithelium, Bowman's layer, corneal stroma, Descemet's Layer, and corneal endothelium[1]. In humans, central corneal thickness is 536 ± 31 μm (mean ±SD)[3].

The corneal epithelium is comprised of stratified squamous cells, with Bowman's layer as its basement membrane. The epithelium forms a barrier to the outside world that keeps microbes out[4]. These cells are continually renewed by corneal stem cells, which reside in the limbus[5]. Newly formed epithelial cells migrate towards the center of the cornea and anteriorly, replenishing the cornea every 1-3 weeks[6].

The cornea stroma forms the bulk of the cornea (~90% of its thickness)[1]. The stroma is composed of aligned collagen fibers with uniform thickness, which are organized into parallel sheets[7]. To maintain transparency, the stroma is kept in a dehydrated state so the distance between fibers is constant (<200 nm)[8]. The highly organized stromal fibers act as Rayleigh scatterers that allow visible light (400-700 nm) to pass through the stroma with minimal interference[7]. On the other hand, UV light (<400 nm) experiences destructive interference when passing through the stroma, and consequently, does not reach the retina.

The stroma's radius of curvature and refractive index accounts for most of the eye's refractive power[9]. Because the refractive index of air is quite dissimilar from that of cornea, the anterior surface of the cornea accounts for most of the refractive power. The refractive power of the cornea is ~43 D (diopters) and does not change through adulthood[1, 8].

The corneal endothelium is the innermost layer of the cornea. It is actually a single layered epithelium – with Descement's layer as its basement membrane – that does not regenerate with age. The cornea endothelium actively pumps water out of the cornea to maintain the relatively dehydrated state of the stroma[10].

1.1.1.2 Iris

The iris (6 in Figure 1.1) serves as a biological aperture (called the pupil, 7 in Figure 1.1) for the neurosensory retina, adjusting the diameter of the pupil depending on ambient light conditions[1]. The iris receives both sympathetic and parasympathetic innervations.

1.1.1.3 Ciliary body

The ciliary body (10 in Figure 1.1) consists of the ciliary muscles and the ciliary processes. The function of the former is to alter the refractive power of the lens by controlling the tension of the zonules, which are fibers that attach the ciliary muscles to the lens[1]. The ciliary muscle forms a ring anchored to the sclera near the scleral spur. When the ciliary muscles contract, the zonules are placed under tension, and the lens is pulled, reducing its radius of curvature and its refractive power, and *vice versa*[11, 12].

The ciliary processes is continuous with the uveal tract. It produce aqueous humor, which is a transparent nutrient-rich fluid derived from blood[13, 14]. The aqueous humor is required to feed the avascular cornea and lens (these tissues are necessarily devoid of blood vessels so as to maintain their transparency). The interior of the ciliary body contains a rich blood vessel network. The ciliary processes is lined by two layers, called the pigmented and unpigmented ciliary epithelium, which sequentially filter blood into aqueous humor[13]. They collectively form the blood-aqueous barrier which keeps blood from leaking into the aqueous humor[15].

1.1.1.4 Aqueous humor

Aqueous humor (8 in Figure 1.1) contains nutrients necessary to feed the corneal epithelium and endothelium, as wells as the lens epithelium, since the cornea and lens are avascular[1]. It is produced by the ciliary epithelium lining the ciliary body. Aqueous humor production (and elimination) is also important in maintaining the intraocular pressure (IOP)[13]. This IOP keeps the eye inflated, which is necessary to maintain the focal plane of the eye on the retina, especially when externally forces are applied on the eye[13]. Elimination of aqueous humor is possible through two paths: the ‘traditional outflow’ and uveoscleral outflow[13, 16]. Traditional outflow occurs through the trabecular meshwork. Fluid flowing through the trabecular meshwork enters Schlemm’s canal, which is a circular channel near the limbus. Fluid collected by Schlemm’s canal is eventually shunted into the episcleral veins[13]. The uveoscleral outflow is usually less than traditional outflow, though there are drugs that can dramatically increase uveoscleral outflow. In uveoscleral outflow, fluid flows through the iris root and into the suprachoroidal space[16]. Aqueous humor production in humans is 2.4 ± 0.6 μL/min, and the characteristic elimination time is approximately 0.01/min[13].

1.1.1.5 Lens

The lens (11 in Figure 1.1) is an avascular transparent tissue that is suspended in the anterior segment by zonules. The lens accounts for about one-third the refractive power of the human eye (with the cornea accounting for the remainder)[17]. It can dynamically adjust the focal plane of the eye when it changes shape. The lens epithelium surround the lens and grown inwards[18]. The lens nucleus is made of enucleate fibers (cells that have lost their nucleus). In young adults, the lens is smaller and can change its shape easily, allowing accommodation. However, with age, the lens becomes larger and more rigid[19]. Lens opacity can result from damage to the lens epithelium, or aggregation of the proteins found in the lens fibers[19].

1.1.2 Posterior segment of the ocular globe

The posterior segment of the eye is responsible for detecting light and transmitting a signal to the brain. The posterior segment consists of the sclera, choroid, retina, optic nerve, and vitreous humor.

1.1.2.1 Retina

The retina (13 in Figure 1.1) is a part of the central nervous system. Total thickness of the human retina is 230 ± 15 μm[20]. The neurosensory retina is a highly organized collection of neural layers responsible for detecting and processing light, and transducing a complex spatiotemporal pattern along the optic nerve to the brain representing light and darkness[1]. The photoreceptors, which are the outermost layer of the retina, are responsible for detecting photons and initiating signal transduction. There are two types of photoreceptors: rod and cone. Rods are capable of detection in low light settings (down to single photons) but have low spatial resolution[5]. There are approximately 91 million rod photoreceptors in the eye, mostly distributed in the periphery[21]. Cones are capable of detection in high light settings with high spatial resolution. Furthermore, there are three subtypes of cones that have maximal sensitivity at 420, 534, and 564 nm, respectively[9]. There are 4.5 million cone photoreceptors, the vast majority of which are found in the center region of the retina called the macula[21]. At the center of the macula is a pit that contain only cone photoreceptors, called the fovea. The fovea is responsible for central vision, allowing for tasks such as reading.

The retinal pigment epithelium (RPE) is a single monolayer of epithelial cells that supports the outer retina (i.e., the photoreceptors) structurally and metabolically[22, 23]. It is located between the outer retina and the choroid[22-25], with Bruch's membrane serving as the basement membrane for both RPE and choroid. The RPE shuttles nutrients from the choroid to the outer retina, while shuttling waste out of the outer retina[26].

Interneurons, such as the bipolar cells, horizontal cells, and amacrine cells, process and convey the information to the retinal ganglion cells[1]. Müller cells support the retina structurally and metabolically. Inner retinal blood vessels supply the inner retina with nutrients[25]. The axons of the retinal ganglion cells coalesce at the optic disc to form the optic nerve. The optic nerve exits the ocular globe, heading towards the brain.

1.1.2.2 Choroid

The choroid (2 in Figure 1.1) is a rich vascular bed that supplies nutrients to the outer layers of the neurosensory retina[26, 27]. Larger caliber vessels are found in the outer choroid, while capillaries, termed choriocapillaris, are found in the inner choroid. The choriocapillaris is one of the densest capillary beds with one of the highest perfusion rates of the body[28, 29]. The total thickness of the choroid in humans is 354 ± 111 μm at the center of the visual axis[30]. Individual choriocapillaries can be classified as non-sinusoidal fenestrated capillaries[31]. The large supply of nutrients and oxygen is necessary for the metabolic demand and health of the retina. Since the oxygen consumption of the outer retina does not deplete the choroid's carrying capacity[29, 32], some have posited that the choroid can function as a heat sink that regulates retinal temperature.

1.1.2.3 Suprachoroidal space

The suprachoroidal space is a potential space that exists between the sclera and the choroid. Pigment can migrate into this space. In healthy adults, the suprachoroidal space is approximately 30 μm thick due to the negative pressure relative to intraocular pressure that keeps the space closed[1, 33, 34]. Furthermore, there are connective tissue fibers that connect the sclera to the choroid and ciliary body[1, 35]. A strain of about "5 g/cm" (calculated to be ~490 Pa) is required to break these fibers[1, 36, 37]. The minimal but nonzero thickness allows the sclera to slide relative to the choroid during accommodation[38]. Due to negligible lymphatics[39], drainage of the suprachoroidal space is through intravascular (into the choroid)[11, 31], trans-scleral[8, 35, 36, 40], and perivascular[16, 41-44] routes.

1.1.2.4 Sclera

The sclera (1 in Figure 1.1) encapsulates the posterior segment of the eye and is continuous with the cornea, meeting at the limbus. The sclera has three layers: the episcleral layer, the sclera proper, and the lamina fusca[1]. The episcleral layer is a composed of loose elastic tissue and attaches the sclera to Tenon's capsule. The sclera proper forms the bulk of the sclera. Unlike the corneal stroma, the scleral stroma is opaque since the sclera's collagen fibers are not aligned nor are they uniform in size[1]. In humans, scleral thickness is 530 ± 140 μm at the limbus, and ~900 μm near the optic nerve[45]. The lamina fusca is the innermost layer of the sclera, and is loosely arranged. The lamina fusca contains many pigment cells.

1.1.2.5 Vitreous humor

The vitreous humor (12 in Figure 1.1) is a jelly-like substance that occupies much of the ocular globe[1]. It is composed mostly of water (99%) with hyaluronic acid[46]. With age, the vitreous can partially liquefy, changing its diffusional properties[47, 48].

1.1.3 Extra-ocular structures

Other structures surround the eye but are not a part of the ocular globe. These include the conjunctiva, Tenon's capsule, extraocular muscles, and eyelid.

1.1.3.1 Eyelid

The eyelids are folds of skin that can close to protect the eye[1]. Muscles can open or close the eyelid. When the eyelids are opened, the cornea and conjunctival surfaces are exposed to the outside world. The blink reflex helps to replenish the tear film and to wash away particulates that may have deposited on the eye[1, 4]. The two muscles that elevate and depress the eyelid are considered extraocular muscles.

1.1.3.2 Conjunctiva

The conjunctiva is a clear membrane that covers the sclera, but not the cornea, and the inner surface of the eyelids[1]. Thus, the only region of the ocular globe actually exposed to the outside world is the cornea. Secretory cells located in the conjunctival membrane produce mucus and tears, which help lubricate the eye. Many blood vessels and lymphatics run in the subconjunctival space[31, 39].

1.1.3.3 Tenon's capsule

Tenon's capsule is a thin membrane that envelops the ocular globe from the optic nerve to the limbus[1]. Tenon's capsule adheres to conjunctiva anteriorly, and to the outer surface of the sclera posteriorly. It helps to keep the retro-orbital tissues (e.g., retro-orbital fat) separated from the eye.

1.1.3.4 Extraocular muscles

There are six extraocular muscles that move the eye in the orbit to position the eye in different directions[1]. The muscles typically work in concert to reposition the eye, as well as hold it stationary. Pairs of muscles work together in a push-pull system. For example, to elevate the eye, the superior rectus muscle contracts, while the inferior rectus relaxes. Since the extraocular muscles are innervated by cranial nerves, they can elucidate the health status of the cranium.

1.2 Ocular Pathology

Many pathologies can affect the eye, which in turn affect vision. Selected ocular diseases are described below to better motivate the need for targeted ophthalmic drug delivery.

1.2.1 Primary open angle glaucoma

Glaucoma is a group of ocular diseases with characteristic optic neuropathy[49]. Patients with glaucoma will slowly and painlessly lose peripheral vision and eventually, central vision. The most common form of glaucoma is primary open-angle glaucoma (POAG). It is a leading cause of blindness in the United States, affecting nearly 3 million individuals with an annual cost of $2.9 billion[50, 51]. POAG is usually associated increased intraocular pressure (IOP) but elevated IOP is neither causative nor requisite for glaucoma[52]. Lowering IOP has been shown to prevent the progression of glaucoma[53, 54], and IOP is strongly linked with aqueous humor production and outflow[4, 13].

Medical and surgical therapy seek to decrease intraocular pressure. Medical therapy is first-line treatment, and calls for of a topical eye drop regimen (common regimens are presented in Table 1.1)[4, 53, 54].

Table 1.1 – Summary of medications used to treat glaucoma

Drug Class	Mechanism of Action	Example	Dose	Dosing Regimen	Dose/day (µg/day)
Beta Blocker	Decrease aqueous humor production	Timolol	0.25%	2/d	250
Prostaglandin analogue	Increase uveoscleral outflow	Latanoprost	0.005%	1/d	2.5
Carbonic anhydrase inhibitor	Decrease aqueous humor production	Dorzolamide	2%	3/d	3000
Alpha-2 adrenergic agonist	Decrease aqueous humor production, increase aqueous humor removal	Brimonidine	0.1%	3/d	150
Miotic agent	Increased aqueous outflow	Pilocarpine	0.5%	3-4/d	750

Patient adherence to eye drop regimens is low, with an estimated adherence of ~60%, in part because patients do not notice the slow painless loss of vision from the periphery [4, 55-58]. The low compliance is due to a number of reasons including regimen difficulties (e.g., refill, cost), patient factors (e.g., knowledge, memory, and motivation), provider factors (e.g., dissatisfaction, communication), or situational/environmental issues (e.g., change in routine, competing activity)[53, 55-58]. Situational/ environmental factors accounted for about half of all adherence barriers[58]. Simplifying the dosing regimen (i.e., using a once-per-day eye drop vs. twice-per-day eye drops) did increase adherence, but did not result in perfect (100%) adherence[56].

1.2.2 Posterior segment diseases

Selected ocular diseases that affect the posterior segment are presented below. The posterior segment can be separated geographically into the macula (necessary for central, high-resolution vision) and the periphery (necessary for vision in dark environments). Since these diseases only affect specific regions, targeted treatment to those regions may be more efficacious and/or mitigate side effects (Table 1.2).

Table 1.2 – Selected posterior segment diseases and their distribution

Disease	**Site of disease** **Macula**	 **Periphery**	**Comments**
Noninfectious posterior uveitis	x	x	Corticosteroids in anterior segment of eye can cause side effects.
Age-related macular degeneration	x		
Retinitis pigmentosa		x	Treatments under investigation include gene therapy; transfection in other regions of eye may be undesirable.
Ocular tumors	?	?	Lesions can develop anywhere in eye. Chemotherapy in other regions of eye can cause side effects.

1.2.2.1 Noninfectious posterior uveitis

Noninfectious posterior uveitis is typically an autoimmune inflammation of the entire choroid[59]. Patients can experience photopsia or pain from light. Current treatment calls for corticosteroids administered systemically, topically, or intravitreally[59-61]. However, long term steroid use causes cataract formation due to inadequate compartmentalization of drug away from nontarget tissues (e.g., lens) [61, 62].

1.2.2.2 Age-related macular degeneration (AMD)

Age-related macular degeneration (AMD) is an ocular disease that affects the macula, or the central part of the retina. AMD affects 10 million Americans[63]. The cause of AMD is not known, but certain genetic mutations, smoking and other forms of oxidative stress, and age increase the risk of developing AMD[64, 65]. AMD can be sub-classified as wet-form or dry-form. In dry AMD, there are subretinal deposits of cellular debris known as drusen in the macular region. Dry AMD progresses slowly towards geographic atrophy of the macula. One the other hand, wet AMD is characterized by the rapid uncontrolled growth of the choroidal vasculature (termed choroidal neovascularization or CNV). These newly formed choroidal vessels are leaky and can disrupt the macula, all of which can cause blindness[66].

There is no FDA-approved treatment for dry AMD. Wet AMD is currently managed with monthly intravitreal injections of anti-VEGF monoclonal antibodies (such as ranibizumab or aflibercept) that suppress CNV and macular edema[67-70]. There is mounting evidence that anti-VEGF therapy can cause visual impairment through the total suppression of VEGF signaling[24, 71-73].

1.2.2.3 Retinitis pigmentosa

Retinitis pigmentosa is a group of genetic diseases where the rhodopsin gene is mutated[74]. Rhodopsin is the photo-pigment found exclusively in rod photoreceptors, and thus the disease primarily affects rod photoreceptors. Patients experience night blindness and tunneling of vision, and eventual blindness. Because of the distribution of rod vs. cone photoreceptors, the peripheral retina is affected in early/mid-stage disease, while the macula is spared.

Though there is no current FDA-approved treatment, there are clinical trials underway that are testing the safety and efficacy of gene therapy to ‘fix’ the mutated rhodopsin gene (e.g., NCT01482195)[75, 76] and a visual prosthesis that electrically stimulates the surviving interneurons to simulate vision (e.g., NCT01603576)[77, 78].

1.2.2.4 Ocular tumors

Primary ocular tumors are typically focal lesions that affect one specific region of the ocular globe. The most common primary tumor in children is retinoblastoma[79] and in adults is uveal melanoma[80]. The goal of treatment is to kill cancer cells (including any metastatic seeds) while sparing noncancerous cells. If the cancerous cells cannot be controlled, the eye is enucleated.

1.3 Ophthalmic Imaging Modalities

The healthy and diseased eye can be readily imaged using *post mortem* and *in vivo* imaging techniques. Since the eye is a largely transparent light detector, imaging the interior surfaces of the eye is possible. In fact, the eye is one of the only regions in the human body where nerves can be visualized. The following subsections briefly review the pros and cons of various imaging techniques.

1.3.1 *Post mortem* imaging techniques

These methods can enable definitive diagnosis, however, they also require tissue harvesting. Thus, they are not useful in clinical medicine, but can be valuable tools in research. Due to tissue processing, kinetic information is lost.

1.3.1.1 Dissection

After enucleation, the eye can be dissected to provide gross visualization of the inner surfaces of the eye. The suprachoroidal space of albino eyes can be easily seen since there is no pigment in the RPE or choroid, and thus, the retina and choroid are transparent[81]. Such a technique is sacrificial as the eye must be cut open. Since enucleation of the eye must occur, temporal resolution is limited (on the order of minutes). However, the eye can be frozen in ethanol chilled over liquid nitrogen to arrest fluid movement.

1.3.1.2 Histology

Histology can be performed to visualize a cross-section of the eye at the cellular level. The eye must be enucleated and fixed to preserve the cellular structure. Thin slices (~10 µm in thickness) are cut in cross-section. Different stains can be applied to accentuate different cellular or extracellular features. For example, a hematoxylin & eosin (H&E) stain is commonly used to identify cells[82]. Care must be taken to choose an appropriate histological processing technique since most techniques are quite harsh and can destroy structures or objects of interest. For example, H&E stains require xylene washes, however, xylene will dissolve polymeric particles and denature fluorescent proteins.

1.3.2 *In vivo* imaging techniques

These techniques can be carried out in live subjects, and can thus be used to study kinetics. Some imaging modalities are not useful in the eye but are covered here since they are commonly used techniques. Since ophthalmology is so visual, many imaging techniques have been developed specifically for the eye[83].

1.3.2.1 Magnetic resonance imaging (MRI)

Magnetic resonance imaging (MRI) enables three-dimension (3D) views of anatomical (and some functional) structures[84, 85]. The subject is placed in a strong magnetic field and radio frequency pulses are used to excite hydrogen atoms; the resulting changes in radio waves can be detected and processed into a 3D stack. No ionizing radiation is used. Anatomical structures in the eye can be seen under MRI. MRI contrast agents exist, though there is not enough resolution to simultaneously track two different contrast agents. Due to the low signal-to-noise ratio (SNR) of radio frequency, long imaging sessions are necessary to ensure sufficient signal. Furthermore, spatial resolution is limited. For example, the Bruker Pharmascan 7T (available in the Institute of Bioengineering and Bioscience (IBB) core facility at Georgia Tech) acquired a 3D image of the eye with a resolution of ~200 µm in 45 min. This temporal and spatial resolution are insufficient to study kinetics in the rabbit eye. Figure 1.2 is an example image of an *ex vivo* rabbit eye after microneedle injection of contrast agent. Due to long image acquisition, the localization of contrast agent is unclear.

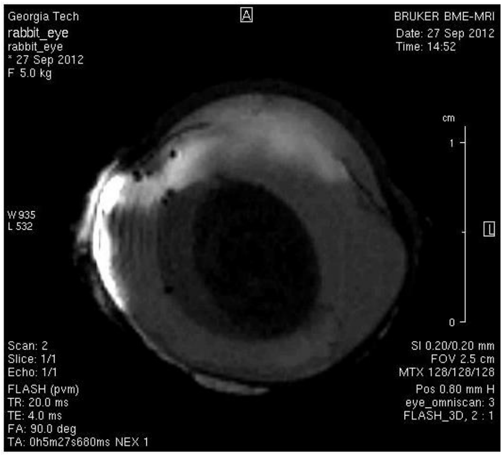

Figure 1.2 – Single slice of ex vivo rabbit eye acquired with Bruker Pharmascan 7T MRI imager after microneedle injection of contrast agent. Contrast agent shows up as bright signal against ocular tissue. Voxel size was a cube with sides ~200 µm. Acquisition time was ~45 min.

1.3.2.2 Computed tomography

Computed tomography (CT) is a technique whereby multiple X-ray images are acquired and processed into a 3D stack. Ionizing radiation is used. Anatomical structures are not visible since all ocular tissue has roughly equal X-ray attenuation properties. Contrast agent can be used. The spatiotemporal resolution of µCT is limited. For example, the Scanco µCT 40 scanner was able to image the whole eye with a resolution of ~50 µm in approximately 1 hr. Since anatomical structures are not readily visible on CT, localization of injected contrast agent in the eye is difficult (Figure 1.3).

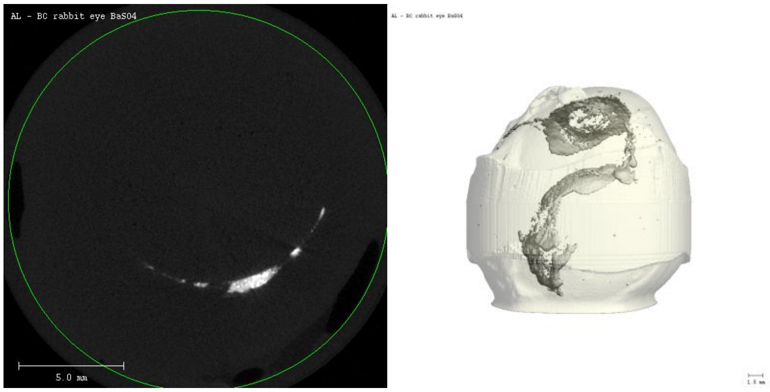

Figure 1.3 – Single slice of ex vivo rabbit eye acquired with Scanco µCT 40 scanner after microneedle injection of contrast agent (Left). 3D render of eye (Right). Note that it was impossible to differentiate ocular tissue from these images. Voxel size was a cube with sides ~50 µm. Acquisition time was ~1 h.

1.3.2.3 Fundus photography

Planar images of the inner surface of the eye can be acquired noninvasively[83]. Optics are needed account for the refractive power of the eye so that a camera can resolve fundus. There are many types of commercial ophthalmic imaging tools, including slit lamp microscopes, direct and indirect ophthalmoscopes, and contact and non-contact retinal cameras[83] Contact retinal cameras (e.g., Clarity Medical Systems Retcam II pediatric ophthalmic imaging system) have wide field lenses that enable visualization into the far periphery (>130° from the optic nerve). Albino subjects can be used so the suprachoroidal space is readily visible. Some cameras also have single wavelength light sources and optical filters that match the excitation and emission spectra of fluorescent molecules, such as fluorescein. Furthermore, these cameras can be modified to visualize fluorescent molecules with other spectra.

1.3.2.4 Ultrasound B-scan

Ultrasonography can be used to acquire cross-sectional views of ocular tissue noninvasively[83, 86]. The ultrasound probe emits high-frequency soundwaves that echo off tissue, and processes the data to show the spatial distribution of density. A single line of information (called an A scan) can be rastered to form a 2D image (called a B scan). Ultrasound B-scan can be used to image through optically opaque tissue (e.g., sclera). Since the suprachoroidal space is a potential space, injection of fluid distends the tissue. This space is visible as a void between the tissues under ultrasound.

1.3.2.5 Optical oherence tomography

Optical coherence tomography (OCT)[83, 87] also generates cross-sectional views of ocular tissue noninvasively using similar techniques as ultrasound (except with shorter wavelengths). Typically, OCT is used to image the retina along the visual axis and is thus not suitable for imaging the far periphery.

1.4 General Overview of Ophthalmic Drug Delivery

1.4.1 Ocular barriers of the eye

Since the retina is a part of the central nervous system, the eye is a site of immune privilege[4, 88]. The difficulty in maintaining a sterile and immune privileged environment are compounded by the fact that a part of the eye (i.e., cornea) is exposed to the outside world. In the healthy eye, multiple barriers maintain this immune privilege by selectively controlling the entry of particulates (e.g., microbes) and molecules into the eye from systemic circulation, as well as the outside world. The barriers that prevent entry from the outside world include the tear flow, the cornea, and aqueous humor flow. The barriers that prevent particulates and molecules floating in systemic blood from reaching the retina include the blood-aqueous barrier and the blood-retinal barrier. Ocular inflammation can override these barriers so immune cells may enter the eye.

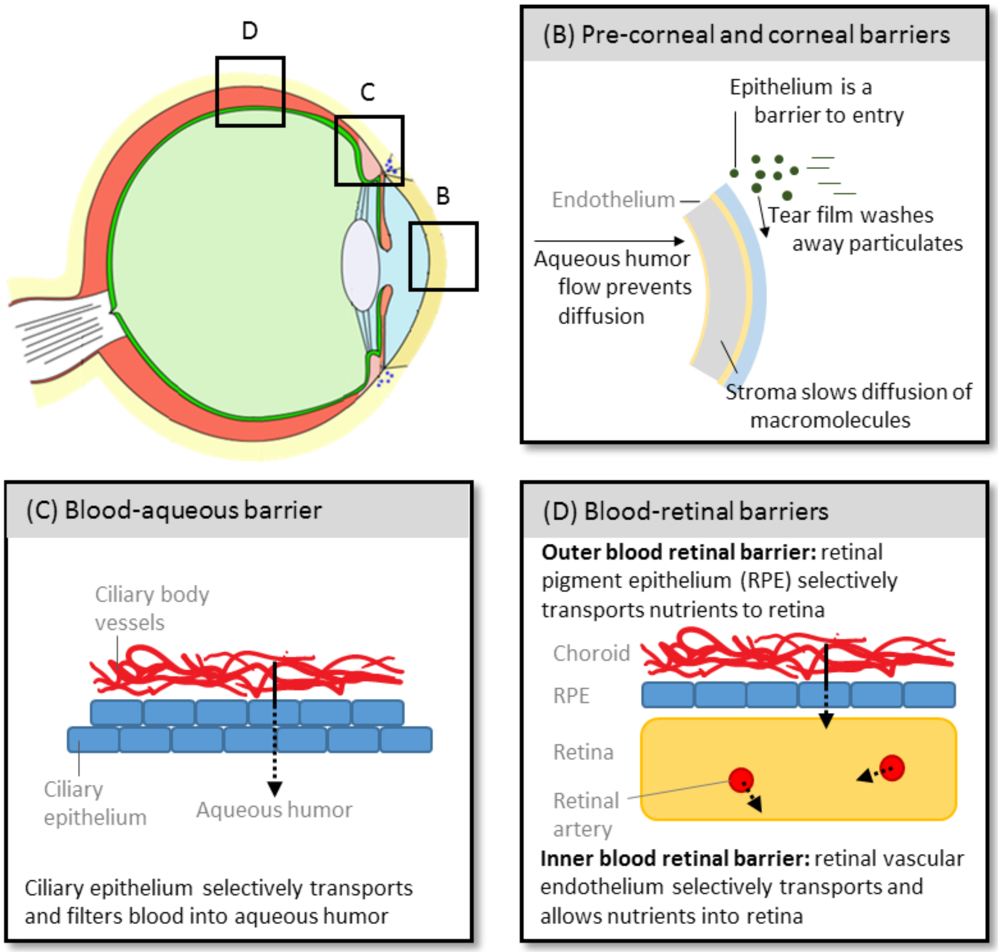

Figure 1.4 – Diagram of the ocular barriers in eye. Adapted from: Talos, colorized by Jakov (https://commons.wikimedia.org/wiki/Human_eye#/media/File:Eye_scheme_mulitlingual.svg)

1.4.1.1 Pre-corneal and corneal barriers

Tear flow and tear drainage form the first barrier to entry into the eye from the outside world (Figure 1.4 B). Glands located in the conjunctiva and eyelids secrete a constant flow of tears that lubricate the eyes and wash away particulates, such as dust or microbes, that may settle on the external surface of the eye. In humans, basal tear film volume is 7.0 ± 2.0 µL and the rate of tear film turnover is 10.3 ± 3.7 %/min[89, 90]. In addition, antimicrobial proteins, such as lactoferrin and lysozymes, are secreted into the tears as an additional means to prevent infection[4].

The cornea is the next barrier to entry from the outside world (Figure 1.4 B). Due to the unique barrier function of the cornea, bioavailability of drugs across the cornea is low, estimated at 1-7%[4]. The corneal epithelium's barrier function and the dense collagen of the stroma inhibit diffusion of particulates and macromolecules through the cornea. Only small molecules within a tight hydrophobic/hydrophilic range may diffuse through the cornea[91].

Corneal epithelial cells form and maintain tight junctions between adjacent cells, which prevent the passage of ions and macromolecules between the cells[92]. Because intracellular transport is limited by tight junctions, the transport of molecules through the epithelium happens via para-cellular or trans-cellular means[91]. In both para-cellular and trans-cellular transport, the diffusing molecule must easily pass into and out of the lipophilic plasma membrane. The corneal stroma is the second structure encountered in the cornea. The collagen fibers and dispersed proteoglycans, which comprise the stroma, are strongly charged and can inhibit the passage of lipophilic molecules. Furthermore, the dense network of collagen fibers physically prevents the movement of particulates and macromolecules. The corneal endothelium provides little barrier function relative to the epithelium and stroma.

Though the barrier function of the sclera is similar to the cornea, the conjunctiva and the subconjunctival space (both of which overlay the sclera) are strong barriers to entry into the eye. The subconjunctival space contains many blood vessels and lymphatics that drain the space; thus, molecules and particulates within the subconjunctival space are preferentially cleared before diffusing through the sclera[4, 93].

Of the fraction of molecules that are able to pass through the cornea into the anterior chamber (1-7%), there is a small but constant convective current caused by aqueous humor outflow that severely limits diffusion deep into the eye to the posterior segment (Figure 1.4 B). Aqueous humor production in humans is 2.4 ± 0.6 μL/min and is directed posterior (from the ciliary body) to anterior (out the trabecular meshwork)[13]. By calculating the Péclet number of the anterior segment, which is dimensionless number that relates the advective transport rate to the diffusion transport rate, we find that advective transport dominates in the anterior chamber[94]. Thus, molecules that cross the cornea will not diffuse towards the back of the eye; rather, they will be pushed by the bulk fluid flow of newly produced aqueous humor into the trabecular meshwork.

1.4.1.2 Blood-retinal barrier

The interior tissues of the eye are separated from the systemic circulation by the blood-aqueous barrier in the ciliary body and the blood-retinal barrier in the retina (Figure 1.4 C and D)[25]. The pigmented and non-pigmented epithelium of the ciliary body form the blood-aqueous barrier (Figure 1.4 C). These cell layers maintain tight junctions that prevent the passage of large macromolecules and cells into the eye[15]. The ciliary epithelium actively transport selected molecules, such as ions, amino acids, and glucose, to form the filtrate that is aqueous humor[14].

Since the retina is a highly metabolically-active tissue, the retina derives nutrients from two separate blood supplies. The inner retina is fed by the retinal vasculature, and the outer retina is fed by the choroid. Each blood supply has its own blood retinal-barrier (i.e., there is an inner and an outer blood-retina barrier) that limits movement from systemic circulation to the retina (Figure 1.4 D)[25]. The inner blood-retinal barrier is inherent to the retinal arteries and their branches. Similar to the vessels that feed the central nervous system, the retinal vasculature is comprised of non-fenestrated capillaries with tight junctions[31]. This limits passive transport of molecules <1 nm (~5kDa) into the inner retina. To enter the inner retina, larger molecules must be actively transported by pericytes that surround the capillary[31]. The outer blood-retinal barrier is comprised of the retinal pigment epithelium (RPE) that separates the outer retina from the choriocapillaris. The choriocapillaris does not have any inherent barrier function because they are fenestrated non-sinusoidal vessels[25, 95, 96]. As with most epithelial layers, the RPE maintains tight junctions that prevent intercellular transport. The RPE actively transports select molecules from the choroid to the outer retina.

1.4.2 Traditional ophthalmic drug delivery techniques

The ability for a pharmacologic agent (i.e., drug) to prevent, treat, or cure a disease has had a profound effect on healthcare. Despite the knowledge that a drug will have a therapeutic effect, it is also essential to deliver drugs to the appropriate site[88]. Optimal drug delivery technologies must balance two sometimes opposing goals: (1) ensuring sufficient drug concentrations are at the drug's site of action to induce a therapeutic effect, and (2) ensuring low drug concentrations are at non-target tissues to minimize side effects. Because of the unique barriers of the eye as well as its small size, targeted drug delivery to specific tissues and regions in the eye can be difficult[88].

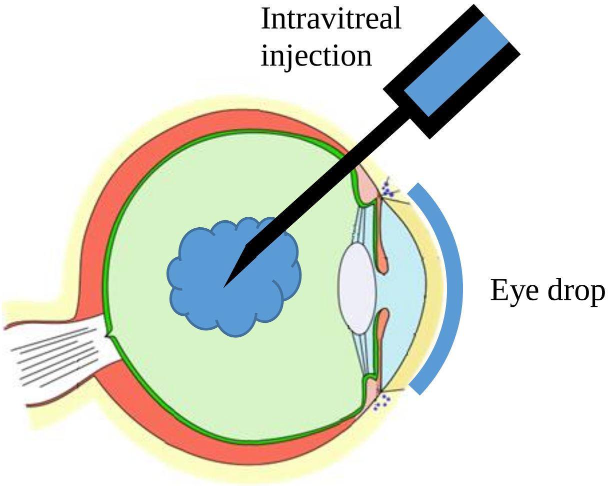

Figure 1.5 – Diagram of the human eye demonstrating the common ophthalmic drug delivery routes: intravitreal injections and topical eye drops. Adapted from : Talos, colorized by Jakov (https://commons.wikimedia.org/wiki/Human_eye#/media/File:Eye_scheme_mulitlingual.svg)

Pharmacokinetics is the study of the movement (including the absorption, distribution, and elimination) of drugs or therapeutic agents in the body. The unique barriers of the eye limit absorption and distribution (e.g., the cornea prevents the bulk movement of drugs into the eye) and increase clearance (e.g., the conjunctival lymphatics clear drug away from the eye into the systemic circulation)[88]. Understanding the pharmacokinetics of each drug delivery method can help us evaluate the advantages and shortcomings of that method. The most common methods for ocular drug delivery are (1) systemic dosing, (2) topical eye drops, and (3) intravitreal injections.

1.4.2.1 Systemic delivery

With systemic dosing, the drug is delivered either orally or parenterally so the entire body is bathed in drug. The drug could distribute into the eye, though the eye's small size (<0.1% of the total mass of an adult) limits the amount of drug that would naturally diffuse into the eye[97]. The actual amount entering the eye is even less due to the blood-retinal barriers. Thus, systemic dosing is inefficient in treating isolated ocular diseases[97]. Instead, systemic dosing is indicated when there is systemic disease with ocular involvement. For example, intravenous injections of an antifungal are appropriate for fungal endophthalmitis in the presence of systemic candidiasis.

1.4.2.2 Topical eye drops

Topical eye drops are a common drug delivery method used for diseases of the anterior segment, such as glaucoma and keratitis[4, 97]. In practice, a patient instills ~50 µL of a drug solution onto their eye. Some manual dexterity and experience are needed to place the drop on the eye and not on the cheek. Tear drainage and corneal barriers limit the total amount of applied drug (~1-7%) that can enter the eye and reach its ultimate site of action[4]. Since the capacity of the lacrimal lake is only about 7-10 uL[4, 89], the vast majority of the eye drop is lost immediately with tear drainage. Drugs that can diffuse through the cornea are moderately-uncharged small molecules[91]. The low bioavailability and fast clearance from the eye necessitate frequent dosing, typically once to four times a day. Because the rate of aqueous humor production is greater than the diffusional rate of the drug (large Péclet number), drugs administered as eye drops do not diffuse deep into the eye[94].

1.4.2.3 Intravitreal injections

Intravitreal injections have become common with the introduction of anti-VEGF monoclonal antibodies (such as bevacizumab and ranibizumab) for wet AMD[69, 98, 99]. Nowadays, intravitreal injections are used for most posterior segment diseases, including AMD, diabetic retinopathy, and uveitis[100]. In the outpatient clinic setting, a trained ophthalmologist uses a 27-30-gauge hypodermic needle to penetrate through all the layers of the eye and inject a drug solution into the vitreous. Such a technique bypasses the ocular barriers of the front of the eye, allowing the delivery of macromolecules (e.g., bevacizumab has a molecular weight of ~146 kDa) into the eye[100]. Unfortunately, intravitreal injections carry a small but significant risk of choroidal hemorrhage, retinal detachment, and infection[101]. After the injection, the vitreous serves as a drug depot, prolonging time between doses. It is estimated that ranibizumab injected intravitreally has a half-life of 2.9 days and was detectable in the vitreous after 29 days[102].

Intravitreal injections are typically intended to treat diseased tissues in the posterior segment diseases (such as the macula in AMD and the choroid in posterior uveitis), not the vitreous itself. The drug must diffuse through the vitreous and reach the site of action in the posterior segment. However, there is no preferential driving force for the injected drugs towards the site of action in the back of the eye, nor is there the ability to direct drug towards specific regions within the back of the eye. The injected drug can freely diffuse throughout the vitreous humor and affect tissue throughout the eye. This nonselective dosing can result in side effects caused by dosing non-target tissues. For example, corticosteroids injected intravitreally for the treatment of uveitis will cause drug-induced cataracts because the corticosteroids can diffuse through the vitreous to the lens[61, 62].

1.4.2.4 Other ophthalmic drug delivery techniques

Other less commonly used ocular drug delivery techniques can be used to deliver drugs around the eye[100]. These techniques are also not targeted towards specific regions or tissues in the eye.

Because the subconjunctival space is a potential space, it is possible to place drug depots inside for extended release applications. This might result in less drug washing away immediately with the tear film. However, clearance by blood and lymphatic vessels from the subconjunctival space is high[95, 103].

Alternatively, drugs can be placed in Tenon's capsule, the fibrous capsule encapsulating the back of the eye[100]. Besides their posterior position, sub-Tenon's injections are similar to conjunctival injections in they do not penetrate into the ocular globe, and thus, are subject to clearance by lymphatics. To have a therapeutic effect in the eye, the drug deposited in the sub-Tenon's space must diffuse through the sclera, which is a diffusional barrier for larger molecules[95, 104].

1.5 Microneedle Injections to Access Suprachoroidal Space

1.5.1 Microneedles

Microneedles are needles with sub-millimeter dimensions. Use of microneedles allows reliable access to superficial tissues that may be difficult to target with conventional means. There are three general classes of microneedles: (1) hollow microneedles enable the injection of drug solutions or suspensions into superficial tissues (Figure 1.6, left); (2) coated microneedles can be used to penetrate into superficial tissues and deliver drugs that are coated on the microneedle (Figure 1.6, middle); and (3) dissolving microneedle are shaped drug-polymer mixtures that can penetrate into superficial tissue and release drug upon dissolution of the polymer (Figure 1.6, right)[8, 81, 105-113].

The main advantage for using microneedles is that they can reliably deliver drug into spaces directly below the body's protective surfaces. In many cases, this can result in less pain, ease of administration, and/or increased efficacy and potency[8, 105-107, 112, 113]. The main disadvantage to using microneedles is the limited amount of drug that can be delivered (<1 µg per microneedle with coated and dissolving microneedles, although multiple microneedles can be used). A dissolving microneedle patch (similar to (Figure 1.6, right) for the delivery of flu vaccine is being investigated in an ongoing phase I clinical trial (NCT02438423).

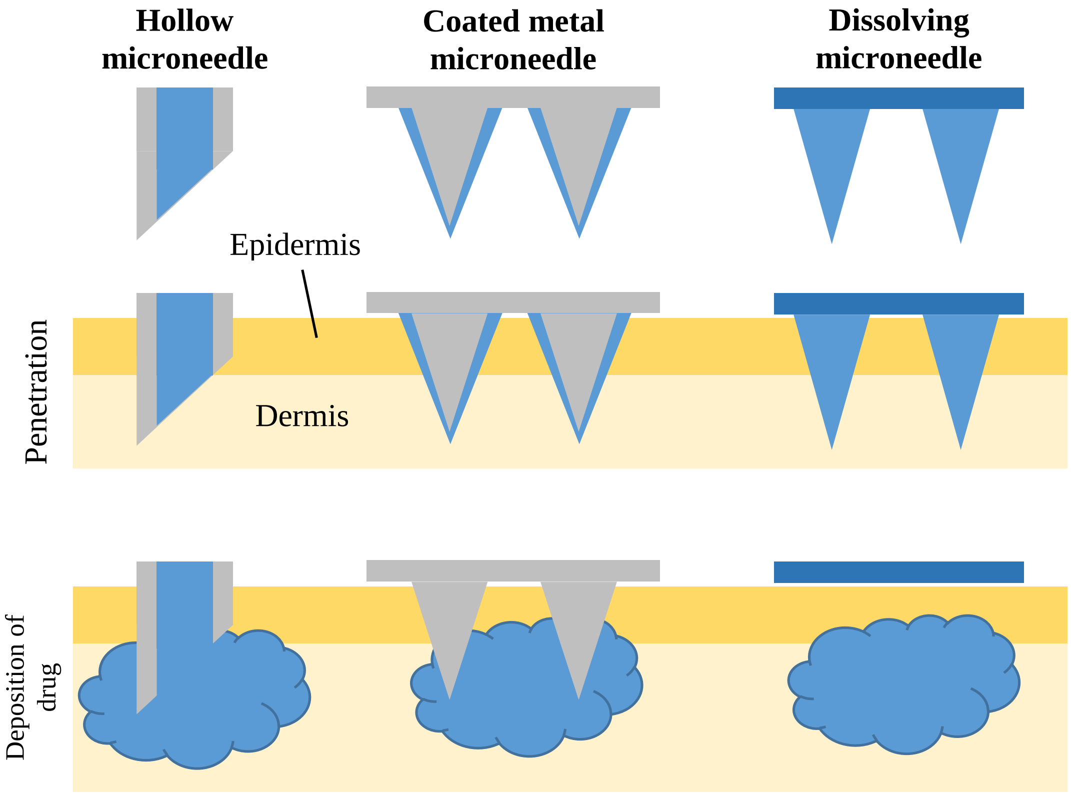

Figure 1.6 – Three types of microneedles that can be used to penetrate the body's superficial barrier (e.g., epidermis) and deliver drugs: (Left) hollow microneedles, similar in function to hypodermic needle, allows infusion of liquid formulations. (Middle) metal studs with dried drug deposited on surface. Upon penetration, the dried drug dissolves. (Right) dissolving polymeric studs with drug interspersed in polymer. Upon penetration, the polymer and drug dissolve. No sharps waste after delivery.

1.6 Suprachoroidal Delivery using Microneedles

Microneedles have been used to deliver drugs to different regions of the eye. Jiang et al. used coated metal microneedles (500-700 µm in length) to deliver small-molecules, proteins, and DNA into the corneal stroma and sclera[109]. Sixty-nine percent bioavailability was possible with this technique compared with ~5% bioavailability with topical eye drops. Kim et al. was able to deliver bevacizumab using coated microneedles to the cornea for the prevention of corneal neovascularization[114].

Figure 1.7 – Hollow Metal Microneedle

Representative image of ½" hypodermic needle (top), 33 G (left), 30 G (middle), and 27 G (right) microneedles.

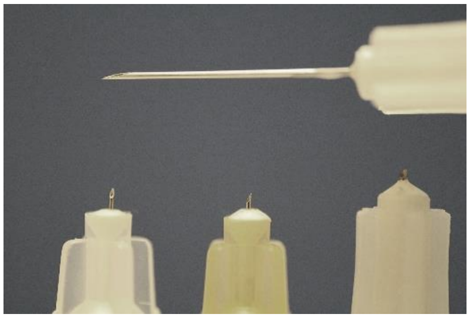

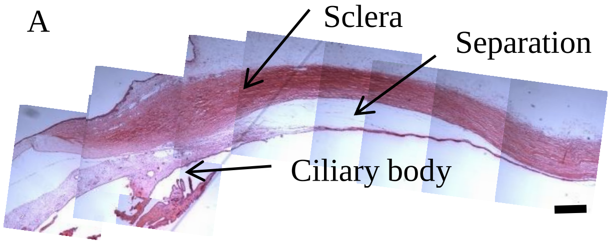

Figure 1.8 – SCS separation caused by microneedle injection. Composite images after saline was injected into the suprachoroidal space of an in vivo rabbit eye. Scale bar = 500 µm. From Chiang et al.[115]

Jiang et al. also used a hollow microneedle to deliver drugs into the scleral stroma[110]. Small molecules and particles up to 1.0 µm in diameter were infused into the scleral stroma. However, it was only possible to infuse up to 35 µL, despite changing injection parameters. Patel et al. found that slightly longer microneedles that fully penetrated through the full thickness of the sclera could deposit drug into the suprachoroidal space[8, 81]. Fluid injected into this space would spread circumferentially within the suprachoroidal space, bathing the choroid with drug. Though drugs had been delivered into this space before using cannulation and/or sclerotomy, [2, 5, 36, 116-118] use of a microneedle simplified the procedure. The microneedle could be used to administer drug in a fashion similar to an intravitreal injection procedure, which is a regularly performed outpatient procedure[8, 69]. Success with injecting a particle suspension was dependent on needle length, needle gauge, infusion pressure, and particle size, and did not depend on intraocular pressure[81].

Preclinical animal studies have shown that suprachoroidal space drug delivery has a similar or better safety profile compared with intravitreal injections[2, 17, 118-120]. Interim results from Phase I/II clinical trials (e.g., NCT01789320) have also been promising[7]. Intraocular pressure immediately after injection increased with increasing injection volume, however, IOP returned to baseline within 1 h post-injection[17, 120]. These IOP changes are similar to those observed with intravitreal injections[98, 101, 102, 121, 122], and are not expected to cause long term ocular damage. Some studies have examined the eye histologically. Einmahl et al. noted that suprachoroidal delivery of hyaluronic acid resulted in retinal atrophy[118], however, no abnormalities were noted by Olsen et al. following suprachoroidal delivery of bevacizumab and hyaluronic acid[9]. Gu et al. observed the eye *in vivo* using indirect ophthalmoscopy and found evidence of choroidal dilation and hyperemia that resolved by 24 h[120]. They were unable to identify parameters that affected this finding in a systematic way. The same group found no changes in electroretinograms before and after injection, indicating suprachoroidal injection did not adversely affect retinal health[119, 120].

Immediately after injection into the suprachoroidal space, higher levels of small molecules and macromolecules where found in the choroidal, RPE, and retinal tissues, compared with intravitreal injections[2, 5, 8, 9, 36, 81, 119, 120, 123-125]. Furthermore, anterior segment tissues, including lens, aqueous humor, and cornea, were largely spared from drug. However, drug was cleared significantly faster with suprachoroidal delivery than intravitreal or subconjunctival injections[5, 9, 126]. The vitreous humor can serve as a depot that slowly releases drug to the retina and choroid[9, 69, 93, 102]. Gu et al. found that the suprachoroidal space collapsed to baseline levels within 1 h[120]. Faster clearance was observed with suprachoroidal delivery of bevacizumab, 4 kDa and 40 kDa FITC dextran than with intravitreal injections[8, 9]. Thus, molecular weight (and molecular size) did not affect this trend, although macromolecules were cleared more slowly from the suprachoroidal space than small molecules. Controlled release systems consisting of triamcinolone in suspension were able to release triamcinolone within the suprachoroidal space for 1 mo or more[2, 7, 119, 127]. Drug properties had an effect on clearance of drug, possibly due to drug binding[123].

Clearance from the suprachoroidal space was reasoned to be by choroidal blood flow. Olsen et al. performed immunohistochemistry to visualize bevacizumab clearance and concluded it occurred through the choroid[9]. Abarca et al. used recently euthanized pigs eyes to study the role of choroidal perfusion in clearance[126]. The study concluded that choroidal perfusion resulted in faster clearance than no perfusion.

Though fluid injected into the suprachoroidal space distributes circumferentially around the eye in the suprachoroidal space, it does not cover the entire space[8, 120, 128]. Similarly, since most ocular diseases do not affect the eye uniformly (e.g., macular degeneration affects the macula while sparing the peripheral retina[64, 66, 67], retinitis pigmentosa affects the peripheral retina while sparing the macula[74]). Therefore, targeting to specific regions of the suprachoroidal space is of interest. Multiple studies have shown that increasing injection volume resulted in increasing coverage area. Gu et al. found that increasing injection volumes resulted in increasing suprachoroidal space cross-sectional area under optical coherence tomography[120]. Seiler et al. looked at the maximal suprachoroidal thickness with different injections volumes[116]. While the thickness resulting from the smallest injection volume tested was different than those from larger injection volumes[116], there did not appear to be a linear trend, especially with intraocular pressure at physiological levels. Kim et al. demonstrated that the density of the microparticles injected could be used to affect the distribution of particle[17]. Denser particles would sink via decreased buoyancy towards the back of the eye if the eye was oriented upright with respect to gravity. Seiler et al. studied the distribution of ultrasound contrast agent injected into the suprachoroidal space[116], but the distribution of these less dense microparticles would not be expected to mimic neutral density microparticles. Kim et al. also studied the distribution of particles injected with liquid formulations of varying viscosities[128]. They found that formulations containing carboxymethyl cellulose were able to localize particles near the site of injection, and that liquid formulations containing hyaluronic acid spread to cover up to 100% of the suprachoroidal space.

1.7 Aims

This work seeks to further elucidate the pharmacokinetics (specifically, distribution and clearance) of particles suspended in liquid formulations injected into the suprachoroidal space using a microneedle. Successful completion of these aims will enable the rational design of injection techniques, formulations, and controlled release systems.

Our central hypothesis is as follows. The formulation exerts a force that is able to separate the weak adhesions between the sclera and the choroid. The thickness and circumferential area covered can be modulated by formulation viscosity, as well as the injection volume. Particles suspended in the liquid formulation become trapped in the suprachoroidal space relative to small molecules, though the formulation viscosity can be used to counteract this entrapment. Anatomical barriers physically limit the suprachoroidal space, and can prevent particle deposition in regions of the eye. Due to the initial high pressure state post-injection, fluid movement is due to convective flow either through leakage sites (e.g., out the injection site or out perivascular drainage routes). Once the pressure returns to baseline, fluid and molecules drain via intravascular clearance by the choroid. As fluid clears from the suprachoroidal space, the sclera and choroid are re-apposed and particles become entrapped in that position until degraded. We will test this central hypothesis in three aims, outlined below.

1.7.1 Aim 1: Identify anatomical barriers that limit spread in the SCS

Previous studies have demonstrated that the suprachoroidal space is bounded by the scleral spur and the optic nerve. These boundaries confine fluid and particles injected into the suprachoroidal space. We hypothesize there are additional anatomical barriers that limit the circumferential spread of particles in the suprachoroidal space. Possible candidates include the vortex veins and the posterior ciliary arteries. Identification of anatomical barriers will motivate the development of strategies that enable the entire suprachoroidal space to be covered.

1.7.2 Aim 2: Study the distribution of particles and molecules in the SCS

Though some studies have described the distribution of particles and molecules injected into the suprachoroidal space, they have not attempted to go beyond observation or study both in concert. The purpose of this study was to investigate the distribution of molecules and particles co-injected into the suprachoroidal space. We further hypothesize that particles become entrapped relative to fluids and small molecules that were co-injected. We will determine the circumferential distribution of fluorescent species via 3D cryo-reconstruction, flat mounts of enucleated eyes, and *in vivo* fundus photography. Finally, we hypothesize that the viscosity of the liquid formulation prevents particle entrapment, and prolongs transport time.

1.7.3 Aim 3: Investigate kinetics of the SCS thickness

Few studies have looked at the distention of the choroid off the sclera (aka, SCS thickness). We set out to determine the effect of injection volume and formulation of a microneedle injection into the suprachoroidal space on SCS thickness and closure kinetics. We hypothesize that injections of varying volumes of a low viscosity fluid has a minor effect on SCS thickness, whereas formulation injected has a major effect on the SCS thickness. We will determine the distribution of suprachoroidal space thickness using high-frequency ultrasound B-scan and a 3D cryo-reconstruction method.

1.7.4 Aim 4: Determine the relative contribution of clearance routes and study the clearance kinetics of molecules from the SCS

Previous studies have investigated clearance of select molecules from the suprachoroidal space. The purpose of this aim is to correlate collapse and clearance with distinct events so that we can better understand these kinetics. We hypothesize that there are two phases of clearance, the first is driven by high pressure, and the second phase is driven by concentration gradient. We will determine the collapse rate of the suprachoroidal space after injection with different liquid formulations using a high-frequency ultrasound B-scan probe in an *in vivo* rabbit model. We will also investigate suprachoroidal space clearance of a wider range of molecular weights. Finally, we will also determine the route of clearance from the suprachoroidal space. These results will guide the rational design of formulations.

1.7.5 Aim 5: Develop controlled-release brimonidine microspheres in the SCS for the treatment of glaucoma

Because glaucoma patients have a low compliance (~50%) in administering eye drops, there is a clinical need for a sustained-release drug delivery system for glaucoma. We hypothesize that a sustained-release polymeric microsphere drug delivery system injected into the anterior suprachoroidal (aka, supraciliary) space will produce a therapeutic effect for 1+ mo. Previous studies have shown that brimonidine lowers intraocular pressure in the albino New Zealand White rabbit. This will be the first demonstration that a controlled release system injected into the suprachoroidal space can be efficacious in treating glaucoma.

2 CIRCUMFERENTIAL FLOW OF PARTICLES IN THE SUPRACHOROIDAL SPACE IS IMPEDED BY THE POSTERIOR CILIARY ARTERIES

This work has been published in Experimental Eye Research[129].

2.1 Summary

Microneedle injection into the suprachoroidal space (SCS) enables targeted drug delivery for treatment of posterior segment diseases (e.g., posterior uveitis). This study sought to identify and characterize anatomical barriers to circumferential spread of particles in the SCS of rabbit and human cadaver eyes. These barriers could make targeting specific regions within the SCS challenging. A hollow microneedle (33-gauge, 750 µm long) was used to inject fluorescent particles into albino New Zealand White rabbit eyes *ex vivo* at six different positions around the limbus and a limited number of conditions *in vivo*. SCS injections were also performed in human cadaver eyes 8 mm and 2 mm from the optic nerve (ON). Eyes were dissected and particle distribution was quantified. In rabbit eyes, injections made in the superior or inferior hemispheres (even when injected temporally immediately adjacent to the long posterior ciliary artery (LPCA)) did not significantly cross into the other hemisphere, apparently due to a barrier formed by the LPCA. The vortex veins had a minor effect on particle deposition, limited to only around the vortex vein root. In human eyes, the short posterior ciliary arteries (SPCAs) prevented circumferential spread towards the macula and ON. In conclusion, the rabbit LPCA and the human SPCA were anatomical barriers to particle spread within the SCS. Therefore, design of drug delivery protocols targeting the SCS need to account

for barriers formed by anatomical structures in order for injected drug to reach target tissues.

2.2 Introduction

Suprachoroidal delivery is being explored as a targeted ophthalmic drug delivery technique to treat posterior segment diseases that affect choroidal, retinal pigment epithelial, and/or retinal tissues [2, 5, 8, 81, 118, 119, 123, 125, 127, 130]. The suprachoroidal space (SCS), which is a potential space between the sclera and choroid, is an attractive drug delivery site because it is directly adjacent to the diseased tissue in many posterior segment diseases, including age-related macular degeneration (AMD) and posterior uveitis [64, 97, 127]. SCS delivery results in increased drug concentrations and bioavailability at the choroid while limiting drug concentrations elsewhere in the ocular globe compared with intravitreal injections [5, 8, 9, 81, 123].

The SCS can be accessed with a hollow microneedle that has a length similar to the thickness of sclera [8, 81]. The microneedle is designed to penetrate the sclera and conjunctiva (but not the chorioretina) and inject material that can flow circumferentially within the SCS, thus bathing the choroid in drug. The safety and tolerability of microneedle injections into the SCS has been studied in an open-label Phase I/II clinical trial (NCT01789320) where triamcinolone acetonide suspension was injected into the SCS to treat noninfectious posterior uveitis [7]. In this clinical trial and supporting pre-clinical studies, the microneedle injection procedure was performed in a manner similar to an intravitreal injection, except it used a much shorter needle and therefore injected into the SCS rather than the vitreous; the procedure was well tolerated in animal and human subjects [7, 8, 81].

Since the chorioretina is typically not uniformly diseased (e.g., AMD affects the macula while sparing the peripheral retina), targeting drugs to specific regions of the chorioretina (i.e., to optimally treat the diseased region of the chorioretina) is of importance. Thus, understanding and controlling the movement of drugs within the SCS is needed to deliver drugs to the diseased tissue using the SCS as a conduit. The purpose of this work is, therefore, to study the movement of particles injected into the SCS and, more specifically, to identify barriers that impede circumferential flow in the SCS, which might influence the ability to target specific regions of the SCS.

Previous experiments show that fluid injected into SCS is limited by the scleral spur anteriorly and the optic nerve (ON) posteriorly [8, 17, 81]. Anatomically, the sclera and the choroid are tightly bound at these two sites, as they delineate the physical extent of the SCS. We hypothesize that there are additional barriers that prevent circumferential flow in the SCS following microneedle injection. Other likely candidates include the posterior ciliary arteries and the vortex veins since the sclera and choroid are bound at these points [118]. Although a previous study reported no anatomical barriers to spread of micro-bubbles within the SCS [116], in that study injections were carried out at the superior (12 o'clock) position near the limbus, which may not optimally assess the existence of barriers throughout the eye, as shown in the present study.

2.3 Methods

2.3.1 Microneedle injection and tissue processing

Enucleated albino New Zealand White rabbit eyes (shipped overnight from Pel-Freeze, Rogers, AR) were stored at -80°C upon arrival until use in *ex vivo* rabbit experiments. Frozen eyes were used to facilitate the testing of many parameters, a subset of which were tested in an *in vivo* rabbit model. In all *ex vivo* eyes, no particles were detected in the vitreous, which suggests that the choroid had not degraded. When needed, frozen eyes were rapidly defrosted in a room-temperature water bath for ~30 min, and muscle, conjunctiva, and fascia were dissected from the ocular globe. The superior prime meridian of the eye (i.e., 12 o'clock) and the injection site were marked with a shallow cut in the adjacent cornea using a scalpel dipped in blue or red food coloring (McCormick, Hunt Valley, MD), respectively.

All injections were performed at room temperature (~23°C). SCS injections were accomplished using a 33-gauge hollow microneedle with a length of ~750 µm (kindly provided by Clearside Biomedical, Alpharetta, GA) and a 250 µL glass chromatography syringe (National Scientific, Rockwood, TN). Injections were performed 3 mm posterior to the limbus, and occurred in 3 s. The fluid injected was 50 µL of 0.5% (w/v) 200 nm diameter red-fluorescent microspheres (580 nm excitation and 605 nm emission wavelength; FluoSpheres, Life Technologies, Carlsbad, CA) in Hank's Balanced Salt Solution (HBSS, Mediatech, Manassas, VA), unless otherwise specified. After waiting 1 min, the needle was withdrawn from sclera.

To arrest fluid flow in SCS, each eye was rapidly frozen 1 min after injection by submersion in 100% ethanol chilled over dry ice. Eight approximately equally-spaced, full-thickness cuts were made in the sclera from the posterior pole to limbus using a scalpel. This yielded eight scleral flaps (a.k.a., "petals") approximately equal in area. One cut was aligned with the injection site and one with the 12 o'clock position. The scleral flaps were splayed open to expose the frozen vitreous humor, lens and aqueous humor, which were removed with forceps and collected to verify no particles were in the vitreous. Three replicates were performed in each condition unless otherwise stated. The following experiments were performed.

2.3.1.1 Effect of injection site on spread in the SCS of rabbits

We performed injections at six positions around the limbus of *ex vivo* rabbit eyes (Figure 2.1A): at the superior (12 o'clock) and inferior (6 o'clock) prime meridians; infratemporal (7.5 o'clock) and supratemporal (10.5 o'clock) locations; and temporally directly superior and inferior to the 90° meridian (9 o'clock). Injections were performed in the temporal hemisphere because, in humans, the macula is temporal to the ON, which we knew limited flow from previous studies [8, 17, 81].

2.3.1.2 Effect of IOP on spread in the SCS of rabbits

To change intraocular pressure (IOP), the eye was cannulated through the ON using a 25-gauge needle connected to a water column of predetermined height [17]. We tested three pressures: unpressurized, 10-12 mmHg (normotensive IOP in rabbits), and 22-25 mmHg (hypertensive IOP in rabbits). After confirming IOP using a rebound tonometer (iCare Tonovet, Helsinki, Finland), we performed an injection at either the temporal position (3 o'clock; directly above the temporal LPCA) or the superior position (12 o'clock) of that eye.

2.3.1.3 Effect of injection volume on spread in the SCS of rabbits

To determine if injection volume would change the flow patterns following a microneedle injection, injections of 50, 100, and 200 µL were performed. Before each experiment, the eye was pressurized to 10-12 mmHg. Injections were performed either at the superior position (12 o’clock) or the temporal position (9 o’clock) directly superior to the LPCA.

2.3.1.4 Effect of particle size on spread in the SCS of rabbits

To study the effect of particle size on spread, we injected one of three mixtures: 0.5% (w/v) 200 nm red fluorescent particles, 0.5% (w/v) 20 nm red fluorescent particles, or 0.025% sulforhodamine B dye (559 Da; 565 nm excitation and 585 nm emission wavelength). The excitation/emission spectra of these three mixtures were comparable. The eyes were pressurized to 10-12 mmHg. Fifty microliters of one of the three formulations were injected at the superior position (12 o’clock) or the temporal position (9 o’clock), directly superior to the LPCA.

2.3.1.5 Effect of bevel orientation on spread in the SCS of rabbits

To study the effect of bevel orientation on spread, injections were performed at the superior position (12 o’clock) with the bevel either directed temporally or nasally. Before each experiment, the eye was pressurized to 10-12 mmHg.

2.3.2 *In vivo* injection into the SCS of rabbits

All *in vivo* experiments were carried out in albino New Zealand White rabbits (Charles River, Wilmington, MA) and were approved by the Georgia Institute of Technology Institutional Animal Care and Use Committee. Practices complied with the ARVO Statement for the Use of Animals in Ophthalmic and Vision Research. Both eyes were used in this study, since the growing body of evidence on SCS injections (pre-clinical animal and human clinical data) indicates that SCS injections are well-tolerated and there have been no reports on vision loss associated with SCS injection.

Animals (N=3 per group) were anesthetized with a subcutaneous injection of ketamine and xylazine. A 50 µL injection of 200 nm fluorescent particles in HBSS was made either in the supratemporal position (10.5 o’clock) or in the temporal position (9 o’clock), directly superior to the LPCA. A superior injection was infeasible as that would have required puncturing through the superior rectus muscle. In some cases, green fluorescent fundus images of the eye after suprachoroidal injection were obtained with a RetCam II with fluorescein angiography attachment (Clarity Medical Systems, Pleasanton, CA). In this case, a 50 µL injection of 200 nm green fluorescent particles was made in the supranasal quadrant. Animals were euthanized with an injection of pentobarbital through the ear vein after two days. The eyes were enucleated and processed as described above.

2.3.3 Dissection of ocular globe of rabbits and humans

To better visualize attachments between choroid and sclera, we dissected *ex vivo* rabbit eyes and human cadaveric posterior poles (Georgia Eye Bank, Atlanta, GA) under a stereoscope (Olympus SZX16, Tokyo, Japan) with a camera (Olympus DP71). The human donors had no history of ocular disease.

2.3.4 Effect of injection site on spread in the SCS of cadaver eyes

Based on findings from the dissections, we hypothesized that the short posterior ciliary arteries (SPCA) would impede particle spread. We tested this hypothesis by injecting particles within and without the SPCA ring. Although this was a different injection site than those used with previous injections (in this and previous studies) and also not clinically relevant, injections made at these positions would adequately test the barrier function of the SPCAs.

Human cadaveric ocular globes (Georgia Eye Bank, Atlanta, GA) with no history of posterior segment disease were obtained 1-3 days after death. We performed injections at two positions: (a) 2 mm from the ON and (b) 8 mm from the ON (N = 4 per group), which were on either side of the SPCAs [131]. To process the eye, the cornea was removed and the eyes were cut with a scalpel through all the ocular tissue, starting anteriorly and leaving the ON and surrounding tissue untouched. Since the eyes were pigmented, the retina and choroid were removed prior to imaging. Other procedures are described above.

2.3.5 Image acquisition and analysis, and statistics

We took two photographs of each mounted eye using a Canon 60d dSLR digital camera (Canon, Melville, NY). Camera settings were held constant at an aperture of 1/2.8 and shutter speed of 1/15 s. All images were captured in the same windowless room with the same light sources. The first image was taken with room light and no filter; the second image was taken with green light (Bluewind Multicolor RGB, HitLights, Baton Rouge, LA) and an optical bandpass filter (610 ± 10 nm; Edmunds Optics, Barrington, NJ) mounted on the camera. This lighting and filter were chosen to match the fluorescence properties of the fluorescent particles used.

After the images were acquired, the red channel of the fluorescent images was thresholded to capture the coverage of the fluorescent particles (ImageJ, National Institutes of Health, Bethesda, MD). The measurement tool in ImageJ was then used to find, for each petal: (a) the area of each petal, (b) the average intensity and (c) standard deviation, and (d) the percentage of the area of each petal that was above the threshold. Alternatively, we used the measurement tool in ImageJ to find the percentage of thresholded area that was superior and inferior to the LPCAs.

Further analysis was performed using Matlab (Mathworks, Natick, MA) and Prism (Graphpad, La Jolla, CA). Values are presented as the mean ± standard error of the mean (SEM), unless otherwise specified. Unpaired Student's t-test and two-way ANOVA analysis were performed to determine statistical significance ($\alpha = 0.05$).

2.4 Results

2.4.1 Effect of injection site on spread in SCS of rabbits

After injecting particles at different positions around the limbus, we identified the LPCA as a barrier to circumferential spread of particles in the SCS of rabbit eyes *ex vivo* (Figure 2.1). Injections at the superior (Figure 2.1B), supratemporal (Figure 2.1C), infratemporal (Figure 2.1F), and inferior (Figure 2.1G) positions resulted in similar particle distributions, where the spatial distributions of particles were roughly normal (i.e., not skewed) (see Figure 2.1, right column for quantification of particle per petal). Furthermore, the spatial distribution of particles was centered near the injection site. Vortex veins, typically located in the supratemporal and infratemporal quadrants, did not produce a noticeable effect on circumferential particle spread when visualized via flat mounts.

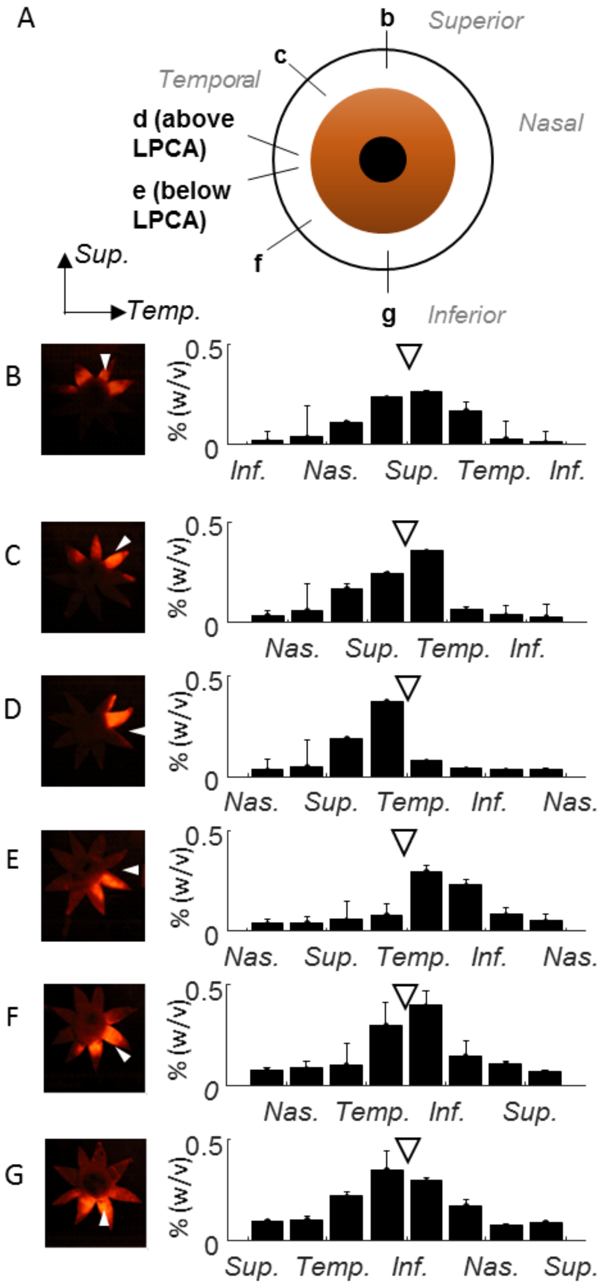

Figure 2.1 – SCS injections at different injection sites, shown in the right eyes ex vivo. [A] Representative images showing spread of fluorescent particles in eyes at the tested injection sites. Eyes are all positioned in the same anatomical orientation – superior is on top and temporal is right. Injections were performed at the superior (12 o'clock, b); supratemporal (10.5 o'clock, b); temporal, directly superior (d) and inferior (e) to the long posterior ciliary artery (9 o'clock); infratemporal (7.5 o'clock, f); and inferior (6 o'clock, g) positions. [B-G] Quantification of the average concentration of particles in each scleral flap for the tested injection sites. Distribution of particles is shown after 50 µl of HBSS containing 200-nm particles was injected into SCS at different sites. Injection site indicated by white arrow in representative images, and hollow arrow in graphs. Sup. = superior (12 o'clock); Temp. = temporal (9 o'clock); Inf. = inferior (6 o'clock); Nas. = nasal (3 o'clock). Since the eye is spherical, leftmost and rightmost bars are adjacent.

In contrast, injections at the temporal (9 o’clock) position (Figure 2.1D and E) had markedly different patterns of spread compared with the others ($p < 0.0001$, 2-way ANOVA). In particular, >95% of particles injected on one side of the 90° meridian did not cross to the other side (i.e., injection superior to the LCPA resulted in few particles in the inferior hemisphere, and *vice versa*). This resulted in a skewed distribution with the tail directed away from the 90° meridian (Figure 2.1 D and E, right column), which indicates an anatomical barrier that impedes flow near the 90° meridian.

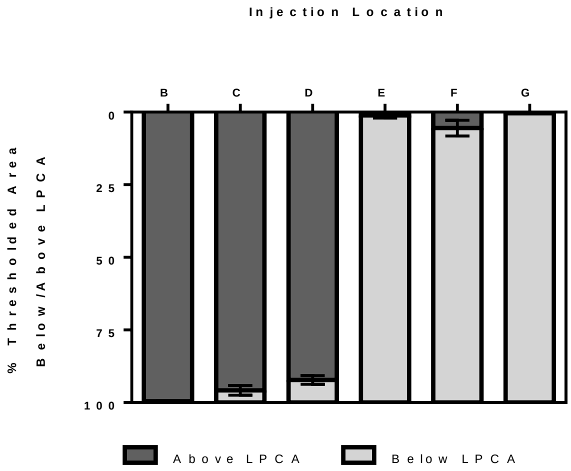

Figure 2.2 – Percentage of particles above versus below LPCA. Data from images like those in Figure 2.1 were re-analyzed to find the percentage of SCS area with fluorescent signal above threshold, indicating presence of injected particles. Injections were carried out in right eyes ex vivo using 50 µl of HBSS containing 200-nm particles. Data show mean±SEM from n=3 replicates.

We reanalyzed the eyes presented in Figure 1 to further examine barrier function at the site of LPCA. We calculated percentage of area with fluorescent signal exceeding background threshold levels above and below LPCA for each injection site (Figure 2.2) and found they were significantly different ($p = 0.0009$, 2-way ANOVA), despite their close proximity. For each of the three injection sites above LPCA (i.e., Figure 2.2 B, C and D), 96±3% (mean±SD) of thresholded area was in the superior hemisphere of the eye. Likewise, in each of the three injections below LPCA (i.e., Figure 2.2 E, F and G), 98+3% (mean±SD) of thresholded area was found in the inferior hemisphere. From these data, we conclude that barriers at the site of LPCA impeded circumferential flow into the opposite hemisphere.

2.4.2 Effect of IOP, injection volume, and particle size on spread in SCS

The effects of IOP, injection volume and particle size on spread in the SCS were evaluated. We found no statistical difference in particle spread at the three different IOPs tested (unpressurized, normotensive IOP, and hypertensive IOP) (Figure 2.3A, p=0.85, 2-way ANOVA).

Varying injection volume did not result in a statistically significant difference in particle spread (Figure 2.3B, p = 0.59, 2-way ANOVA). It is important to note that the eye was able to accommodate the entire 200 µL volume when injected at the 12 o'clock position but not when the injection occurred temporally above the LPCA (i.e., there was leakage out the injection site, supporting the hypothesis that the LPCA formed a barrier to flow). Furthermore, particles injected at 12 o'clock had entirely covered the superior hemisphere and could be found partially in the inferior hemisphere. On the other hand, the 200 µL injection above the LPCA had a smaller coverage area compared to the injection at 12 o'clock. The presence of LPCA might have decreased the expandability of SCS enough so that 200 µL could not be injected temporally.

No differences in particle spread were detected when particle size was varied (Figure 2.3C, p=0.28, 2-way ANOVA) with >90% of delivered compounds retained in the superior hemisphere. We conclude that particle size did not significantly affect particle spread circumferentially past LPCA. Moreover, since very little sulforhodamine B was found in the inferior hemisphere, LPCA appears to physically prevent fluid flow into the opposite hemisphere and did not just sieve particles. Indeed Gu et al. noted that saline injected into the suprachoroidal space of guinea pigs did not cross the "horizontal midline" and was not found in the inferior hemisphere [120].

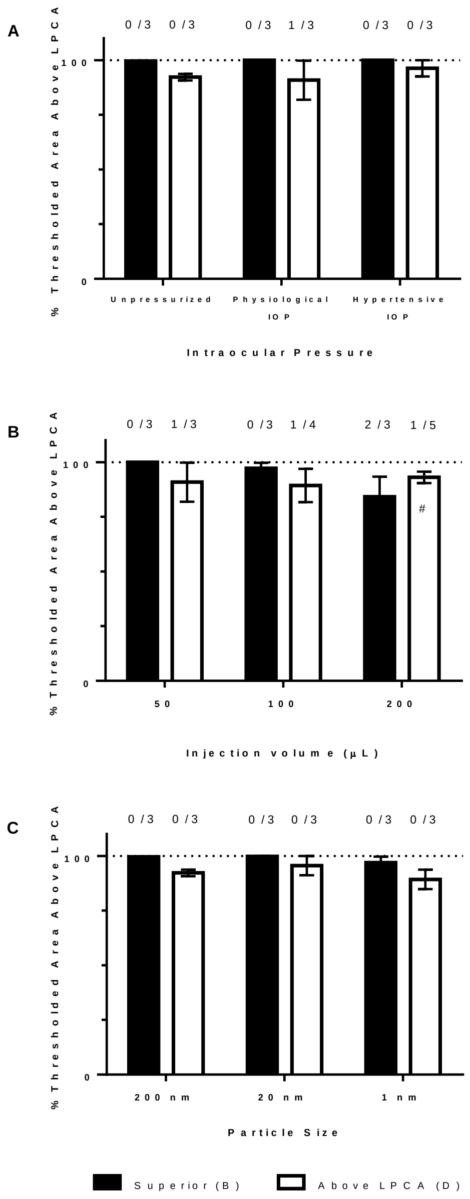

Figure 2.3 – Effect of IOP (A), injection volume (B), and particle size (C) on LPCA barrier function. The fraction of eyes in which particles were detected inferior to LPCA is shown above each tested condition. Data show mean±SEM from n=3-5 replicates. (A) Injections were carried out in left eyes ex vivo using 50 µl of HBSS containing 200-nm particles. The percentage of SCS area with fluorescent signal above threshold is shown in unpressurized eyes, eyes at physiological IOP (10 - 12 mmHg), and eyes with hypertensive IOP (22 – 25 mmHg). (B) Injections were carried out in right eyes ex vivo using 50, 100 or 200 µl of HBSS containing 200-nm particles. Pound sign (#) indicates that significant leakage out the injection site occurred. (C) Injections were carried out in right eyes ex vivo using 50 µl of HBSS containing 200 nm fluorescent particles, 20 nm fluorescent particles, or a small molecule fluorescent dye (559 Da ≈ 1 nm).

2.4.3 Effect of bevel orientation on spread in SCS

When the bevel was directed either temporally or nasally during injection, particle spread was indistinguishable (data not shown). This result was expected, since the needle length, including bevel, was designed to penetrate only conjunctiva and sclera.

2.4.4 *In vivo* injection into SCS

Guided by findings in the *ex vivo* eye, we performed injections in the rabbit eye *in vivo* at the supratemporal position or temporal position above LPCA, and found no statistical difference between these injection sites (p = 0.71, 2-way ANOVA). The supratemporal position was chosen instead of the superior position (as in the *ex vivo* eyes) because a superior injection would require puncturing the superior rectus muscle. In eyes injected supratemporally, 87±13% (mean±SD) of thresholded area was above LPCA and in eyes injected temporally, 92±12% (mean±SD) of thresholded area was above LPCA (Figure 2.4A-F). One of the eyes injected temporally had particles present in the inferior hemisphere (Figure 2.4F).

We next visualized the rabbit fundus (Figure 2.4G) and imaged spread of green-fluorescent particles (Figure 2.4H) after supranasal injection in the rabbit eye *in vivo* using an ophthalmic digital imaging system. Since these rabbits were albino, the choroid was readily visible, with the inner retinal vessels shadowing the choroid. The LPCA could be seen (Figure 2.4G, blue arrowheads) after penetrating through sclera anteriorly (rightmost arrowhead) and as it traversed deep to sclera, sending small branches through sclera. When visualized with fluorescein angiography, the injected green fluorescent particles were clearly seen in SCS. Fluorescence was shadowed by the inner retinal and choroidal vessels, confirming particles' localization in SCS between choroid and sclera.

The microneedle injection (Figure 2.4H, white arrowhead) occurred in the supranasal quadrant and spread until flow was impeded by LPCA and its branches (blue arrowheads) anteriorly, as indicated by bright fluorescence superior to LPCA and dimmer fluorescence elsewhere. When we imaged the superior region of the eye, the area immediately adjacent (within 0.5 mm) to the vortex vein was devoid of fluorescent particles (Figure 2.4I). We hypothesize that vessels feeding into the vortex vein were sufficiently dense to prevent particle deposition or, alternatively, particles deposited were efficiently cleared. Thus, the vortex veins had a minor effect on particle deposition that was visible on fundus exam but not flat mounts.

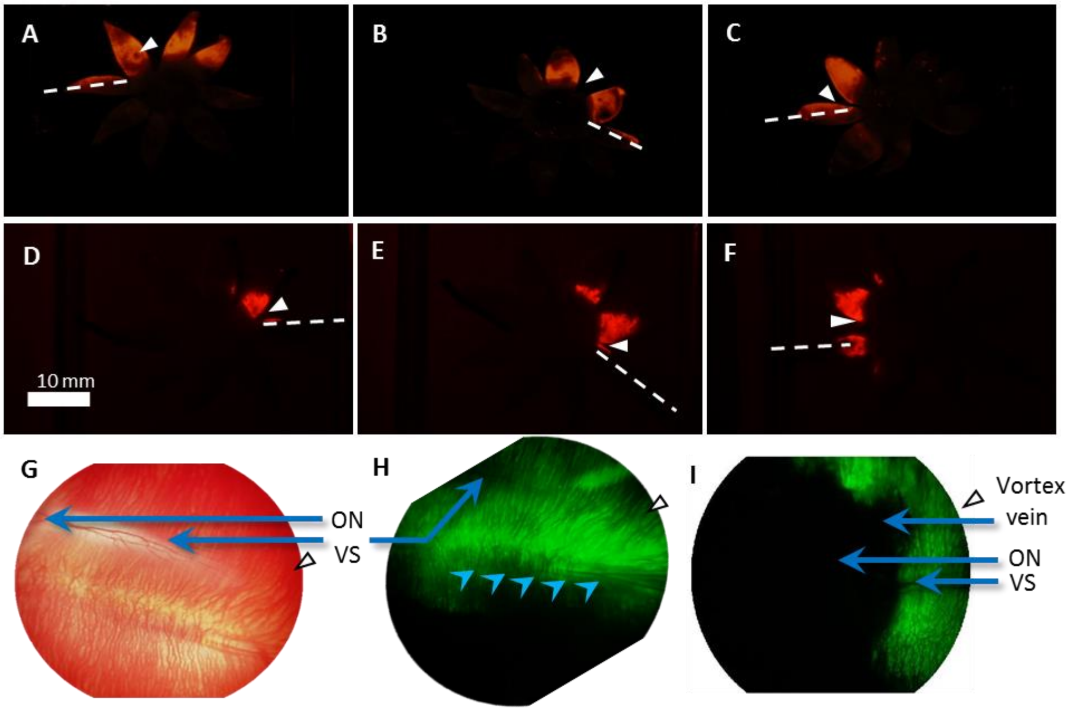

Figure 2.4 – Distribution of particles in SCS after injection into rabbit eyes in vivo. (A-F) The path of LPCA (dotted line) and injection site (white arrow) are shown, based on examination of tissue using brightfield optics (not shown). Supratemporal (A, B, C) and temporal, above the LPCA, (D, E, F) injections are shown. One eye (F) had some particles present in the inferior hemisphere presumably by flowing anteriorly bypassing the LPCA. Temporal injections were carried out in left (D, E) and right (F) eyes in vivo using 50 µl of HBSS containing 200-nm particles. RetCam image after supranasal injection illuminated with white light (G) and fluorescein angiography attachment (H and I). Particles were not found near the root of the vortex vein (I). White arrow = injection site; ON = optic nerve; VS = visual streak; blue arrowheads = LPCA with its branches.

2.4.5 Dissections of *ex vivo* rabbit eyes and human eyes

Previous studies have reported that branches of the LPCA pass through sclera via multiple tightly packed perforations [132, 133]. To confirm this anatomy in this study, we dissected *ex vivo* rabbit eyes to better visualize the path of LPCA as it penetrated through sclera. During dissection, choroid easily separated off sclera for most of the globe, consistent with a potential space between these tissues, but was strongly attached to sclera where LPCA penetrated through sclera near and anterior to the equator (Figure 2.5). The vortex vein did not tightly adhere sclera and choroid together, possibly due to tissue processing. We hypothesize that multiple sites of adhesion associated with penetration of branches of LPCA across SCS in the rabbit eye are responsible for LPCA's barrier to circumferential flow.

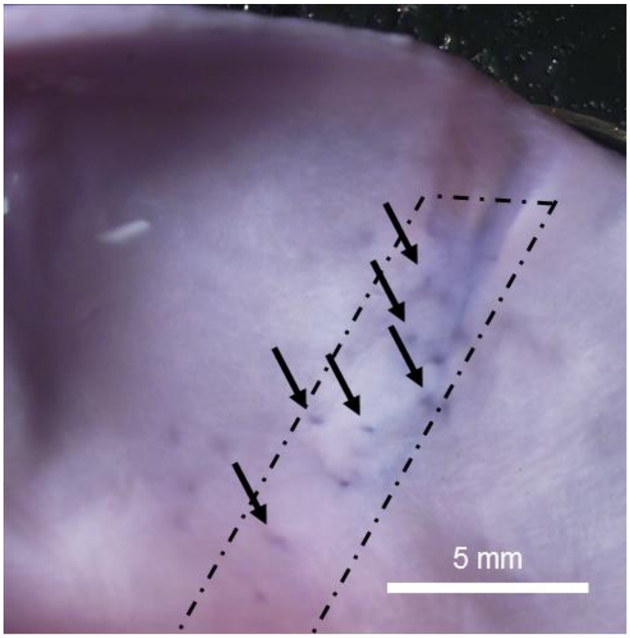

Figure 2.5 – Image of rabbit sclera showing LPCA perforations through sclera. The temporal LPCA is a branch of the ophthalmic artery that penetrates through sclera near the equator to supply choroid, ciliary body, and iris (Gray, 1918). In the rabbit, the LPCA branches before penetrating through sclera; these LPCA branches appeared to strongly adhere choroid to sclera during dissection. Dashed lines indicate the path of LPCA. Arrows indicate sites where LPCA branches perforated sclera. The representative image was taken with a brightfield stereoscope in an ex vivo rabbit eye after dissection. No SCS injection was performed.

The literature indicates that in human eyes, the LPCA anatomy is different from rabbit eyes [132]. Dissection in human cadaver eyes demonstrated that the LPCA penetrated through sclera more posteriorly (relative to the equator) than in the rabbit eye, and then travelled within SCS for at least 5 mm before anastomosing with the circulus arteriosus (Figure 2.6A). Notably, the two LPCAs penetrated into SCS at just one location and did not have multiple branches penetrating into SCS, as seen in the rabbit eye. It is possible that the presence of a section of LPCA running within SCS may be able to facilitate, rather than impede, distention of SCS during microneedle injection in humans, especially anterior to the equator.

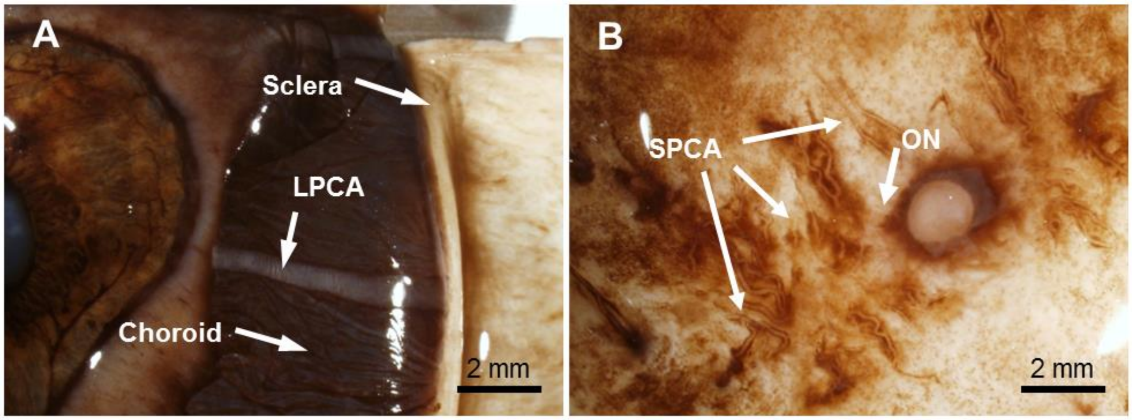

Figure 2.6 – Images of the posterior pole of a representative human cadaver eye showing LPCA and SPCAs. (A) Choroid was lifted off sclera and folded over to show the LPCA, which penetrated more posteriorly than in the rabbit and traveled within SCS for at least 5 mm before anastomosing with the ciliary body. (B) Retina/choroid was removed to show SPCAs, which are vessels originating from the ophthalmic artery that penetrate sclera to form a ring around the optic nerve and macula (Gray, 1918). Images were taken with a brightfield stereoscope in a representative human cadaver eye after dissection. No SCS injection was performed.

However, we found that the choroid was tightly attached to the sclera in a region surrounding the ON and roughly corresponding to sites of the SPCA penetration into the eye. The six-to-twelve SPCAs found in the human eyes formed an ellipsoid around the ON with a major radius of ~5 mm and minor radius of ~1 mm (Figure 6B), which is consistent with previous findings [131]. Since retina had peeled off choroid, we were unable to locate the macula in relation to SPCA. However, it is likely that the macula was within the ellipsoid demarcated by SPCAs [134]. This suggests that in human eyes, flow within SCS may also be impeded, but not anteriorly by LPCAs, as seen in the rabbit eye, but more posteriorly by SPCAs in the human eye. This might affect the ability of an injection in the SCS to target the macula due to a possible barrier formed by the SPCAs.

2.4.6 Microneedle injection into human cadaver eyes

To test the hypothesis that the SPCAs impede flow in the human eye, we performed injections inside the SPCA ring (2 mm from the ON, Figure 2.7A) and outside the SPCA ring (8 mm from the ON, Figure 2.7B) in human cadaver eyes. The SPCAs could be found between the chosen injection sites at ~3 mm from the ON. Although these injection sites were not clinically relevant, they allowed us to assess the barrier function of the SPCAs; we reasoned that if the SPCAs formed a barrier when an injection was made immediately adjacent to the vessels, then an injection made near the limbus (i.e., >20 mm from the ON) would experience similarly impeded flow, provided particles could flow that far.

The particle distributions of these conditions were statistically different ($p = 0.0035$, 2-way ANOVA, Figure 2.7C). When injection occurred within the SPCA ring, 66±8% (mean±SD) of particles were within 5 mm of the ON. When injection occurred outside the SPCA ring, 18 ± 7% (mean ± SD) of particles were found within 5 mm of the ON. These data indicated that the SPCAs provided a barrier to circumferential spread towards the ON and macula when an injection occurred more anteriorly than the SPCAs.

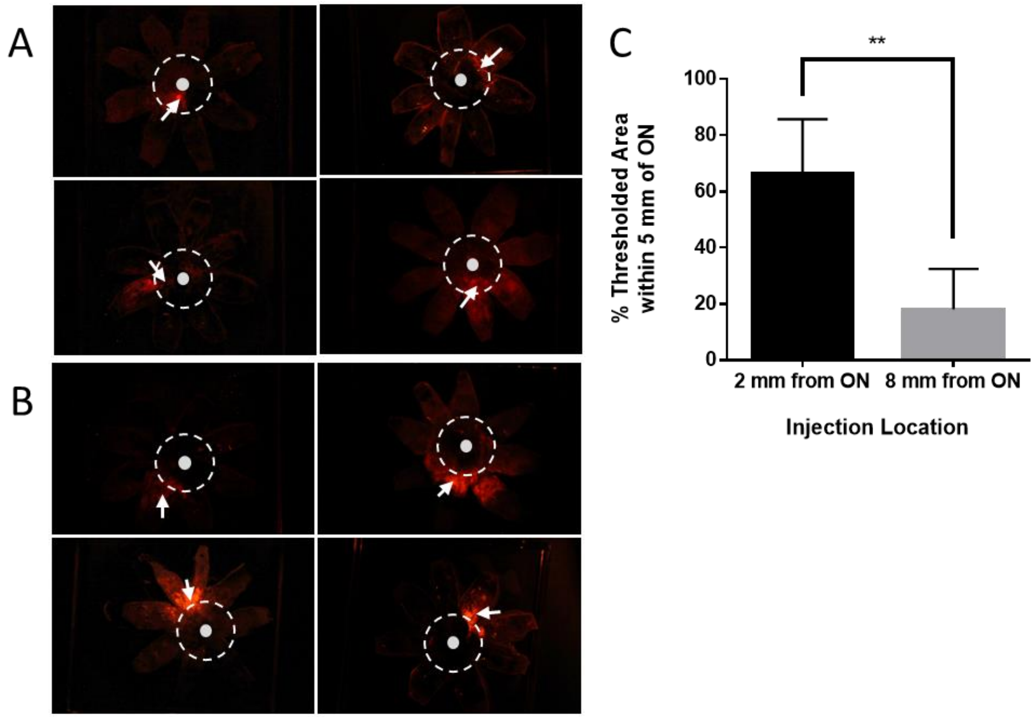

*Figure 2.7 – Images of human cadaver eye after microneedle injection (A) 2 mm from the optic nerve (ON), and (B) 8 mm from the ON. Solid gray circle denotes location of ON, dashed line denotes location of SPCAs and white arrow denotes injection location. (C) Quantification of images following injection within the SPCA ring and without the SPCA ring. ** indicates p<0.005.*

2.5 Discussion

The SCS is an attractive site of drug delivery targeted to the chorioretina [2, 5, 8, 81, 118, 119, 123, 125, 127, 130]. However, targeting within the SCS is important as well, since sites of disease are often localized to specific regions of the chorioretina, such as localization of AMD to the macula and localization of tumors at their sites of growth. This study addressed the possible existence of barriers to flow in the SCS due to its anatomy, more specifically due to sites where the posterior ciliary arteries, but not the vortex vein, cross the SCS and thereby limit its distention. This study showed that sites where the LPCA crosses the SCS in the rabbit eye and where the SCPA crosses the SCS in the human eye were associated with limited movement of particles in the SCS. The vortex veins had a minor effect on particle deposition, limited only to near the vortex vein root. In the rabbit eye, the LPCA barrier limited flow of particles between the upper and lower hemispheres of the eye, which was similar to distribution of saline seen with guinea pigs [120]. In the human eye, the SPCA barrier limited flow of particles posteriorly to the macula and ON.

We believe that previous studies have not reported this barrier because they were not designed to look for it and, in some cases, used animal models with different anatomy [8, 116]. One studies mentions injected fluid not crossing the midline but does not offer an explanation as to why this is [120] . Other studies have shown that formulations designed to keep SCS open after injection allow particles to redistribute within SCS and cover both hemispheres of the eye [128], although re-analysis of particle spread indicates lower particle concentration overlaying LPCAs compared with elsewhere (data not shown).

Vortex veins, another likely candidate that may have had barrier function in the SCS, did not have a large effect on particle distribution. Any effect by the vortex vein on particles spread was not apparent when viewed in flat mount, but was visible when imaged fundoscopically *in vivo.* We noted that few particles were deposited within 0.5 mm of the vortex vein upon funduscopic exam. It is important to note that each vortex vein penetrates through sclera as a single large vessel, which does not form a large region of physical attachment between sclera and choroid [41]. We posit that morphological differences between how branches of LPCAs penetrate sclera at multiple locations, whereas each vortex vein penetrates at just a single vessel, govern the ability of vessels to block circumferential flow.

Results from our *ex vivo* studies agreed with *in vivo* rabbit studies, suggesting that particle distribution was insensitive to vital processes, such as blood flow, for the injection formulation tested (i.e., particles suspended in HBSS). Previous studies using particles suspended in HBSS have indicated that particle spread occurs at the time of injection, after which the particles do not move [6, 8, 17, 81, 128].

Dissection of the choroid from the sclera demonstrated that the choroid is strongly attached to the sclera where multiple branches of the LPCA penetrate through sclera to anastomose with the choroid. These branches of the LPCA may act like staples to secure sclera and choroid together, thus physically impeding fluid flow. We hypothesize that it is possible to bypass this barrier by (i) flowing anteriorly or posteriorly around attachment sites, (ii) distending the choroid between the vessels, or (iii) tearing the small vessels. Further studies are needed to test this hypothesis.

Human eye dissection was consistent with prior studies [44, 131, 133], which indicated that the LPCA pierces the sclera more posteriorly and does not tightly adhere the sclera to the choroid, as compared to rabbit eyes. In contrast, SPCAs do tightly adhere choroid to sclera in a ring around the ON. This ring likely encompasses the macula, which may make SCS delivery to the macula and ON more difficult in humans. Consistent with these findings, Olsen et al. found that there were more and “stronger connections” between sclera and choroid in the macular region of porcine eyes [2], which is where the SPCAs penetrate through the sclera [135].

Limitations of this study include the use of *ex vivo* rabbit eyes, inability to determine kinetics of particle movement, lack of blood flow in *ex vivo* experiments, and inability to study temporal effects on LPCA’s barrier function. Furthermore, the conclusion of anatomy affecting particle spread (expected to be driven by convective flow) cannot be applied to distribution of small molecules (expected to be driven by both convection and diffusion). These barriers may not affect drugs diffusing within the SCS since they are on different length scales. Factors, such as physiochemical properties and clearance, are more likely to affect drug distribution [9, 123]. More comprehensive testing of anatomical barriers present in the SCS of human eyes is warranted.

In conclusion, we found that circumferential fluid flow in the SCS was impeded by the LPCA in rabbit eyes *ex vivo* and *in vivo*. It appeared that multiple tightly clustered vessels perforating through the sclera (such as those seen with branches of the LPCA in New Zealand White rabbits) result in strong attachment between sclera and choroid, and that these strong attachments form a physical barrier to circumferential flow. On the other hand, singular large vessels (e.g., vortex veins) had a minor effect on impeding circumferential particle spread. Human cadaver eyes exhibited a similar pattern of tightly clustered vascular perforations at the SPCAs near the ON, which impeded particle spread near the ON. This may make specifically targeting the SCS overlaying the macula and ON more difficult. Development of drug delivery and other applications requiring fluid flow in the SCS should take these anatomical barriers into account and either accept limitations they may impose or develop strategies to overcome or circumvent them.

3 DISTRIBUTION OF PARTICLES AND MOLECULES IN THE SUPRACHOROIDAL SPACE AFTER MICRONEEDLE INJECTION

3.1 Summary

The purpose of this study was to determine the effect of injection volume, formulation composition, and time on the circumferential spread of particles and molecules in the suprachoroidal space (SCS) after microneedle injection into New Zealand White rabbit eyes *ex vivo* and *in vivo*.

Microneedle injections of 25 to 150 µL of Hank's Balanced Salt Solution (HBSS) containing 0.2 µm particles and fluorescein were performed in rabbit eyes *ex vivo*. Spread of the compounds within the SCS was visualized via flat mount and 3D cryo-reconstruction. In the living rabbit, red-fluorescent microparticles and the following molecules were co-injected into the SCS: fluorescein, fluorescein isothiocyanate (FITC)-labeled Discovisc, and FITC-labeled carboxymethyl cellulose (CMC) in HBSS. Microparticles of different diameters (0.02 – 2 µm) were also injected in HBSS. Fluorescent fundus images were acquired over time to determine area of particle and molecule spread, as well as their co-localization.

We found that increasing injection volume increased area of particle and fluorescein spread in the SCS *ex vivo*. Particles occupied a smaller area than fluorescein, suggesting additional barriers to particle flow. In the living rabbit, injection of particles in viscous polymeric formulations led to initial localization of particles near the site of injection, followed by spreading of polymer and particles together until the formulation

polymers were cleared after 2 – 3 weeks for polymers that did not crosslink to form a gel. There was no significant effect of particle size on spreading in the SCS.

We conclude that (i) the area of particle spread generally increased with increasing injection volume and was unaffected by particle size, (ii) particles suspended in low-viscosity liquid formulations were entrapped in the SCS after injection, whereas molecules were not, (iii) increased formulation viscosity delayed particle entrapment in the SCS, allowing movement subsequent to injection and (iv) when using polymeric formulations that crosslink, particles can be entrapped within the formulation at the site of injection.

3.2 Introduction

Ophthalmic drug delivery into the potential space between the sclera and the choroid (aka. suprachoroidal space or SCS), is a new drug delivery technique actively under pre-clinical and clinical investigation[2, 7, 8, 81, 118, 119, 127, 136]. Unlike traditional ophthalmic drug delivery techniques, such as topical eye drops and intravitreal injections, SCS injection enables targeted delivery to the choroid, retinal pigment epithelium, and retina with high bioavailiability[8, 9, 81, 117-119, 123, 126, 130]. Additional advantages of SCS delivery include increased bioavailability, dose sparing, and avoiding the visual axis. A hollow-bore needle with a length of ~1 mm or less (aka. microneedle) can be used to reliably access the SCS without piercing the chorioretina[8, 81]. Performing such an injection is similar to an intravitreal injection and has been performed in the outpatient clinic setting[8, 81, 109]. Ongoing clinical trials are assessing the safety and efficacy of microneedle injections for indications such as posterior noninfectious uveitis (NCT01789320 and NCT02595398)[7].

When administering drugs via the SCS, it is important to control the area over which the drug formulations spread within the SCS. This targeting within the SCS may be used to treat diseased tissue while sparing non-diseased tissue. In some cases, it is desirable to have drug distributed over a large area of the SCS to broadly deliver drug to the chorioretina (e.g., to treat posterior uveitis[7]). In other cases, it may be desirable to localize the drug near the site of injection (e.g., to treat glaucoma)[6, 115].

Previous studies have used the two- dimensional (2D) circumferential spread of particles injected into the SCS as the primary metric of distribution[6, 8, 17, 81, 128]. Though many studies have investigated the distribution of particles[8, 17, 81, 119, 128] and molecules[5, 6, 8, 9, 124] independently, to our knowledge, no study has examined the distribution of particles and molecules injected into the SCS simultaneously, or imaged the distribution of polymeric formulation excipients in the SCS. Because of the large differences in diffusivity between particles and molecules, distribution of particles and molecules are expected to be different.

The purpose of this work was to investigate particle and molecule distribution following microneedle injection into the rabbit SCS. We hypothesize that (i) the area of particle spread generally increases with increasing injection volume, (ii) particles suspended in low-viscosity liquid formulations are entrapped in the SCS after injection, whereas molecules are not, (iii) increased formulation viscosity delays particle entrapment in the SCS, allowing movement subsequent to injection and (iv) at very high liquid formulation viscosity, particles can be entrapped within the formulation at the site of injection.

3.3 Materials and Methods

All reagents and chemicals were purchased from Sigma-Aldrich (St. Louis, MO) unless otherwise specified. Red-fluorescent polystyrene particles (Excitation: 580 nm; Emission: 605 nm) and green-fluorescent polystyrene particles (Excitation: 505 nm; Emission: 515 nm) with diameters ranging from 0.02 – 2 µm were purchased from Life Technologies (Fluosphere, Carlsbad, CA). Eyes of pigmented Silver Fox and American Blue rabbits (Broad River Pastures, Elberton, GA) and albino New Zealand White rabbits (Pel Freeze, Rogers, AR) were obtained within 1 day after euthanasia until use. All *in vivo* experiments were carried out in albino New Zealand White rabbits (Charles River Laboratories, Wilmington, MA) and were approved by the Georgia Institute of Technology Institutional Animal Care and Use Committee. Practices complied with the ARVO Statement for the Use of Animals in Ophthalmic and Vision Research. Four replicates per experimental group were performed unless otherwise specified.

3.3.1 *Ex vivo* injection procedure

Extraocular tissues were carefully removed from the rabbit ocular globe. To simulate a physiological intraocular pressure (IOP) of 10-12 mmHg, a water column was raised to ~14 cm and connected to the eye via a 25-gauge needle penetrated through the optic nerve[17]. A microneedle (750 µm in length, 33-gauge; kindly provided by Clearside Biomedical, Alpharetta, GA) attached to a 250 µL glass chromatography syringe (National Scientific, Rockwood, TN) was used to make injections. Injections were performed 3 mm posterior to the limbus at the 12 o'clock position (superior) to be as far as possible from anatomical barriers created by the long posterior ciliary artery that impede circumferential flow[129].

Depending on the experimental condition, each injection consisted of 25 to 150 µL of 0.5% (w/v) red-fluorescent particles (0.2 µm diameter; Excitation: 580 nm; Emission: 605 nm) and 0.025% (w/v) fluorescein suspended in Hank's Balanced Salt Solution (HBSS; Gibco, Life Technologies). After each injection, the needle was held in place for 1 min to minimize reflux[121]. The eye was then frozen via submersion in 100% ethanol chilled over dry ice 3 min post-injection depending on experimental condition.

3.3.2 Flat mount to characterize 2D circumferential spread

After SCS injection and freezing, eyes were prepared to assess the 2D spread of particles and fluorescein, as described previously[8, 128, 129]. The frozen eye was sliced open from the limbus to the posterior pole to generate eight approximately equidistant scleral flaps. The resulting scleral flaps were splayed open and the frozen vitreous humor, lens, and aqueous humor were removed.

A digital SLR camera (Canon 60D, Canon, Melville, NY) with a 100 mm lens (Canon) was used to acquire brightfield and fluorescence images. Camera parameters were held constant at shutter speed = 1/15 s and aperture = F/2.8. To acquire the area of fluorescein spread, a green optical band-pass filter (520 ± 10 nm; Edmunds Optics, Barrington, NJ) was placed on the lens, and the sample was illuminated by a lamp with the violet setting of a multicolor LED bulb (S Series RGB MR16/E26. HitLights, Baton Rouge, LA). To visualize the location of the red-fluorescent particles, a red filter (610 ± 10 nm; Edmunds Optics) was placed on the lens, and the sample was illuminated with the same lamp switched to green light. The area of green and red fluorescence that was above threshold was calculated for each eye using ImageJ (National Institutes of Health, Bethesda, MD). Thresholding was set manually based on visual inspection of background signal.

3.3.3 3D cryo-reconstruction to determine 3D distribution of particles and fluorescein

Rabbit eyes that received a microneedle injection of 25 to 150 µL containing 0.5% w/v red-fluorescent particles (0.2 µm diameter) and 0.025% w/v fluorescein were processed using the 3D cryo-reconstruction procedure (detailed procedure in Section 4.3.3 on page 87). Briefly, the eye was frozen in chilled ethanol after 3 or 15 min. The frozen pigmented eye was sliced with a cryostat, and fluorescence images of the cryo-block were acquired every 300 µm. Imaging the block reduced apparent drift and simplified reconstruction compared with previous methods[137, 138]. To acquire the green fluorescence (from fluorescein), a green optical band-pass filter (520 ± 10 nm; Edmunds Optics) was placed on the lens, and the sample was illuminated with blue/violet LED light (HitLights). To visualize the location of the red fluorescent particles, a red filter (610 ± 10 nm; Edmunds Optics) was placed on the lens, and the sample was illuminated with green LED light (HitLights).

The resulting image stack consisting of only the green or red fluorescence images was imported into a custom Matlab (Mathworks, Natick, MA) script. The eye was modeled as a sphere and discretized into 100x100 points. For each of these 100x100 points, a ray originating from the centroid of the eye (determined manually by visual inspection) through each point was identified (Figure 4.1B). The intensity along each ray was used to find the location of the fluorescence in the SCS (Figure 4.1C). If the ray had a segment >25 µm in length with an intensity above threshold, we considered the point to be occupied by the fluorescent species. This procedure was repeated for all 100x100 rays to yield a 2D map projection or a 3D surface plot (Figure 4.1D and E). The resulting 100x100 array was viewed as a surface plot in Matlab, and the thresholded area was calculated as a percentage of total ocular globe minus the cornea. Thresholding was determined manually by visual inspection.

3.3.4 Fluorescent tagging of excipient formulation

To visualize spread of polymer formulation excipients, we fluorescently labeled polysaccharides that have been shown to significantly influence spread of particles within the SCS[128] using previously described methods[139]. Carboxymethyl cellulose (CMC; 700 kDa high viscosity, Sigma-Aldrich) has been shown to impede spread of particles, allowing for localized delivery of particles that stay near the injection site[6, 128]. On the other hand, Discovisc (Alcon Laboratories, Fort Worth, TX) and hyaluronic acid have been shown to promote spread up to 100% of SCS area by a slow process after injection[128].

To label CMC, 250 mg of CMC and 10 mg of fluorescein isothiocyanate (FITC) was added to 25 mL of 0.1 M NaOH in DI water. The solution was mixed in the dark at room temperature (22 °C) for 4.5 days. The solution was then transferred into a dialysis tube (30 kDa cutoff, Spectra/Por, Spectrum Laboratories, Rancho Dominguez, CA) in a DI water bath. The water bath was changed daily for 5 days to remove unreacted FITC. The contents of the dialysis tube were transferred into a 50 mL centrifuge tube and frozen prior to vacuum drying. Care was taken to minimize light exposure at all steps to minimize bleaching. A similar procedure was performed with Discovisc; 500 μL of

Discovisc and 1 mg of FITC were added to 2.5 mL of 0.1 NaOH. The other methods were the same as those used for FITC labeling of CMC.

3.3.5 *In vivo* SCS injections and image acquisition

Albino rabbits were anesthetized with isoflurane and treated with proparacaine eye drops (Bausch & Lomb, Rochester, NY). All injections were 50 µL in volume and performed 3 mm posterior to the limbus at the supranasal quadrant (4 mm nasal to the edge of the superior rectus extraocular muscle).

To determine the effect of polymeric formulation on particle spread, the following injections (N=4 eyes per group) were performed: [i] 50 µL of 2% (w/v) red-fluorescent particles (0.2 µm diameter) and 0.025% fluorescein in HBSS; [ii] 50 µL of 2% (w/v) red-fluorescent particles (0.2 µm diameter) and 5% FITC-CMC in HBSS; [iii] 50 µL of 2% (w/v) red-fluorescent particles (0.2 µm diameter) and 1x FITC-Discovisc re-constituted in HBSS.

To determine if particles ranging from 0.02 µm to 2 µm co-localize, the following injections (N=4 eyes per group) were performed: [i] 50 µL of 1% (w/v) red-fluorescent particles (0.2 µm diameter) and 1% (w/v) green-fluorescent particles (0.02 µm in diameter) suspended in HBSS; [ii] 50 µL of 1% (w/v) red-fluorescent particles (0.2 µm diameter) and 1% (w/v) green-fluorescent particles (0.2 µm diameter) suspended in HBSS; [iii] 50 µL of 1% (w/v) red-fluorescent particles (0.2 µm diameter) and 1% (w/v) green-fluorescent particles (2 µm diameter) suspended in HBSS; and [iv] 50 µL of 1% (w/v) red-fluorescent particles (0.02 µm diameter) and 1% (w/v) red-fluorescent particles (2 µm diameter) suspended in unlabeled Discovisc.

At predetermined time points, the animals were imaged with a modified RetCam II system (Clarity Medical Systems, Pleasanton, CA). Prior to imaging, tropicamide (Akorn Pharmaceuticals, Lake Forest, IL), phenylephrine (Akorn Pharmaceuticals), and proparacaine (Akorn Pharmaceuticals) eye drops were given. The built-in fluorescein attachment was used to capture green fluorescence. For the red fluorescence, green light was generated by placing a 575±50 nm bandpass filter (Edmunds Optics) in line with the fiber optic line. A red-emission filter (610 ± 10 nm, Omega Optical, Brattleboro, VT) was placed over the camera to capture red fluorescence. Animals were euthanized with an injection of pentobarbital through the ear vein at the end of the experiment.

Post-processing of the RetCam images was used to generate a collage for each imaging condition, since the camera did not have built-in image stitching algorithms. Co-localization was determined using a previously described method[140]. Briefly, the 2D correlation coefficient of the red- and green-fluorescent images was calculated, and compared against the 2D correlation of 100 randomly assigned image pairs using a one-sided unpaired t-test. A low p-value indicated statistically significant co-localization greater than chance, and a high p-value indicated no significant co-localization.

3.3.6 Statistical analysis

Image analysis was performed using Matlab and ImageJ. Statistical analysis was performed using Prism (Graphpad, La Jolla, CA). Values are presented as the mean ± standard error of the mean (SEM), unless otherwise specified. Two-way ANOVA and Student's t-test analyses ($\alpha = 0.05$) were performed to determine statistical significance.

3.4 Results

3.4.1 Distribution of particles and molecules immediately after injection into the SCS

The first objective was to test the hypothesis that the circumferential area of particle coverage increases with increasing injection volume. We therefore calculated the percentage area of the SCS that had red and green fluorescence greater than threshold after injection of increasing volumes into the rabbit SCS *ex vivo* using flat mounts (Figure 3.1) and 3D cryo-reconstruction (Figure 3.2) measurement methods.

Consistent with the hypothesis, area covered by fluorescein and particles generally increased with increasing injection volume, although the rate of increase was larger at lower volumes (Figure 1). A linear fit to the data yielded a poor correlation (r^2 = 0.51 for particles and 0.67 for fluorescein), whereas an exponential fit was better (r^2 = 0.90 for particles), which is consistent with the observation that area initially increases and appears to approach a plateau value slightly below 50% area coverage for particles and slightly above 50% for fluorescein. We hypothesize that this apparent plateauing behavior is due to anatomical barriers that inhibit coverage in the inferior hemisphere, especially for particles[129].

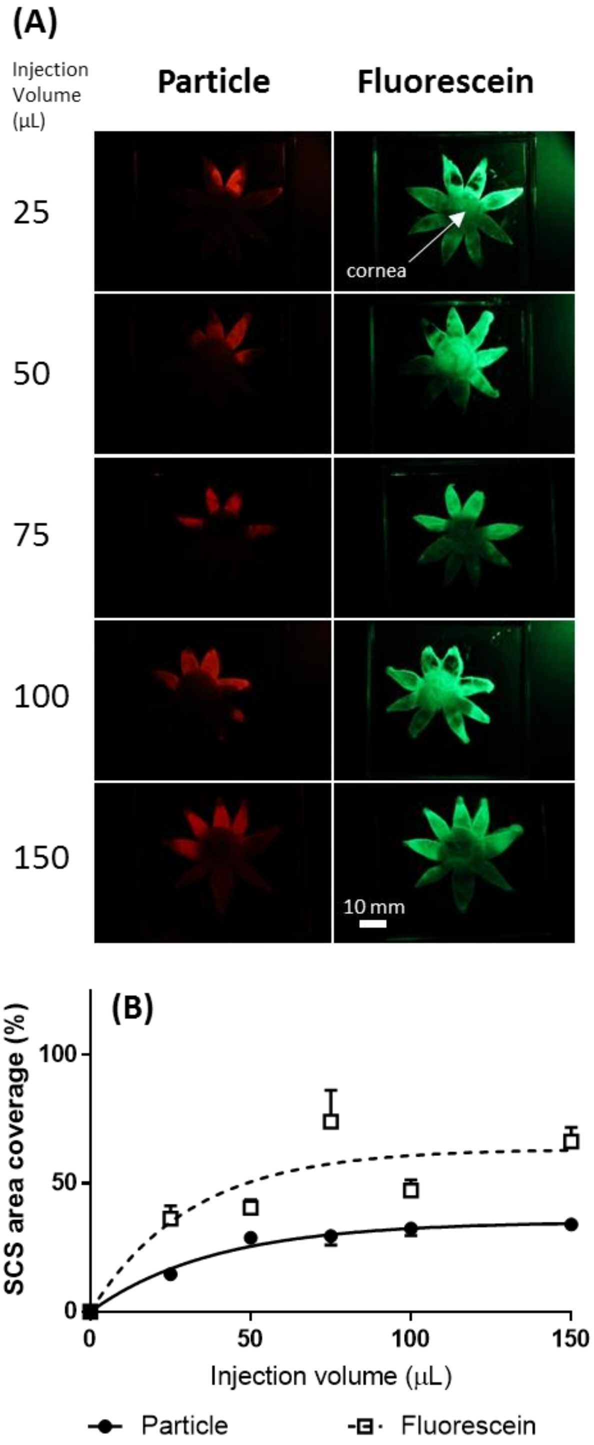

Figure 3.1 – Percentage area of SCS containing injected particles and fluorescein molecules, as determined by flat-mount measurement method. (A) Representative red and green fluorescence flat-mount images to visualize the spread of particles (0.2 µm diameter) and fluorescein after microneedle injection in ex vivo rabbit eyes. Eyes frozen and processed 3 min after injection. (B) Quantification of percent area (mean±SEM, N=3-5 replicates) of SCS covered by red particles or fluorescein. Exponential fits to the data are shown.

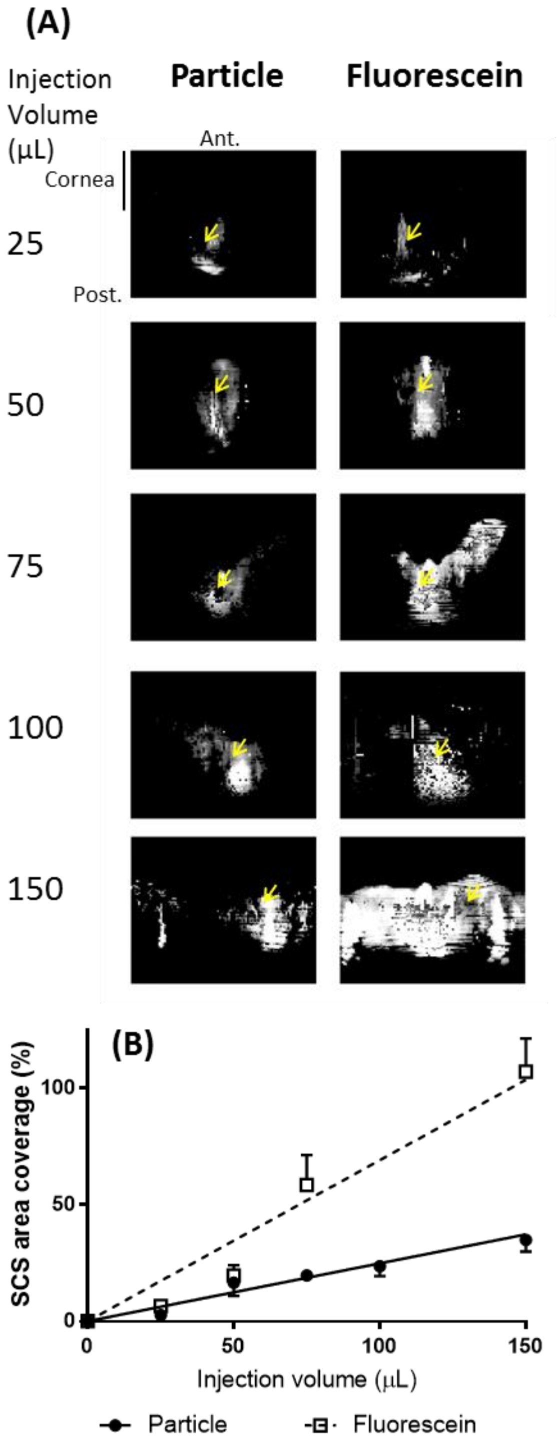

Figure 3.2 – Percentage area of SCS containing injected particles and fluorescein molecules, as determined by 3D cryo-reconstruction method. Eyes frozen and processed 3 min post-injection. (A) Representative equatorial map projections of red fluorescence of 0.2 µm diameter particles and green fluorescence of fluorescein after microneedle injection in ex vivo rabbit eyes. Injection site indicated by yellow arrow. Note that like a Mercator map projection of Earth, there is distortion at the poles (anterior and posterior). (B) Quantification of percent area (mean±SEM, N=2-6) covered by red particles or fluorescein. Linear fits to the data are shown.

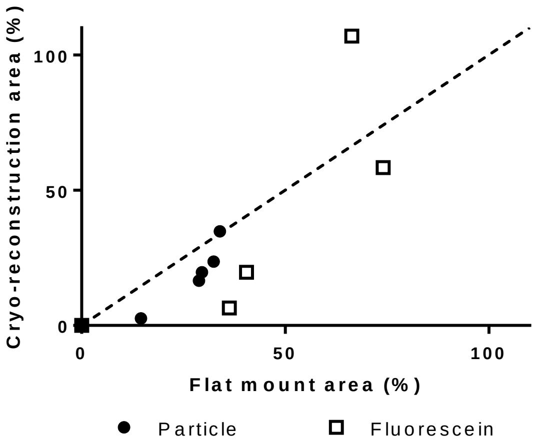

Figure 3.3 – Parity plot comparing area calculated from flat mount and cryo-reconstruction methods. Pooled data had a slope of 0.91 ± 0.14 (mean ± SEM; r^2 = 0.65), which was not statistically different from 1 indicating methods agree.

For all injection volumes, the fluorescein occupied a larger area than the red fluorescent particles ($p<0.0001$, ANOVA). The ratio of area covered by fluorescein versus particle was 2.05±0.24 (mean±SEM), which did not significantly depend on injection was found when comparing the percentage areas of eye covered by fluorescein versus particles. There was no discernible pattern in the ratio when comparing high- and low-volume injections. This difference in area could be explained by the higher diffusuvuty of fluorescein versus particles (which are assumed to transport only by convection). However, diffusion of fluorescein for 3 min after injection is expected to account for an area increase of only ~20% (based on a calculation assuming a fluorescein diffusivity of 4.3×10^{-6} cm^2/s [141] and a covered SCS area of ~200 mm^2 in the rabbit eye [142]). Because this small predicted increase is much less than the roughly two-fold measured increase, this results suggest, which is less than 2.05. This result suggests that there are additional factors at play in the SCS that limit movement of particles relative to small molecules (i.e., fluorescein).

3.4.2 Distribution of particles and molecules over time after injection into the SCS *in vivo*

We further investigated the role of formulation and time on particle distribution in the SCS. The distribution of red-fluorescent particles suspended with green fluorescently-tagged formulation excipients in HBSS after injection into the SCS of live rabbits was imaged using red and green fluorescence simultaneously. Fluorescence was imaged using RetCam imaging, which was preferred to other non-contact fundus imaging methods, since it enabled visualization of the posterior pole as well as the far periphery (i.e., the injection site). We then calculated the percentage of the SCS area in the composite images that had red/green fluorescence values at least 0.1% of the starting concentration, which we used as a proxy of true coverage; and determined the incidence of co-localization of the red and green fluorescence greater than chance.

To study the distribution of red-fluorescent particles and green-fluorescent fluorescein molecules injected in HBSS (Figure 3.4), we measured the SCS area over which the particles and fluorescein spread for 21 days after injection *in vivo*. The particle area coverage was constant at all time points from 3 min to 14 d post-injection ($p=0.99$, Sidak’s multiple comparison test), with a small decrease in area at 21 d. In contrast, the fluorescein area increased from 3 min to 1 h post-injection before being cleared by 2 d. At the 3 min and 1 h time points, fluorescein covered a larger area than the red particles ($p<0.01$, Sidak’s multiple comparison test). Moreover, the time point at which the maximum fluorescein coverage was measured was later than the red particle maximum. Statistical analysis showed that the particles co-localized with fluorescein immediately after injection, but not at later time points. Taken together with the *ex vivo* data, we conclude that particles suspended in HBSS became immobilized immediately post-injection even though fluorescein was able to move within the SCS well after the injection.

We next investigated how the addition of viscous formulation excipients affected particle distribution over time. When the formulation consisted of red particles suspended in 5% FITC-CMC in HBSS (Figure 3.5), particle area coverage increased from 3 min until 2 d post-injection ($p<0.01$, Sidak's multiple comparison test). Then, from 2 d to 35 d, there was no significant change in particle distribution in the SCS ($p=0.61$, Sidak's multiple comparison test). The co-injected FITC-labeled CMC initially followed a pattern similar to the particles, increasing in area for the first two days ($p<0.005$, Sidak's multiple comparison test). However, from 2 d until 21 d, the area of FITC-CMC decreased ($p<0.005$, Sidak's multiple comparison), and from 21 d until 35 d, there was essentially no detectable FITC-CMC in the SCS. The FITC-CMC never occupied an area larger than the red particles ($p>0.07$, Sidak's multiple comparison test). The maximum red particle coverage and maximum FITC-CMC coverage occurred at the same time point, i.e., 2 d post injection. The last time point of co-localization was at 4 d. This suggests that the particles and FITC-CMC were transported together during the injection and for up to 2 days thereafter, after which the particles remained immobilized and the FITC-CMC was cleared.

When the formulation consisted of red particles suspended in FITC-Discovisc (Figure 3.6), particle area coverage changed over time. Particle coverage was constant from 3 min to 1 h ($p=0.98$, Sidak's multiple comparison test), and increased by 2 d ($p<0.05$, Sidak's multiple comparison test). There was no significant change in particle coverage from 2 d to 21 d ($p>0.24$, Sidak's multiple comparison test). The co-injected FITC-labeled Discovisc molecules initially followed a pattern similar to the particles, increasing in area for the first two days ($p<0.005$, Sidak's multiple comparison test). However, from 2 d until 7 d, the area of FITC-Discovisc decreased ($p<0.005$, Sidak's multiple comparison), and from 7 d until 21 d, there was essentially no detectable FITC-Discovisc in the SCS. The FITC-Discovisc never occupied an area larger than the red particles ($p>0.05$, Sidak's multiple comparison test). The maximum red particle coverage and maximum FITC-Discovisc coverage occurred at the same time point, i.e., 2 d post injection. The last time point of co-localization was at 2 d. This suggests behavior similar to that seen with FITC-CMC, where the particles and FITC-Discovisc were transported together during the injection and for up to 2 days thereafter, after which the particles remained immobilized and the FITC-Discovisc was cleared, although the FITC-Discovisc was cleared faster than the FITC-CMC and, on an absolute scale, the area coverage of FITC-Discovisc and co-injected particles was roughly twice as large as the area coverage of FITC-CMC and co-injected particles.

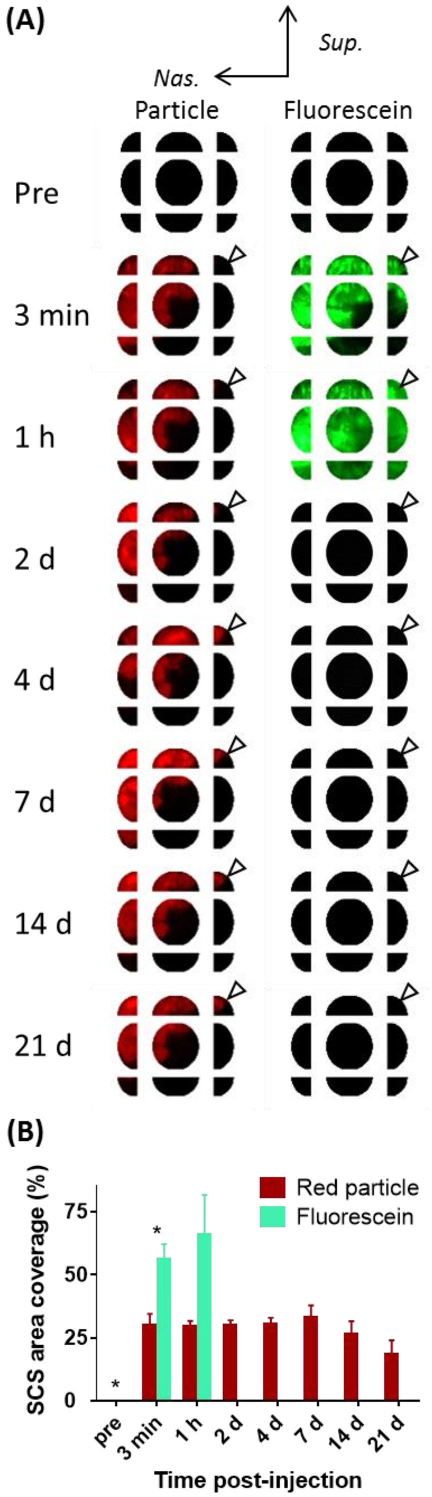

*Figure 3.4 – Spread of particles and fluorescein molecules in the SCS after injection of HBSS formulation in vivo. (A) Representative fluorescent fundus collages after microneedle injection of red-fluorescent particles (0.2 µm diameter) and fluorescein in HBSS in the supranasal position in vivo (injection site indicated by white arrow). The same animal was imaged for the duration of the experiment. Sup.=superior. Nas.=nasal. (B) Quantification of area covered (mean±SEM, N=3) by red-fluorescent particles and fluorescein in HBSS. * represents time points where red particle and fluorescein signals co-localize.*

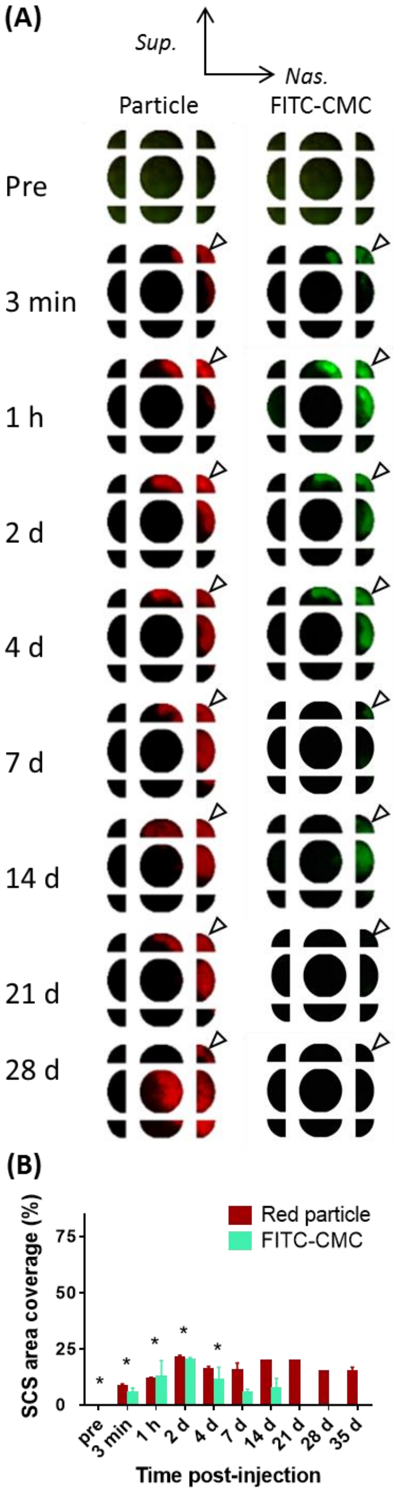

*Figure 3.5 – Spread of particles and fluorescein molecules in the SCS after injection in FITC-CMC formulation in vivo. (A) Representative fluorescent fundus collages after microneedle injection of red-fluorescent particles (0.2 µm diameter) and FITC-CMC in HBSS in the supranasal position (injection site indicated by white arrow). The same animal was imaged for the duration of each experiment. Sup. = superior. Nas.= nasal. (B) Quantification of area covered (mean±SEM, N=2-4) by red fluorescent particles and FITC-CMC in HBSS. * represents time points where red particle and FITC-CMC signals co-localize.*

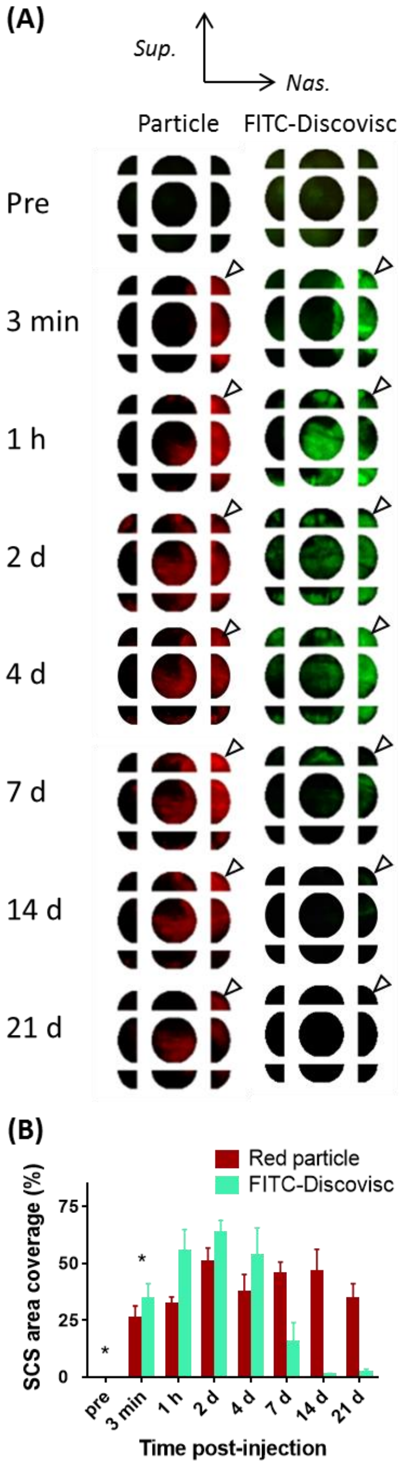

*Figure 3.6 – Spread of particles and fluorescein molecules in the SCS after injection in FITC-Discovisc formulation in vivo. (A) Representative fluorescent fundus collages after microneedle injection of red-fluorescent particles (0.2 µm diameter) and FITC-Discovisc reconstituted in HBSS in the supranasal position (injection site denoted by white arrow). The same animal was imaged for the duration of each experiment. Sup.=superior. Nas.=nasal. (C) Quantification of area covered (mean±SEM, N=2-4) by red fluorescent particles and FITC-Discovisc in HBSS. * represents time points where red particle and FITC-Discovisc signals co-localize.*

Considering all of these data (Figure 3.4 – Figure 3.6), the spread of particles immediately after injection depended on formulation composition, such that spreading went from smallest to largest with: FITC-CMC (8.5%) < FITC-Discovisc (26%) < HBSS (30%). At 14 d, the rank list for particle coverage for the tested excipients was FITC-CMC (20%) < HBSS (27%) < FITC-Discovisc (46%). The maximum area coverage was achieved at 3 min when formulated only in HBSS, and at 2 d for FITC-CMC and FITC-Discovisc. The particles injected with a low-viscosity formulation (i.e. HBSS only) did not experience a change in area coverage over time. On the other hand, particles injected with viscous formulations (FITC-CMC and FITC-Discovisc) experienced an increase in coverage of two-fold when comparing coverages at 3 min and 14 d post-injection. Thus, we can conclude that the viscous formulations prolonged particle transport time compared with the low-viscosity formulation. There was a strong association between transport time compared with viscosity (Figure 3.7). Initial viscosity of the formulation was a poor predictor of final spread of particles, possibly due to physical crosslinking of CMC[143] that effectively increased viscosity after injection and thereby limited spreading (Figure 3.8).

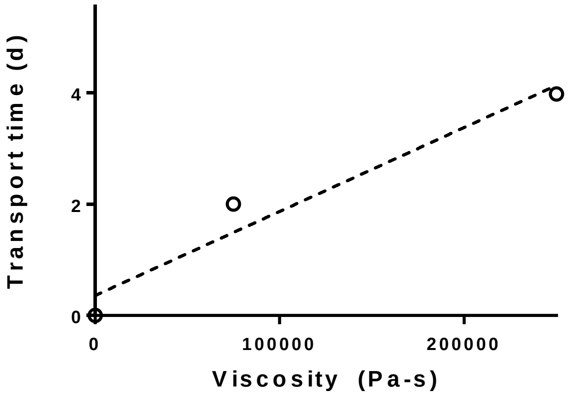

Figure 3.7 – Plot of transport time (mean±SEM) vs. formulation viscosity. Transport time defined as greater of (a) time in which co-localization stops, and (b) time in which particle area stops increasing. Linear regression fits data well (r^2=0.90)

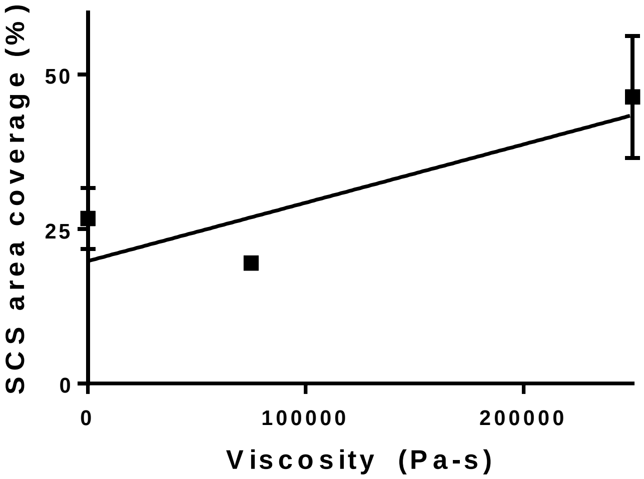

Figure 3.8 – Plot of SCS area coverage (mean±SEM) vs. formulation viscosity. SCS area coverage determined from RetCam II collages. Linear regression did not fit data well (r^2=0.44)

Fluorescein in HBSS occupied 66% of the visible SCS, which was the largest area of all the fluorescent species injected. In comparison, peak FITC-CMC spreading was 20% of SCS area, and occurred at 2 d. Peak FITC-Discovisc coverage was 63% and occurred at 2 d. Total clearance of the fluorescently-tagged formulation excipients occurred by 2 d for HBSS, 21 d for FITC-CMC, and 14 d for FITC-Discovisc.

Co-localization of particles and the formulation excipients was seen up until 3 min for HBSS, 4 d for FITC-CMC, and 3 min for FITC-Discovisc.

3.4.3 Effect of particle size on particle distribution over time after injection into the SCS *in vivo*

To determine the effect of particle size on distribution, particles of different sizes (20 nm – 2 µm) were suspended in HBSS and Discovisc, and co-injected into the rabbit SCS *in vivo*. Injections ysed pairwise combinations of red- and green-fluorescent particles of different sizes to determine whether the particles co-localized in the SCS. In all cases, the pairs of co-injected particles all co-localized for at least 4 d post-injection (Figure 9). With all HBSS conditions, particle area did not change with time (p>0.06, 2-

way ANOVA). For particles in Discovisc, the particle area increased until 2 d for both the 20 nm and 2 μm particles.

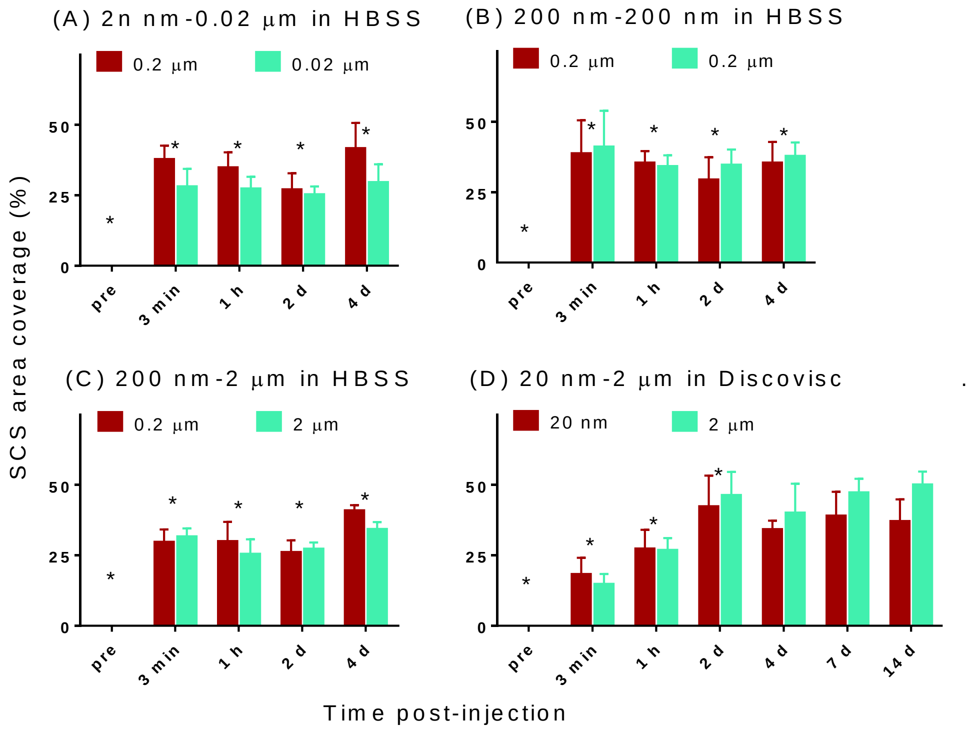

*Figure 9 – Quantification of area covered (mean±SEM, N=3-4) after SCS injection with (A) 2 nm red- and 200 nm green-fluorescent particles in HBSS, (B) 200 nm red- and 200 nm green-fluorescent particles in HBSS, (C) 200 nm red- and 2 μm green- fluorescent particles in HBSS, and (D) 20 nm red- and 2 μm green-fluorescent particles in Discovisc over time in vivo. The same animal was imaged for the duration of each experiment. * represents time points where red- and green-fluorescent particles signals co-localize.*

3.5 Discussion

Traditional ophthalmic drug delivery techniques, namely topical eye drops and intravitreal injections, do not precisely target diseased tissues in posterior segment indications. Compared with these conventional routes of administration, suprachoroidal delivery enables targeted drug delivery to the choroid, retina, ciliary body, and sclera with higher bioavailability[5, 6, 8, 9, 81, 115], and can be performed in the outpatient clinic setting[7, 8, 81]. The extent and distribution of posterior-segment diseases are typically not uniform. For example, glaucoma treatment requires localization near the ciliary body, which is near the site of microneedle injection[6, 115]; while noninfectious posterior uveitis requires spreading throughout the SCS[7]. Deposition within the suprachoroidal space can be geographically controlled so as to target diseased tissues while sparing non-diseased tissues[17, 118, 124, 128, 129]. This work investigated the distribution of particles and molecules injected into the rabbit SCS over time as a function of injection volume and formulation.

3.5.1 Distribution of particles and molecules injected into the SCS

One goal of this work was to study the distribution of particles and molecules co-injected into the SCS of rabbits. We found that, as injection volume increased, circumferential area of SCS containing particles and molecules also generally increased. However, we were not able to conclude if area increased linearly with injection volume or followed an exponential or other relationships. Thus, increasing injection volume was a reasonable strategy to increase coverage, but may limit particle spreading across certain anatomical barriers[129]. For example, in rabbits and guinea pigs, anatomical barriers prevented particle spread into the inferior hemisphere when injections were made superior to the long posterior artery [120, 129]. To address this limitation, Kim et al. showed that it is possible to achieve particle spread >50% (and up to 100%) by optimizing the injection formulation[128].

3.5.2 Distribution of particles relative to molecules

Another goal of this study was to determine the relative distributions of particles and molecules co-injected into the SCS. We found that, with HBSS as the formulation, the area covered by fluorescein was larger than the area covered by particles for all injection volumes tested. On average, the fluorescein occupied an area twice as large as that occupied by particles *ex vivo* and *in vivo*. The discrepancy in area covered could be due to either barriers in the SCS that preferentially limit movement of particles or increased diffusion of fluorescein in the SCS post-injection relative to the particles. Because the contribution of fluorescein diffusion was estimated to increase coverage by only ~20%, entrapment of particles is the more likely explanation.

Because molecules distributed to cover a larger area than particles in the SCS, the delivery of molecules may be preferred if the goal is to achieve full coverage of the SCS. However, the use of particles (e.g., containing drug molecules for slow release over time[7, 115]) may be preferable to injecting free drug molecules, which are usually cleared from the SCS within a day[6, 8, 9, 120].

3.5.3 Effect of formulation on distribution of particles

For the purposes of our *in vivo* formulation excipient experiments, we defined transport time as the greater of (a) the time at which particle area stopped changing and (b) the time in which co-localization of particles and formulation excipients stopped. The data showed that there was a strong association between transport time and viscosity of the liquid formulation, where increased viscosity facilitated longer transport time (i.e., for days after the injection). In contrast, viscosity of the formulation had a much weaker association with area coverage, probably because certain viscous formulations like CMC may become physically cross-linked, effectively increasing viscosity after injection and thereby limiting spread.

3.5.4 Effect of particle size on distribution of particles

Finally, particles with diameters ranging from 0.02 to 2 µm co-localized within the SCS independent of particle size. Furthermore, the size of the particles did not influence transport time. Particles of different sizes may be preferred for different applications, such as micron-scale particles to serve as slow-releasing drug delivery systems, nanoscale virus particles as gene delivery vectors, and micron-sized cells as cell-based therapies. This study shows that particles spanning two orders of magnitude in size distributed on the SCS to a similar extent with similar kinetics, which should simplify design of particle delivery to the SCS. Of course, other particle parameters may also play a role, such as particle density, shape, surface properties and composition.

3.5.5 Study limitations

Limitations of the study include use of *ex vivo* rabbit eyes, and shortcomings of equipment and measurement methods. There are physiological and anatomical differences between rabbit and human eyes. These species differences may or may not alter suprachoroidal distribution. For example, as we showed previously[129], there are different anatomical barriers in rabbits versus humans that affect circumferential particle spread. Human clinical trials will be needed to investigate suprachoroidal distribution, as it applies to human health. This study used *ex vivo* eyes for some studies, which may not be fully representative of living animals. However, the use of *ex vivo* eyes made certain measurements possible; for example, using *ex vivo* (and enucleated) eyes allowed rapid freezing of the eye to stop particle and molecule movement. The distribution of molecules and particles suspended in HBSS was studied in both *ex vivo* and *in vivo* rabbit eyes, and the results were similar, at least initially post-injection.

The RetCam II fluorescent fundus imaging system did not have the ability to automatically stitch image fields together. Instead, collages were used, and this may have introduced errors in the actual coverage of fluorescence (e.g., two neighboring images in the collage may overlap). However, the RetCam allowed visualization into the far periphery, which would be difficult with other non-contact fundus imaging modalities.

3.5.6 Conclusion

In conclusion, we studied the distribution of particles and molecules co-injected into the SCS of rabbits. We found that as injection volume increased, the area the injected fluid in the SCS generally increased. Particles did not spread to cover as large an area as fluorescein molecules, suggesting barriers to particle movement in the SCS. With high-viscosity formulations, the transport time of particles was significantly extended (to 2 d), and particles were often co-localized with viscous polymer excipients during spreading. These studies will aid in the development of formulations that can be injected via microneedle to control particle spread within the SCS.

4 THICKNESS AND CLOSURE KINETICS OF THE SUPRACHOROIDAL SPACE FOLLOWING MICRONEEDLE INJECTION OF LIQUID FORMULATIONS

4.1 Summary

The purpose of this study was to determine the effect of injection volume and formulation of a microneedle injection into the suprachoroidal space (SCS) on SCS thickness and closure kinetics. Microneedle injections containing 25 – 150 µL of Hank's Balanced Salt Solution (HBSS) were performed in the rabbit SCS *ex vivo*. Distribution of SCS thickness was measured by ultrasonography and 3D cryo-reconstruction. Microneedle injections were performed in the rabbit SCS *in vivo* using HBSS only; Discovisc; and 1, 3, and 5% carboxymethyl cellulose (CMC) in HBSS. Ultrasonography was used to track SCS thickness over time. We found that increasing HBSS injection volume increased the area of expanded SCS, but did not increase SCS thickness *ex vivo*. With SCS injections *in vivo*, the SCS initially expanded to thicknesses of 0.43±0.06 mm with HBSS, 1.5±0.4 mm with Discovisc, and 0.69 – 2.1 mm with 1 – 5% CMC. After injection with HBSS, Discovisc and 1% CMC solution, the SCS collapsed to baseline with time constants of 19 min, 6 h and 2.4 d, respectively. In contrast, injections with 3 – 5% CMC solution resulted in SCS expansion to 2.3 – 2.8 mm over the course of 2.8 - 9.1 h after which the SCS collapsed to baseline with time constants of 4.5 – 9.2 d. Thus, we concluded that with low-viscosity formulations, increasing injection volume has a negligible effect on SCS thickness. Increasing injection fluid viscosity had a major effect on SCS thickness. SCS expansion is hypothesized to be controlled by a balance between

the viscous forces of the liquid formulation and the resistive biomechanical forces of the tissue.

4.2 Introduction

The suprachoroidal space (SCS) is a potential space found between the sclera and choroid. Due to its close proximity to the ciliary body, choroid, retina, and sclera, this space has recently drawn attention as a site for targeted drug delivery[2, 7, 8, 81, 118, 119, 125, 127], placement of glaucoma drainage devices[144-147], and implantation of retinal prostheses[148]. As a site of drug administration, delivery into the SCS is noted for high bioavailability at targeted tissues in posterior segment diseases, as well as fast clearance by the choroidal vasculature[8, 9]. Access to the SCS is possible via surgical procedures of varying complexity[2, 117, 118, 124, 126, 130, 149] and microneedle injections that offer greater simplicity [8, 81]. A hollow microneedle with a length similar to the thickness of the sclera can be used to reliably access the SCS while preventing penetration deeper into the eye[8, 81]. Microneedle injections can be performed by ophthalmologists in the outpatient clinic setting, similar to the intravitreal injection procedure. The safety and efficacy of these microneedle injections have been demonstrated in a recent open-label Phase I/II clinical trial (NCT01789320) where triamcinolone acetonide suspension was injected into the SCS to treat posterior uveitis[7]; a Phase III clinical trial is ongoing (NCT02595398) to further study the efficacy of the SCS injection.

Although many studies have investigated the circumferential spread of particles [8, 17, 81, 119, 120, 128, 129] and molecules[5, 9, 116, 120, 125] within the SCS, few have studied the third dimension: the distensibility of the choroid off the sclera, a.k.a. the SCS thickness. Seiler et al. measured the maximum suprachoroidal space thickness over the injection site in *ex* *vivo* porcine and canine eyes, and found that there was no difference in thickness with three injection volumes, especially once the eyes were inflated to a physiological intraocular pressure[116]. They also determined the 3D distribution of microbubbles in the porcine eye[116], however, the microbubbles are not expected to distribute the same as neutral-density materials[17]. Patel et al. used a fluorophotometer to assess the SCS thickness along the visual axis in rabbits[8, 81]. Gu et al. used optical coherence tomography to study the SCS thickness along the visual axis in guinea pigs[120]. Since the injection occurs in the far periphery (near the limbus), the SCS thickness at the posterior pole may not be representative of the entire globe. Kadam et al. showed that the physiochemical properties of molecules injected into the SCS affected affinity to certain ocular layers, which may indirectly affect measured SCS thickness[123].

These prior studies made measurements of SCS thickness at individual locations at individual time points using individual liquid formulations. To provide a more comprehensive understanding the distribution of SCS thicknesses and the factors that affect SCS thickness after microneedle injection, this study measured SCS thickness at multiple locations at multiple time points using multiple different liquid formulations of multiple different volumes. More specifically, this work evaluated the effect of increasing injection volume and liquid formulation viscosity on SCS thickness at the time of injection and over time after the injection.

We used two companion approaches to report on the distribution of the SCS thickness throughout the entire ocular globe (i.e., ultrasonography and 3D cryo-reconstruction). We hypothesize that for a given liquid formulation, the SCS thickness expands to a constant value independent of the volume of fluid injected; that increasing viscosity of the liquid formulation increases the SCS thickness; that SCS thickness may continue to expand after injection of concentrated carboxymethyl cellulose (CMC) solutions that form physically crosslinked hydrogels that swell; and that SCS thickness collapses to baseline over time after SCS injection.

4.3 Materials and Methods

All reagents and chemicals were purchased from Sigma-Aldrich (St. Louis, MO) unless otherwise specified. Red fluorescent polystyrene particles (excitation: 580 nm; emission: 605 nm) with diameters of 200 nm were purchased from Life Technologies (Fluospheres, Carlsbad, CA). Eyes of pigmented Silver Fox and American Blue rabbits (Broad River Pastures, Elberton, GA) and albino New Zealand White rabbits (Pel Freeze, Rogers, AR) were obtained within 1 d after slaughter and stored in a -80°C freezer immediately upon arrival. All *in vivo* experiments were carried out in albino New Zealand White rabbits (Charles River Laboratories, Wilmington, MA) and were approved by the Georgia Institute of Technology Institutional Animal Care and Use Committee. Practices complied with the ARVO Statement for the Use of Animals in Ophthalmic and Vision Research. Four replicates per group were performed unless otherwise specified.

4.3.1 *Ex vivo* injection procedure

The conjunctiva, fascia, and extraocular muscles were carefully dissected off the rabbit eye. The eye was pressurized to a physiological intraocular pressure (IOP) of 10-12 mmHg by penetrating a 25 gauge needle through the optic nerve, which was connected to a water reservoir raised to ~14 cm above the eye[17]. A 750 µm-long, 33-gauge hollow microneedle (Clearside Biomedical, Alpharetta, GA) attached to a 250 µL glass chromatography syringe (National Scientific, Rockwood, TN) was used to make injections. All injections were performed 3 mm posterior to the limbus at the 12 o'clock position (superior) to be as far as possible from anatomical barriers that impede circumferential flow[129]. Depending on the experimental condition, each injection consisted of 25, 50, 75, 100, or 150 µL of 0.5% (w/v) red-fluorescent particles suspended in Hank's Balanced Salt Solution (HBSS; Gibco, Life Technologies, Carlsbad, CA). After each injection, the needle was held in place for 1 min to prevent reflux[121].

4.3.2 Ultrasound imaging to determine SCS thickness

A high-frequency ultrasound (U/S) probe (UBM Plus, Accutome, Malvern, PA), with a minimum axial resolution of 15 µm, was used to generate 2D cross-sectional images of the SCS in rabbit eyes *ex vivo* after injecting volumes ranging from 25 to 150 µL. An U/S probe cover (Clearscan, Eye-Surgical-Instruments, Plymouth, MN) was attached to the UBM Plus to facilitate U/S image acquisition. Three minutes after injection, the U/S probe was used to acquire eight sagittal views around the eye (12, 1.5, 3, 4.5, 6, 7.5, 9, and 10.5 o'clock). Post-processing of the U/S B scans was performed to find the thickness from the outer sclera to the inner retina at 1, 5, and 9 mm posterior to the scleral spur. The mean, median, and standard deviation for each eye were calculated.

4.3.3 3D cryo-reconstruction to determine 3D distribution of particles and fluorescein

Microneedle injections of 25 – 150 µL containing red-fluorescent particles were performed in pigmented rabbit eyes, as described above. The eyes were frozen 3 min post-injection using ethanol chilled to -80°C. Frozen eyes were put into cryomolds loaded with Optical Cutting Temperature embedding medium (OCT; Tissue-Tek, Sakura Finetek, Tokyo, Japan) and India Ink (Higgins Ink, Leeds, MA). The cryomolds were then half-submerged in liquid nitrogen until the OCT was solid. The eye was removed from the plastic mold for sectioning. The pigmentation in the eye and the India Ink in the OCT prevented fluorescence from out of plane during imaging (see below).

Each cryomold was connected to the mount of a cryostat (CryoStar NX70 cryostat, Thermo Fisher Scientific, Waltham, MA or Leica CM 3050 cryostat, Wetzlar, Germany). A digital SLR camera (Canon 60D, Canon Inc., Melville, NY) with 100 mm prime lens was positioned on a tripod such that the camera was along the longitudinal axis of the cryo-block (to minimize apparent motion of the sample as it was cut and any keystoning effect). Camera parameters were held constant at shutter speed = 1/15 s and aperture = F/2.8. The camera was placed close enough such that the sample occupied >80% of the image sensor.

One red fluorescent images of the cryo-block was obtained every 300 µm by slicing the sample with the cryostat (Figure 4.1). Since the cryo-block was locked in place for each image and the camera was stationary, determining the orientation of one image relative to other images was simplified compared with other reconstruction methods[137, 138]. To visualize the location of the red-fluorescent particles, a red filter was placed on the lens, and the sample was illuminated with green LED light (HitLights, Baton Rouge, LA). Care was taken not to shift the camera when connecting the filter. After every 300 µm of tissue was removed by the cryostat, the procedure was repeated (including imaging measurements) until the entire eye was imaged.

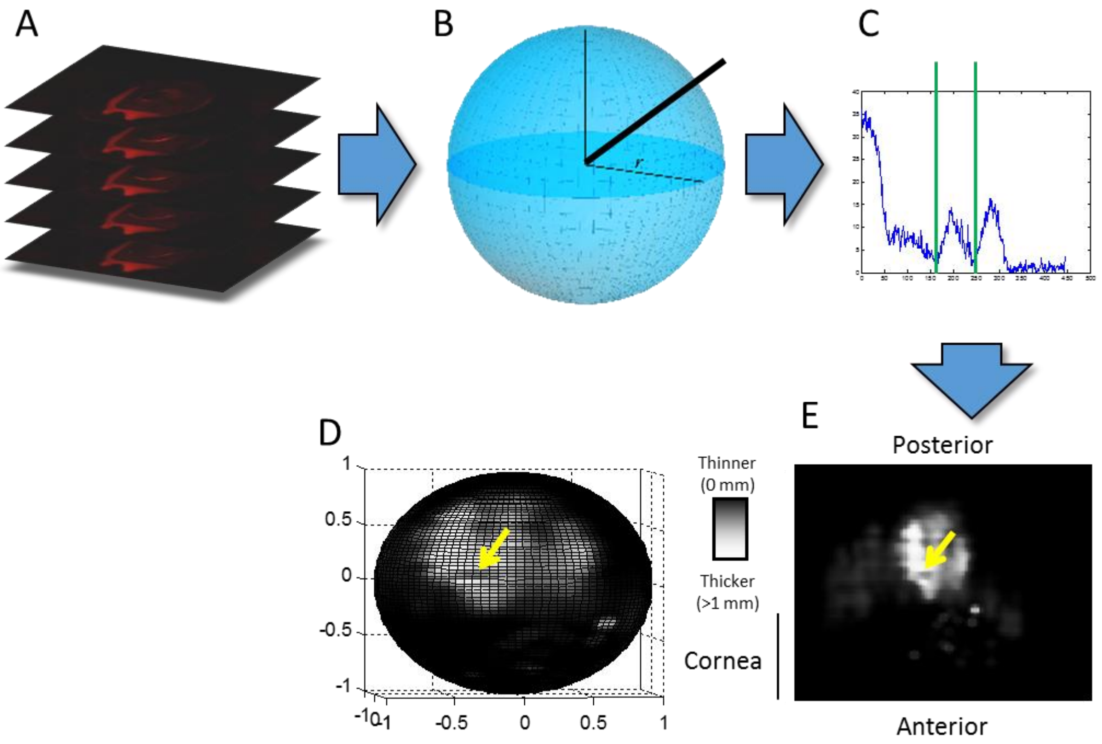

Figure 4.1 – Diagram of 3D cryo-reconstruction methods. Microneedle injection of particles suspended in HBSS is made in the suprachoroidal space (SCS). (A) Eye is cryo-sectioned. Every 300 µm, fluorescence images of the block are taken. (B) Image stack is uploaded to Matlab script. The centroid of the eye is identified manually by visual inspection, and 100 x 100 rays originating from the centroid are calculated. (C) The intensity along each ray is used to calculate the SCS thickness. (D and E) The SCS thicknesses for each of the 10,000 rays are calculated and displayed as either a (D) spherical representation or (E) 2D equatorial map representation. Similar to a Mercator projection of Earth, the regions near the anterior and posterior pole in (E) are greatly distorted. Injection site indicated with yellow arrow.

Image stacks consisting of red fluorescence images were imported into a custom Matlab (Mathworks, Natick, MA) script. The image stack was preprocessed by spatially transforming each image so the four corners of the mold matched up, using the Matlab functions ‘cp2tform’ and ‘imtransform’. The spatial transformation accounted for angular deviations (e.g., roll around the longitudinal axis of the sample), linear deviations (e.g., shifting the camera), apparent changes in sample size due to changes in distance from sample to camera (i.e., as the sample was cut), and perspective deviations (i.e., viewing the sample from off the longitudinal axis).

The eye was modeled as a sphere and discretized into an array of 100 x 100 pixels. For each of these 10,000 pixels, a ray originating from the centroid of the eye through each point was identified (Figure 4.1B). The intensity along each ray was used to map the SCS thickness, as determined by the distribution of red particles, in the SCS (Figure 4.1C). The SCS thickness was determined by finding the distance between the first appearance and first disappearance of red fluorescence, as determined with an absolute intensity threshold and the first derivative of the intensity (to ensure an edge). This procedure was repeated for all 10,000 rays to yield a 2D map projection or a 3D surface plot (Figure 4.1D and E). Note that only SCS thickness per ray was calculated, not particle concentration.

A low-pass filter was used on the 100 x 100 array to remove aberrant signals. The resulting array was viewed as a surface plot in Matlab. Key parameters from each sample included distribution of thickness (5th, 25th, 50th, 75th, and 95th percentile, mean, and standard deviation) excluding thicknesses < 25 µm, thresholded area, and thresholded volume.

4.3.4 Mechanical testing of sclera-choroid attachments

To assess the mechanical properties of attachments between the sclera and choroid, a peel test (modification of ASTM D1876 method[150]) was performed on sclera/chorioretina strips with and without microneedle injection of HBSS into the SCS (N=8 per condition). Albino rabbit eyes *ex vivo* were used for this experiment.

Either the superior and inferior hemisphere was randomly assigned to receive a microneedle injection of 100 µL HBSS. After injection, two sagittal strips – one with no injection and one with SCS injection – from the same eye, approximately 10 mm in width and 14 mm in length, were cut from the eye. The actual width was measured with a caliper. A scalpel blade was gently run along the edges of the strip to ensure the edges were clean. The ciliary body was cut posterior to the scleral spur so the choroid could be separated off the sclera. A 5 mm biopsy punch was used to make a hole through the cornea. The strip was mounted on a force displacement station (ESM301 motorized stand, Mark-10 Corp., Copiaque, NY) with a 50 gF force sensor (Series 5 Force Gauge, Mark-10 Corp.). A hook attached to the force sensor was threaded through the hole in the cornea, and the ciliary body was clamped to a stationary platform. The force displacement station was programmed to pull (i.e., peel) the sclera from the choroid at a rate of 60 mm/min. The force readings were collected in real time by the MESUR Lite gauge software. The average force per width of sclera/choroid tissue strip was calculated.

4.3.5 SCS collapse rate with different liquid formulations

The rabbit was anesthetized with isoflurane. Topical proparacaine was given to further anesthetize the eye. To study the effect of viscosity on SCS collapse time, one of the following formulations was injected: [i] 50 µL of HBSS; [ii] 50 µL of Discovisc (Alcon Laboratories, Fort Worth, TX); [iii] 50 µL of 1% carboxymethyl cellulose (CMC; 700 kDa high viscosity) dissolved in HBSS; [iv] 50 µL of 3% CMC in HBSS; [v] 50 µL of 5% CMC in HBSS; and [vi] 25 µL of 5% CMC in HBSS. High-frequency ultrasound B-scan was used to determine the rate of SCS collapse. Eight sagittal views over the pars plana were acquired: (a) supranasal, over the injection site; (b) superior; (c) nasal; (d) supratemporal; (e) temporal; (f) infratemporal; (g) inferior; and (h) infranasal. Image acquisition for these formulations occurred for up to 28 d *in vivo*.

Off-line post processing was performed on the U/S views to measure the SCS thickness. The U/S probe used has a minimum axial resolution of 15 µm. For each U/S view, a line segment 5 mm posterior to the scleral spur and perpendicular to the sclera was created (Figure 4.2). The line started at the outer surface of the sclera and ended at the inner surface of the retina. The sclera and chorioretina were included in the measurement to ensure the line was perpendicular. SCS thickness was then calculated by subtracting the tissue thickness from the measured line length. Curve fitting was done to determine the rate of SCS collapse.

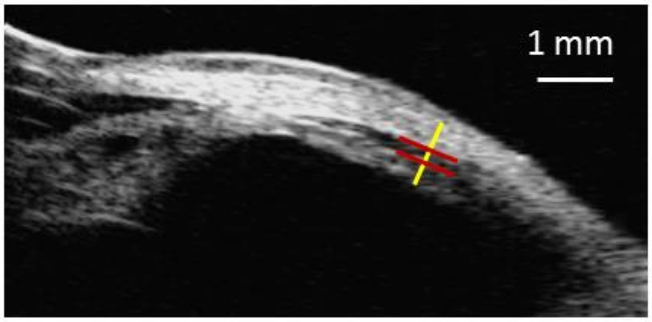

Figure 4.2 – Calculation of SCS thickness in ultrasound B scans. A line segment perpendicular to the sclera and choroid, from the outer sclera to the inner retina, is found. The conjunctiva is excluded from the measurement. The tissue thickness is found and subtracted out, resulting in the SCS thickness.

4.3.6 Determination of SCS clearance kinetics by fundus imaging

To study the effect of viscosity on fluorescein movement in the SCS, a 50 µL microneedle injection of the following formulations were tested: [i] 0.025% (w/v) fluorescein sodium (25% AK-Fluor, Akorn, Lake Forest, IL diluted with HBSS); and [ii] 0.025% fluorescein sodium (25% AK-Fluor, diluted with HBSS) and 5% CMC in HBSS.

The approximate clearance rate of injected fluorescent material from the SCS was found by taking fluorescence fundus images over time in the rabbit eye *in vivo*. Topical eye drops of tropicamide and phenylephrine (Akorn, Lake Forest, IL) were administered prior to each imaging session to dilate the eye. A RetCam II (Clarity Medical Systems, Pleasanton, CA) with the 130° lens attachment and the built-in fluorescein angiography module was used to acquire the images. Multiple images were taken with the blue light output from the RetCam II set at 0.0009, 1.6, and 2.4 W/m^2. In an attempt to capture the entire interior surface of the ocular globe, nine images were captured: central, supranasal, superior, supratemporal, temporal, infratemporal, inferior, infranasal, and nasal. This allowed imaging into the far periphery. Imaging was done immediately after injection, at 1 h, every 3 h for 12 h, and every two days post-injection.

The total clearance time, which we defined as the first time point in which fluorescence was not detectable by visual observation, was determined for all eyes injected.

4.4 Results

4.4.1 Effect of injection volume on SCS thickness: cryo-reconstruction measurement

We measured the thickness of the SCS and investigated its distribution in rabbit eyes after microneedle injection *ex vivo* using a 3D cryo-reconstruction method. 2D mapping of the spread of particles (Figure 4.3A) in the SCS after injection of different volumes of fluid indicated that the area of spreading increased with injection volume.

Quantification of the SCS thickness throughout the area of spreading produced histograms (Figure 4.3B) of the SCS thickness for each injection volume. Sites where SCS thickness was less than 25 µm were considered to have “unopened” SCS and were therefore not included in the analysis. All particle thickness histograms showed a characteristic spike at ~160 µm (i.e., the average mode value among the histograms collected at all conditions shown in Figure 4.3 is 160±25 µm (mean±SEM), and there were very few portions of the SCS open to smaller thicknesses. This peak value of SCS thickness did not significantly change as a function of injection volume (p=0.43, one-way ANOVA). This indicates that if the SCS is opened up, it readily expands to a thickness of at least ~160 µm.

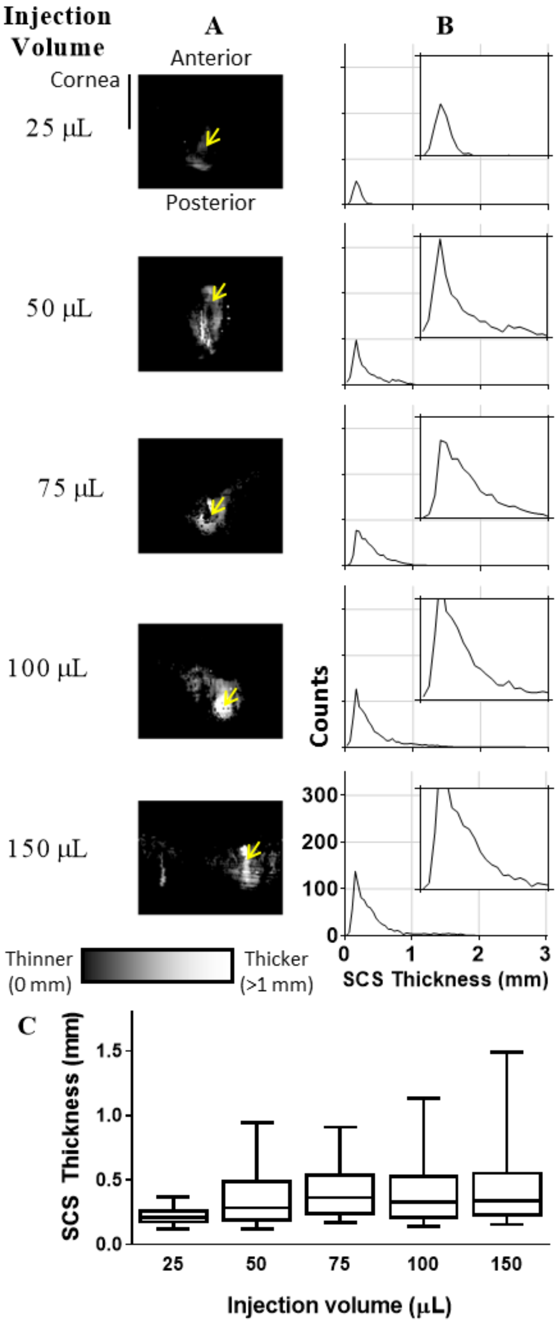

Figure 4.3 – Distribution of SCS thickness after injection of particles suspended in HBSS into the SCS of the rabbit eye ex vivo. Ex vivo rabbit eyes were frozen 1 min after SCS injection and analyzed by 3D cryo-reconstruction. (A) Representative thickness maps of 200 nm particles, where brighter white color indicates thicker SCS spreading. Yellow arrow indicates site of injection, at the 12 o'clock superior position. Each 2D map is an equatorial projection oriented such that anterior (i.e., cornea) is up and posterior (i.e., optic nerve) is down. As with 2D map projections of globes, the area represented by pixels at the upper and lower poles are distorted. (B) Data from these thickness maps are presented as histograms for different injection volumes (indicated on the left side of the figure). Y-axis is counts with every 100 counts marked. (C) Box and whiskers represent 5th, 25th, 50th (median), 75th, and 95th percentile of SCS thickness after injection (N=3-7 replicates per condition).

The median value of SCS thickness was found to be 330±30 µm, which was significantly different from the mode value ($p<0.001$, unpaired t-test) indicating few points where the thickness was less than 150 µm. The median SCS thickness was independent of injection volume ($p=0.15$, F test for zero slope), as shown in Figure 4.3C. This finding is notable, because injection of larger volumes of fluid can increase the area of fluid spread in the SCS and/or the thickness of the SCS. These data indicate that the SCS expands to a maximum thickness, and that injection of additional fluid increases area of spreading in direct proportion to the volume injected. To further test this hypothesis, we plotted area of spreading versus injection volume and found they increased in direct proportion to each other (Figure 4.4).

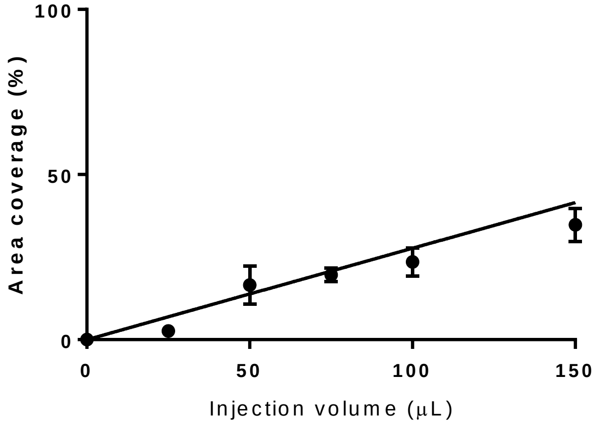

Figure 4.4 – Area of SCS coverage with increasing injection volume. Injection volumes ranging from 25 – 150 µL were performed in ex vivo rabbit eyes and the area of circumferential coverage was determined by 3D cryo-reconstruction. Values represent mean±SEM. Linear regression performed on data indicated that area was directly related to injection volume ($R^2 = 0.92$).

Finally, the mean values of SCS thickness were found to be 340±40 µm among all the conditions tested. The mean values had a slight dependence on injection volume ($p=0.04$, F test for zero slope). The 5th, 25th, median, and 75th percentile SCS thickness was approximately constant for injection volumes greater than 25 µL, but the 95th percentile increased with injection volume. The fact that there was a spread of SCS thicknesses to values up to a few-fold larger than the median value indicates that SCS thickness can be spread well beyond ~ 300 µm in some cases. These sites of greater SCS thickness occurred in patches (see bright spots on Figure 4.3A) that were often located near the site of injection.

4.4.2 Effect of injection volume on SCS thickness: ultrasound B-scan measurement

To validate the SCS thickness measurements calculated by the cryo-reconstruction method, we conducted additional experiments to measure SCS thickness by ultrasound B-scan in the rabbit eye *ex vivo* (Figure 4.5). This U/S measurement yielded a median SCS thickness of 160±20 µm, which was independent of injection volume (p=0.67, F test for zero slope) and was about half the value obtained by the cryo-reconstruction method (i.e., 330±30 µm). The two methods both showed that SCS thickness values were independent of injection volume and had a median value of roughly 150 – 350 µm. Since the eyes used in the U/S measurement were at room temperature and measured in real time shortly after injection and the eyes used in 3D cryo-reconstruction were frozen shortly after injection and measured later, still in the frozen state, the observed differences in thickness may be due to differences in timing, temperature, solid vs. liquid state tissue fluids or artifacts due to freezing. Furthermore, the U/S measurement was not able to assess the SCS thickness at the posterior pole, which may have biased the results.

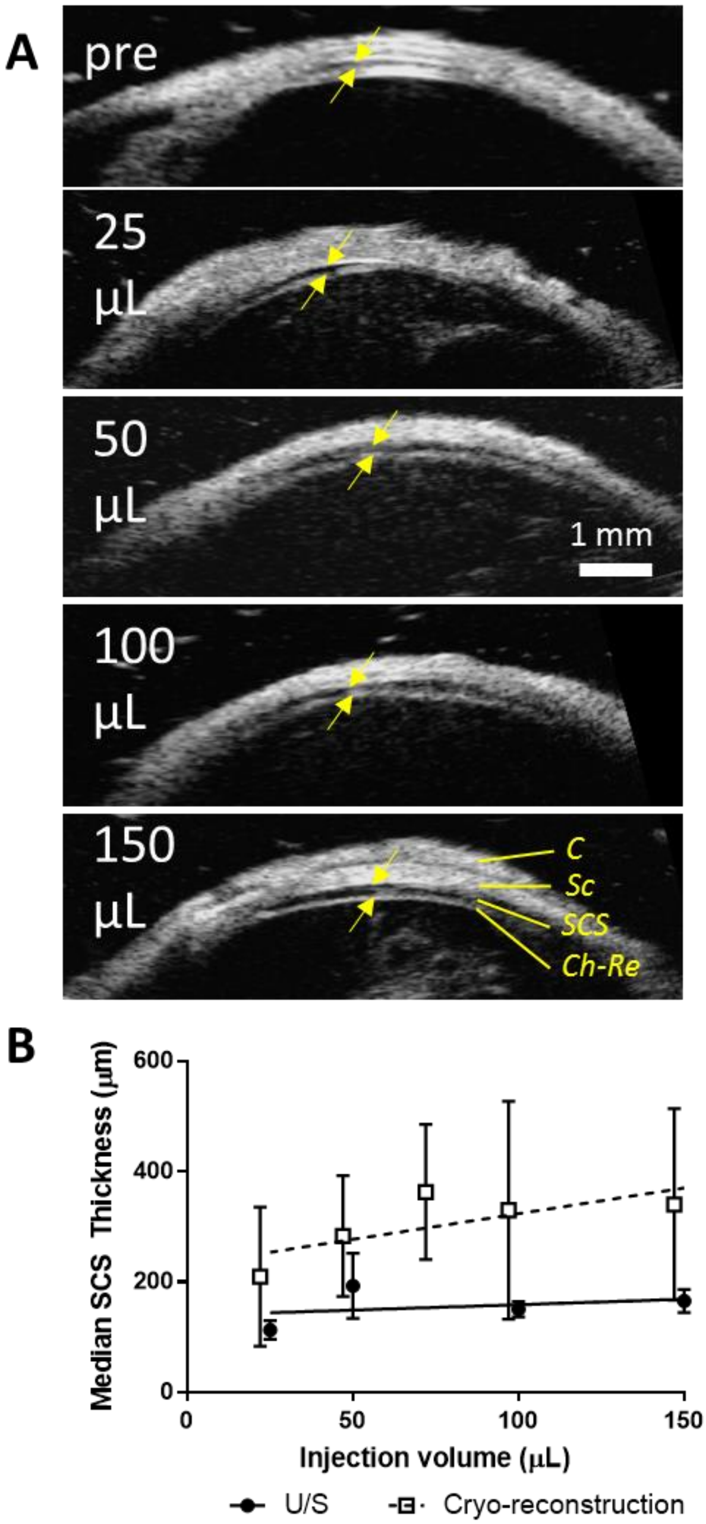

Figure 4.5 – SCS thickness measured with ultrasound B-scan in the rabbit eye ex vivo. (A) Representative ultrasound B scans. (B) Quantification of median SCS thickness ± SEM based on ultrasound (U/S) and cryo-reconstruction methods (N=3-7 replicates). Lines on the graph indicate best fits by linear regression. C = conjunctiva; Sc = sclera; SCS = suprachoroidal space; Ch-Re = choroid-retina. Arrows indicate SCS thickness.

4.4.3 Measurement of force of adhesion between sclera and choroid

We investigated further why median SCS thickness was constant over the range of injection conditions studied. The presence of lamellae that attach the sclera to the choroid might explain this constant thickness, as they may limit expansion of the SCS beyond a certain thickness. The literature suggests that such lamellae exist[1, 37, 149]. We therefore performed a peel test (modified ATSM 1876, Figure 4.6A) on scleral/chorioretinal strips from rabbit eyes that had either received or not received a SCS injection of HBSS *ex vivo*. We found that eyes with previous injection in the SCS required only 51% of the force to separate the sclera from the choroid compared with eyes having no SCS injection ($p<0.005$, unpaired t-test, Figure 4.6B). This suggests that the process of SCS injection weakens the adhesion strength between the sclera and choroid, possibly due to reorganizing, weakening, breaking or otherwise altering fibers adhering the sclera to the choroid. Since the force to separate the tissue does not become zero after injection, adhesive forces between the sclera and choroid, possibly involving connective fibers, may play a role in limiting SCS expansion.

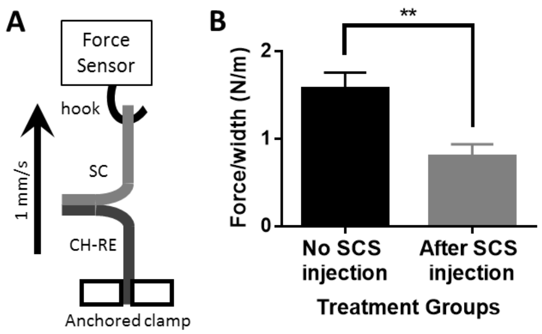

*Figure 4.6 – Modified ATSM 1876 peel test performed on scleral/chorioretinal (Sc-Ch-Re) strips from eyes that had either received (gray bar) or not received (black bar) a 100 µL SCS injection of HBSS ex vivo.(A) A diagram of the experimental setup is shown. (B) Mean ± SEM of the force to separate sclera from choroid per width of tissue strip is shown (N=8 replicates). P<0.005 = **, unpaired t-test.*

To further interpret these findings, we examined histological sections for anatomical structures within the SCS of rabbit eyes that had either received or not received a SCS injection of HBSS in the live rabbit. With no injection, the sclera and choroid were tightly apposed (Figure 4.7A). After injection, the sclera and choroid were no longer tightly adhered (Figure 4.7B), even more than one month after injection (Figure 4.7C). Furthermore, there was evidence of structures that appear to be fibrils connecting the sclera and choroid (Figure 4.7B and C). It cannot be determined at this time if these fibrils were intact or not. In companion experiments, the SCS thickness measured *in vivo* by U/S 30 min or longer post-injection was found to be indistinguishable from pre-injection thickness (i.e., zero), suggesting that processes in the living rabbit (e.g., intraocular pressure) were able to minimize the SCS thickness *in vivo* but were unable to maintain it after death. This finding further supports the hypothesis that there has been a loss in adhesion strength, possibly due to changes to the SCS lamellae.

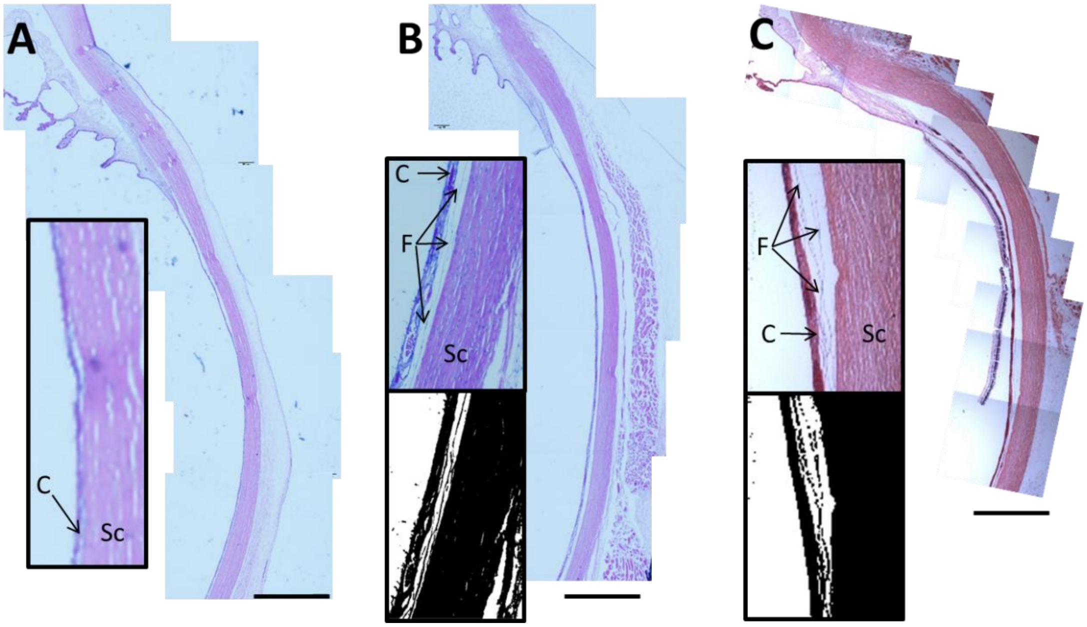

Figure 4.7 – Representative histological images showing SCS fibrils. (A) In eyes with no injection, the sclera and choroid are tightly adhered. (B) In eyes 30 min after HBSS injection, the sclera and choroid are no longer closely adherent. There are SCS fibrils visible, especially when image is transformed to black & white (insets). (C) In eyes 1+ mo after HBSS injection, the sclera and choroid are still not adherent. There are SCS fibrils visible, especially when image istransformed to black & white (insets). When animals were viewed under U/S in vivo, no SCS expansion was visible. Sc = sclera; C = choroid; F = SCS fibril. Scale bar = 1 mm.

4.4.4 Effect of liquid formulation on SCS thickness and collapse time

We next evaluated the effect of liquid formulation on SCS thickness, as well as the SCS collapse rate over time in the living rabbit (Figure 4.8A). We chose solutions of carboxymethyl cellulose (CMC) at different concentrations in HBSS and the commercial viscoelastic product, Discovisc® as liquid formulations for this study, because these liquid formulations were previously shown to distribute differently in the SCS, compared with HBSS[128].

The initial SCS thickness over the injection site varied greatly with choice of liquid formulation from 0.43±0.06 mm with HBSS to 2.1±0.1 mm with 5% CMC in HBSS (Figure 4.8B and Figure 4.9). The value for HBSS found here in the living rabbit eye is larger than what was found above in the rabbit eye *ex vivo*. This could be because the *in vivo* measurement was made at the injection site, which was the site of maximum SCS thickness, whereas the *ex vivo* measurement was reported as the average SCS thickness through the expanded SCS. Use of Discovisc, which had previously been reported to initially remain near the site of injection in the SCS[128], had a SCS thickness of 1.5±0.4 mm, which was significantly larger than the value for HBSS ($p<0.01$, Sidak's multiple comparison test). SCS injection of solutions containing 1%, 3% and 5% CMC in HBSS (viscous solutions that have also been reported to localize at the injection site[128]) had initial SCS thicknesses of 0.7±0.1 mm, 1.6±0.2 mm and 2.1±0.1 mm, respectively (Figure 4.8B). These data indicate that changing the formulation (to increase viscosity) had a larger effect on SCS thickness than increasing injection volume for a given formulation.

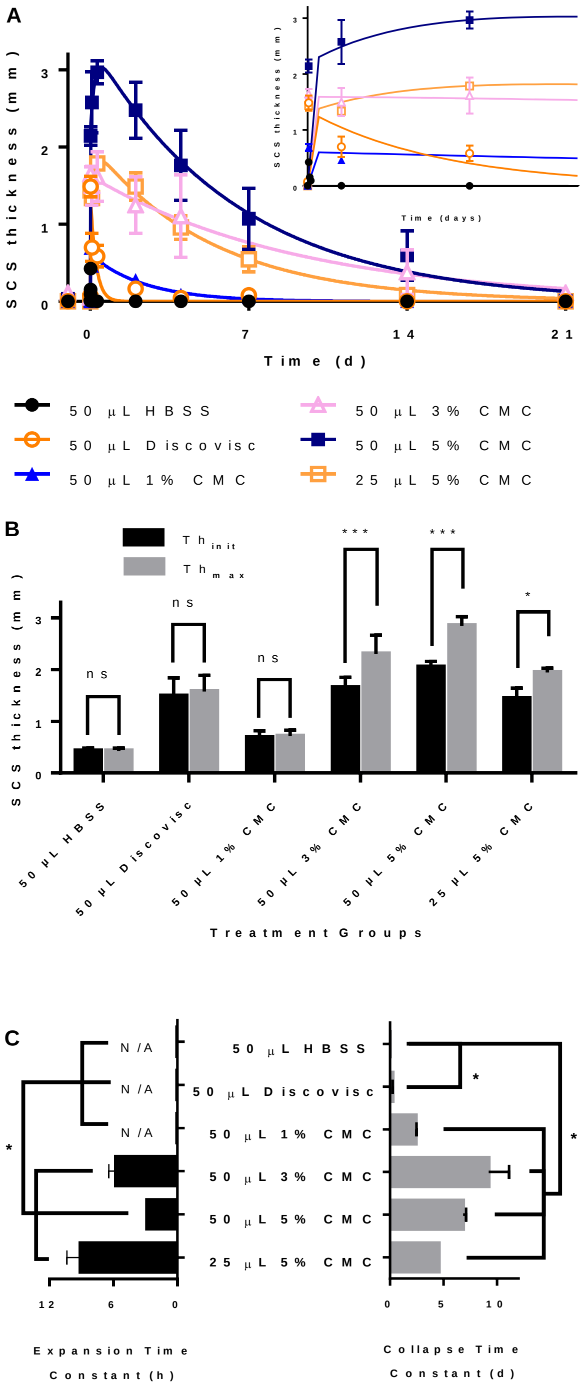

*Figure 4.8 – Quantification of median SCS thickness after injection of different liquid formulations as a function of time. (A) Time course of SCS thickness after injection with six liquid formulations. Inset shows first 24 h. (B) SCS thickness measured immediately post-injection (θ_0) and the maximum SCS thickness reached (θ_{max}) when using different liquid formulations. (C) The time constants associated with SCS expansion and collapse when using different liquid formulations. All values are mean±SEM (N=4 replicates) (ns = no significant difference, $p<0.05$ = *; $p<0.0005$ = ***, F test)*

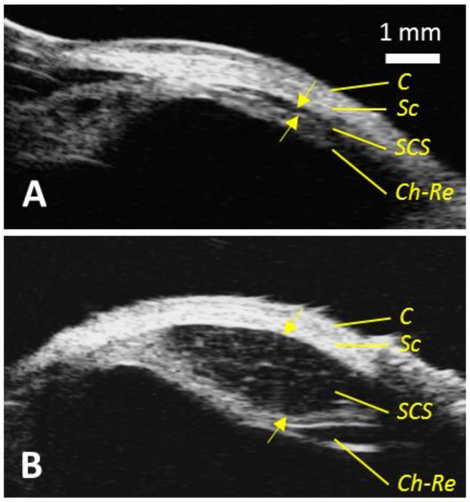

Figure 4.9 – Representative ultrasound B-scan images of the SCS after 50 µL injection of (A) HBSS and (B) 5% CMC solution. C = conjunctiva; Sc = sclera; SCS = suprachoroidal space; Ch-Re = choroid-retina. Arrows indicate SCS thickness.

We next monitored SCS thickness over time at eight positions around the globe for all the formulations tested (Figure 4.10A). After injection of HBSS, the SCS thickness over the injection site achieved its peak value immediately after injection and then decreased according to a roughly first-order exponential decay, i.e., there was no significant difference between SCS thickness immediately post-injection (θ_0) and the maximal SCS thickness (θ_{max}) ($p > 0.99$, Sidak's multiple comparison test, Figure 5B). Measurements at other locations around the globe behaved similarly.

There was also no difference between initial and maximal SCS thickness over the injection site for Discovisc and 1% CMC ($p \geq 0.97$, Sidak's multiple comparison test). However, the SCS thickness measured at the other sites behaved differently, which is consistent with a previous study[128]. With Discovisc, the decrease in SCS thickness at the injection site over time was accompanied by a concomitant increase in SCS thickness at adjacent sites in the SCS (Figure 4.10A, 4 h). By 2 d, the SCS thickness throughout the entire eye had returned to baseline. In contrast, 1% CMC only expanded the SCS at or near the injection site for the entire time course (data not shown). Because Kim et al.[128]

had shown that Discovisc was able to facilitate the distribution of particles throughout the SCS and that CMC was able to localize particles near the injection site, we hypothesize that the expansion of a region of SCS was necessary for particle deposition in that region.

With 3% CMC and 5% CMC solutions, θ_0 over the injection site was different than θ_{max} ($p<0.01$, 2-way ANOVA) because the SCS thickness initially increased over the course of hours after the injection. This expansion of the SCS could be explained by an osmotic and hydration effect of the CMC within the SCS, which could draw in water from the surrounding tissue to dilute the CMC and cause swelling of the gel. Besides the swelling, the behavior of the SCS thickness at other positions (Figure 4.10B) was similar to those found with 1% CMC.

To describe the timecourse of SCS thickness changes after injection over the injection site, we used a 2nd order exponential equation that could account for both the observed expansion and collapse of the SCS:

$$\theta(t) = -Ae^{-t/\tau_{exp}} + Be^{-t/\tau_{col}}, \qquad \text{Eq. 4.1}$$

where t is the time post-injection, $\theta(t)$ is the SCS thickness as a function of time, A and B are thickness constants, τ_{exp} is the expansion time constant, and τ_{col} is the collapse time constant (Figure 4.8C). This equation described the data from all the liquid formulations well (Pearson coefficient $r^2>0.76$).

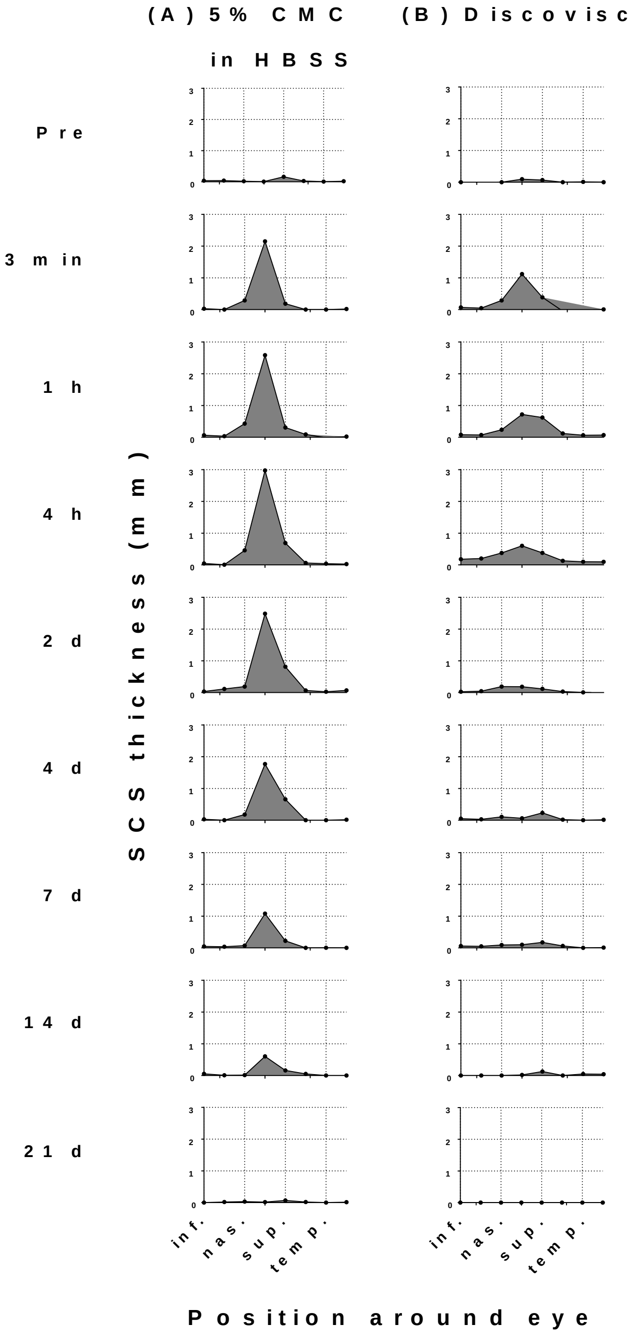

Figure 4.10 – Time course of SCS thickness following microneedle injection of (A) 50 µL Discovisc and (B) 50 µL 5% carboxymethyl cellulose in HBSS. Injection was performed supranasal and U/S B scans were acquired at eight positions around the ocular globe. Each time point represents the mean of 3-5 replicates. X-axis divisions at Inf. = inferior; Nas. = nasal; Sup. = superior; Temp. = temporal. SCS thickness (y-axis) marked every 1 mm.

Using this equation, we calculated the characteristic times associated with each of the liquid formulations. As expected, the liquid formulations that did not cause further expansion of the SCS after injection (i.e., HBSS, Discovisc, and 1% CMC), the calculated τ_{exp} values were all on the order of seconds (Figure 4.8C, left). In contrast, τ_{exp} values for the 3% CMC and 5% CMC liquid formulations ranged from 2.8 to 9.1 h, and there was no significant difference among these τ_{exp} values (p=0.77, F test).

There were significant differences in τ_{col} values among the liquid formulations tested (Figure 4.8C, right). With HBSS as the liquid formulation, τ_{col} was 19±3 min. With the Discovisc liquid formulation, τ_{col} was 6±2 h, which was significantly different than the HBSS value (p<0.005, F test). With all of the CMC liquid formulations, τ_{col} ranged from 2.4 – 9.2 days, which were different than HBSS (p<0.0001, F test) but not different from each other (p=0.47, F test). It is notable that collapse of SCS containing 1% CMC solution (that did not swell after injection) and SCS containing 5% CMC solution (which did swell after injection) had comparable τ_{col} values, which suggests that dissociation of the crosslinks found in CMC gels[143] is the rate limiting step to CMC clearance from the SCS resulting in collapse.

4.4.5 Effect of liquid formulation on clearance of fluorescent molecules from the SCS

We investigated the effect of liquid formulation viscosity on the timescale of clearance of fluorescein from the SCS. Using fundus microscopy, we identified how long it took for there to be no visual evidence of fluorescein in the SCS. Total clearance of fluorescein injected into the SCS in HBSS was 0.33±0.05 d, which was significantly faster than the clearance of fluorescein injected in 5% CMC solution, which was 2.7±0.7

d (p<0.0005, unpaired t-test, Figure 4.11). This can probably be explained by the long-lived presence of viscous CMC gel in the SCS (as evidenced by the SCS remaining open for many days, Figure 4.8 and Figure 4.10), which can slow diffusion of fluorescein out of the SCS.

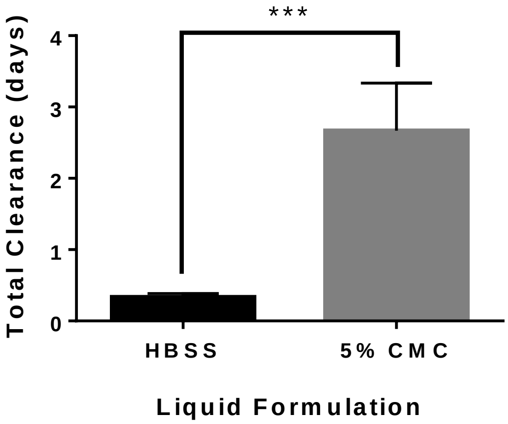

*Figure 4.11 – The total clearance time of fluorescein from the SCS after injection in HBSS or 5% CMC solution. Total clearance time is defined as the first time point at which fluorescein was not detectable under fluorescent fundus exam. All values are mean±SEM (N=3-6 replicates). p<0.0005 = ***, unpaired t-test.*

4.5 Discussion

4.5.1 SCS thickness is independent of injection volume

This study examined the effects of injection volume and liquid formulation on the thickness and closure kinetics of the SCS following microneedle injection. We found that the SCS was spread to a roughly constant thickness, independent of injection volume. The observation was made in the rabbit eye *ex vivo* using two different measurement methods: 3D cryo-reconstruction and U/S B-scan imaging. This result was not necessarily expected. Injection of an increasing volume of fluid into the SCS could be accommodated by an increase in SCS thickness, SCS area, or a combination of both. Our data indicate that the SCS readily expands to a certain thickness, after which additional fluid fills the SCS by expanding the SCS area containing fluid without expanding the

SCS thickness further. This explanation was supported by demonstration that the area of fluid in the SCS increased in direct proportion with the volume injected.

We and others hypothesized that the constant SCS thickness could be due to fibrils running between the sclera and choroid that resist expansion of the thickness of this space[1, 125]. Results from a modified peel test to determine the strength of adhesion between sclera and choroid showed that a fluid injection into the SCS as a pretreatment reduced, but did not eliminate, the force needed to subsequently separate the tissues. This could be explained by a partial weakening of the adhesions between sclera and choroid, possibly due to reorganizing, weakening, breaking or otherwise altering the fibrils with an injection. We also imaged evidence of these fibrils in the SCS, which was consistent with previous reports[1, 37].

Previous studies were inconclusive regarding the relationship between SCS thickness and injection volume. Seiler et al. concluded that, in *ex vivo* canine and porcine eyes, there was a difference between the maximum thickness achieved with the smallest injection volume tested (250 µL), and higher injection volumes tested (500, 800 and 1000 µL)[116]. However, no difference in maximum thickness was seen once the eyes were inflated to physiological intraocular pressures[116]. Moreover, the Seiler study assessed maximum thickness, rather than median thickness reported here, and it used much larger volumes of fluid, which are much greater than those used in current clinical trials[7].

Gu et al. found that, in guinea pigs, the cross-sectional area of the SCS increased with increasing injection volume[120]. However, as seen in Figure 4.5A of this study, not all the SCS was expanded, especially at small injection volumes. Thus, increases in cross-sectional area could be attributed to either expanding previously-unexpanded SCS (i.e., to enlarge the area of SCS expansion), or increases in SCS thickness.

4.5.2 SCS thickness depends strongly on injection liquid formulation

We found that liquid formulation had a major effect on SCS thickness, possibly related to fluid viscosity. While HBSS spread over large areas of the SCS, Discovisc and CMC solutions were largely retained near the site of injection initially, probably due to their high viscosity. This might be explained by the viscous forces resisting spread of the injected fluid in the SCS leading to the fluid further expanding the SCS near the site of injection in order to accommodate the injected fluid volume. Interestingly, in some cases (i.e., 3% CMC and 5% CMC solutions), SCS thickness continued to expand for hours after the injection, probably due to the diffusion of water into the hydrogel, which resulted in swelling it.

At later times, SCS thickness decreased and ultimately returned to baseline within hours for HBSS and within days to weeks for the viscous solutions. These slow kinetics were probably controlled by clearance of the polymer components of the hydrogels from the SCS, which was significantly slower for CMC, which forms a physically crosslinked gel[143].

4.5.3 SCS thickness controlled by balance between viscous forces of the liquid formulation and biomechanical forces of the tissue

We propose that SCS thickness is controlled by a balance between the viscous forces of the liquid formulation and the biomechanical forces inherent to the tissue (such as the viscoelastic properties of the sclera and choroid, as well as the viscoelastic and failure mechanics of the SCS fibrils). A cartoon of this is presented in Figure 4.12. When fluid first enters the SCS, it can expand the thickness of the SCS at the site of injection and/or it can expand the area of the SCS that it occupies. We propose that what determines how the SCS expands to accommodate the fluid is based on whether there is less physical resistance to increasing thickness or to increasing area. Increasing thickness will require overcoming biomechanical forces (e.g., from fibrils connecting sclera to choroid) and elastic restoring forces of the sclera and choroid tissues[151] [13, 151, 152]. Intraocular pressure differences between the SCS and adjacent tissues may also play a role[34]. Increasing area will require overcoming the viscous forces opposing flow of fluid circumferentially in the SCS.

We further propose that the required force increases with increasing SCS expansion in thickness, while the required force of viscous flow within the SCS is a function of fluid viscosity and SCS thickness. We hypothesize that when the SCS is fully collapsed, the force required to expand the thickness of the SCS is less than the force to flow liquid through the adjacent collapsed SCS to expand the area. As more fluid is forced into the SCS, the SCS thickness continues to expand until the force required for further expansion of thickness of SCS exceeds the force required to flow fluid out into adjacent SCS. This switch occurs due to two factors: (i) as the SCS thickness increases, the force required to further increase thickness escalates and (ii) as the SCS thickness increases, the viscous forces to flow into adjacent SCS decrease because flow through wider channels exhibits less resistance to flow.

When injecting HBSS (with a low viscosity comparable to water) into SCS of the rabbit, the force balance switches when the SCS is expanded to 150 – 350 µm in the rabbit eye *ex vivo* and to 400 – 500 µm in the rabbit eye *in vivo*; we can call this thickness the “equilibrium thickness,” because it represents the thickness when the force needed to expand thickness equals the forces needed to expand area of the SCS. In this way, SCS expansion readily expands to the equilibrium thickness, because increasing SCS area requires less force than further increasing SCS thickness. A distribution of equilibrium thicknesses is expected, as seen in Figure 4.12, due to variation in the mechanical properties of the SCS.

When injecting Discovisc or CMC, which have higher viscosity than HBSS (e.g., >170,000 cP for 1.7% CMC (700 kDa) in HBSS[128, 143]), the force balance should be altered. The force to expand SCS thickness may only be marginally affected by the increase in viscosity, because the main resistance to expansion is from the ocular tissues, not from viscous flow. In contrast, the force to expand SCS area may be significantly affected, because expansion of area requires flow of fluid into narrow channels of SCS that becomes increasingly difficult as viscosity increases. Thus, the equilibrium thickness of the SCS increases, because expansion of SCS area requires greater force.

In the case of 3% CMC and 5% CMC solutions, there is an additional force in play. After the fluid has been injected and the SCS expanded to its equilibrium value, diffusive forces pulling fluid into the CMC gel formed in the SCS cause the gel to expand. Because the gel has physical crosslinks, it cannot easily flow through SCS to expand area, but instead expands in place, which primarily expands SCS thickness. In this case, a new force balance is set up between the expansive swelling force of the gel and the resistive biomechanical forces of the ocular tissue. This results in a new equilibrium thickness based on the balance of these two forces.

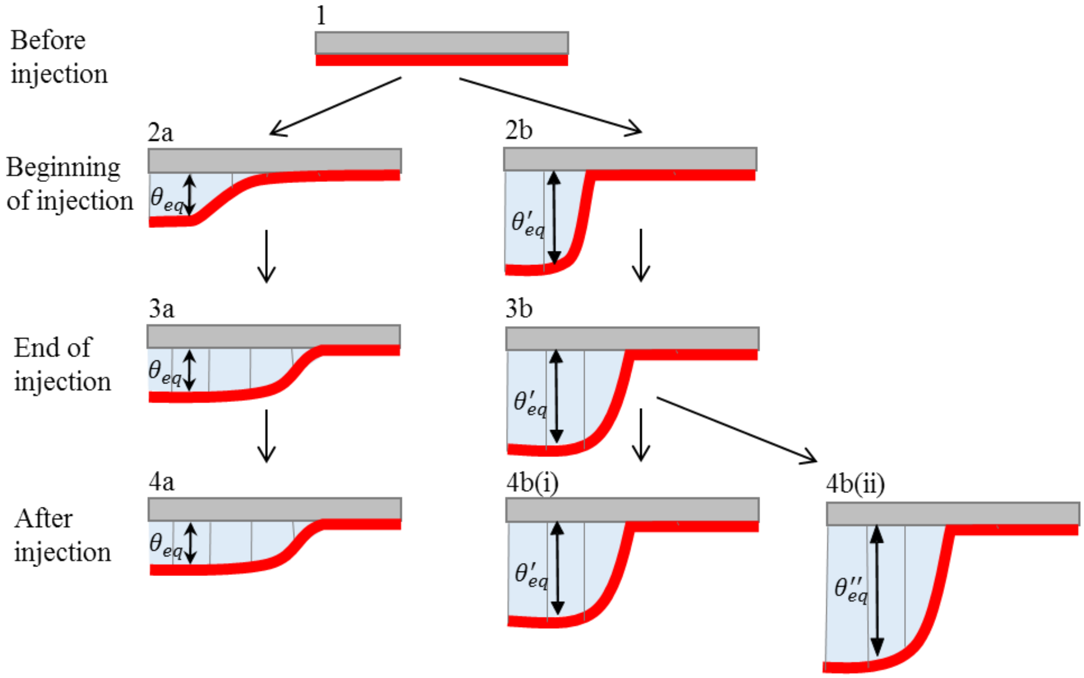

Figure 4.12 – Schematic of SCS expansion after injection of fluid. (1) The SCS is closed before injection. (2) Upon injection the SCS expands to an equilibrium thickness (θ_{eq}*) determined by a balance between viscous forces of the liquid formulation and the resistive biomechanical forces of the tissue. This thickness is smaller for low-viscosity fluids (*θ_{eq}* in 2a) than for high-viscosity fluids (*θ_{eq}*' in 2b), due to increased resistance to flow. (3) As the injection proceeds, the area of expanded SCS increases to accommodate the additional fluid, but the SCS thickness remains constant. (4) After injection is complete, no further growth of the SCS usually occurs (4a, 4b(i)), but a gel that continues to swell could further increase SCS thickness (*θ_{eq}*" in 4b(ii))*

4.5.4 Additional comments

The ability to modulate SCS thickness could have implications on emerging SCS technologies, such as targeted drug delivery, placement of glaucoma drainage devices, and suprachoroidal retinal prostheses. For example, increasing liquid formulation viscosity has a dual effect of expanding the SCS and localizing the circumferential spread at the site of injection. This might be useful in treating localized diseases, such as placing anti-glaucoma agents in the anterior SCS near their site of action in the ciliary body[6, 115] or localizing anti-cancer agents in the SCS adjacent to intraocular tumors. In another application, SCS injections of sodium hyaluronate have been made as an alternative to scleral buckling for the treatment of retinal detachment[153, 154]. As shown in the present study, greater distension and localization are achievable with CMC, which continues to expand after injection, compared with hyaluronic acid (i.e., a major component of Discovisc), which does not. Perhaps use of CMC as a liquid formulation may yield better results. Finally, microneedle injection of a viscous liquid formulation could be made prior to surgical implantation of suprachoroidal devices. This could transiently weaken sclera – choroid adhesion (e.g., stretch or break SCS fibrils), allowing for easier implantation.

There was a difference between the *ex vivo* and *in vivo* SCS thickness. *Ex vivo* eyes were chosen to remove the confounding effect of fluid clearance from the eye that occurs *in vivo*. Intraocular pressure changes in *post mortem* eyes were significantly faster than eyes in the living rabbit, indicating faster normalization of ocular volume, presumably by clearance of fluid. This difference in behavior could be explained by loss of tissue integrity (e.g., loss in the biomechanical strength of sclera or SCS fibrils), the absence of living process (e.g., choroidal perfusion, intraocular pressure), or consequences of these effects (e.g., increased trans-scleral and perivascular drainage).

Increasing formulation viscosity had a modest effect on the residence time of small molecules dissolved in the formulation. This effect could be explained by decreased diffusivity through the viscous formulation compared with less viscous formulations. Controlled-release polymeric systems[115] may be more suitable if the goal is drug delivery for one month or longer.

Limitations of the study include use of *ex vivo* rabbit eyes in some experiments. Species differences between rabbit and human eyes may affect the translation of these findings to clinical medicine. Further experiments in human eyes are warranted. The U/S was only able to image the far periphery, not the posterior aspect of the eye. This may bias the SCS thickness measurements but should not change the general trends observed.

4.6 Conclusions

In conclusion, microneedle injection of fluid into the SCS results in distension of the choroid off the sclera, which expands the thickness of the SCS. Liquid formulation injected into the SCS had a major effect on SCS thickness, where highly viscous fluids expanded SCS thickness more than low-viscosity HBSS. Surprisingly, increasing injection volume of HBSS had no significant effect on SCS thickness, such that injection of increasing volume of fluid was accommodated by increasing area of fluid spread in the SCS while maintaining constant SCS thickness. Expansion of SCS thickness *in vivo* ranged from 0.43±0.06 mm after injection of HBSS and 0.7 – 2.8 mm after injection of viscous formulations. Injection of CMC solutions led to further expansion of SCS thickness over the course of hours after the injection was completed, which could be explained by swelling of CMC gel in the SCS. Clearance of HBSS from the SCS occurred within 1 h and clearance of Discovisc and CMC took days to weeks.

These observations could be explained by SCS expansion controlled by a balance between the viscous forces of the injected liquid formulation (which increase with fluid viscosity) and the biomechanical forces that hold the sclera and choroid together (which are unaffected by fluid viscosity or fluid volume). There is evidence that the forces that limit expansion of SCS thickness may be in part related to fibrils that bind the sclera and choroid and that may need to stretch and/or break to accommodate SCS expansion. These findings that affect the extent and duration of expanded SCS thickness and area, may be used to improve control over targeted drug delivery and placement of devices in the SCS for therapeutic applications.

5 CLEARANCE KINETICS AND CLEARANCE ROUTES OF MOLECULES FROM THE SUPRACHOROIDAL SPACE AFTER MICRONEEDLE INJECTION

5.1 Summary

The purpose of this work was to determine clearance kinetics and routes of clearance of molecules injected into the suprachoroidal space (SCS) of live New Zealand White rabbits.

The SCS collapse rate was determined by ultrasonography after microneedle injection of Hank's Balanced Salt Solution (HBSS). Fluorescent fundus images were acquired to determine clearance rates of fluorescent molecules ranging in molecular mass from 323 Da to 2 MDa and 20-nm green-fluorescent polymeric particles. A microneedle injection containing fluorescein in HBSS was performed, and samples were taken over time to determine amount of fluorescein on the scleral surface at the injection site, on the anterior surface and on the posterior surface, including sites where vortex veins penetrated through sclera. Blood was also sampled from the vortex vein. Clearance transport was modeled theoretically and compared to data.

We found that after injection of 50 µL of HBSS solutions, intraocular pressure (IOP) spiked and then returned to baseline over a characteristic time of ~5 min. There was no significant difference between pressure in the SCS and the vitreous humor. After injection, SCS expanded and then collapsed over a characteristic time of ~20 min, which provides a measure of the time scale of fluid clearance from the SCS. Characteristic time of clearance of molecules from the SCS ranged from 4 h to 26 h, in proportion to molecular mass. Total clearance time from the SCS (i.e., below detection limit) ranged

from 22 h for fluorescein to 21 d for 2 MDa FITC-dextran. Nanoparticles were not cleared from the SCS at all. One hour after fluorescein injection, 57% was still present in the eye, 14% had transported through the sclera, 6% had been cleared by the choroidal vasculature, and 3.8% had refluxed out the injection site or via perivascular leakage pathways. These data generally agreed with predictions from a two-dimensional model of clearance transport.

In conclusion, clearance of molecules from the SCS occurred in three regimes: (i) on a time scale on the order of 10 min, fluid and molecules were cleared from the SCS by pressure-driven reflux out leakage sites across the sclera (i.e., injection site and perivascular drainage) and remaining molecules were transported out of the SCS into the choroid and sclera, (ii) on a time scale of 1 – 10 h, molecules were cleared from the choroid by blood flow and (iii) on a time scale of days up to weeks, molecules were cleared from the sclera by diffusion as well as IOP-driven convection. Clearance kinetics were strongly dependent on molecular size, where 2 MDa FITC-dextran was cleared significantly slower than smaller molecules.

5.2 Introduction

Suprachoroidal drug delivery is an emerging route of administration that targets diseased tissues in posterior segment diseases, such as age-related macular degeneration and uveitis[2, 7, 81, 119]. Since the suprachoroidal space (SCS) is bounded by the ciliary body, choroid, and sclera, significantly higher bioavailability at these tissues can be achieved with SCS delivery compared with eye drops or intravitreal (IVT) injections[5, 8, 123, 124, 126]. Due to higher bioavailability, significant dose sparing can be achieved with drugs that have their site of action at these tissues[6, 9]. Fewer ocular side effects are expected due to dose sparing and also because drugs are compartmentalized away from non-target tissues (e.g., lens). Furthermore, a short needle, with a length matched to the thickness of the sclera (aka, a microneedle), can be used in an outpatient procedure similar to an IVT injection[7, 8]. Indeed, the safety and tolerability of a microneedle injection has been demonstrated in a Phase I/II clinical trial (NCT01789320) where triamcinolone acetonide was injected into the SCS to treat non-infectious posterior uveitis[7]. Other indications are also actively being pursued.

When comparing the pharmacokinetics of molecules in the SCS against IVT injections, higher levels of injected molecules have been found in the chorioretina with significantly faster clearance. Olsen et al. reported that 12 h after SCS injection, higher levels of bevacizumab were found in the chorioretina compared with IVT injection[9]. However, at 7 days, bevacizumab was undetectable in the SCS group, but remained relatively high in the IVT group. Patel et al. observed a clearance half-life of 3.6 – 7.9 h for various macromolecules injected into the SCS[8, 81]. Tyagi et al. reported that sodium fluorescein concentration in the chorioretina was 25-fold higher after SCS injection compared with IVT injection; however, 2 h after injection, fluorescein levels in the chorioretina were higher in the IVT injection group than in the SCS group[124]. Similarly, Wang et al. found that the elimination half-life of ketorolac was longer with intravitreal injections than SCS delivery (3.1 hr vs. 1.2 hr)[5]. Interestingly, Wang et al. reported a lower C_{max} in the chorioretina for the SCS group than the IVT group. Gu et al. found that the SCS collapsed to baseline levels within 1 h[120]. To our knowledge, no studies have systematically investigated factors that affect clearance from the SCS.

Although prior studies have investigated the pharmacokinetics of SCS delivery, only limited information exists about different routes of clearance from the SCS and their relative contributions to clearance. Moseley et al. found that the clearance of Xenon and radioactive water injected intravitreally was due to choroidal blood flow[11, 155]. Indeed, Olsen et al. and Tyagi et al. hypothesized that molecules injected into the SCS are rapidly cleared by choroidal blood flow[9, 123]. Abarca et al. demonstrated significantly faster clearance of fluorescein from the SCS with choroidal perfusion than without in a postmortem porcine model[126]. Classical experiments performed by Bill et al. in elucidating the uveoscleral outflow pathway showed that microspheres injected into the anterior chamber were found trapped in the SCS where blood vessels penetrated through the sclera[41, 43]. These particles were able to exit the eye through perivascular drainage routes. Since SCS injections expand the SCS and generate a significant pressure gradient out of the SCS, we believe the mechanisms elucidated by either Moseley et al. or Bill et al. do not provide the complete picture.

The purpose of this work is to measure clearance kinetics and to identify the dominant routes of clearance from the rabbit SCS after microneedle injection. We hypothesize that clearance of fluid and dissolved molecules injected into the SCS occurs initially through leakage sites across the sclera (i.e., injection site and perivascular drainage) and then by trans-scleral transport. Later, clearance from the SCS is by diffusion into and clearance by the choriocapillaries.

5.3 Methods

All reagents and chemicals were purchased from Sigma-Adrich (St. Louis, MO) unless otherwise specified. All experiments were performed in albino New Zealand

White rabbits (Charles River, Wilmington, MA) and were approved by the Georgia Institute of Technology Institutional Animal Care and Use Committee. Practices complied with the ARVO Statement for the Use of Animals in Ophthalmic and Vision Research.

5.3.1 Microneedle injection

The rabbit was anesthetized with isoflurane and an eye drop of proparacaine (Bausch & Lomb, Rochester, NY) was given as a topical anesthetic prior to injection. For all experiments, a 50 µL injection was performed in each eye with a 33-gauge microneedle approximately 750 µm in length (Clearside Biomedical, Alpharetta, GA) and a 1 mL syringe. All injections were made in the supranasal quadrant 3 mm posterior to the limbus and 4 mm nasal to the superior rectus muscle. Four eyes were used in each group unless otherwise specified. The 50 µL injection occurred in 3 s. After injection, the needle was kept in place for 1 min to limit reflux at the injection site.

5.3.2 Determination of SCS collapse rate by ultrasonography

High-frequency ultrasound B-scan (U/S; UBM Plus, Accutome, Malvern, PA) was used to determine the rate of SCS collapse after a microneedle injection of 50 µL Hank's Balanced Salt Solution (HBSS; Mediatech, Manassas, VA) into the SCS. Three sagittal views were acquired: (a) supranasal, over the injection site; (b) superior, 45° lateral to the injection site; and (c) nasal, 45° nasal to the injection site. Image acquisition occurred every minute for 10 min, and then every 2 min for 1 h.

Off-line post processing was performed on the U/S views to determine the SCS thickness. For each U/S image, a line segment 5 mm posterior to the scleral spur and perpendicular to the sclera was found. The line started at the outer surface of the sclera and ended at the inner surface of the retina, which were readily identifiable on the U/S images. The sclera and chorioretina were included in the measurement to ensure the line was perpendicular. SCS thickness was determined as the length of the line segment minus the thickness of the sclera and chorioretina. The characteristic time of SCS collapse was determined by modeling SCS thickness versus time as an exponential decay.

5.3.3 Fluorescent labeling of monoclonal antibody

Bevacizumab (Avastin, Genentech, South San Francisco, CA) was fluorescently labeled with fluorescein isothiocyanate (FITC) using previously described methods[40]. Briefly, 40 mg FITC was added to a 1.0 mL sodium bicarbonate (pH = 9) solution, and 3 mL of bevacizumab solution (25 mg/mL) was added to the FITC solution and stirred in the dark for 2 h at room temperature. The solution was dialyzed against phosphate buffered saline (PBS) using dialysis tubing with a cutoff of 30 kDa (Spectra/Cor, Spectrum Laboratories, Rancho Dominguez, TX). The PBS was changed daily for 5 days to remove unreacted FITC.

5.3.4 Determination of SCS clearance kinetics by fundus imaging

To study the effect of molecular radius on clearance from the SCS, a 50 µL microneedle injection of the following formulations were tested: [i] 0.025% (w/v) fluorescein sodium in HBSS; [ii] 0.5% (w/v) 70 kDa FITC–dextran in HBSS; [iii] 00.5% (w/v) 500 kDa FITC-dextran in HBSS; [iv] (w/v) 2 MDa FITC–dextran in HBSS; [v] 1.5% (w/v) FITC–bevacizumab in HBSS; and [vi] 1% (w/v) 20 nm green-fluorescent particles (Excitation: 505 nm, Emission: 515 nm; FluoSpheres, Life Technologies, Carlsbad, CA) in HBSS.

The clearance rate of injected fluorescent material from the SCS was estimated by taking fluorescence fundus images over time. Topical eye drops of tropicamide and phenylephrine (Akorn, Lake Forest, IL) were administered prior to each imaging session to dilate the eye. A RetCam II (Clarity Medical Systems, Pleasanton, CA) with the 130° lens attachment and the built-in fluorescein angiography module was used to acquire the images. Multiple images were taken with the blue light output from the RetCam II set at 0.0009, 1.6, or 2.4 W/m^2. In an attempt to capture the entire interior surface of the ocular globe, nine images were captured: central, supranasal, superior, supratemporal, temporal, infratemporal, inferior, infranasal, and nasal. This allowed imaging into the far periphery. Imaging was done 3 min after injection, at 1 h, every 3 h for 12 h, and every other day post-injection for up to 28 days.

The relative concentration of the injected fluorescent molecules was estimated for each eye at each time point by comparing the average fluorescence intensity with aliquots of known concentrations imaged using the same lighting conditions for calibration. The characteristic times of SCS clearance rate and total clearance time were determined by modeling these processes as exponential decays in fluorescein concentration in the SCS over time.

5.3.5 Intraocular pressure measurements

A custom-designed pressure measurement system was used to measure pressure in the vitreous humor (VH) and in the SCS after either an IVT or SCS injection. The animal was terminally anesthetized with a subcutaneous injection of a ketamine and xylazine cocktail. A 33 gauge, 0.5 inch hypodermic needle was penetrated through the pars plana into the VH, and a 33 gauge microneedle was penetrated through the sclera 3 mm posterior to the limbus to access the SCS. Both needles were connected by polyethylene tubing (I.D. 1.14 mm, Becton Dickinson and Company, Sparks, MD) to a T-junction (i.e., to switch between the SCS and VH) that was in fluid communication with a second T-junction. The second T-junction allowed switching between either a 1 mL syringe (to inject HBSS into either the SCS or the VH) or a pressure transducer (Honeywell 142PC01, Morris Plains, NJ). The pressure transducer was zeroed to the height of the eye, and the height difference of the needle openings was also found (<10 mm height difference). A custom Labview (National Instruments, Austin, TX) script was used to record the pressure trace.

A 50 µL SCS or IVT injection (N=4 per injection site) was made either in the SCS or the VH, respectively. The pressure in the SCS and VH was measured by switching the T-junction between the two sites every few minutes. The pressure was monitored until the pressures had reached their original baseline values from before the injection (i.e., ~15 mmHg). After the measurements, the animal was euthanized with a lethal dose of pentobarbital injected intravenously. A second set of SCS and IVT injections was made in the animal postmortem. In the postmortem measurements, pressure was only measured in the tissue space (i.e., SCS or VH) where the injection was made.

The characteristic times of elevated pressure in the SCS and VH were determined by modeling these processes as exponential decays in pressure over time.

5.3.6 Collection of fluorescein by different clearance routes

For this terminal experiment, the rabbit (N=4 eyes per group) was anesthetized with a subcutaneous injection of ketamine and xylazine before microneedle injection;

additional injections were given every 30 min to maintain anesthesia. A subcutaneous injection of 60 mL saline was also given on the rump to counteract fluid loss. The amount of fluorescein exiting the eye by four routes was determined by collecting samples over time from the [i] sclera anterior to the equator; [ii] anterior sclera with injection site plugged; [iii] sclera posterior to the equator; and [iv] posterior sclera with vortex vein transected.

Prior to the microneedle injection, the conjunctiva in the supranasal quadrant was carefully dissected off the sclera. A 50 µL microneedle injection was performed supranasally 4 mm nasal to the superior rectus muscle and 3 mm posterior to the limbus. In the [i] anterior sclera and [iii] posterior sclera conditions, samples were collected every minute for 10 min, and every 2 min for 1 h by swabbing the space with a 1 cm x 1 cm paper tissue (Kimwipe, Kimberley-Clark, Irving, TX) for the entirety of time between each time point (i.e., one or two minutes). Care was taken to swab only anterior or posterior to the equator, depending on the condition. The tissue was then placed in 1 mL of HBSS until analysis.

To determine the amount of fluorescein leaving [ii] the anterior sclera with injection site plugged, a similar experiment was performed. Immediately post-injection, the site of injection was plugged by carefully applying cyanoacrylate glue (Loctite 4013, Düsseldorf, Germany) with a 30 gauge needle to the microneedle hub to seal the gap between the microneedle and surrounding scleral tissue. After the microneedle injection occurred, the microneedle was left in the eye. Other methods were the same as above.

For the eyes that had a vortex vein cut [iv], the superior vortex vein was transected prior to injection. Heparin (5 mL of 10,000 IU/mL; Hospira, Lake Forest, IL) was given intravenously prior to the start of the experiment to prevent coagulation. The vortex vein was found under the nasal edge of the superior rectus muscle. The rectus muscle was lifted off the ocular surface to expose the vortex vein. The vortex vein was confirmed by verifying its path, i.e., originating from within the sclera and traveling posteriorly along the ocular surface towards the optic nerve. A transfer pipette was used to collect the blood exiting the vortex vein every 1 min post-injection for 10 min, and every 2 min for 1 h. The volume of collected blood collected was recorded and HBSS was added to reach a final volume of 2 mL per sample for analysis.

Immediately after the last time point, all animals were euthanized with an injection of pentobarbital through the marginal ear vein. The eyes were enucleated to measure the amount of fluorescein remaining in the vitreous humor and within the tissue (including the SCS). An incision in the cornea was made so the aqueous humor, vitreous humor, and lens could be drained from the ocular globe and collected. The remaining ocular tissues (with undisturbed SCS) were collected. The Kimwipe paper tissue and ocular tissue samples were placed in HBSS at 4 °C for 2 days to allow the fluorescein to diffuse out and equilibrate with the HBSS. It is possible that fluorescein bound to the Kimwipe tissue paper but it should have done so equally for all conditions tested. The amount of fluorescein in all samples was measured using a multiplate reader (Synergy H4, BioTek, Winooski, VY) with parameters set to excitation = 494 nm and emission = 521 nm.

Further analysis was performed using Matlab (MathWorks, Natick, MA) and Prism (Graphpad, La Jolla, CA) software. The characteristic times of clearance rate via each route were determined by modeling these processes as exponential decays in fluorescein concentration over time.

5.3.7 Data and Statistical Analysis

Prism and Matlab software were used to perform data and statistical analysis. Data were fit to exponential decays to find relevant parameters (e.g., time constant) using the formula $y(t) = Y_0 e^{(-t/\tau)}$, where t is the time post-injection, y(t) is the SCS thickness or fluorescent-molecule fluorescence at time t, Y_o is the maximum SCS thickness or fluorescent-molecule fluorescence, and τ is the characteristic time constant of SCS collapse or fluorescent molecule clearance, respectively. Other data were fit to an exponential approach function, $\mathrm{N}(t) = N_0\left(1 - e^{(-t/\tau)}\right)$, where t is the time post-injection, N(t) is cumulative amount of fluorescein collected at time t, N_o is the maximum amount of fluorescein, and τ is the characteristic time constant.

All values are reported either as mean ± standard error of the mean (mean±SEM), or mean and 95% confidence interval (mean [95% CI]), unless otherwise specified. One-way ANOVA analysis was performed to determine statistical significance (α=0.05) among multiple conditions. F test was used to compare parameters generated by curve fits.

5.4 Results

5.4.1 SCS collapse rate as a measure of fluid clearance rate from the SCS

We determined the SCS collapse rate in live rabbits after microneedle injection of HBSS into the SCS (Figure 5.1). Under typical conditions before injection, the sclera and choroid in rabbits were apposed since the SCS is normally collapsed (Figure 5.1A, pre).

Upon microneedle injection, fluid was introduced into the SCS, which caused the choroid to distend off the sclera. This created a gap between the sclera and choroid when viewed under ultrasound B scan (Figure 5.1A, 1 min), which we tracked over time and used as a proxy for SCS collapse rate and fluid clearance rate. Since the SCS expansion due to HBSS can be measured directly, no tracers or contrast agents were added to the fluid.

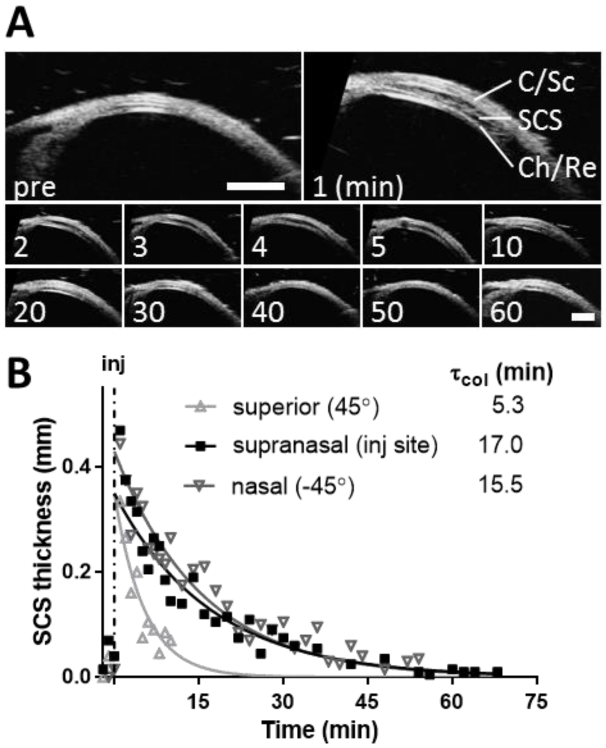

Figure 5.1 – SCS thickness over time determined by ultrasound B-scan images acquired during supranasal injection of 50 µL HBSS into the SCS of the live rabbit. (A) Representative B-scans of time course. C/Sc = conjunctiva/sclera interface; SCS = expanded suprachoroidal space; Ch/Re = choroid/retina interface. Scale bar represents 1 mm. (B) Quantification of SCS thickness (mean only, N = 2-6 replicates) 2 mm posterior to scleral spur at three locations. The SEM for all time points ranged from 0.00 to 0.21 mm with a mean of 0.06 mm. Reported time constants (τ_{col}) were derived from exponential-decay curve fitting.

After a 50 µL injection in the supranasal position, we tracked collapse of the SCS as a function of time directly over the injection site and also superiorly and nasally (Figure 5.1B). The data were fit to an exponential decay (r^2=0.62-0.71). One minute after the injection, the SCS thickness over the injection site was 470 ± 60 µm (mean±SEM). The collapse time constant (τ_{col}) was 19 min [15; 27 min 95% confidence interval]. The

SCS expansion was indistinguishable from pre-injection thickness by 40 min post-injection. There was no significant difference in the curve fits for the measurements made supranasal or nasal ($p=0.89$, F test). Collapse rate of the superior SCS ($\tau = 5.5$ min [3.9; 9.4 min]) was significantly faster than the other two positions measured ($p<0.05$, F test). This could be due to nearby perivascular drainage routes, but more experiments are warranted to explore this hypothesis.

5.4.2 Clearance rate of fluorescent molecules from the SCS

We determined the clearance rates of different-sized fluorescent molecules and a fluorescent nanoparticle injected as solutions into the SCS of live rabbits. The molecules ranged in molecular weight from 332 Da (fluorescein) to 2 MDa (FITC-dextran), which corresponds to effective molecular diameters of roughly 1 nm[38] to 54 nm[156, 157], respectively. The nanoparticle measured 20 nm in diameter. Bright-field and fluorescence fundus images were acquired for each fluorescent molecule tested over time (Figure 5.2). Since the rabbits were albino, the eyes were unpigmented, which made the choroidal vessels readily visible beneath the inner retinal vessels (Figure 5.2, pre (brightfield)). Furthermore, there was no detectable green autofluorescence with the light level used (Figure 5.2, pre).

After injection, the fluorescent molecules and nanoparticles were visible in the SCS (Figure 5.2, 3 min and 14 d); localization in the SCS (i.e., behind the choroid) was confirmed by the shadowing of the choroidal vessels over the green fluorescence. Three minutes after injection, fluorescein in HBSS and 2 MDa FITC-dextran in HBSS distributed similarly in the SCS, occupying 56±6% and 58±7% of the visible SCS respectively ($p=0.95$, Dunnett's test). Both fluorescein and 2 MDa FITC-dextran covered larger areas of SCS than the nanoparticles (28±6%; $p<0.05$, Dunnett's test).

We further determined the rate of clearance by determining (i) the total clearance time and (ii) the clearance time constant ($\tau_{clearance}$) calculated using a curve fit derived from the normalized concentration of fluorescein over time. We defined total clearance time as the first time point post-injection where fluorescence was not detected in the fundus images. Representative time courses for fluorescein (Figure 5.2, upper row and Figure 5.3A) and 2 MDa FITC-dextran (Figure 5.2, middle row and Figure 5.3B) show the rates of clearance and the calculated total clearance time. In the representative images in Figure 5.3A and B, the fluorescein is not visible by 1 d, whereas the 2 MDa FITC-dextran was not totally cleared until 21 d.

The fluorescence was tracked via fundus examinations with a series of lighting conditions, and used to estimate relative concentration of the fluorescent molecules over time in the SCS. For each fluorescent molecule, the data were fit to an exponential decay ($r^2 > 0.84$; Figure 5.3C). The time constants from the curve fits are shown in Figure 5.3D (closed squares), along with the total clearance time (Figure 5.3D, open circles) for all the fluorescent species tested.

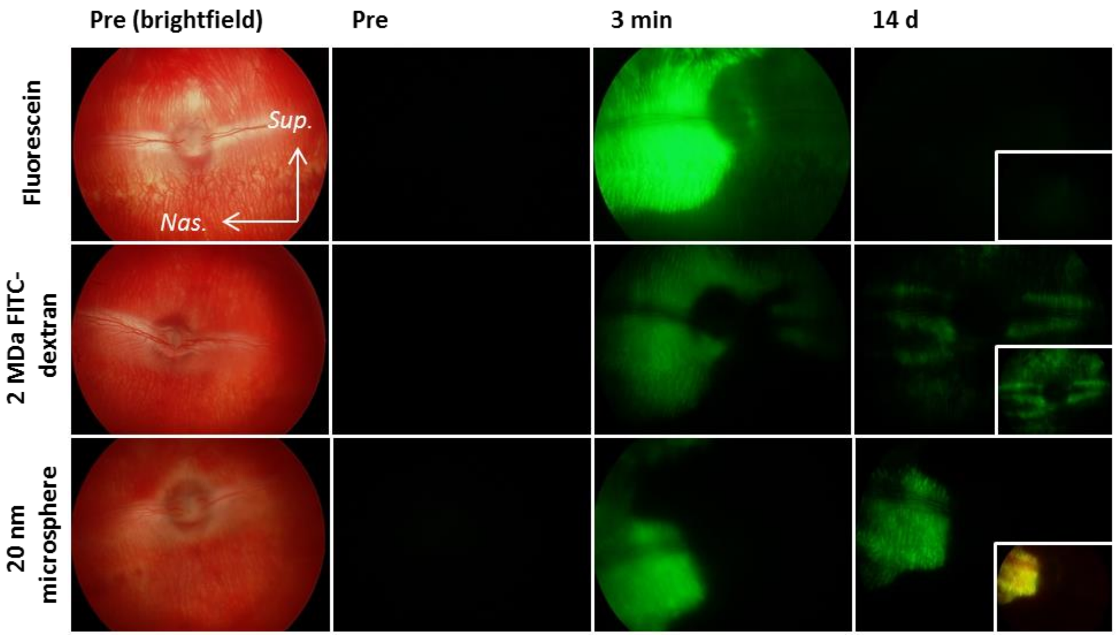

Figure 5.2 – Representative brightfield and fluorescent fundus images of the live rabbit eye before, 3 min post- and 14 days post-injection of 50 µL of fluorescein, 2 MDa FITC-dextran, or 20 nm polystyrene particles. Three minutes post-injection, the fluorescein and 2 MDa FITC-dextran were distributed approximately equally. The microspheres occupied less area than the other formulations. The 2 MDa FITC-dextran is still visible 14 days post-injection The particles were visible for at least 2 mo (data not shown). Inset depicts fundus image taken under brighter light setting, enabling visualization of regions with lower level of fluorescence. All eyes oriented such that up is superior (sup.) and nasal is left (nas.). Fundus field of view is 130°.

Clearance time constant was linearly dependent on molecular diameter (Figure 5.3D, r^2=0.87), varying from 4.3 ± 0.4 h for fluorescein and 26 ± 9.8 h for 2 MDa FITC-dextran. Total clearance time could also be fit to a line (Figure 5.3D, r^2=0.43), but appears to show nonlinearity at high molecular size. While clearance time constant had a similar value to total clearance time for the smaller molecules, total clearance time was bigger for the larger molecules, suggested a biphasic clearance rate for which a fraction of the larger molecules persist in the SCS for a long time. The nanoparticle was not cleared from the SCS for the duration of the study (> 2 months). Despite differences in molecular weight and chemical structure between FITC-dextran and FITC-bevacizumab, clearance times were similar due to comparable hydrodynamic diameter of 70 kDa FITC-dextran (~12 nm[38]) and FITC-bevacizumab (~11 nm[158]), further indicating the dominant role of molecular diameter in determining SCS clearance.

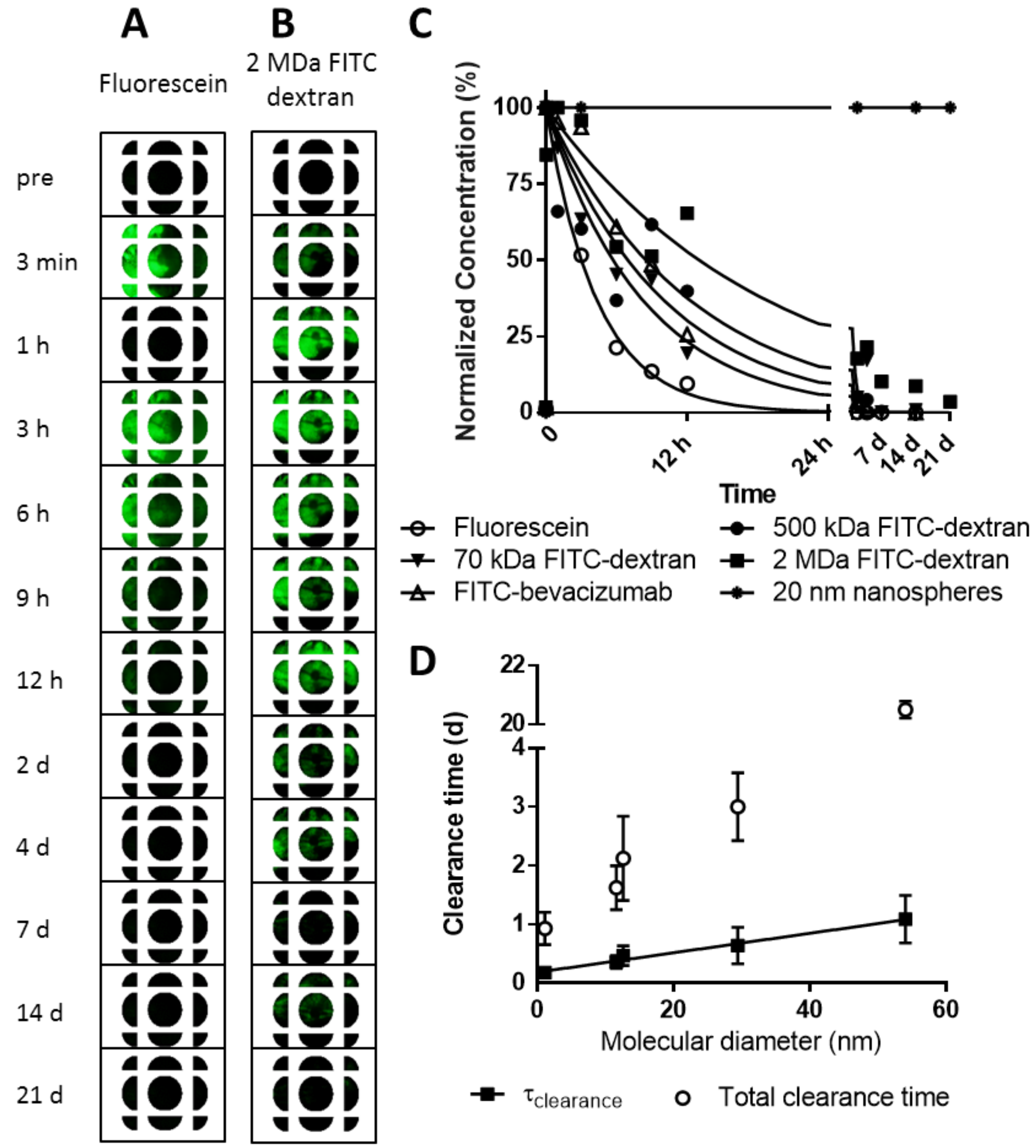

Figure 5.3 – Analysis of rates of clearance from the SCS after 50 µL SCS injection with molecules ranging from 1 – 60 nm in diameter and a 20 nm polystyrene particle. (A) Representative fundus collages after injection with fluorescein in HBSS. (B) Representative fundus collages after injection with 2 MDa FITC-dextran in HBSS. (C) Quantification of fluorescein/FITC- concentration with curve fit to an exponential decay. (D) Clearance time constant from ($\tau_{clearance}$, from curve fit in C) and total clearance time plotted against hydrodynamic molecular diameter. All values are mean±SEM (N=3-7 replicates).

5.4.2.1 Intravitreal and SCS pressure measurements

We measured pressure in the VH and suprachoroidal spaces after IVT or SCS injection using a custom-designed setup. The VH pressure trace after IVT injection was consistent with prior literature, showing a roughly exponential decay in pressure that returned to within 10% of baseline value within 15 min[17, 98]. After SCS injection, the VH pressure followed a similar timecourse, returning to within 10% of baseline value by 15 min too. The VH and SCS pressure traces were within ±1 mmHg of each other throughout the length of the experiment.

Each data set was fit to an exponential decay, from which a pressure-decay time constant ($\tau_{pressure}$) was calculated (Figure 5.4). Although the pressure-decay time constants after SCS injection (~3 min) appear to be smaller than after IVT injection (~5.5 min), there was no significant difference between any of the four time constants derived from the VH and SCS pressure curve fits after IVT or SCS injection *in vivo* ($p=0.98$, 2-way ANOVA). Thus, we conclude that the time course of pressure decay in the eye is the same after IVT or SCS injection. We also conclude that there is no significant pressure different between the VH and SCS after IVT or SCS injection.

Injections made postmortem in the companion eye resulted in significantly faster depressurization (~ 1 min) than injections *in vivo* ($p<0.05$, 2-way ANOVA). Since the eye was not enucleated and tissue degradation had likely not yet happened, we believe the main difference between the *in vivo* eye and the postmortem eye is the lack of living processes, such as choroidal perfusion. Our data suggest that these living processes have a major effect on SCS clearance. With no blood flow through the vortex veins, they are likely collapsed upon SCS injection, and therefore, SCS clearance through perivascular drainage routes is expected to be greater postmortem than *in vivo*, which may explain the faster decay in IOP in the postmortem eye. Another possible explanation is that blood volume was expelled from the eye upon SCS injection (as there was no resistance to venous flow).

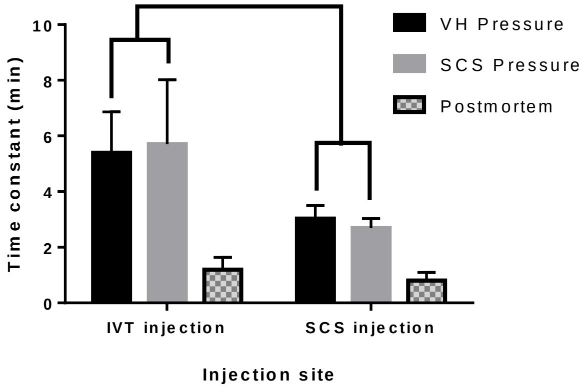

Figure 5.4 – Pressure measurement in vivo and postmortem after SCS injection of 50 µL HBSS. Pressure-decay time constants derived from fitting data to an exponential decay. No difference in time constants from SCS or VH pressure traces after SCS or IVT injections in vivo. In vivo time constants were different than postmortem time constants. All values are mean±SEM (N=4 replicates).

5.4.3 Route of clearance after SCS injection

To determine the contributions of different routes of clearance, we collected fluorescein from multiple collection sites after SCS injection *in vivo* (Figure 5.5). Fluorescein was collected over the course of 1 h from four sites: [i] sclera anterior to the equator; [ii] anterior sclera with injection site plugged; [iii] sclera posterior to the equator; and [iv] posterior sclera with vortex vein transected. The cumulative fluorescein from these collection sites was determined as a function of time (Figure 5B). The amount of fluorescein leaving through the injection site (Figure 5.5B, upper right) was found by subtracting site [i] from site [ii]. And the amount of fluorescein leaving through the blood (Figure 5.5B, lower right) was found by subtracting site [iv] from site [iii]. Though the physiological data is inherently noisy and performing calculations on the data might yield errors, it should nevertheless yield an order of magnitude estimate of the underlying processes (which can be compared to a 2D model of transport below).

The cumulative amount of fluorescein collected at 1 h, as well as the residual amounts in the ocular tissues, was calculated and expressed as a function of the total fluorescein injected into the SCS (Figure 5.5C). One hour post-injection, 46±18% was still within the tissue (e.g., in the sclera, choroid, SCS, etc.); 15±0.3% had passed transsclerally to the subconjunctival space (anterior and posterior combined); and 6.3±4% was found in the blood. We calculated that 1.3±4% exited via the injection site and 2.5±0.3% exited via perivascular drainage around the vortex vein. We were unable to account for 28% of the fluorescein, though we assume it to be roughly equally distributed in the collection sites due to difficulty to achieve efficient fluorescein collection during dynamic transport to the scleral surfaces, and the expected efficiency of fluorescein extraction from the ocular tissues.

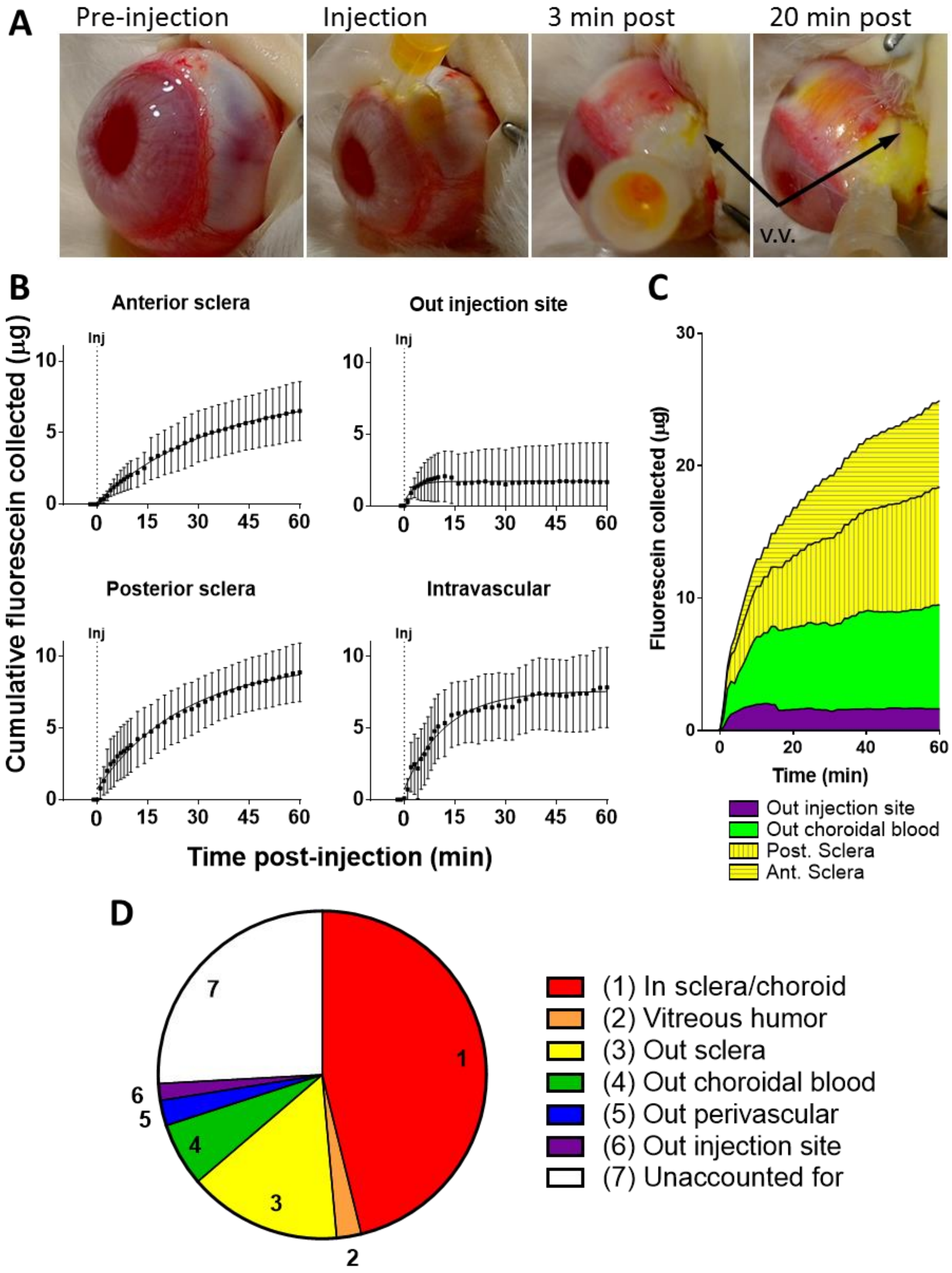

Figure 5.5 – Fluorescein collected from four routes out of the SCS after 50 µL SCS injection of fluorescein in HBSS. (A) Representative series of images of eye with the injection site plugged. (B) Cumulative fluorescein collected by swabbing anterior sclera after plugging injection site (B upper left), collected by swabbing posterior sclera (B lower left), calculated by comparing amount collected from anterior sclera with and without plugging injection site (B upper right), and calculated by comparing amount collected from posterior subconjunctiva with and without transecting vortex vein (B lower right). All values are mean±SEM (N=4 replicates) (C) Quantification of total fluorescein distribution in and out of the eye after SCS injection based on data in (B) and analysis of residual fluorescein content in the eye after enucleation.

5.5 Discussion

Microneedle injections enable targeted access to the SCS and can be performed with an out-patient procedure similar to intravitreal injections. Due to the high bioavailability at the sclera, choroid, ciliary body, and retina achieved with suprachoroidal drug delivery, this route of administration is well suited for targeting tissues diseased in posterior segment diseases. Ongoing clinical trials are testing the safety and efficacy of microneedle injections for the treatment of posterior noninfectious uveitis, as well as other indications. Although drug delivery via the SCS is receiving increasing attention, little is known about how molecules and fluid are cleared from the SCS in terms of clearance kinetics and routes of clearance.

In this study, we investigated the clearance kinetics of molecules injected into the SCS of live rabbits using a microneedle. Previous studies demonstrated decay of IOP after SCS injection on a time scale of minutes[17], which is expected to correlate with the time scale of fluid clearance from the SCS, and reported clearance of various molecules from the SCS on a time scale of hours[5, 8, 9, 120, 124, 125], both which we corroborated in this study. Previous studies have also found that the clearance times after suprachoroidal delivery were significantly faster than after IVT injections[102]. We also found that the complete collapse of the SCS occurred by 40 min, which is consistent with previous studies[120]. During the first hour post-injection, approximately half of injected fluorescein was cleared from the ocular globe, with approximately half still remaining. The remaining fluorescein was not visible by 12 h post-injection.

5.5.1 Modeling clearance from the SCS

We developed a two-dimensional model (2D) of small-molecule transport after microneedle injection into the SCS to corroborate our experimental results. A Cartesian coordinate system was used such that the x-direction was a ‘radial’ measure into and out of the eye and the y-direction was the ‘circumferential’ measure; at small distances (like the one used in the model), the curvature of the eye was ignored. The convection-diffusion equation (Eq. 5.1)[159] describes the rate of change in the amount of molecule in a control volume, and attributes changes in concentration due to diffusion (first term), convective flow (second term), and reaction or clearance (third term). The equation is as follows:

$$\frac{\partial c}{\partial t} = \nabla \cdot (\nabla D c) - \nabla \cdot \left(v_f c\right) - Bc \qquad \text{Eq. 5.1}$$

where c is the concentration of molecule, t is the time, D is the diffusion coefficient of the molecule through tissue, v_f is the velocity of flow, and B is a reaction or clearance coefficient.

Due to the complex ocular anatomy across different tissues, an analytic solution of the above was not found. Instead, this model utilized a modified random walk algorithm[160] to study the position and disposition of molecules by displacing the molecule at each time point in 2D based on the characteristic diffusional length a molecule would move in that time period, as well as additional rules as defined below. We defined the regions in the eye corresponding with the choroid, SCS, and sclera, which were set as 0.1, 0.05, and 0.3mm thick, respectively[161] (Figure 5.6A(i)).

Rules governing molecule movement at each time point (Δt) of the random walk algorithm was set as follows. The diffusivity within the choroid and sclera (both of which are limited largely by the proteoglycan extracellular matrix[162]) was set to 5×10^{-11} m^2/s (diffusion coefficient of fluorescein in sclera[163], corresponding to a characteristic diffusional length of 0.1 mm in 1 min. The diffusivity in the SCS was 5×10^{-10} m^2/s (diffusion coefficient of fluorescein in water[141]) corresponding to a characteristic diffusional length of 0.34 mm in 1 min.

Furthermore, we defined additional behaviors for regions in the model corresponding to ocular anatomy and physiology, in particular (region i) the choroid, (region ii) the sclera, and (region iii) a drainage pathway through the sclera analogous to the injection site (Figure 5.6A(i)). The choroid (region i) was subdivided into an inner and outer region, corresponding to the choriocapillaris and Haller's/Sattler's layers[164], respectively. The choriocapillaris[31] (as opposed to Haller's and Sattler's layers) possessed fenestrae capable of clearing molecules, which we modeled with a clearance rate B, whereas we assumed that no clearance occurred in Haller's and Sattler's layers.

The sclera (region ii) was able to bind fluorescein (and prevent diffusion or convection) with second-order kinetics[163], as described by the following equation:

$$C_b = \frac{B_{max} C_f}{K_D + C_f} \qquad \text{Eq. 5.2}$$

where C_b is the concentration of bound fluorescein, C_f is the concentration of free fluorescein, B_{max} is the apparent maximum binding capacity of the sclera (experimental determined to be 1440 µM by Lin et al.[163]) and K_D is the apparent equilibrium dissociation constant (experimentally determined to be 110 µM by Lin et al.[163]). Since the scleral binding of molecules was hypothesized to be mediated by collagen[38], no binding to the choroid was included in the model.

In addition, the sclera had convective flow directed outwards due to the pressure drop of the IOP across the sclera. We can find the convective flow rate using Darcy's Law:

$$v_f = -\frac{K_h}{\mu}\nabla P = -\frac{K_h}{\mu}\frac{dP}{dx} \qquad \text{Eq. 5.3}$$

where K_h is the hydraulic conductivity of the flow pathway medium (10^{-18} m^2 for rabbit sclera)[35, 165, 166], μ is the viscosity of the fluid (7×10^{-4} Pa s for water at 37°C)[167], P is the pressure and x is position in the radial direction. We only considered pressure changes in the radial direction and not in the circumferential direction. Because there was no (or very little[34]) pressure differential between the vitreous humor and the SCS, there should be little pressure-driven flow into the choroid. The significant pressure drop was therefore between the SCS and the extraocular environment across the sclera. We could assume the pressure drops linearly across the sclera, i.e., across a representative distance of 300 µm [161]. We could use the experimental data (Figure 5.4) to describe the pressure drop over time as an exponential decay with a maximum of 100 mmHg and a time constant of ~5 min.

There was also convective flow via the drainage pathway (region iii), which had a y-dimension equivalent to the outer diameter of a microneedle (i.e., 0.25 mm), and had a convective flow two orders of magnitude greater than that in the rest of sclera.

5.5.1.1 Modeling predictions of clearance from SCS

At time t=0, 1000 molecules were randomly 'injected' into the SCS (Figure 5.6A(ii)). At each subsequent time point (time step Δt=1 min), molecules were moved following the rules described above depending on each molecule's location at the previous time point (Figure 5.6A). The location and fate of each molecule was recorded (i.e., in the eye, outside the sclera, or cleared via choroid).

After 5 min (Figure 5.6A(iii)), molecules were cleared from the SCS. A fraction of the molecules were rapidly convected across the sclera via leakage pathways at the site of injection and via perivascular routes (treated in the simulation as a single shunt pathway through the center of the sclera, as depicted in (Figure 5.6A(i)). The remaining molecules were transported into the choroid or the sclera as the SCS collapsed (in the simulation, the SCS did not collapse). Transport into the choroid was exclusively by diffusion, since no pressure gradient from the SCS across the choroid was expected. Transport into the sclera (i.e., not via leakage pathways) was through a combination of diffusion as well as convection driven by the decaying pressure gradient across the sclera. Molecules that entered the choroid were eventually cleared by choroidal vasculature. Molecules that entered the sclera were eventually cleared across the outer scleral surface.

Within 15 min after injection (Figure 5.6A(iv)), molecules penetrated deeper into the choroid and sclera, and began to be cleared from these tissues. At 1 h (Figure 5.6A(v)), most molecules within the choroid had been cleared into the bloodstream, while molecules in the sclera continued to be cleared. The rate of clearance from the choroid was determined by the rate of diffusion of molecules to capillaries and the odds of being taken up by a capillary (i.e., the B term). At 4 and 12 h (Figure 5.6A(vi) and Figure 5.6A(vii)), transported across the sclera continues. The rate of clearance from the sclera was determined by the rate of transport to the outer scleral surface by diffusion, as well as convection driven by the normal IOP of the eye (i.e., 15 mmHg in the rabbit). Our model, as well as previous literature[168], predicted that both of these driving forces may play a role in the sclera.

By 24 h (Figure 5.6A(viii), the clearance process was largely complete. It was worth noting that this modeling result was for the low-molecular weight compound fluorescein (Figure 5.6A – C). We predict that molecules that do not bind, e.g., ethacrynic acid[163] (Figure 5.6D) or have higher molecular weight, e.g., 70 kDa dextran (Figure 5.6E) were cleared similarly, but with different kinetics, especially for diffusion-based processes.

The snapshots shown in Figure 5.6A were supplemented with continuous time course results over the course of one hour (Figure 5.6B) and one day (Figure 5.6C). Within 10 min, most molecules were removed from the SCS, a fraction of the molecules were cleared from the eye via transscleral leakage pathways and the remaining molecules were transported into choroid and sclera. Over the course of hours, molecules were slowly cleared from the choroid and sclera. Molecules in the choroid were cleared more quickly (i.e., within 1 h, because of the shorter diffusional distances to choroidal capillaries that remove molecules via blood flow). Molecules in the sclera were steadily removed as they exit the eye, mostly within 24 h.

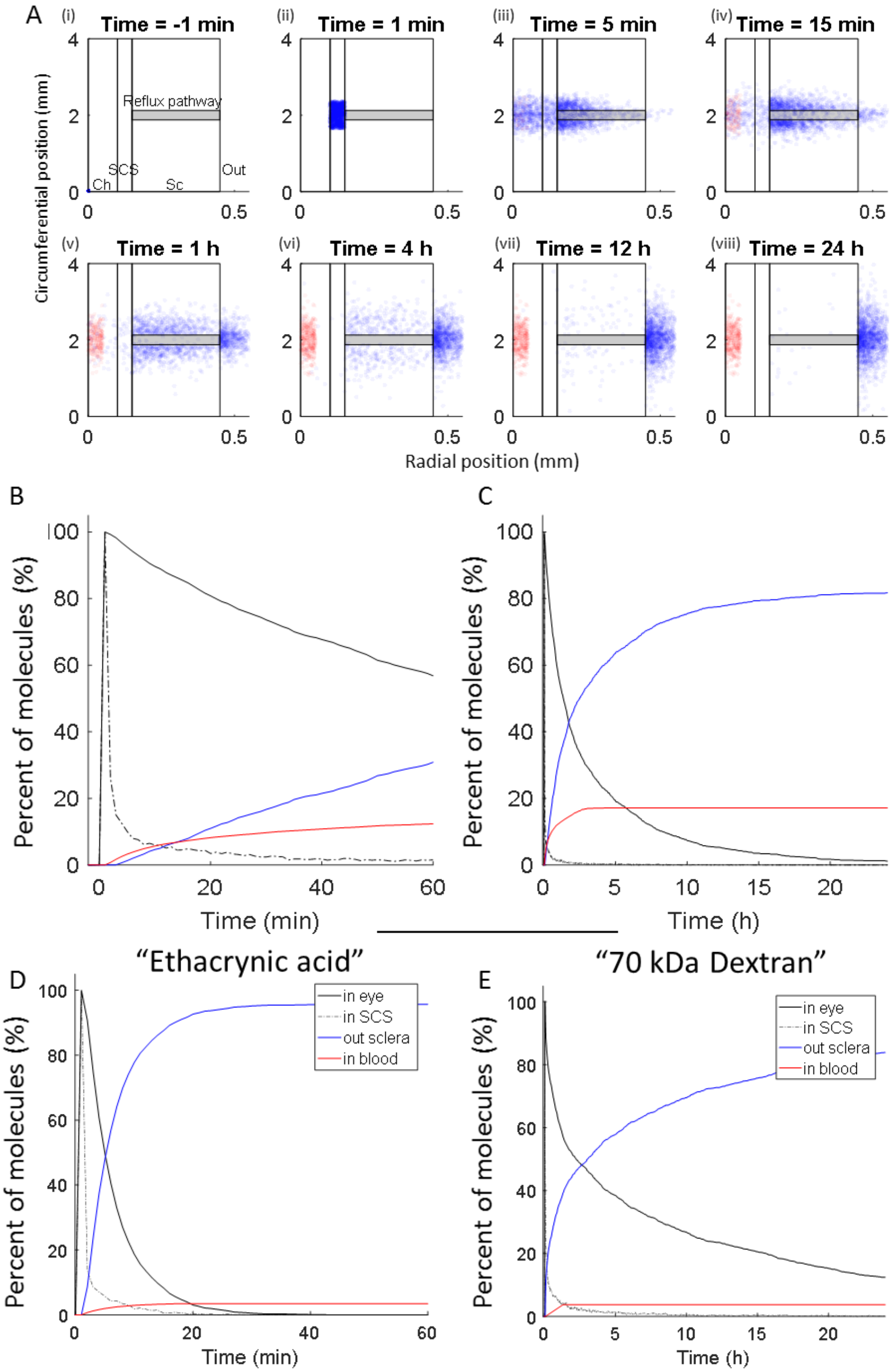

Figure 5.6 - Results from 2D model of molecule transport in the SCS. Transport after SCS injection with (A-C) 'fluorescein'; (D) molecule with no binding, "ethacrynic acid"; and (E) high-molecular weight molecule, "70 kDa dextran". (A) Cross-sectional view of eye showing position of molecules (blue dots) and molecules that were cleared in blood (red dots) at different times post injection. Ch=choroid; SCS=suprac horoidal space; Sc=sclera. Percentage of particles found in the eye, in the SCS, on the exterior surface of the sclera, and in the blood via the choroid (B)within 1 h after injection and (C) within 24 h after injection. Summarized fate of (D) small molecule that does not bind sclera and (E) large molecule, 70 kDa dextran.

The model suggested that the sclera accounted for more clearance than the choroid. This could be explained as follows. After injection into the SCS, a molecule experienced isotropic transport (recall that there was no pressure differential in the eye interior to the sclera) and was thus able to diffuse either circumferentially within the SCS or radially (towards the choroid or towards the sclera) at similar rates. Circumferential diffusion did not affect clearance very much, but radial transport played a major role in a molecule's eventual clearance route. If the molecule diffused into the sclera, there was sufficient diffusive transport and convective flow due to physiological IOP across the sclera to ensure clearance of the molecules across the thickness of the sclera. Alternatively, if the molecule diffused into the choroid, the molecule had a probability of clearing as it diffused through the choroid. If the molecule within the choroid did not clear immediately (which is unlikely considering $B = 0.05\ \text{min}^{-1}$) it could diffuse towards the sclera and consequently become driven trans-sclerally. About one-third of molecules that diffused into the choroid initially were eventually cleared through the sclera.

Exponential curve fits were generated from the model results in Figure 5.6C. The percentage of molecules found in the eye was fit to a 1st order exponential decay, which yielded a time constant of 3.38 h [3.34, 3.41; 95% confidence interval] (r^2=0.98). The cumulative percentage of molecules that had entered the blood via the choroid was fit to a 1st order exponential approach function with a time constant of 0.93 h [0.92, .94] (r^2=0.99). The cumulative percentage of molecules that had exited the eye via trans-scleral transport routes was fit to a 1nd order exponential approach with time constants of 3.84 h [3.80, 3.87] (r^2=0.99).

Since the time constants of molecule clearance from the eye and the time constant of trans-scleral clearance were on the same order of magnitude of hours (with intravascular clearance being significantly faster), the model suggested that trans-scleral diffusion was the dominant route of clearance. The model generated a clearance time constant similar to the time constant of 4.3 h that we found based on fundus imaging (Figure 5.2).

Guided by the experimental data in the context of model predictions, the characteristic times of key transport phenomena following SCS injection were summarized in Table 5.1.

Table 5.1 - Characteristic times of transport phenomena in the eye

Characteristic time (order of magnitude)	**Transport phenomena in eye**
1 min	• SCS loaded with molecules and fluid during injection
10 min	• Fluid and molecules cleared from SCS by convection through leakage pathways • Remaining molecules transported into choroid and sclera • SCS collapses • IOP drops to baseline
1 h	• Molecules cleared by choroidal blood flow
1 - 10 h	• Molecules cleared from sclera by diffusion and convection

We also modeled the behavior of a small molecule that did not bind to sclera[163] and a large molecule[38], which were summarized in Figure 5.6 D and E respectively. To model a small molecule that did not bind sclera, we used experimentally derived values for ethacrynic acid[163]; in particular, we increased the diffusivity to 5×10^{-6} cm^2/s[163] and decreased B_{max} to 5 µM[163] (other parameters kept the same as the fluorescein condition). The model predicted that half-life of "ethacrynic acid" in the eye to be 4.8 min with complete clearance by 25 min (Figure 5.6D). These values were similar to the SCS collapse time (which could be viewed as a proxy for clearance of water from the SCS). Comparison of these characteristic times to those for fluorescein showed the dramatic effect that binding could have on clearance rates.

The clearance of a large macromolecule was modeled by using values experimentally determined for 70 kDa FITC-dextran[38]. In particular, we decreased the diffusivity to $5x10^{-8}$ cm^2/s (by assuming the experimental derived scleral permeability of $1.5x10^{-6}$ cm/s[38] was at steady state across the thickness of the sclera), decreased the choroidal clearance rate to 0.005 min^{-1} (since larger molecules should have more difficulty passing through the fenestrae of the choriocapillaris[31]), and decreased the binding affinity B_{max} to 1000 μM[38] while keeping the other parameters the same as the fluorescein condition. The model predicted that the half-life of this macromolecule to be 5.2 h and the total clearance time to be 3.8 d. Both values were within two-fold of the values we found experimentally. For all three model molecules tested, the dominant route of clearance was via trans-scleral transport with a lesser contribution from intravascular clearance.

5.5.1.2 Sensitivity analysis of model predictions

To provide greater insight into the transport phenomena, we performed sensitivity analysis on the model to determine the relative contributions of different parameters to the overall clearance in the eye (Figure 5.7). In general, the model predicted that small changes (within 1 order of magnitude) in parameter values did not significantly change the model results. The rank order of parameter sensitivity was, from most sensitive to least: diffusivity of the molecule in the SCS and in the tissue (Figure 5.7A), scleral binding capacity (Figure 5.7B) and equilibrium dissociation constant (Figure 5.7C), vascular clearance rate (Figure 5.7D), scleral hydraulic permeability (Figure 5.7E), size of leakage sites (Figure 5.7F), $\tau_{pressure}$ (the rate at which elevated IOP dissipated, Figure 5.7G), and baseline physiological IOP (Figure 5.7H). Since the model suggested that the rate limiting step in SCS clearance was the trans-scleral transport, it stood to reason that the parameters that modified the trans-scleral transport rate affected the clearance time constant and total clearance time the most. Nevertheless, as evidenced by the graphs in Figure 5.7, the clearance time constant was a linear combination of the trans-scleral and vascular clearance time constants.

Diffusivity (D) had the greatest effect on clearance times (Figure 5.7A); for example, reducing D (the diffusivities of fluorescein) by one order of magnitude to one-tenth the diffusivity of fluorescein (0.1xD) resulted in a doubling of the clearance time constant. Intuitively, changes in diffusivity will have a significant effect on clearance time since the characteristic time for a molecule to move across the sclera (300 μm in the radial dimension) increases with the diffusivity. As seen in Figure 5.7A and in our experimental results (Figure 5.3D), the model correctly predicted nonlinearity in the clearance time at 0.01x D. Experimental data suggested that the nonlinearity occurs at >500 kDa, which should be ~0.01x D based on the Stokes-Einstein equation.

Scleral binding of molecules (as modulated by B_{max} and K_D; Figure 5.7B and C, respectively) also had a major effect on clearance times. Intuitively, increasing scleral binding effectively behaved like a decreased diffusivity by drastically slowly molecule transport. However, scleral binding affected molecule transport on short time scales (before saturating the sclera) whereas diffusivity equally affected transport at all times. Unlike the results seen with changing D, changes in B_{max} and K_D had a biphasic effect whereby small changes resulted in almost no change in clearance time but a large change caused a disproportionate increase in clearance time. This could be due to changes in the binding saturation point of the sclera.

The choroidal clearance rate had a moderate effect on characteristic clearance time constant and a minor effect on total clearance time (Figure 5.7D). At high clearance rates by choroidal vasculature, the choroidal perfusion contributed at most 50% of total clearance of molecules from the eye. We reasoned that this 50% makes sense since molecules leaving the SCS have an approximately 50% chance to enter the choroid (as opposed to the sclera). With clearance rates set to low or nonexistent (time constants excluded in Figure 5.7D), most or all molecules left via trans-scleral pathways, which set an upper limit on the clearance time (i.e., it takes ~25 h for all molecules to leave the eye trans-sclerally).

The scleral hydraulic permeability (Figure 5.7D) and size of the leakage pathways (Figure 5.7E), had a moderate effect on clearance time. These parameters were indirectly related to trans-scleral transport. Parameters that increased the convective flow rate ($\tau_{pressure}$ and physiological baseline IOP) had a modest effect on clearance time. This suggested that convective flow through the sclera was not a major contributor to clearance.

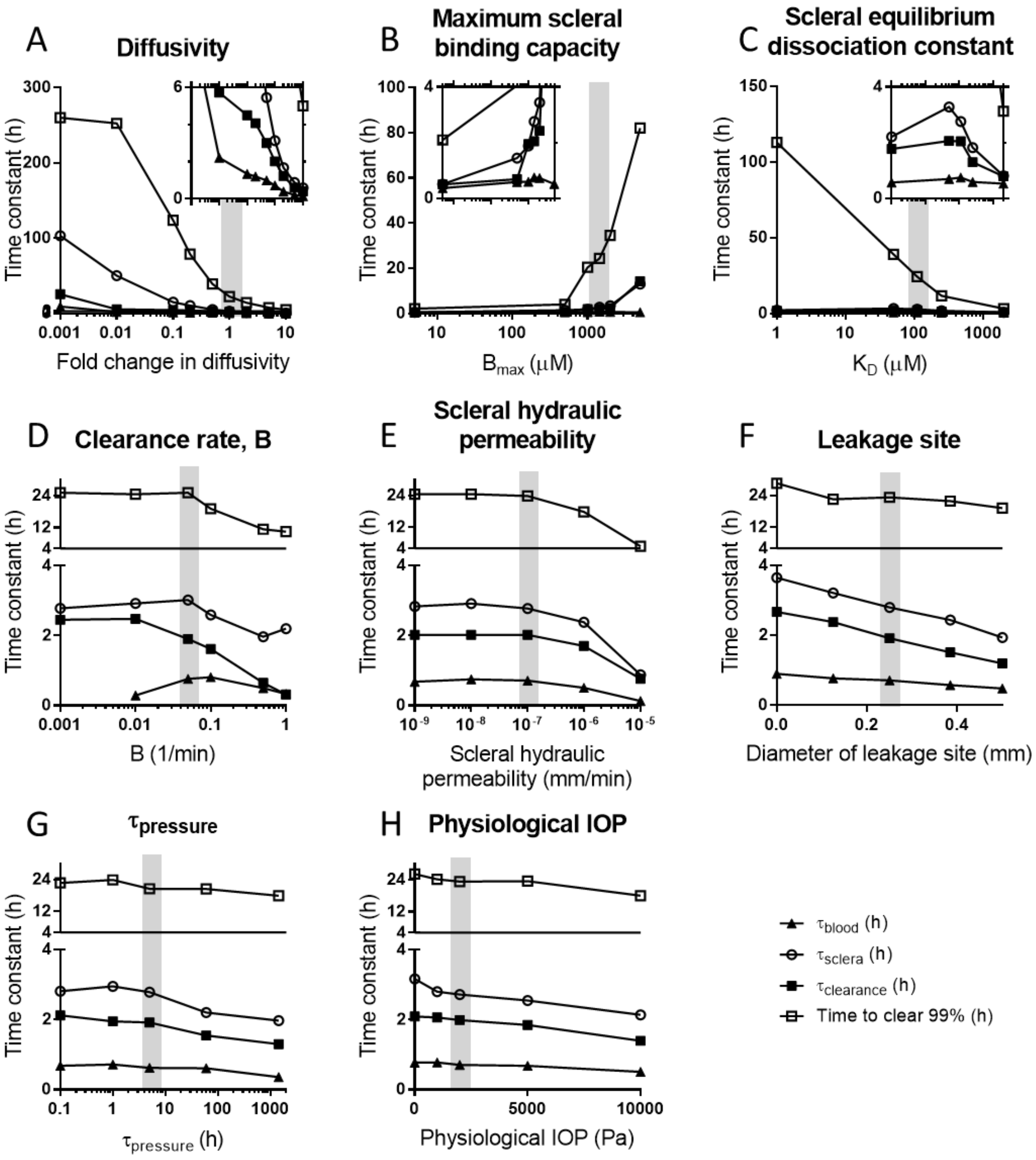

Figure 5.7 – Sensitivity analysis of parameters used in two-dimensional model of molecule transport from the SCS. Parameters were varied at least one order of magnitude from the value used in the model (value used in base condition highlighted in gray). The clearance time constant (black square) and time to clear 99% (open squares) of molecules are plotted against each variable. In addition, the time constants for intravascular clearance (τ_{blood}, triangle) and trans-scleral transport (τ_{sclera}, open circle) were also found. Note that the y-axes of the first three graphs (A-C) are on a different scale than the others (D-H).

Of the parameters tested, diffusivity and size of the leakage site could be changed by optimizing formulation or microneedle injection technique, respectively and thereby modulate clearance rate. Diffusivity was the most sensitive variable and changes by an order of magnitude could change the clearance time constant from 5 min to 18 h. The Stoke-Einstein equation indicated that diffusivity could be modulated by changes in formulation viscosity and the molecular radius (which is in turn a function of molecular weight). In addition, using a smaller-bore microneedle did have a moderate effect on the clearance times. On the other hand, changes in physiological parameters (e.g., physiological IOP, scleral hydraulic conductivity, and clearance rate) did not drastically change the behavior of the model, and clearance changed by less than 2-fold with up to 10-fold changes in the parameter value. Thus, the model may be applicable to other species, like humans.

5.5.1.3 Additional comments on the model

A limitation of the model was that it only investigated in two dimensional transport using Cartesian coordinates, although the actual clearance process occurred in three dimensions in spherical coordinates. This limited the ability of the model to predict distribution. To simplify the model, variation in SCS area and thickness were not accounted for, as these additional considerations would complicate the model with dynamic boundary conditions. Many other simplifying assumptions were also employed, such as no convective flow simulating the process of injection, no aqueous turnover via uveoscleral outflow[16], and no influences of biomechanical tissue properties. Despite these limitations, model predictions were in general agreement with experimental data.

Previous studies had hypothesized that clearance from the SCS is predominantly due to either choroidal perfusion[9, 124, 126] or perivascular leakage routes[43]. However, as shown in the present study, a combination of routes was utilized in clearing the SCS. Some studies showed that molecular clearance into the choroid was important[9, 126]. Other studies demonstrated the importance of perivascular drainage routes[43]. Furthermore, periocular injections into the subconjunctival space revealed that transscleral diffusion was possible, albeit in the opposite direction of transport in this study[35, 36, 40, 104, 125].

To our knowledge, this was the first study to provide experimental and computational evidence of the relative contributions of different routes of clearance from the suprachoroidal space. In particular, we identified pressure-driven flow through leakage routes (e.g., perivascular leakage routes and reflux out the injection site) and transscleral transport; and diffusion-mediated transport across the sclera and into the choroid for intravascular clearance. We also identified the time scales and relative contributions of each of these routes of clearance for the first time.

5.5.2 Effect of molecular size on residence time

We found experimentally and computationally that increasing molecular radius had a major effect on clearance time. Fluorescein (~1 nm in diameter[38]) was cleared by 24 h, while 2 MDa FITC-dextran (~50 nm in diameter[156]) was not fully cleared until 21 d. The prolonged residence time did not increase as a linear function of molecular mass, but was dramatically longer above a threshold of ~10^6 Da. The difficulty for very large macromolecules to pass through the fenestrae of the choriocapillaris and through the extracellular matrix of the sclera is the likely explanation for this behavior.

As shown in this study, the bulk of clearance occurs via diffusion across the sclera, as well as through the choroid into choriocapillaris. The physiological upper limit of pore size of the choriocapillaris is estimated to be ~6 nm[31]. Thus, the hydrodynamic radius of 2 MDa FITC dextran is much larger than the choriocapillaris pore size. Because macromolecules are not rigid and are constantly changing shape, even 2 MDa FITC-dextran is eventually able to adopt a conformation that allows passage through the fenestra of a choriocapillary. On the other hand, small polystyrene microspheres (20 nm in diameter), which are rigid and are not able to adopt different conformations, were still visible upon fundus examination 2 months after injection[8, 128]. Diffusion across sclera is the other main mechanism for clearance. Experimental studies and theoretical analysis have shown that scleral permeability decreases as a steep function of molecular mass[91, 169].

5.5.3 Implications for drug delivery

The findings in this study may be instructive for controlling drug delivery via the SCS. The observation that pressure-driven flow occurs through leakage sites indicates the importance of minimizing leaking from the site of injection (e.g., by keeping the microneedle in place after injection). It also suggests that there are diminishing returns on increasing injection volume; larger volumes lead to larger IOP which lead to more loss of fluid through pressure-driven flow through leakage pathways.

Most molecules injected in the SCS are cleared into the systemic circulation via the choriocapillaris or transsclerally into the subconjunctival space. Drugs cleared via the choroid can interact with possible drug targets in that tissue, and possibly diffuse across the retinal pigment epithelium into the retina, where additional drug targets are also located. Drugs cleared across the sclera (or via leakage pathways) do not enter the choroid or retina, and therefore do not reach targets in those tissues.

Residence time in the SCS depends on what is injected. It has previously been reported that molecules are cleared from the SCS within one day and that particles are not cleared at all[5, 8, 9, 81, 120, 125]. This study corroborated those findings, which suggest that extending the residence time of drugs in the SCS requires their incorporation into particulate controlled release systems[115]. However, this study also suggests a new approach, which involves the use of drug molecules of very high molecular mass, possibly by conjugation to a large polymer, incorporation into a biodegradable polymer, use of a prodrug or other strategies[46, 170-172].

5.5.4 Limitations

There were several limitations to this study. There are anatomical and physiological differences between rabbit and human eyes. Human clinical trials will be needed if these findings are to be applied to human medicine. However, sensitivity analysis indicates that changes in hydraulic conductivity and scleral thickness did not have major effects on the results of the model. Another possible concern is that we have an incomplete mass balance from the fluorescein collection experiments (i.e., 28% unaccounted for in Figure 5). While we assume that incomplete capture was equally due to all the collection routes, it is possible this collection was biased (i.e., unequal loss of fluorescein from the different routes, especially the intravascular route that was most difficult to collect). Since this study was performed with fluorescent tracer molecules and not a real drug, pharmacokinetic studies with drugs of interest are needed.

5.5.5 Conclusions

In summary, we used live New Zealand White rabbits to study molecular clearance from the SCS after microneedle injection. We identified that clearance occurs in three regimes. (i) There was immediate loss of fluorescein from pressure-driven leakage at the injection site and via perivascular routes associated with vortex veins on a time scale of minutes which accounted for a few percent of clearance from the SCS under the conditions of this study. The remaining molecules were transported out of the SCS and into the sclera or the choroid where they formed depots. (ii) Concentration-driven diffusion into the choroid and subsequent clearance of the choroidal depot by choriocapillaries took place on a time scale of an hour. (iii) Diffusion and physiological IOP-mediated convection across the sclera cleared the remaining fluorescein from the eye over the course of hours. These experimental data were supported by a two-dimensional model of small-molecule transport in the eye. Increasing the molecular radius of injected molecules significantly slowed the rate of clearance. These experiments will guide development of strategies to better control drug delivery via the SCS.

6 SUSTAINED REDUCTION OF INTRAOCULAR PRESSURE BY SUPRACILIARY DELIVERY OF BRIMONIDINE-LOADED POLY(LACTIC ACID) MICROSPHERES FOR THE TREATMENT OF GLAUCOMA

This work has been published in Journal of Controlled Release[115].

6.1 Summary

Although effective drugs that lower intraocular pressure (IOP) in the management of glaucoma exist, their efficacy is limited by poor patient adherence to the prescribed eye drop regimen. To replace the need for eye drops, in this study we tested the hypothesis that IOP can be reduced for one month after a single targeted injection using a microneedle for administration of a glaucoma medication (i.e., brimonidine) formulated for sustained release in the supraciliary space of the eye adjacent to the drug's site of action at the ciliary body. To test this hypothesis, brimonidine-loaded microspheres were formulated using poly (lactic acid) (PLA) to release brimonidine at a constant rate for 35 days and microneedles were designed to penetrate through the sclera, without penetrating into the choroid/retina, in order to target injection into the supraciliary space. A single administration of these microspheres using a hollow microneedle was performed in the eye of New Zealand White rabbits and was found to reduce IOP initially by 6 mm Hg and then by progressively smaller amounts for more than one month. All administrations were well tolerated without significant adverse events, although histological examination showed a foreign-body reaction to the microspheres. This study demonstrates, for the first time, that the highly-targeted delivery of brimonidine-loaded microspheres into the

supraciliary space using a microneedle is able to reduce IOP for one month as an alternative to daily eye drops.

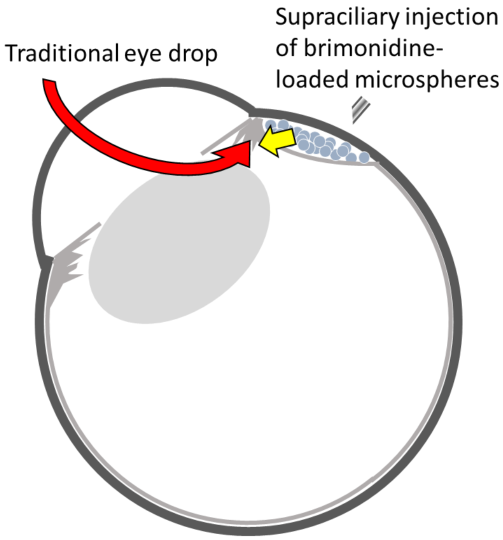

Figure 6.1 – Graphical description of rationale to target ciliary body. Higher bioavailability achievable with supraciliary injection of briomindine-loaded microspheres compared with topical eye drops.

6.2 Introduction

Primary open-angle glaucoma is a leading cause of blindness in the United States, affecting nearly 2 million individuals with an annual cost of \$2.9 billion [50, 51]. Glaucoma is the most common form of optic neuropathy, where loss of retinal ganglion cell axons permanently disrupts transmission of visual information from the retina to the brain [1, 49, 50]. Over decades, patients experience a painless and gradual loss of vision starting from the periphery and eventually claiming central vision [1, 53]. Intraocular pressure (IOP) is the only modifiable risk factor [52, 173] and reducing IOP prevents the progression of glaucoma-related vision loss [53, 54].

IOP is mediated by the balance of aqueous humor production and aqueous humor removal [13]. Aqueous humor is a clear liquid that is secreted by the ciliary body. Clearance of aqueous humor occurs through either the trabecular meshwork into the episcleral veins or the uveoscleral outflow pathway into the suprachoroidal space [13, 16]. Medical and surgical therapy for glaucoma seeks to control IOP by reducing production of aqueous humor and/or increasing clearance of aqueous humor [4, 53]. Topical eye drops, such as timolol, latanoprost, and brimonidine, are commonly-used FDA-approved medical therapies for glaucoma patients. Brimonidine is an α_2-adrenergic agonist that both decreases aqueous humor secretion by the ciliary body and increases aqueous humor clearance [174]. Because topical eye drops can have low bioavailability through the cornea (<5%), some regimens call for multiple eye drops per day to ensure sufficient drug dosing (e.g., brimonidine eye drops are prescribed three times per day) [4, 175].

6.2.1 The need for improved patient adherence with administration of IOP-lowering drugs

Patient adherence to topical eye drops is low, estimated to be only 41% to 76% [4, 55-58, 176]. Due to the chronic nature of glaucoma and the rigorous administration schedule, it can be difficult for patients to administer their eye drops on a regular basis. Since any loss of vision is permanent, increasing patient adherence to the regimen will preserve functional vision and decrease progression to blindness [4].

Patient adherence to the eye drop regimen can be increased through methods, such as memory tools that remind patients, and improved formulations that do not require refrigeration or require simpler administration regimens [4]. But perhaps the most attractive method to improve eye drop adherence is through the use of controlled-release drug delivery systems that obviate the need for the patient to take eye drops at all. While brimonidine-loaded drug delivery systems for the management of glaucoma have been studied before [177-180], we seek to determine the efficacy of a targeted controlled-release system delivered using a microneedle adjacent to brimonidine's site of action in the ciliary body.

6.2.2 Injections targeting the supraciliary spacing using microneedles

The supraciliary space is the anterior-most region of the suprachoroidal space. The suprachoroidal space is a potential space in the eye found between the sclera (the fibrous collagenous layer that contains the eye) and the choroid (the rich vascular network that supplies nutrients to the outer retina). The suprachoroidal space has been explored as a site for ophthalmic drug delivery in preclinical and recent clinical studies (e.g., NCT01789320 and NCT02255032) [2, 5, 7-9, 17, 36, 81, 97, 116-118, 123, 124, 126, 127], motivated by higher bioavailability compared with topical eye drops [8, 81] and the ability to target drug delivery to the choroid that lines the suprachoroidal space, the adjacent retina or, most recently, the ciliary body that forms its most anterior boundary.

Injections are targeted to the suprachoroidal (and supraciliary) space using individual hollow microneedles with a length matched to the thickness of the sclera and conjunctiva that enable access to the suprachoroidal space with a procedure comparable to an intravitreal injection, which is a method of ophthalmic drug delivery regularly performed in the outpatient clinic setting [8, 81, 88]. Microneedle injections in the suprachoroidal space were originally designed as a treatment for posterior-segment diseases. This study seeks to treat glaucoma, which is currently treated with therapies targeted at the anterior-segment, by targeting drug delivery to the supraciliary space [6].

In our initial study, a bolus microneedle injection of glaucoma drugs (including brimonidine) into the supraciliary space was able to reduce IOP with significant dose sparing compared with topical eye drops [6]. Furthermore, fewer ocular side effects are expected since the drug is compartmentalized in the suprachoroidal space away from other non-target tissues (e.g., lens, cornea, etc).

In this study, we hypothesize that IOP can be reduced for one month after a single microneedle injection of brimonidine formulated for sustained release using PLA into the supraciliary space of the eye. Brimonidine was chosen because it is an FDA-approved IOP-lowering agent currently prescribed to glaucoma patients [174, 175, 181] and is pharmacologically active in the rabbit [6, 177-180]. Due to increased bioavailability, a microneedle injection into the supraciliary space should reduce the dose needed, compared with topical eye drops, thereby allowing a relatively small injection to contain sufficient drug for extended therapy. The successful implementation of this technique could enable a sustained-release treatment for glaucoma patients without the need to administer topical eye drops.

6.3 Materials and Methods

6.3.1 Materials

Brimonidine tartrate, poly-lactic acid (PLA) with an inherent viscosity (i.v.) of 0.20 dL/g (free acid terminated, RESOMER® 202H), and polyvinyl alcohol (PVA, 80% hydrolyzed, MW ~9,000-10,000) were purchased from Sigma Aldrich (St. Louis, MO). PLGA (75:25, i.v. = 1.13 dL/g, ester terminated) was purchased from Durect (Cupertino, CA). All solvents used were HPLC grade and were purchased from Fisher Scientific (Waltham, MA), and unless otherwise noted, all other chemicals were purchased from Sigma Aldrich.

6.3.2 Removal of low molecular weight acids from PLA

PLA (~5 g) was dissolved in 10 mL CH_2Cl_2 at room temperature and then added to a stirring ddH_2O bath maintained at 60°C. After evaporating CH_2Cl_2 for 3 h the aqueous phase containing water-soluble, low molecular weight acids was removed while the water-insoluble, higher MW polymer remained as a solid in the vessel as a result of the organic solvent evaporation. The resulting higher MW polymer was dried under vacuum and stored at -20°C until use [182].

6.3.3 Microsphere preparation

Microspheres were prepared using oil-in-water (o/w) emulsion solvent-evaporation methods. First, brimonidine and the selected polymer(s) (Table 6.1) were dissolved in 1 mL CH_2Cl_2. Two mL 5.0% (w/v) PVA was added and vortexed to create the o/w emulsion, which was then poured into a stirring bath of 0.5% (w/v) PVA to allow for CH_2Cl_2 evaporation and microsphere hardening. After 3 h, the hardened microspheres were screened to 20-45 µm using sieves, washed with ddH_2O, then lyophilized and stored at -20°C for future use.

Table 6.1 – Microsphere formulation parameters

Formulation Name	Polymer	Polymer Concentration (mg/mL-CH_2Cl_2)	Theoretical w/w Loading (L_T)
800PLA	PLA	800	6.00%
1000PLA	PLA	1000	5.00%
800PLA-T	PLA hot-water treated	800	6.25%
PLA/PLGA	50 : 50 Blend PLGA : PLA	500	10.00%

6.3.4 Scanning electron microscopy

Prior to imaging, lyophilized microspheres were mounted using double-sided carbon tape and coated with a thin layer of gold under vacuum. Scanning electron microcopy (SEM) images were then taken using a Hitachi S3200N scanning electron microscope (Hitachi, Japan). Images were obtained using EDAX software.

6.3.5 Determination of brimonidine loading and encapsulation efficiency

Prepared microspheres (~5 mg) were dissolved in 1 mL acetonitrile. The resulting solution was filtered and analyzed for brimonidine content by ultra-performance liquid chromatography (UPLC), as described below. Percentage loading and encapsulation efficiency were calculated using Equations 6.1 and 6.2, respectively.

$$\% \frac{w}{w} loading\ (LA) = \frac{mass\ of\ brimonidine}{total\ mass\ of\ microspheres}\, x\ 100 \qquad \text{Eq. 6.1}$$

$$\%\ encapsulation\ efficiency\ (EE) = \frac{actual\ loading}{theoretical\ loading}\ x\ 100 \qquad \text{Eq. 6.2}$$

6.3.6 In vitro release kinetics of brimonidine

Microspheres (~5 mg) were suspended in 1 mL phosphate-buffered saline + 0.02% Tween 80 (PBST, pH 7.4) at 37°C under mild agitation. As brimonidine tartrate is highly water soluble[183], 1 mL of release media was sufficient to ensure sink conditions for the duration of release. Microspheres were separated from media at each time point by centrifugation at 8,000 rpm for 5 min. Then, release media was completely removed and replaced at 1, 3, 5 and 7 days and weekly thereafter for 7 weeks. Release media was assayed for brimonidine content by UPLC, as described below.

6.3.7 Brimonidine quantification

Brimonidine content in loading solutions and release media was determined using a UPLC system (Waters, Milford, MA). The mobile phase was composed of 40 : 60 (acetonitrile : ddH2O) and the flow rate was set to 0.5 mL/min. Samples and standards prepared in either acetonitrile or PBST were injected (8 µL) onto a C18 (Acquity BEH

C18, 1.7 µm, 2.1 x 100 mm) column maintained at 30°C. Brimonidine was detected at 254 nm.

6.3.8 Microneedle fabrication

A 27-gauge (OD = 0.41 mm; ID = 0.21 mm) hypodermic needle (Becton Dickinson, Franklin Lakes, NJ) was used as the starting material. The needle was shortened to ~1.5 mm in length by cutting the needle using a cordless rotary tool (Dremel 800, Robert Bosch Tool Corporation, Mount Prospect, IL). The bevel was produced by grinding the shortened needle at a 60° angle against the sanding band attachment of the rotary tool. A constant stream of water was flowed through the needle bore to prevent heat buildup and the metal from melting. This was done under a stereoscope to ensure the needle length was 750 ± 50 µm. If the needle was too long, the process was repeated; if the needle was too short, the plastic hub was carefully removed with a razor. Each needle was inspected for needle length, absence of metal shavings, and sharpness. If needed, the needle was filed with sandpaper and/or electropolished (ESMA E399, South Holland, IL), as previously described [8].

6.3.9 *In vivo* experimental treatment groups

All *in vivo* experiments were carried out in albino New Zealand White rabbits (Charles River, Wilmington, MA) and were approved by the Georgia Institute of Technology Institutional Animal Care and Use Committee. Practices complied with the ARVO Statement for the Use of Animals in Ophthalmic and Vision Research. Although bioavailability and distribution of brimonidine is affected by presence of pigment in the eye, albino rabbits were used to facilitate visualization of microspheres and since an albino rabbit animal model was used in a previous study [6, 184]. The treatment groups are listed in the Table 6.2.

Table 6.2 – Summary of in vivo experimental treatment groups

Treatment Group	Fluid Carrier	Description
SC-HBSS	50 µL of HBSS	Supraciliary delivery of saline
SC-CMC	50 µL of 5% (w/v) CMC in HBSS	Supraciliary delivery of CMC
SC-blank	50 µL of 5% (w/v) CMC in HBSS	Supraciliary delivery of blank microspheres
SC-low dose	50 µL of 5% (w/v) CMC in HBSS	Supraciliary delivery of brimonidine-loaded microspheres (20-45 µm) [low dose]
SC-high dose	100 µL of 5% (w/v) CMC in HBSS	Supraciliary delivery of brimonidine-loaded microspheres (20-45 µm) [high dose]
Top	N/A	Topical delivery of brimonidine

Before the injection procedure, animals were anesthetized with a subcutaneous injection of ketamine and xylazine. An eye drop of proparacaine (Akorn, Lake Forest, IL) was given 5 min prior to the injection. The eye was proptosed to facilitate injection. A hollow microneedle with a length of 750 µm (see Figure 6.3) and a 250 µL glass chromatography syringe (National Scientific, Rockwood, TN) were used to make injections 3 mm posterior to the limbus.

To ensure delivery near the ciliary body, the total injection volume was divided into multiple injections of 10-20 µL each. Injections were spaced approximately equally around the limbus while avoiding the extraocular muscles. To inject a total volume of 50 µL, three injections of 16.7 µL each were made supranasal, supratemporal, and infranasal. To inject 100 µL, five injections of 20 µL each were made; the same 3 injection sites, as in the 50 µL dose, were used with an additional 2 injections infratemporal and temporal. The fluid carrier was 5% (w/v) carboxymethyl cellulose (CMC; average M_w 700 kDa; Sigma-Aldrich) in Hank's buffered salt solution (HBSS;

Mediatech, Manassas, VA). For all groups, only one eye per rabbit received treatment; the contralateral eye did not receive any treatment during the study.

For the supraciliary delivery of HBSS group (SC-HBSS), a total of 100 µL of HBSS was injected into the supraciliary space. For the supraciliary delivery of CMC group (SC-CMC), 50 µL of 5% (w/v) CMC in HBSS was injected. For the supraciliary delivery of blank microspheres group (SC-blank), 50 µL of 30% blank microspheres (w/v) and 5% (w/v) CMC in HBSS was injected. For the low-dose delivery of brimonidine-loaded microspheres group (SC-low dose), 50 µL of 30% brimonidine-loaded microspheres (w/v) and 5% (w/v) CMC in HBSS was injected into the supraciliary space. For the high-dose delivery of brimonidine-loaded microspheres group (SC-high dose), 100 µL of 30% brimonidine-loaded microspheres (w/v) and 5% (w/v) CMC in HBSS was injected into the supraciliary space. The total injected volume was increased from the SC-low dose to SC high-dose because particle concentrations higher than 30% (w/v) particle in 5% CMC clogged the 27 gauge microneedle.

After the injection, animals were monitored until mobile. If there was significant redness, inflammation, or irritation, a steroid/antibiotic ointment was applied to the eye. If the animal looked agitated or in pain after the procedure, 200 µL of buprenorphine was given subcutaneously. Animals were euthanized with an injection of pentobarbital through the marginal ear vein at the end of the experiment. The eyes were enucleated and some were processed histologically.

For the topical delivery group (TOP), brimonidine eye drops (0.15% Alphagan, Allergan, Irvine, CA) were administered 3 times per day at 8:30 am, 2:30 pm, and 8:30 pm unilaterally to the upper conjunctival sac without anesthesia.

6.3.10 Intraocular pressure monitoring

For the animals that received a microneedle injection, IOP was measured in both eyes with a TonoVet (iCare, Vantaa, Finland) rebound tonometer between 10 am and 2 pm. To measure IOP, the animal was removed from the cage and restrained in a towel for at least 5 min. IOP was measured at least 3 times in both eyes. If there was significant variation between recordings, additional time was given to acclimate the animal to its surroundings before attempting to measure IOP again. The baseline IOP was established by measuring IOP daily for a week prior to the injection. IOP was not taken on the day of injection because the ketamine cocktail used had a significant impact on IOP [6]. IOP was monitored on 1, 3, 5, 7, 10, 14, 17, 20, 24, 27, 30, 33, and 43 days post-injection. Animals that received topical eye drops had their IOP measured at 4 pm daily for a week using the same methods.

The rebound tonometer had been calibrated 6 mo prior against a rabbit whose eye was in fluid communication to a water column eye different heights[6]. The rebound tonometer reported values that were offset by 3 mmHg with no slope adjustment.

6.3.11 Histology

After the animals were euthanized, some eyes were enucleated and immediately fixed in 10% formalin. The eyes were serially sectioned, and sections were stained with hematoxylin-eosin (H&E) or periodic acid Schiff (PAS). Light microscopic examination was performed on all histologic sections for any signs of anatomical changes and foreign body reaction. Histological sections were photographed at 20× magnification (DP 71; Olympus, Tokyo, Japan).

6.3.12 Statistical analysis

All values are mean ± standard error of the mean (SE), unless otherwise specified. Time traces of IOP were calculated in two ways: by finding the difference from the average IOP pre-treatment and by finding the difference between the treated and contralateral eyes. Repeated-measures ANOVA was used to compare the time course data. The dose-response curve was generated by calculating the area under the curve (AUC) using the trapezoid rule. Fisher's Least Square Difference test ($\alpha = 0.05$) was performed to determine statistical significance for individual time points.

6.4 Results

6.4.1 Characterization of brimonidine-loaded microspheres

Our first goal was to encapsulate brimonidine into microspheres for sustained release for up to one month (Figure 6.2). We initially encapsulated brimonidine in free-acid terminated PLA (800PLA), which resulted in low efficiency and high initial burst (24-hour release; Figure 6.2). This is probably because brimonidine is highly water-soluble, which caused leaching of brimonidine into the aqueous phase during microsphere formulation, leading to poor loading [185]. The highly water-soluble nature of brimonidine also probably contributed to high initial burst due to rapid dissolution of poorly encapsulated, surface-associated drug. Initial burst is generally an undesirable property of controlled-release formulations, as it may cause exposure to toxic drug levels.

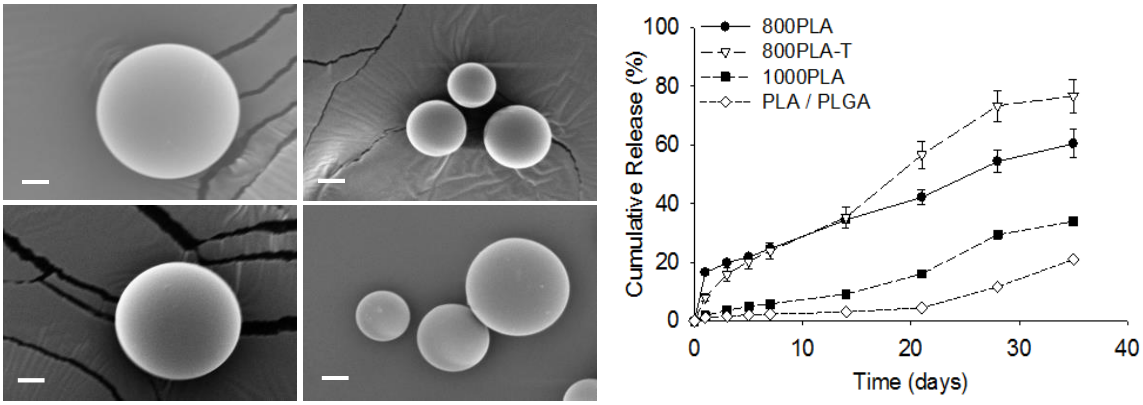

Figure 6.2 – Representative SEM images of four microsphere formulations: (A) 800PLA, (B) 800PLA-T, (C) 1000PLA, (D) PLA/PLGA. Scale bars represent 10 µm. (E) Brimonidine release from four polymer microsphere formulations in vitro. The media was PBST (pH 7.4, 37ºC). Data are expressed as mean ± SE (n = 3 replicates per group).

To improve loading efficiency and decrease initial burst from microspheres, we employed three alternative formulation strategies for encapsulation of brimonidine: (i) increasing PLA concentration to 1000 mg/mL (abbreviated 1000PLA), (ii) blending PLA with PLGA (PLA/PLGA), and (iii) treating the PLA to remove low molecular weight acids (800PLA-T). The first two strategies increased brimonidine loading and decreased initial burst, believed to be due to a denser polymer matrix, which is more efficient in trapping the molecule during microsphere formulation [186]. Although these formulations improved loading and burst, the long-term release from these microspheres in vitro was incomplete through five weeks and was thus deemed unfavorable (Figure 6.2).

To further optimize the brimonidine release kinetics, we removed acidic monomers and oligomers to improve polymer stability during storage and effectively increase molecular weight of the bulk PLA. It has been shown that biodegradable polymers may contain 10-20 µmoles of acid per 100 mg of polymer following synthesis. Furthermore, the lactic acid monomers and oligomers formed during polymerization may catalyze the degradation of the polymer during storage, leading to a decline in PLA molecular weight and a buildup of additional acidic byproduct [182]. Higher molecular weight polymers create a denser matrix during microsphere manufacturing, leading to more efficient encapsulation [182].

This final formulation was prepared with the same free-acid terminated PLA 202H as used in our initial formulation. However, prior to microsphere manufacturing, we stirred the dissolved polymer in a hot water bath to remove low molecular weight, water-soluble acids; a strategy that been used successfully in the past to encapsulate the peptide leuprolide with high efficiency and resulting in low initial burst [182]. Using these methods, we were able to greatly improve brimonidine loading in PLA to achieve 85 ± 0.4% efficiency (Table 6.3) These microspheres also exhibited reduced initial burst *in vitro* (8.0 ± 1.3 %) as compared to the initial 800PLA microspheres (16.5 ± 0.2 %). Although this formulation did not achieve complete drug release at the end of the experiment, it was more than 75%.

Table 6.3 – Characterization of brimonidine encapsulation in microspheres. Data expressed as mean ± SE (n = 3).

Formulation Name	Description	Loading (w/w %)	Encapsulation Efficiency (%)	Initial Burst (%)
800PLA	Starting PLA concentration at 800 mg/mL	2.3 ± 0.1	38 ± 1	16.5 ± 0.2
800PLA-T	Starting PLA concenration at 800 mg/mL. Heat treatment to remove low molecular weight acids	5.3 ± 1.3	85 ± 0.4	8.0 ± 1.3
1000PLA	Starting PLA concentration at 1000 mg/mL	3.3 ± 0.3	67 ± 6	1.8 ± 0.3
PLA/PLGA	Blending of PLA and PLGA	5.3 ± 0.7	53 ± 8	1.2 ± 0.1

6.4.2 Targeted injection localized to the supraciliary space

Our next objective was to target injection of the brimonidine-loaded microspheres to the supraciliary space adjacent to the ciliary body. Microneedles (750 ± 50 µm in length) were fabricated for this study (Figure 6.3). We and others have seen that injection of larger volumes leads to spread over a larger area of the suprachoroidal space [6, 119, 120, 128]. To localize our formulation at the site of injection at the supraciliary space, we wanted to minimize the injection volume and therefore needed to give multiple injections in order to deliver the target dose. Histological images were acquired for all supraciliary microsphere injection groups (SC-blank, SC-low dose, and SC-high dose) to assess the degree of localization of the particles at the injection site. These images showed that the injected particles were localized at the anterior suprachoroidal space, which is bordered by the ciliary body (Figure 6.4), which we call the supraciliary space.

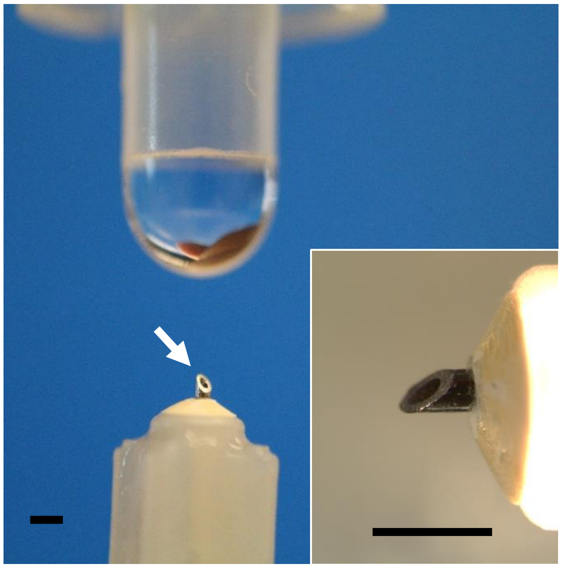

Figure 6.3 – Hollow microneedle measuring 750 µm in length is shown opposite a 50 µL drop from a conventional eye dropper. Scale bars represent 1 mm

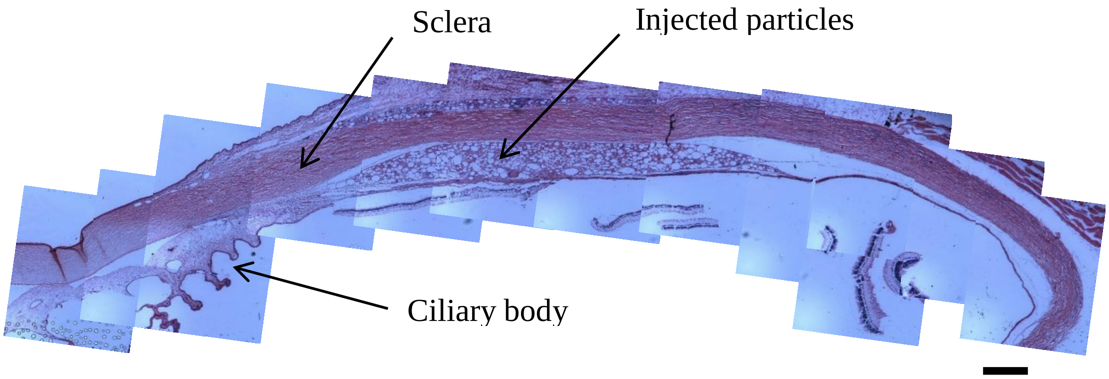

Figure 6.4 – Representative histological image of a section from the rabbit eye showing brimonidine-loaded microspheres suspended in 5% (w/v) CMC/HBSS 46 days after injection into the supraciliary space. Scale bar indicates 500 µm.

To further image supraciliary injection, we added 1% (w/v) red-fluorescent microspheres (1 µm diameter) to blank microspheres injected into the supraciliary space at multiple locations around the limbus. Sixty-nine days after injection, fluorescence imaging of eyes cut radially from the posterior pole to the limbus and then splayed open similarly show localization of the injected microspheres at the sites of injection in the anterior suprachoroidal space near the ciliary body (Figure 6.5). This result is consistent with previous reports that a low volume injection of CMC was able to be localized in the anterior suprachoroidal space [6].

Figure 6.5 – Representative fluorescence image showing localization of red-fluorescent microspheres to the supraciliary space. Eyes were enucleated and imaged 69 days after injection of 1% (w/v) fluorescent polystyrene microspheres (1 µm diameter; ex: 580 nm, em: 605 nm; FluoSpheres, ThermoFisher Scientific, Waltham, MA) and 5% (w/v) blank microspheres suspended in 5% (w/v) CMC in HBSS. Bright-field image (A) displays the interior surface of rabbit eye. The center of the sample is the anterior segment, and the distal ends of the "petals" form the posterior pole. Each petal contains, from superficial to deep, the sclera (white), choroid, and retina. Fluorescence image (B) of same eye shows microspheres localized to the anterior suprachoroidal space.

6.4.3 Effect of supraciliary delivery of brimonidine-loaded microspheres on intraocular pressure

Next, our goal was to inject brimonidine-loaded microspheres into the supraciliary space of rabbit eyes to reduce IOP for one month. The rabbits had a baseline IOP of 12.2 ± 2.1 mmHg (mean±SD). As a positive control, brimonidine was given topically (TOP group) in the form of the clinical product Alphagan®, which was administered topically three times per day for five days to mimic chronic use. This dosing regimen corresponds to approximately 75 µg of brimonidine administered per eye drop and 1,125 µg of brimonidine administered over the course of five days.

In the TOP group, we saw a consistent IOP drop of 2 – 4 mm Hg in the treated eye (one-way ANOVA, p = 0.003, Figure 6.6A) with a magnitude similar to those reported previously for the length of the treatment [187]. Five days after stopping eye-drop administration, the IOP of the treated eye had returned to baseline (Fisher's LSD test, p = 0.86). The IOP of the contralateral eye in the TOP group also showed a significant reduction (one-way ANOVA, p = 0.03, Figure 6.6A) with a magnitude similar to the treated eye (two-way ANOVA, p = 0.26, Figure 6.6B). Because the body weight of the rabbits (2-4 kg) was more than an order of magnitude less than a human, it is likely that the brimonidine that cleared from the treated eye (that was administered a human dose of drug) was sufficient to cause an effect on the contralateral effect, either through a systemic cardiovascular effect or a contralateral therapeutic effect [188].

Guided by this positive control, we next injected brimonidine-loaded microspheres into the supraciliary space. To improve localization of delivery to the ciliary body by avoiding flow of the injectate away from the injection site, the microspheres were formulated with CMC to increase viscosity, and the total material injected was divided into multiple small injections (10-20 µL) at multiple locations around the eye, as was done previously to localize to the supraciliary space[6]. We delivered 15 mg (SC-low dose, containing 0.45 mg of brimonidine, Figure 5C-D) and 30 mg (SC-high dose, containing 0.9 mg of brimonidine, Figure 6.6E-F) of microspheres into the supraciliary space. To control for the effect of the injection of microspheres, we also injected 15 mg of blank microspheres (SC-blank) as a negative control (Figure 6.6G-H).

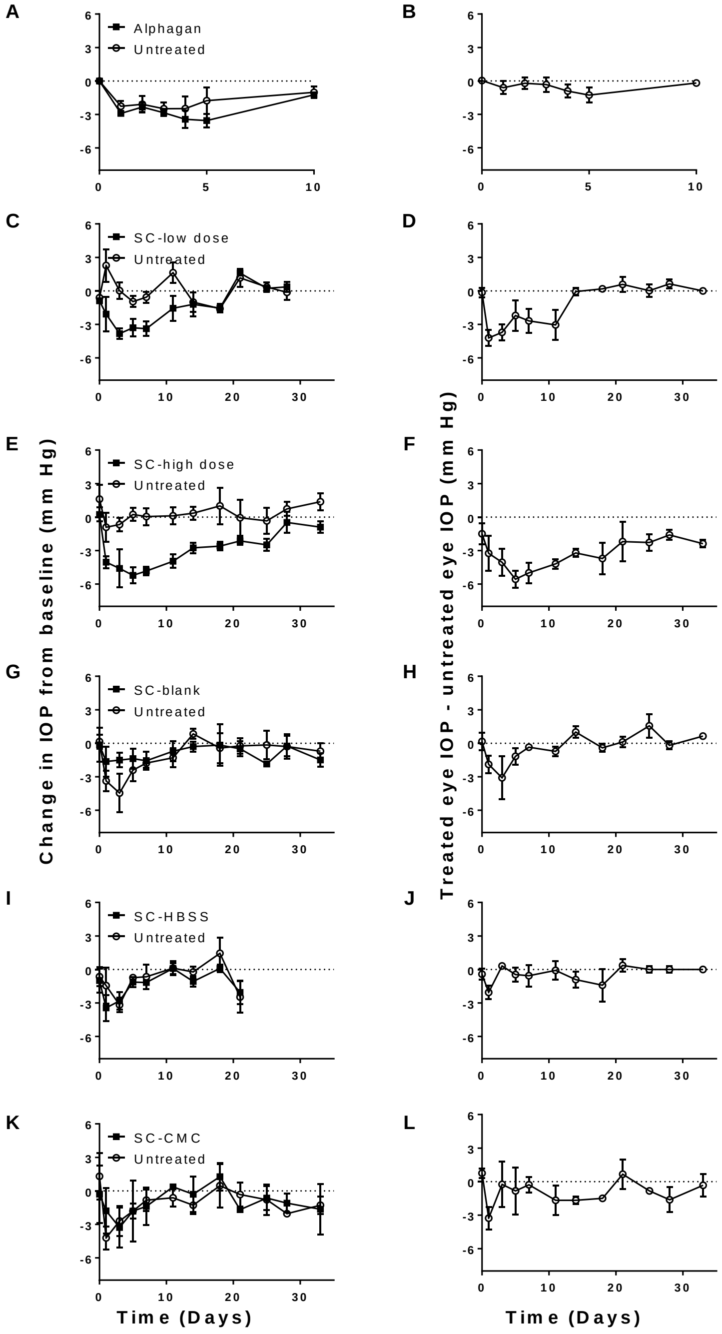

Figure 6.6 – Effect of brimonidine delivery on IOP in the rabbit eye. Change in IOP from baseline over time for topical brimonidine eye drops three times per day (A), brimonidine microspheres (low dose) (C), brimonidine microspheres (high dose) (E), blank microspheres (G) , HBSS only (I), and 5% (w/w) CMC (K). Difference in IOP between treated and contralateral eye over time for topical brimonidine eye drops 3 per day (B), brimonidine microspheres (low dose) (D), brimonidine microspheres (high dose) (F), blank microspheres (H), HBSS only (J), and 5% (w/w) CMC (L). Data are expressed as mean ± SE (n = 3-6).

Both groups that received brimonidine-loaded microspheres (i.e., SC-low dose and SC-high dose) experienced a decline in IOP of the treated eye of as much as 6 mm Hg when compared to the contralateral eye (repeated-measures ANOVA, p = 0.025 and 0.002, respectively). It is notable that the contralateral eye showed no significant change in IOP (repeated-measures ANOVA, p = 0.92 and 0.73, respectively), which is consistent with localization of the drug to the site of injection. The SC-low dose group showed a reduction in the IOP of the treated eye for 14 days after the injection (Fisher's LSD test, p = 0.005). The SC-high dose group showed a reduction in the IOP of the treated eye for 33 days (Fisher's LSD test, p = 0.03). These data are consistent with our central hypothesis that IOP can be reduced for one month after a single injection of brimonidine formulated for sustained release in the supraciliary space.

In the negative control (SC-blank), the "treated" eye had an IOP reduction of 3 mm Hg compared to the contralateral eye 3 days after injection (one-way ANOVA, p = 0.02), which returned to baseline within 5 days (Fisher's LSD test, p = 0.35). This effect seen in the negative control might be due to an inflammatory response caused by the injection, reduced aqueous humor production due to disruption of the ciliary body, or increased uveoscleral outflow due to stretching of the ciliary muscles [189, 190].

6.4.4 Effect of fluid carrier on intraocular pressure

To further elucidate the cause of IOP reduction in the SC-blank group, we examined the effect of the injection technique and fluid carrier on IOP. We injected HBSS (SC-HBSS, Figure 6.6I-J) or 5% (w/v) CMC in HBSS (SC-CMC, Figure 6.6K-L) into the supraciliary space to monitor their impact on IOP. There was a change in IOP from baseline for both SC-HBSS and SC-CMC groups that was evident immediately after injection (Fisher's LSD test, p = 0.01), but was no longer evident at the next measurement 2 days later (Fisher's LSD test, p = 0.84). Possible explanations of this brief IOP reduction include: increased uveoscleral outflow due to ciliary muscle stretching, a short inflammatory reaction causing blood-aqueous-barrier breakdown and decreased aqueous humor production due to ciliary body distention. Further studies are needed to explore this phenomenon.

There was no difference between treated eyes of SC-CMC (Figure 6.6C-D) and SC-blank groups (Figure 6.6G-H) (repeated-measures ANOVA, p = 0.22). This result shows that blank microspheres had little intrinsic effect on IOP. Therefore, the IOP reduction in the treated eye seen in the SC-low dose and SC-high dose groups is believed to be due primarily to the effect of brimonidine release from the microspheres.

6.4.5 Integrated pharmacodynamic response of treatment groups

As a characterization of the integrated pharmacodynamic responses, we determined the area under the curve (AUC) for all treatment groups by integrating the difference in IOP between the treated and contralateral eyes over time (Figure 6.7). The expected response of the brimonidine eye drop (TOP) regimen extrapolated over 30 days was 70 mmHg-days (Figure 6, dotted line). Unlike the other values presented in Figure 6, the response was calculated by finding the IOP reduction of the treated eye minus the IOP of the baseline (i.e., before eye drop application) over the course of one day of eye drop application, and extrapolating the effect by 30 days There was no statistical difference between the SC-blank group and the SC-HBSS group (Fisher's LSD test, p = 0.99) or the SC-CMC group (Fisher's LSD test, p = 0.93). The SC-low dose group also did not reach statistical significance compared with the SC-blank group (Fisher's LSD test, p = 0.38) because there was considerable variation in the response among the five animals in the SC-low group. There was a significant response with the SC-high dose of brimonidine-loaded microspheres compared with the SC-blank group (Fisher's LSD test, p = 0.017).

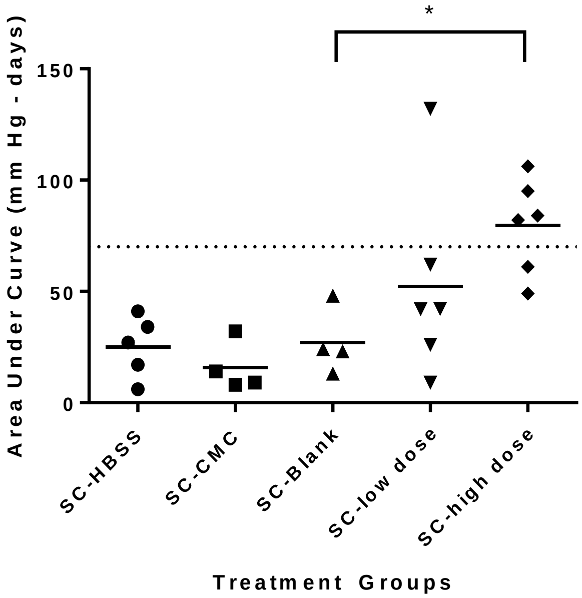

*Figure 6.7 – Integrated pharmacodynamic response of treatment groups. Values were calculated by determining the area under the curve for differences in IOP between the treated and contralateral eyes (data from Figure 6.6) for each animal. Bars represent mean values. Dotted line indicates the expected response achievable with brimonidine eye drops. * = p<0.05.*

The high-dose brimonidine-loaded microspheres were necessary to ensure a consistent sustained effect for one month. All animals in the SC-high dose group had a sustained reduction in IOP for at least three weeks. On the other hand, there was appreciable variation among the responses of the six animals in the SC-low dose group. Out of the six rabbits in the SC-low dose group, one rabbit experienced no IOP drop in the treated eye and another had the strongest response out of all the rabbits tested. This variation in IOP response is possibly due to inter-animal differences in sensitivity to brimonidine or the microspheres releasing at the lower limit needed for a pharmacologic response. Since an increased dose resulted in a prolongation of the effective duration, the release rate from the microspheres might have decreased after 14 days, suggesting nonlinear drug release rate.

6.4.6 Initial safety assessment

During the experiment, rabbits were inspected on a daily basis by veterinary staff and/or study investigators. The microneedle injection site was barely visible immediately post-injection (Figure 6.8A) and was not visible 1 day post-injection (Figure 6.8B). Some rabbits had mild redness 1 day after injection, and were subsequently treated with an antibiotic/steroid ointment. Three days after injection, all eyes were quiet and there were no signs of redness or irritation, or apparent distress in the rabbits. No serious adverse events were noted, and the rabbits at least maintained their weight from pre-injection. Assessment of visual acuity and visual fields were not performed on the rabbits though we would be unlikely to detect any deficit since the injection was localized to the far periphery of the suprachoroidal space.

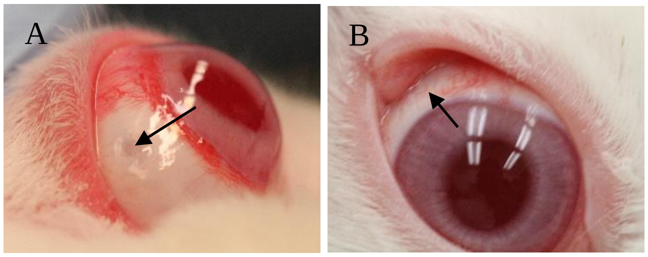

Figure 6.8 – Representative images of the rabbit eye 5 min (A) and 1 day (B) after microneedle injection. Microneedle injection site marked with arrow.

To further assess the safety of brimonidine-loaded microspheres in the supraciliary space, we performed histology on the enucleated eyes. The slides were read by a board-certified ocular pathologist. All eyes that received a supraciliary injection demonstrated separation of the suprachoroidal space at the anterior region (Figure 6.9). However, further studies are required to determine if this might be an artifact from the histology process.

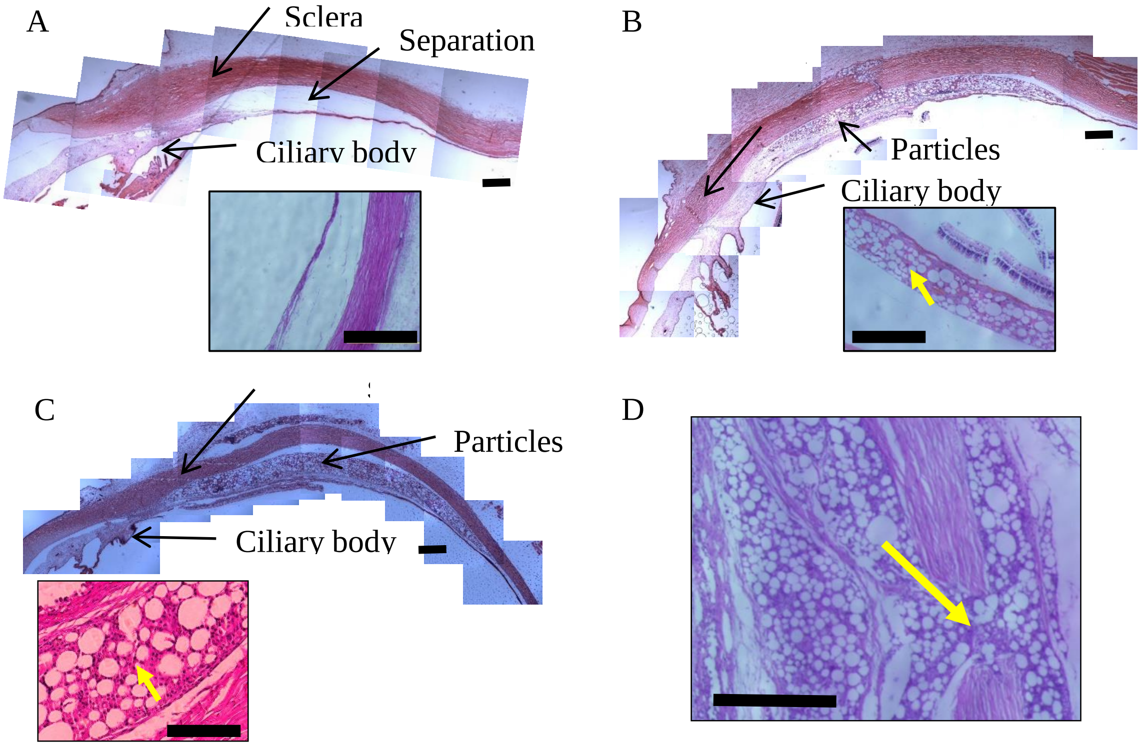

Figure 6.9 – Representative histological images after microneedle injection of HBSS only (SC-HBSS, A) 88 days post-injection; blank microspheres (SC-blank, B) 46 days post-injection; and brimonidine-loaded microspheres (SC-low dose, C) 69 days post-injection. No inflammatory cells were noted in the SC-HBSS group (A inset), whereas accumulation of macrophages was seen in eyes that received SC-blank (B inset) and SC-low dose (C inset), as indicated by the darkly-stained nuclei (arrows) among the voids of where the microspheres were. The microspheres and associated foreign-body response could also be seen in the site of microneedle puncture across the sclera, indicated by the yellow arrow, and in the subconjunctival space 69 days after injection (D). Scale bars indicate 500 µm.

Due to the histologic/staining process, the PLA microspheres were dissolved leaving behind voids where the microspheres were located. There was significant foreign body response among the microspheres in the supraciliary and subconjunctival space (Figure 6.9). We hypothesize this response may be due to the acidic byproducts of the PLA microsphere degradation or impurities in the microsphere from the fabrication process, because previous injections of polystyrene microspheres did not cause inflammation [8, 81]. The foreign body response was present in both blank (Figure 6.9C) and brimonidine-loaded microspheres (Figure 6.9B), which further suggested that the accumulation of macrophages was due to the presence of microspheres (i.e., and not due to the drug itself). The presence of the PLA microspheres and associated foreign-body reponse also appeared at the injection site (Figure 6.9D, arrow) [191]. Nevertheless, it is important to note that the eye did not look inflamed and the animals did not show signs of pain, irritation or distress. Further experiments are needed to investigate this.

We were not able to observe the time frame of complete microsphere degradation. The PLA microspheres were still present 46 and 69 days after the injection (Figure 6.9B-D). It is important to note that all brimonidine was released by these times (as seen with the in vitro drug release). As the degradation rates of this polymer are well known [192, 193] and certainly much slower than the release rate of the drug, especially *in vivo*, and intact microspheres remained at the end of the release experiment, we did not explore the erosion and degradation behavior of the microspheres further. Now that we have initial proof-of-principle data on the success of *in vivo* delivery, further formulation work on PLGA microspheres for brimonidine and related drug molecules is warranted.

The inability of the injection site to heal was concerning. A delayed healing response may be due to the release of byproducts from the particles that delayed healing, or the mass effect of the particles. This hole through the sclera may be a risk for infection, although it is expected the conjunctiva healed over the wound limiting access to the wound.

6.5 Discussion

Current glaucoma medical therapies are dominated by topical administration. Due to the low bioavailability of eye drops, typically less than 5% of the drug penetrates into the eye and reaches the target site (i.e., ciliary body) [4]. The remaining 95% of the drug enters systemic circulation and can cause side effects throughout the body [4]. For example, brimonidine use causes dry mouth in 33% of patients [194]. Because of the low bioavailability of drug at the ciliary body, patients are often required to administer multiple eye drops daily. Patient adherence suffers due to the complexity and rigor of the treatment required to control glaucoma [55-58, 176, 195, 196]. It is estimated that adherence with use of topical eye drops is as low as 41% [4, 196].

Glaucoma therapy delivered in a highly-targeted manner to the ciliary body could reduce side effects by lowering the required dose. Supraciliary delivery allows the highly targeted delivery of glaucoma drugs to the ciliary body with significant dose sparing [6]. This dose sparing translates into a lower daily dose as well as fewer side effects. In this study, we delivered 0.9 mg of brimonidine loaded into slow-releasing polymeric microspheres as a single injection and demonstrated an IOP reduction for more than one month in the treated eye. The amount of brimonidine delivered via commercial eye drops three times per day for an equivalent time would result in a 7.5-times greater dose. Consistent with the lower administered dose, IOP reductions in the contralateral eye were not seen with the brimonidine-loaded microspheres groups compared with the topical eye drop administration. This increase in bioavailability during controlled release of brimonidine is lower than previously reported for bolus delivery of brimonidine in the suprachoroidal space[6]. We hypothesize that this may be due to the strong binding affinity of brimonidine to a_2 adrenergic receptors [181, 187] and the fast clearance from the SCS [5, 9]. With a bolus injection, brimonidine is expected to bind all available receptors and causes a biological response for up to 12 h [6]. However, with a controlled release system, brimonidine is continually released in small quantities, and this must overcome the clearance of brimonidine from the SCS. Because of its strong binding affinity, not all the brimonidine release will be able to bind receptors since the receptors are already occupied by previously released brimonidine. This brimonidine is essentially ‘wasted’, which may at least partially explain the lower than expected dose sparing. To our knowledge, this is the first time that controlled-release drug delivery systems for the management of glaucoma have been injected into the supraciliary space.

In this study, we have shown reduced IOP for one month, however further optimization of microsphere formulation and injection procedure could increase the duration of effect and further reduce the required dosage. Since glaucoma patients typically make regular visits to the eye clinic every 3 - 6 months, we envision an outpatient procedure performed by an ophthalmologist consisting of a single supraciliary microneedle injection of glaucoma drugs encapsulated within microspheres to adequately control IOP for the next 3 - 6 months. This would obviate the need for the patient to administer eye drops multiple times per day, and thus drastically raise patient adherence. Future studies will address the development of microparticles that release glaucoma drugs for 3 – 6 months and their use in the eye.

Histology sections showed foreign body response due to the presence of microspheres in the supraciliary space. This may be due to impurities in the microsphere fabrication process, or particle degradation byproducts, though further studies are needed to determine the cause. Nevertheless, the animals did not show signs of distress or redness in the eye. Furthermore, the microspheres persisted in the supraciliary space despite complete drug release. Further studies are required to improve the biocompatibility of materials injected into the supraciliary space.

The success of our approach is based on the combination of two advances: the development of sustained-release brimonidine microspheres and their placement adjacent to the drug's site of action in the ciliary body using microneedles. Roughly zero-order release of brimonidine with minimal burst effect was achieved by formulating the drug into PLA microspheres using PLA which was first treated to remove acidic monomers and oligomers to improve polymer stability during storage and effectively increasing molecular weight of the bulk PLA used for formulation. The resulting PLA microspheres had higher molecular weight and a denser matrix, which enabled efficient encapsulation, slow and continuous release with minimal burst in the first day. By increasing the PLA molecular weight or using an ester end-capped PLA in future studies, the release rate could be extended further, perhaps to achieve the target of 3 – 6 months of sustained release. Using different biodegradable polymers, such as poly(trimethylene carbonate), could reduce the inflammatory response to the microspheres because this polymer does not produce acidic byproducts during its degradation by surface erosion [197, 198]. Other polymers might also biodegrade in a time frame matched to the drug release.

Placement of the sustained-release microspheres in the supraciliary space served a number of functions. First, forming a drug depot adjacent to the ciliary body enabled dose sparing, which is not only of interest to reduce side effects, but also enables a smaller injection to contain enough drug for a longer duration of effect. Second, the supraciliary space is not in the visual axis and therefore should not affect vision the way eye drops or intravitreal injections can [97, 199].

Third, injection into the supraciliary space is expected to be safe and straightforward to perform on an outpatient basis. This is because the microneedle used for injection inherently targets the supraciliary space due to its length and the injection procedure is almost identical to how current intravitreal injections are routinely performed, except for using a shorter needle. Studies in animals and humans have shown that microneedle injections into the suprachoroidal space have been well tolerated [2, 7, 119, 124, 127].

Finally, the supraciliary space is believed to be a safe place to deposit drug formulations. The sclera and choroid are not tightly attached and thereby form a potential space that can be temporarily expanded without apparent long-term adverse effects [7, 9, 119, 136, 146, 199-202]. Sustained-release formulations placed into the suprachoroidal space of animals and humans have been well tolerated [7, 118, 124, 127]

7 CONCLUSION

Patients experiencing ocular pathology and/or disease can have devastating loss of vision and blindness, and consequently significant loss in quality of life[203-206]. Although many medications exist, delivering these drugs to the site of disease in a spatially and temporally controlled manner is challenging due to the eye's small size and unique barriers. Traditional ophthalmic drug delivery techniques, namely topical eye drops and intravitreal injections, are not able to target specific tissues within the eye, resulting in low bioavailability at the diseased tissue(s) and/or possible side effects due to drug affecting non-target tissues.

The suprachoroidal space (SCS) is a potential space found between the sclera and the choroid. Due to its proximity to the choroid, this space is an attractive site of drug delivery for posterior segment diseases because high bioavailability within the choroid and retina can be achieved[9, 125]. Thus, a lower drug dose can be used to achieve similar efficacy compared with traditional routes of administration[6]. Furthermore, the drug is compartmentalized in the SCS away from non-diseased tissues, which is expected to result in a more favorable side effect profile[9, 125]. Because of these reasons, drug delivery to the SCS has been achieved through invasive procedure and/or surgery[2, 116-118, 130].

A microneedle injection enables reliable and more efficient access to the SCS[8, 81], compared with previous methods[2, 117, 118, 130]. The length of the microneedle is matched to the thickness of the conjunctiva and sclera so the microneedle is physically unable to penetrate deeper into the eye (i.e., through the choroid and retina). When fluid is injected at this position (deep to the sclera but superficial to the choroid), it will flow circumferentially within the SCS, bathing the choroid in drug. Furthermore, microneedle injections can be performed in the outpatient clinic setting by ophthalmologists, and are well tolerated[7].

7.1 Kinetics of Suprachoroidal Space Delivery using Microneedles

To aid in the rational design of drug delivery strategies utilizing the SCS, we studied the distribution and clearance of particles and molecules, as well as a controlled release system, injected into the SCS using a microneedle. First, we identified anatomical barriers to circumferential spread within the SCS. We studied the circumferential spread of particles and molecules co-injected into the SCS, as well as the effect of viscous formulations on distribution. Then, we investigated the SCS thickness and the effect of injection volume and formulation on this parameter over time. Next, we examined clearance kinetics and the routes of clearance of molecules injected into the SCS. Finally, we developed and tested a controlled release drug delivery system within the SCS for the treatment of glaucoma.

7.1.1 Distribution in the suprachoroidal space

The first three studies described the distribution of molecules and particles injected into the SCS of rabbits and humans using microneedles. We found anatomical barriers (the long posterior ciliary arteries in rabbits *ex vivo* and *in vivo* and the short posterior ciliary arteries in human cadaver eyes) that prevented circumferential particle spread within the SCS. Particles injected in close proximity to these vessels did not spread isotropically like particles injected far from these anatomical features. We posited that this behavior was due to a physical barrier within the SCS caused by a multitude of vessels that bound the sclera and choroid together tightly. In contrast, the human long posterior ciliary artery did not bind the sclera and choroid tightly, and was not expected to form a barrier to spread. Instead, we found that the short posterior ciliary arteries in humans are morphologically similar to the long posterior ciliary arteries in rabbits, and we showed that these vessels also limited spread. Furthermore, solitary large attachments (i.e., the vortex vein) did not result in altered particle distribution. If the goal is to target the optic nerve and/or macula in human patients, further studies in live human subjects are warranted.

We studied the distribution of particles and molecules co-injected into the SCS of *ex vivo* and *in vivo* rabbits. The purpose of this study was to ascertain if particles and molecules that were co-injected distributed differently. With particles suspended in HBSS, we found that, as injection volume increased, the area of particle spread increased, though the area of molecule coverage was greater than that of particles. Particle entrapment could be ameliorated by increasing formulation viscosity. Akin to Stoke's Law, the viscous liquid formulation could form a 'sheath' around the particle and influence its interactions with the walls of the SCS. We also found that particles ranging from 20 to 2,000 nm in diameter also co-localized, suggesting particles of varying sizes behave similarly.

We next investigated amount of distension between the sclera and the choroid, which we termed the SCS thickness. We found that increasing injection volume of HBSS did not change the thickness. We looked into why this might be the case, as the injected fluid could spread circumferentially or increase SCS thickness. We provide evidence that there are SCS fibrils that bind the sclera and the choroid, and that these fibrils limit the expansion of the SCS. Changing the viscosity of the formulation injected had a major effect on SCS thickness, presumably since the viscous formulation could overcome the biomechanical forces of the tissues.

From these three studies, we provide a model of how fluids and particles distribute in the SCS. The volume of fluid injected attempts to distribute itself within the SCS so as to minimize forces. Fluid can distribute circumferentially and/or increase the SCS thickness. Low-viscosity formulations are unable to overcome the biomechanical forces of the tissue beyond a certain SCS thickness, and thus fluid is distributed in a disc-like region within the SCS that has a near-constant thickness. Initially, high-viscosity formulations resist flow and are able to overcome the tissue biomechanics, resulting in a localization of the fluid at the site of injection with an expanded SCS thickness. Over time, the viscous formulation may imbibe water to balance the increased osmotic forces of the fluid. This will cause swelling of the fluid at the site of injection. Alternatively, the viscous formulation can creep circumferentially in the SCS. Regardless of formulation, there are anatomical barriers in the SCS that physically limit circumferential flow (probably of a convective nature). These anatomical barriers are formed by tight adhesions as vessels traverse the sclera to anastomose with the choroid. If there is a solitary adhesion (as in the rabbit vortex), the effect is small and limited to just around the vessel. If there are many adhesions (as in the rabbit LPCA), an entire region can be blocked off. We hypothesize that these barriers are to convective flow so it may be possible to diffuse through or around them.

Particles injected as a suspension within these formulations appear to be carried by the formulation. The viscosity of the formulation influences when the particles ‘fall out’ of suspension. ‘Falling out’ may be due to gravitational, electrostatic, or morphological effects of the particles or rheological changes of the fluid. Since the viscosity of the formulation can change in the SCS over time due to dilution, prediction of particle transport time may be challenging.

7.1.2 Clearance from the suprachoroidal space

The second overall goal of this thesis was to study the clearance of molecules from the rabbit SCS *in vivo*. We began by investigating the rate of SCS collapse after microneedle injection of different liquid formulations. The rate of collapse varied from 40 min to 14 days depending on formulation composition. Surprisingly, some viscous formulations expanded within the SCS well after the injection. This phenomenon was likely due to the viscous gel imbibing water from the local tissue environment to equalize osmotic (and hydration) pressure[143].

We then determined the rate of clearance of fluorescent molecules ranging from 400 Da to 2 MDa. Whereas, small molecules (e.g., fluorescein) cleared from the SCS within 12 h, very large macromolecules were still in the SCS at 21 d. These very large macromolecules had significantly delayed clearance from the SCS likely due to the macromolecule being larger than the fenestrae of choriocapillaris[31]. Since clearance time of 2 MDa FITC-dextran matched the clearance of monoclonal antibodies injected intravitreally, this might be a viable strategy for controlled release in the SCS. Microspheres with similar dimensions as 2 MDa FITC-dextran were still visible in the SCS after 2 mo[8]. The macromolecule has deformable shape compared with the rigid microsphere, so clearance of 2 MDa FITC-dextran should still be possible.

We set out to determine the route of clearance from the SCS. Previous studies have hypothesized the route of clearance as intravascular clearance from the SCS[9, 126].

We collected fluorescein from different routes after microneedle injection. Contrary to those previous studies, we identified three regimes of clearance: (i) initial leakage of fluorescein from the injection site and perivascular leakage sites; (ii) pressure-driven trans-scleral movement of fluorescein, and (iii) diffusion into the choroid and subsequent intravascular clearance. These results were corroborated with a one-dimensional mathematical model of the SCS and surrounding tissues.

7.1.3 Controlled release systems within the suprachoroidal space

Due to the fast clearance from the SCS, we hypothesized that microparticle-based controlled-release drug delivery system could be used to extend time between dosing. We showed that such a system injected into the anterior SCS had a therapeutic effect for up to 1 mo.

However, this system achieved dose sparing of ~13% of the topical dose, which was not as much as the 1% of the topical dose achieved with bolus injections into the suprachoroidal space adjacent to the ciliary body (i.e., the supraciliary space)[6]. We hypothesized that this may be due to the strong binding affinity of brimonidine to a_2 adrenergic receptors and the fast clearance from the SCS. With a bolus injection, brimonidine was expected to bind all available receptors and cause a biological response for up to 12 h. However, with a controlled-release system, brimonidine was continually released in small quantities, and this must overcome the clearance of brimonidine from the SCS. Because of its strong binding affinity, not all the brimonidine release would be able to bind receptors since the receptors were already occupied by previously released brimonidine. This brimonidine was essentially ‘wasted’, which may at least partially explain the lower than expected dose sparing.

Using a more hydrophobic drug (such as latanoprost) might shrink this discrepancy in dose sparing between bolus and controlled release delivery. For example, suspensions of triamcinolone acetonide have been shown to release drug in the SCS for up to 2 mo[2, 7, 119, 127]. Another approach to have controlled release in the setting of fast clearance might be a drug delivery system that releases bursts of drug periodically. Drug would only be released during these bursts and not between the bursts. The periodicity of these bursts would match the time of efficacy for the drug encapsulated.

7.2 Role of Formulation on Kinetics

7.2.1 Liquid formulation

Changes in formulation can have a dramatic effect on distribution, both circumferentially and in SCS thickness. In particular, we studied the effect of injection volume and formulation viscosity on distribution. Increasing injection volume had a reasonable effect on circumferential spread and a negligible effect on SCS thickness. On the other hand, increasing formulation viscosity had the dual effect of initial localization at the injection site, as well as increased SCS thickness. Depending on the formulation composition, the formulation could remain localized (for example, if the formulation contains physically cross-linked polymers) or it could spread. We are unsure of the mechanism by which viscous formulations spread, though we hypothesize it is associated with the biomechanical properties of the tissue.

We achieved increased viscosity by adding high molecular weight macromolecules to the formulation. It would be interesting to find out if viscous formulations achieved with low molecular weight species would behave similarly.

7.2.2 Polymeric microparticles

We and others have shown that polymeric microparticles distribute in the SCS and are resistant to clearance. We provide evidence that particles ranging from 20 nm to 2,000 nm behave similarly. Even the smallest particles in this range are thought to be too large to fit through the fenestrae of the choriocapillaris. Thus, they are resistant to clearance.

The fabrication and composition of microspheres suitable for the SCS need to be optimized. Although the brimonidine-loaded microsphere system was efficacious for up to 1 mo, the microspheres seemed to cause a significant foreign body response in the SCS. This might be due to the fabrication process (e.g., incomplete removal of solvent) or the materials used. Since the SCS is exposed to the choroidal vasculature (which is one of the densest vascular beds in the body), there is the strong possibility of a potent immune response. Furthermore, we have an incomplete understanding of the immune system in the SCS. Perhaps a detailed study of immune responses to materials in the SCS is warranted.

Particles suspended in liquid formulations do not travel as far as the formulation. A theory on why this is has been presented above. This behavior might be modifiable by changing properties other than size.

7.3 Limitations of the Studies

The bulk of the studies were performed in albino New Zealand White rabbits, and there are inherent anatomical/physiological differences between rabbits and humans. The rabbit animal model was used because ocular dimensions of rabbit eyes are similar to humans while enabling visualization of fluorescence within the SCS. The use of smaller animals (e.g., rats and mice) would be significantly more difficult since a shorter microneedle would need to be developed, which might decrease reliability[81, 105]. Larger animals (e.g., pigs and monkeys, for which Georgia Tech has no housing facilities) would require significantly more cost and study coordination. Thus, the rabbit is a good animal model to study suprachoroidal delivery.

Despite limitations of the rabbit model, we believe the results of these studies are relevant to human health. For example, scaling microneedle dimensions is sufficient for reliable microneedle injections in rabbits and humans. Injection volumes should also be able to scale with respect to eye size. Some species-dependent parameters were deemed unimportant. For example, the scleral permeability of rabbits is different from that of humans, but sensitivity analysis indicates this parameter contributes very little to overall clearance.

To study kinetics, fluorescent tracer molecules were used as proxies for drugs. While parameters such as molecular radius can be matched, other physiochemical properties (such as partition coefficient and protein affinity) cannot be matched. It is possible these physiochemical properties also play a role in clearance[123]. Thus, studies with drugs of interest should be performed to determine their kinetics.

7.4 Final Note

These studies provide an in depth look at the kinetics of microneedle injections into the SCS, and lay the foundation for future developments in suprachoroidal delivery as a route of administration that targets diseased tissues in posterior segment indications.

8 FUTURE DIRECTIONS

This work investigated the kinetics (e.g., distribution and clearance) of molecules and particles injected into the SCS using a microneedle. In particular, we showed that (1) SCS thickness can be modulated with different excipient formulations; (2) particles become entrapped in the SCS to a greater extent relative to molecules; and (3) very large macromolecules (2 MDa) have significantly slower clearance times relative to smaller molecules. Since the bulk of this work was performed in rabbits, correlation in human subjects is also warranted. We will briefly discuss applications based on these findings, and possible ways forward.

8.1 SCS Thickness can be Modulated with Liquid Formulation

With low viscosity formulations (e.g., HBSS), the SCS reaches a constant thickness irrespective of injection volume. With high viscosity formulations (e.g., 5% CMC in HBSS), the SCS can reach a maximum thickness of ≥3 mm. Though this phenomenon has limited practicality in ophthalmic drug delivery, it can be useful in modulating biomechanical properties of the eye, including aqueous humor production and/or clearance, axial length of the eye, and re-apposition of the choroid with the retina (to treat retinal detachment).

We showed that intraocular pressure (IOP) dropped after the injection of a viscous formulation (with or without the drug, brimonidine). This could be due to disruption of the ciliary epithelium causing decreased aqueous humor production, stretching of the iris root causing increased uveoscleral outflow, or stretching of Schlemm’s canal causing increased aqueous humor outflow. Examination of the mechanism of this IOP reduction is warranted. A combined drug-device implant, wherein the implant could reduce IOP via biomechanical effects as well release glaucoma medications, could be developed to treat glaucoma. Suprachoroidal drainage stents (see CyPass® micro-stent[144, 147, 201] or iStent® Trabecular Micro-Bypass[145, 207]), which are biomechanical devices that function under similar principles, require surgery whereas the proposed drug-device implant could be injectable in an outpatient setting.

Refractive errors caused by myopia are due to misalignment of the retina relative to the focal plane of the eye[1]. Typically, myopia is caused by an increased axial length of the eye. We propose treating myopia by injecting a semi-permanent viscous formulation into the SCS to shift the retina (and choroid) forward so the focal plane of the eye lies on the retina.

A retinal detachment is a medical emergency where the retina detaches from the choroid, and can result in irreparable loss of retinal cells[1]. Typically, a scleral buckle is surgically placed around the ocular globe in an attempt to re-appose the retina to the choroid[208]. A suprachoroidal bleb could be used, instead of a scleral buckle, to achieve the same goal. And indeed, such a surgical procedure has been attempted with positive results[153, 154, 209]. We propose a procedure to treat retinal detachments by injecting a viscous formulation into the SCS to re-appose the retina to the choroid. Since time is of the essence with a retinal detachment, a microneedle injection is advantageous over other methods because it can be performed in the clinic or the emergency department, and would not require surgery. A follow-up surgical intervention could be performed if needed.

We noted some ischemia caused by the CMC bleb. This might be useful to prevent or control choroidal blood vessel growth (as in the case of choroidal neovascularization or retinopathy of prematurity.

8.2 Strategies for Controlled Release Treatments of Posterior Segment Diseases

Many therapeutics to treat posterior segment diseases are monoclonal antibodies (mAbs) that bind up soluble proteins or polypeptide[24, 68, 210, 211]. For example, wet age-related macular degeneration is treated with monthly intravitreal injections of mAbs against vascular endothelial growth factor (VEGF)[68, 69]. Since we and others[8, 9] have shown that macromolecules on the order of 150 kDa clear from the SCS within 1 d, controlled release of these macromolecules has been proposed[124]. Most controlled release systems rely on the encapsulation of the therapeutic agent in polymeric microspheres or monolithic implants. However, encapsulation can affect the stability and functionality of mAbs[212, 213]. Furthermore, we have shown that microspheres do not distribute well in the SCS relative to molecules.

Improving the formulation through the addition of viscous excipients should improve distribution of particles. Another approach might be to inject a solution of mAbs dissolved in a viscous solution. This should slow down the diffusion rate of mAbs to achieve some level of controlled release. And another approach might be to conjugate mAbs together to create very large macromolecules.

8.3 Visualization of SCS Injections in Human Subjects

Most of these studies were carried out in the *in vivo* and *ex vivo* albino New Zealand White rabbit eye, and species differences with humans are enough to warrant further experimentation. It was possible to visualize and track the kinetics of fluorescein (and derivatives) in the SCS of albino rabbits since there was no pigment in the retinal pigment epithelium and choroid. However, most humans (and other model animals) are not albino and thus visualization with this method would not work. We propose the use of indocyanine green[214] (or other fluorescent molecules with excitation/emission in the infrared spectra) as a marker of fluid distribution in the SCS. A near-infrared (NIR) dye should be visible regardless of the presence of visible-light pigment. Furthermore, indocyanine green is an FDA-approved molecule and there are ophthalmic imaging tools that have optics to visualize this molecule[215].

8.4 Future Outlook of Suprachoroidal Delivery

Microneedle injections into the suprachoroidal space (SCS) enable reliable and efficient access to the SCS[8, 81]. The SCS is an emerging route of administration to treat ocular disease affecting the posterior segment and ciliary body. This work investigated distribution and clearance of particles and molecules injected into the SCS using a microneedle. We showed that distribution of particle suspensions are limited by anatomical barriers[129]; that particles spread to a lesser area than molecules; that clearance of molecules is by a combination of reflux, trans-scleral transport, and choroidal clearance; that very large macromolecules are cleared slower; and that controlled-release polymeric drug delivery systems in the SCS are efficacious[115] but did not achieve the dose sparing seen with bolus injections[6]. From these experimental results, we generated theories to describe SCS kinetics.

The knowledge gained from this thesis should aid in the rational design of formulations and injection strategies to attain better targeting within the SCS. Some ideas are highlighted in this chapter. At the same time, others are advancing the acceptability of

SCS injections in human medicine. Based on encouraging results from a Phase II clinical trial that tested the safety of a microneedle injection of triamcinolone to treat posterior uveitis (NCT02255032), a Phase III clinical trial (NCT02595398) is actively recruiting to determine the efficacy of this system in the clinic. Overall, the future for microneedle injections into the suprachoroidal space is bright.

REFERENCES

1. Tasman W, Jaeger E. *Duane's Ophthalmology*. 15 ed. Philadelphia, Pa: Lippincott Williams & Wilkins; 2009.
2. Olsen TW, Feng X, Wabner K, et al. Cannulation of the suprachoroidal space: a novel drug delivery methodology to the posterior segment. *Am J Ophthalmol* 2006;142:777-787.
3. Doughty MJ, Zaman ML. Human Corneal Thickness and Its Impact on Intraocular Pressure Measures: A Review and Meta-analysis Approach. *Surv Ophthalmol* 2000;44:367-408.
4. Ghate D, Edelhauser HF. Barriers to glaucoma drug delivery. *J Glaucoma* 2008;17:147-156.
5. Wang M, Liu W, Lu Q, et al. Pharmacokinetic comparison of ketorolac after intracameral, intravitreal, and suprachoroidal administration in rabbits. *Retina* 2012;32:2158-2164.
6. Kim YC, Edelhauser HF, Prausnitz MR. Targeted delivery of antiglaucoma drugs to the supraciliary space using microneedles. *Invest Ophthalmol Vis Sci* 2014;55:7387-7397.
7. Goldstein DA. A phase 1/2 open-label, safety and tolerability study of triamcinolone acetonide administered to the suprachoroidal space in patients with non-infectious uveitis. *Invest Ophthalmol Vis Sci* 2015;56:3557-3557.
8. Patel SR, Berezovsky DE, McCarey BE, Zarnitsyn V, Edelhauser HF, Prausnitz MR. Targeted administration into the suprachoroidal space using a microneedle for drug delivery to the posterior segment of the eye. *Invest Ophthalmol Vis Sci* 2012;53:4433-4441.
9. Olsen TW, Feng X, Wabner K, Csaky K, Pambuccian S, Cameron JD. Pharmacokinetics of pars plana intravitreal injections versus microcannula suprachoroidal injections of bevacizumab in a porcine model. *Invest Ophthalmol Vis Sci* 2011;52:4749-4756.
10. Stiemke MM, Edelhauser HF, Geroski DH. The developing corneal endothelium: correlation of morphology, hydration and Na/K ATPase pump site density. *Curr Eye Res* 1991;10:145-156.
11. Moseley H, Foulds WS, Allan D, Kyle PM. Routes of clearance of radioactive water from the rabbit vitreous. *Br J Ophthalmol* 1984;68:145-151.
12. Fisher RF. The force of contraction of the human ciliary muscle during accommodation. *J Physiol* 1977;270:51-74.
13. Ethier CR, Johnson M, Ruberti J. Ocular biomechanics and biotransport. *Annu Rev Biomed Eng* 2004;6:249-273.
14. Cole DF. Secretion of the aqueous humour. *Exp Eye Res* 1977;25 Suppl:161-176.
15. Cunha-Vaz J. The blood-ocular barriers. *Surv Ophthalmol* 1979;23:279-296.
16. Alm A, Nilsson SF. Uveoscleral outflow--a review. *Exp Eye Res* 2009;88:760-768.
17. Kim YC, Edelhauser HF, Prausnitz MR. Particle-stabilized emulsion droplets for gravity-mediated targeting in the posterior segment of the eye. *Adv Healthc Mater* 2014;3:1272-1282.

18. Wistow GJ, Piatigorsky J. Lens crystallins: the evolution and expression of proteins for a highly specialized tissue. *Annu Rev Biochem* 1988;57:479-504.
19. Andley UP. Crystallins in the eye: Function and pathology. *Prog Retin Eye Res* 2007;26:78-98.
20. Hee MR, Izatt JA, Swanson EA, et al. Optical coherence tomography of the human retina. *Arch Ophthalmol-Chic* 1995;113:325-332.
21. Curcio CA, Sloan KR, Kalina RE, Hendrickson AE. Human photoreceptor topography. *J Comp Neurol* 1990;292:497-523.
22. Strauss O. The retinal pigment epithelium in visual function. *Physiol Rev* 2005;85:845-881.
23. Spraul CW, Lang GE, Grossniklaus HE, Lang GK. Histologic and morphometric analysis of the choroid, Bruch's membrane, and retinal pigment epithelium in postmortem eyes with age-related macular degeneration and histologic examination of surgically excised choroidal neovascular membranes. *Surv Ophthalmol* 1999;44 Suppl 1:S10-32.
24. Saint-Geniez M, Kurihara T, Sekiyama E, Maldonado AE, D'Amore PA. An essential role for RPE-derived soluble VEGF in the maintenance of the choriocapillaris. *Proc Natl Acad Sci U S A* 2009;106:18751-18756.
25. Runkle EA, Antonetti DA. The blood-retinal barrier: structure and functional significance. *Methods Mol Biol* 2011;686:133-148.
26. Bhutto I, Lutty G. Understanding age-related macular degeneration (AMD): relationships between the photoreceptor/retinal pigment epithelium/Bruch's membrane/choriocapillaris complex. *Mol Aspects Med* 2012;33:295-317.
27. Linsenmeier RA, Padnick-Silver L. Metabolic dependence of photoreceptors on the choroid in the normal and detached retina. *Invest Ophthalmol Vis Sci* 2000;41:3117-3123.
28. Ciulla TA, Harris A, Martin BJ. Ocular perfusion and age-related macular degeneration. *Acta Ophthalmol Scand* 2001;79:108-115.
29. Kiel JW, van Heuven WA. Ocular perfusion pressure and choroidal blood flow in the rabbit. *Invest Ophthalmol Vis Sci* 1995;36:579-585.
30. Ikuno Y, Kawaguchi K, Nouchi T, Yasuno Y. Choroidal thickness in healthy Japanese subjects. *Invest Ophthalmol Vis Sci* 2010;51:2173-2176.
31. Sarin H. Physiologic upper limits of pore size of different blood capillary types and another perspective on the dual pore theory of microvascular permeability. *J Angiogenes Res* 2010;2:14.
32. Lau JC, Linsenmeier RA. Oxygen consumption and distribution in the Long-Evans rat retina. *Exp Eye Res* 2012;102:50-58.
33. Fatt I, Shantinath K. Flow conductivity of retina and its role in retinal adhesion. *Exp Eye Res* 1971;12:218-226.
34. Emi K, Pederson JE, Toris CB. Hydrostatic pressure of the suprachoroidal space. *Invest Ophthalmol Vis Sci* 1989;30:233-238.
35. Jackson TL, Hussain A, Hodgetts A, et al. Human scleral hydraulic conductivity: age-related changes, topographical variation, and potential scleral outflow facility. *Invest Ophthalmol Vis Sci* 2006;47:4942-4946.

36. Kim SH, Galban CJ, Lutz RJ, et al. Assessment of subconjunctival and intrascleral drug delivery to the posterior segment using dynamic contrast-enhanced magnetic resonance imaging. *Invest Ophthalmol Vis Sci* 2007;48:808-814.
37. Moses RA. Detachment of ciliary body--anatomical and physical considerations. *Invest Ophthalmol* 1965;4:935-941.
38. Ambati J, Canakis CS, Miller JW, et al. Diffusion of high molecular weight compounds through sclera. *Invest Ophthalmol Vis Sci* 2000;41:1181-1185.
39. Nakao S, Hafezi-Moghadam A, Ishibashi T. Lymphatics and lymphangiogenesis in the eye. *J Ophthalmol* 2012;2012:783163.
40. Pescina S, Ferrari G, Govoni P, et al. In-vitro permeation of bevacizumab through human sclera: effect of iontophoresis application. *J Pharm Pharmacol* 2010;62:1189-1194.
41. Bill A. Quantitative determination of uveal blood flow in rabbits. *Acta Physiol Scand* 1962;55:101-110.
42. Nillson SF. The uveoscleral outflow routes. *Eye (Lond)* 1997;11:149-154.
43. Inomata H, Bill A. Exit sites of uveoscleral flow of aqueous humor in cynomolgus monkey eyes. *Exp Eye Res* 1977;25:113-118.
44. Krohn J, Bertelsen T. Corrosion casts of the suprachoroidal space and uveoscleral drainage routes in the human eye. *Acta Ophthalmol Scand* 1997;75:32-35.
45. Olsen TW, Aaberg SY, Geroski DH, Edelhauser HF. Human sclera: thickness and surface area. *Am J Ophthalmol* 1998;125:237-241.
46. Kontermann RE. Half-life extended biotherapeutics. *Expert Opin Biol Ther* 2016.
47. Tan LE, Orilla W, Hughes PM, Tsai S, Burke JA, Wilson CG. Effects of vitreous liquefaction on the intravitreal distribution of sodium fluorescein, fluorescein dextran, and fluorescent microparticles. *Invest Ophthalmol Vis Sci* 2011;52:1111-1118.
48. Meral I, Bilgili Y. Diffusion changes in the vitreous humor of the eye during aging. *AJNR Am J Neuroradiol* 2011;32:1563-1566.
49. Weinreb RN, Khaw PT. Primary open-angle glaucoma. *Lancet* 2004;363:1711-1720.
50. Quigley HA, Broman AT. The number of people with glaucoma worldwide in 2010 and 2020. *Br J Ophthalmol* 2006;90:262-267.
51. Quigley HA, Cassard SD, Gower EW, Ramulu PY, Jampel HD, Friedman DS. The cost of glaucoma care provided to Medicare beneficiaries from 2002 to 2009. *Ophthalmology* 2013;120:2249-2257.
52. Sommer A. Relationship between intraocular pressure and primary open angle glaucoma among white and black Americans. *Archives of Ophthalmology* 1991;109:1090.
53. Gooch N, Molokhia SA, Condie R, et al. Ocular drug delivery for glaucoma management. *Pharmaceutics* 2012;4:197-211.
54. Lavik E, Kuehn MH, Kwon YH. Novel drug delivery systems for glaucoma. *Eye (Lond)* 2011;25:578-586.
55. Gurwitz JH, Glynn RJ, Monane M, et al. Treatment for glaucoma: adherence by the elderly. *Am J Public Health* 1993;83:711-716.

56. Robin AL, Novack GD, Covert DW, Crockett RS, Marcic TS. Adherence in glaucoma: objective measurements of once-daily and adjunctive medication use. *Am J Ophthalmol* 2007;144:533-540.
57. Rotchford AP, Murphy KM. Compliance with timolol treatment in glaucoma. *Eye (Lond)* 1998;12 (Pt 2):234-236.
58. Tsai JC, McClure CA, Ramos SE, Schlundt DG, Pichert JW. Compliance barriers in glaucoma: a systematic classification. *J Glaucoma* 2003;12:393-398.
59. Sudharshan S, Ganesh SK, Biswas J. Current approach in the diagnosis and management of posterior uveitis. *Indian J Ophthalmol* 2010;58:29-43.
60. Jaffe GJ, Martin D, Callanan D, et al. Fluocinolone acetonide implant (Retisert) for noninfectious posterior uveitis: thirty-four-week results of a multicenter randomized clinical study. *Ophthalmology* 2006;113:1020-1027.
61. Kok H, Lau C, Maycock N, McCluskey P, Lightman S. Outcome of intravitreal triamcinolone in uveitis. *Ophthalmology* 2005;112:1916-1921.
62. Williamson J, Paterson RW, McGavin DD, Jasani MK, Boyle JA, Doig WM. Posterior subcapsular cataracts and glaucoma associated with long-term oral corticosteroid therapy. In patients with rheumatoid arthritis and related conditions. *Br J Ophthalmol* 1969;53:361-372.
63. Klein R, Chou CF, Klein BE, Zhang X, Meuer SM, Saaddine JB. Prevalence of age-related macular degeneration in the US population. *Arch Ophthalmol-Chic* 2011;129:75-80.
64. Ambati J, Fowler BJ. Mechanisms of age-related macular degeneration. *Neuron* 2012;75:26-39.
65. Nowak J. Age related macular degeneration (AMD): pathogenesis and therapy. *Pharmacological Reports* 2006;58:353.
66. Zarbin MA. Pathogenesis of Age-Related Macular Degeneration. *Medical Retina* 2012;1:125-133.
67. Cheung LK, Eaton A. Age-related macular degeneration. *Pharmacotherapy* 2013;33:838-855.
68. Group CR, Martin DF, Maguire MG, et al. Ranibizumab and bevacizumab for neovascular age-related macular degeneration. *N Engl J Med* 2011;364:1897-1908.
69. Avery RL, Pieramici DJ, Rabena MD, Castellarin AA, Nasir MA, Giust MJ. Intravitreal bevacizumab (Avastin) for neovascular age-related macular degeneration. *Ophthalmology* 2006;113:363-372 e365.
70. Heier JS, Brown DM, Chong V, et al. Intravitreal aflibercept (VEGF trap-eye) in wet age-related macular degeneration. *Ophthalmology* 2012;119:2537-2548.
71. Hartnett ME, Wittchen ES, Hartnett ME. Breaking barriers: insight into the pathogenesis of neovascular age-related macular degeneration. *Eye and Brain* 2011;19.
72. Lois N, McBain V, Abdelkader E, Scott NW, Kumari R. Retinal pigment epithelial atrophy in patients with exudative age-related macular degeneration undergoing anti-vascular endothelial growth factor therapy. *Retina* 2013;33:13-22.
73. Tolentino M. Systemic and ocular safety of intravitreal anti-VEGF therapies for ocular neovascular disease. *Surv Ophthalmol* 2011;56:95-113.
74. Hartong DT, Berson EL, Dryja TP. Retinitis pigmentosa. *The Lancet* 2006;368:1795-1809.

75. Beltran WA, Cideciyan AV, Lewin AS, et al. Gene therapy rescues photoreceptor blindness in dogs and paves the way for treating human X-linked retinitis pigmentosa. *Proc Natl Acad Sci U S A* 2012;109:2132-2137.
76. Deng WT, Dyka FM, Dinculescu A, et al. Stability and Safety of an AAV Vector for Treating RPGR-ORF15 X-Linked Retinitis Pigmentosa. *Hum Gene Ther* 2015;26:593-602.
77. Yue L, Falabella P, Christopher P, et al. Ten-Year Follow-up of a Blind Patient Chronically Implanted with Epiretinal Prosthesis Argus I. *Ophthalmology* 2015;122:2545-2552 e2541.
78. Humayun MS, Dorn JD, da Cruz L, et al. Interim results from the international trial of Second Sight's visual prosthesis. *Ophthalmology* 2012;119:779-788.
79. Dimaras H, Kimani K, Dimba EAO, et al. Retinoblastoma. *The Lancet* 2012;379:1436-1446.
80. Shields JA, Shields CL. Management of posterior uveal melanoma: past, present, and future: the 2014 Charles L. Schepens lecture. *Ophthalmology* 2015;122:414-428.
81. Patel SR, Lin AS, Edelhauser HF, Prausnitz MR. Suprachoroidal drug delivery to the back of the eye using hollow microneedles. *Pharm Res* 2011;28:166-176.
82. Fischer AH, Jacobson KA, Rose J, Zeller R. Hematoxylin and eosin staining of tissue and cell sections. *CSH Protoc* 2008;2008:pdb prot4986.
83. Yannuzzi LA, Ober MD, Slakter JS, et al. Ophthalmic fundus imaging: today and beyond. *Am J Ophthalmol* 2004;137:511-524.
84. Li SK, Lizak MJ, Jeong EK. MRI in ocular drug delivery. *NMR Biomed* 2008;21:941-956.
85. Edelman RR, Warach S. Magnetic resonance imaging (1). *N Engl J Med* 1993;328:708-716.
86. Pavlin CJ, Harasiewicz K, Sherar MD, Foster FS. Clinical Use of Ultrasound Biomicroscopy. *Ophthalmology* 1991;98:287-295.
87. Huang D, Swanson E, Lin C, et al. Optical coherence tomography. *Science* 1991;254:1178-1181.
88. Rowe-Rendleman CL, Durazo SA, Kompella UB, et al. Drug and gene delivery to the back of the eye: from bench to bedside. *Invest Ophthalmol Vis Sci* 2014;55:2714-2730.
89. Mishima S, Gasset A, Klyce SD, Jr., Baum JL. Determination of tear volume and tear flow. *Invest Ophthalmol* 1966;5:264-276.
90. Mochizuki H, Yamada M, Hatou S, Tsubota K. Turnover rate of tear-film lipid layer determined by fluorophotometry. *Br J Ophthalmol* 2009;93:1535-1538.
91. Edwards A, Prausnitz MR. Predicted permeability of the cornea to topical drugs. *Pharmaceutical research* 2001;18:1497-1508.
92. Mandell KJ, Berglin L, Severson EA, Edelhauser HF, Parkos CA. Expression of JAM-A in the human corneal endothelium and retinal pigment epithelium: localization and evidence for role in barrier function. *Invest Ophthalmol Vis Sci* 2007;48:3928-3936.
93. Nomoto H, Shiraga F, Kuno N, et al. Pharmacokinetics of bevacizumab after topical, subconjunctival, and intravitreal administration in rabbits. *Invest Ophthalmol Vis Sci* 2009;50:4807-4813.

94. Fischbarg J. *Biology of the Eye*. 1 ed: Elvesier; 2006.

95. Ranta VP, Mannermaa E, Lummepuro K, et al. Barrier analysis of periocular drug delivery to the posterior segment. *J Control Release* 2010;148:42-48.

96. Nickla DL, Wallman J. The multifunctional choroid. *Prog Retin Eye Res* 2010;29:144-168.

97. Kim YC, Chiang B, Wu X, Prausnitz MR. Ocular delivery of macromolecules. *J Control Release* 2014;190:172-181.

98. Benz MS, Albini TA, Holz ER, et al. Short-term course of intraocular pressure after intravitreal injection of triamcinolone acetonide. *Ophthalmology* 2006;113:1174-1178.

99. Beer PM, Bakri SJ, Singh RJ, Liu W, Peters GB, Miller M. Intraocular concentration and pharmacokinetics of triamcinolone acetonide after a single intravitreal injection. *Ophthalmology* 2003;110:681-686.

100. Edelhauser HF, Rowe-Rendleman CL, Robinson MR, et al. Ophthalmic drug delivery systems for the treatment of retinal diseases: basic research to clinical applications. *Invest Ophthalmol Vis Sci* 2010;51:5403-5420.

101. Jonas JB, Spandau UH, Schlichtenbrede F. Short-term complications of intravitreal injections of triamcinolone and bevacizumab. *Eye (Lond)* 2008;22:590-591.

102. Bakri SJ, Snyder MR, Reid JM, Pulido JS, Ezzat MK, Singh RJ. Pharmacokinetics of intravitreal ranibizumab (Lucentis). *Ophthalmology* 2007;114:2179-2182.

103. Robinson MR, Lee SS, Kim H, et al. A rabbit model for assessing the ocular barriers to the transscleral delivery of triamcinolone acetonide. *Exp Eye Res* 2006;82:479-487.

104. Olsen TW, Edelhauser HF, Lim JI, Geroski DH. Human scleral permeability. Effects of age, cryotherapy, transscleral diode laser, and surgical thinning. *Invest Ophthalmol Vis Sci* 1995;36:1893-1903.

105. Davis SP, Landis BJ, Adams ZH, Allen MG, Prausnitz MR. Insertion of microneedles into skin: measurement and prediction of insertion force and needle fracture force. *Journal of Biomechanics* 2004;37:1155-1163.

106. Park JH, Allen MG, Prausnitz MR. Biodegradable polymer microneedles: fabrication, mechanics and transdermal drug delivery. *J Control Release* 2005;104:51-66.

107. Park JH, Allen MG, Prausnitz MR. Polymer microneedles for controlled-release drug delivery. *Pharm Res* 2006;23:1008-1019.

108. Gill HS, Prausnitz MR. Coating formulations for microneedles. *Pharm Res* 2007;24:1369-1380.

109. Jiang J, Gill HS, Ghate D, et al. Coated microneedles for drug delivery to the eye. *Invest Ophthalmol Vis Sci* 2007;48:4038-4043.

110. Jiang J, Moore JS, Edelhauser HF, Prausnitz MR. Intrascleral drug delivery to the eye using hollow microneedles. *Pharm Res* 2009;26:395-403.

111. Sullivan SP, Koutsonanos DG, Del Pilar Martin M, et al. Dissolving polymer microneedle patches for influenza vaccination. *Nat Med* 2010;16:915-920.

112. Gupta J, Felner EI, Prausnitz MR. Rapid pharmacokinetics of intradermal insulin administered using microneedles in type 1 diabetes subjects. *Diabetes Technol Ther* 2011;13:451-456.

113. Kim YC, Park JH, Prausnitz MR. Microneedles for drug and vaccine delivery. *Adv Drug Deliv Rev* 2012;64:1547-1568.
114. Kim YC, Grossniklaus HE, Edelhauser HF, Prausnitz MR. Intrastromal delivery of bevacizumab using microneedles to treat corneal neovascularization. *Invest Ophthalmol Vis Sci* 2014;55:7376-7386.
115. Chiang B, Kim YC, Doty AC, Grossniklaus HE, Schwendeman SP, Prausnitz MR. Sustained reduction of intraocular pressure by supraciliary delivery of brimonidine-loaded poly(lactic acid) microspheres for the treatment of glaucoma. *J Control Release* 2016;228:48-57.
116. Seiler GS, Salmon JH, Mantuo R, Feingold S, Dayton PA, Gilger BC. Effect and distribution of contrast medium after injection into the anterior suprachoroidal space in ex vivo eyes. *Invest Ophthalmol Vis Sci* 2011;52:5730-5736.
117. Peden MC, Min J, Meyers C, et al. Ab-externo AAV-mediated gene delivery to the suprachoroidal space using a 250 micron flexible microcatheter. *PLoS One* 2011;6:e17140.
118. Einmahl S, Savoldelli M, D'Hermies F, Tabatabay C, Gurny R, Behar-Cohen F. Evaluation of a novel biomaterial in the suprachoroidal space of the rabbit eye. *Invest Ophthalmol Vis Sci* 2002;43:1533-1539.
119. Chen M, Li X, Liu J, Han Y, Cheng L. Safety and pharmacodynamics of suprachoroidal injection of triamcinolone acetonide as a controlled ocular drug release model. *J Control Release* 2015;203:109-117.
120. Gu B, Liu J, Li X, Ma Q, Shen M, Cheng L. Real-Time Monitoring of Suprachoroidal Space (SCS) Following SCS Injection Using Ultra-High Resolution Optical Coherence Tomography in Guinea Pig Eyes. *Invest Ophthalmol Vis Sci* 2015;56:3623-3634.
121. Rodrigues EB, Grumann A, Jr., Penha FM, et al. Effect of needle type and injection technique on pain level and vitreal reflux in intravitreal injection. *J Ocul Pharmacol Ther* 2011;27:197-203.
122. Doshi RR, Bakri SJ, Fung AE. Intravitreal injection technique. *Semin Ophthalmol* 2011;26:104-113.
123. Kadam RS, Williams J, Tyagi P, Edelhauser HF, Kompella UB. Suprachoroidal delivery in a rabbit ex vivo eye model: influence of drug properties, regional differences in delivery, and comparison with intravitreal and intracameral routes. *Mol Vis* 2013;19:1198-1210.
124. Tyagi P, Barros M, Stansbury JW, Kompella UB. Light-activated, in situ forming gel for sustained suprachoroidal delivery of bevacizumab. *Mol Pharm* 2013;10:2858-2867.
125. Tyagi P, Kadam RS, Kompella UB. Comparison of suprachoroidal drug delivery with subconjunctival and intravitreal routes using noninvasive fluorophotometry. *PLoS One* 2012;7:e48188.
126. Abarca EM, Salmon JH, Gilger BC. Effect of choroidal perfusion on ocular tissue distribution after intravitreal or suprachoroidal injection in an arterially perfused ex vivo pig eye model. *J Ocul Pharmacol Ther* 2013;29:715-722.
127. Gilger BC, Abarca EM, Salmon JH, Patel S. Treatment of acute posterior uveitis in a porcine model by injection of triamcinolone acetonide into the suprachoroidal space using microneedles. *Invest Ophthalmol Vis Sci* 2013;54:2483-2492.

128. Kim YC, Oh KH, Edelhauser HF, Prausnitz MR. Formulation to target delivery to the ciliary body and choroid via the suprachoroidal space of the eye using microneedles. *Eur J Pharm Biopharm* 2015;95:398-406.
129. Chiang B, Kim YC, Edelhauser HF, Prausnitz MR. Circumferential flow of particles in the suprachoroidal space is impeded by the posterior ciliary arteries. *Exp Eye Res* 2016.
130. Tzameret A, Sher I, Belkin M, et al. Transplantation of human bone marrow mesenchymal stem cells as a thin subretinal layer ameliorates retinal degeneration in a rat model of retinal dystrophy. *Exp Eye Res* 2014;118:135-144.
131. Hayreh SS. Posterior ciliary artery circulation in health and disease: the Weisenfeld lecture. *Invest Ophthalmol Vis Sci* 2004;45:749-757; 748.
132. Rucker CW, Stein HA, Wakim KG. In vivo studies on the choroidal circulation of rabbits. *AMA Arch Ophthalmol* 1956;56:726-735.
133. Okubo H, Gherezhiher T, Koss MC. Long posterior ciliary arterial blood flow and systemic blood pressure. *Invest Ophthalmol Vis Sci* 1990;31:819-826.
134. Mok KH, Lee VW. Disc-to-macula distance to disc-diameter ratio for optic disc size estimation. *J Glaucoma* 2002;11:392-395.
135. Ninomiya H, Inomata T. Microvascular anatomy of the pig eye: scanning electron microscopy of vascular corrosion casts. *J Vet Med Sci* 2006;68:1149-1154.
136. Ianchulev T. *Suprachoroidal space as a therapeutic target*. New York: Springer; 2014.
137. Zhang YL, Chang SJ, Zhai XY, Thomsen JS, Christensen EI, Andreasen A. Non-rigid landmark-based large-scale image registration in 3-D reconstruction of mouse and rat kidney nephrons. *Micron* 2015;68:122-129.
138. Song Y, Treanor D, Bulpitt AJ, Magee DR. 3D reconstruction of multiple stained histology images. *J Pathol Inform* 2013;4:S7.
139. Nielsen LJ, Eyley S, Thielemans W, Aylott JW. Dual fluorescent labelling of cellulose nanocrystals for pH sensing. *Chem Commun (Camb)* 2010;46:8929-8931.
140. McDonald JH, Dunn KW. Statistical tests for measures of colocalization in biological microscopy. *J Microsc* 2013;252:295-302.
141. Culbertson C. Diffusion coefficient measurements in microfluidic devices. *Talanta* 2002;56:365-373.
142. Bozkir G, Bozkir M, Dogan H, Aycan K, Guler B. Measurements of axial length and radius of corneal curvature in the rabbit eye. *Acta Med Okayama* 1997;51:9-11.
143. Benchabane A, Bekkour K. Rheological properties of carboxymethyl cellulose (CMC) solutions. *Colloid and Polymer Science* 2008;286:1173-1180.
144. Garcia-Feijoo J, Rau M, Grisanti S, et al. Supraciliary Micro-stent Implantation for Open-Angle Glaucoma Failing Topical Therapy: 1-Year Results of a Multicenter Study. *Am J Ophthalmol* 2015;159:1075-1081 e1071.
145. Wellik SR, Dale EA. A review of the iStent((R)) trabecular micro-bypass stent: safety and efficacy. *Clin Ophthalmol* 2015;9:677-684.
146. Patrianakos TD. Anatomic and physiologic rationale to be applied in accessing the suprachoroidal space for management of glaucoma. *J Cataract Refract Surg* 2014;40:1285-1290.

147. Hoh H, Grisanti S, Grisanti S, Rau M, Ianchulev S. Two-year clinical experience with the CyPass micro-stent: safety and surgical outcomes of a novel supraciliary micro-stent. *Klin Monbl Augenheilkd* 2014;231:377-381.
148. Ayton LN, Blamey PJ, Guymer RH, et al. First-in-human trial of a novel suprachoroidal retinal prosthesis. *PLoS One* 2014;9:e115239.
149. Touchard E, Berdugo M, Bigey P, et al. Suprachoroidal electrotransfer: a nonviral gene delivery method to transfect the choroid and the retina without detaching the retina. *Mol Ther* 2012;20:1559-1570.
150. ASTM Standard D1876 "Standard test method for peel resistance of adhesives (T-Peel Test)". West Conshohocken, PA: ASTM International; 2008 (2015).
151. Ugarte M, Hussain AA, Marshall J. An experimental study of the elastic properties of the human Bruch's membrane-choroid complex: relevance to ageing. *Br J Ophthalmol* 2006;90:621-626.
152. Daxer A, Misof K, Grabner B, Ettl A, Fratzl P. Collagen fibrils in the human corneal stroma: structure and aging. *Invest Ophthalmol Vis Sci* 1998;39:644-648.
153. El Rayes EN, Oshima Y. Suprachoroidal buckling for retinal detachment. *Retina* 2013;33:1073-1075.
154. Poole TA, Sudarsky RD. Suprachoroidal implantation for the treatment of retinal detachment. *Ophthalmology* 1986;93:1408-1412.
155. Moseley H, Foulds WS. The movement of xenon-133 from the vitreous to the choroid. *Exp Eye Res* 1982;34:169-179.
156. Kano MR, Bae Y, Iwata C, et al. Improvement of cancer-targeting therapy, using nanocarriers for intractable solid tumors by inhibition of TGF-beta signaling. *Proc Natl Acad Sci U S A* 2007;104:3460-3465.
157. Dreher MR, Liu W, Michelich CR, Dewhirst MW, Yuan F, Chilkoti A. Tumor vascular permeability, accumulation, and penetration of macromolecular drug carriers. *J Natl Cancer Inst* 2006;98:335-344.
158. Wen H, Hao J, Li SK. Characterization of human sclera barrier properties for transscleral delivery of bevacizumab and ranibizumab. *J Pharm Sci* 2013;102:892-903.
159. Bird R, Stewart W, Lightfoot E. *Transport Phenomena, 2nd edition*: John Wiley & Sons; 2006.
160. Berg HC. *Random walks in biology*: Princeton University Press; 1993.
161. Zhang Y, Li Z, Liu L, Han X, Zhao X, Mu G. Comparison of riboflavin/ultraviolet-A cross-linking in porcine, rabbit, and human sclera. *Biomed Res Int* 2014;2014:194204.
162. Edwards A, Prausnitz MR. Fiber matrix model of sclera and corneal stroma for drug delivery to the eye. *AIChE Journal* 1998;44:214-225.
163. Lin CW, Wang Y, Challa P, Epstein DL, Yuan F. Transscleral diffusion of ethacrynic acid and sodium fluorescein. *Mol Vis* 2007;13:243-251.
164. Esmaeelpour M, Ansari-Shahrezaei S, Glittenberg C, et al. Choroid, Haller's, and Sattler's layer thickness in intermediate age-related macular degeneration with and without fellow neovascular eyes. *Invest Ophthalmol Vis Sci* 2014;55:5074-5080.
165. Fatt I, Hedbys BO. Flow of water in the sclera. *Exp Eye Res* 1970;10:243-249.

166. Missel PJ. Finite and Infinitesimal Representations of the Vasculature: Ocular Drug Clearance by Vascular and Hydraulic Effects. *Annals of Biomedical Engineering* 2002;30:1128-1139.
167. Kestin J, Sokolov M, Wakeham WA. Viscosity of liquid water in the range −8 °C to 150 °C. *Journal of Physical and Chemical Reference Data* 1978;7:941.
168. Rudnick DE, Noonan JS, Geroski DH, Prausnitz MR, Edelhauser HF. The effect of intraocular pressure on human and rabbit scleral permeability. *Invest Ophthalmol Vis Sci* 1999;40:3054-3058.
169. Prausnitz MR, Noonan JS. Permeability of cornea, sclera, and conjunctiva: a literature analysis for drug delivery to the eye. *J Pharm Sci* 1998;87:1479-1488.
170. Conway A, Vazin T, Spelke DP, et al. Multivalent ligands control stem cell behaviour in vitro and in vivo. *Nat Nanotechnol* 2013;8:831-838.
171. Pollock JF, Ashton RS, Rode NA, Schaffer DV, Healy KE. Molecular characterization of multivalent bioconjugates by size-exclusion chromatography with multiangle laser light scattering. *Bioconjug Chem* 2012;23:1794-1801.
172. Stebbins ND, Faig JJ, Yu W, Guliyev R, Uhrich KE. Polyactives: controlled and sustained bioactive release via hydrolytic degradation. *Biomater Sci* 2015;3:1171-1187.
173. Gordon MO, Beiser JA, Brandt JD, et al. The Ocular Hypertension Treatment Study: baseline factors that predict the onset of primary open-angle glaucoma. *Arch Ophthalmol-Chic* 2002;120:714-720; discussion 829-730.
174. Toris CB, Gleason ML, Camras CB, Yablonski ME. Effects of brimonidine on aqueous humor dynamics in human eyes. *Arch Ophthalmol-Chic* 1995;113:1514-1517.
175. Konstas AG, Stewart WC, Topouzis F, Tersis I, Holmes KT, Stangos NT. Brimonidine 0.2% given two or three times daily versus timolol maleate 0.5% in primary open-angle glaucoma. *Am J Ophthalmol* 2001;131:729-733.
176. Patel SC, Spaeth GL. Compliance in patients prescribed eyedrops for glaucoma. *Ophthalmic Surg* 1995;26:233-236.
177. Ibrahim MM, Abd-Elgawad AH, Soliman OA, Jablonski MM. Natural bioadhesive biodegradable nanoparticle-based topical ophthalmic formulations for management of glaucoma. *Transl Vis Sci Technol* 2015;4:12.
178. Fedorchak MV, Conner IP, Medina CA, Wingard JB, Schuman JS, Little SR. 28-day intraocular pressure reduction with a single dose of brimonidine tartrate-loaded microspheres. *Exp Eye Res* 2014;125:210-216.
179. Deokule SP, Baffi JZ, Guo H, Nazzaro M, Kaneko H. Evaluation of extended release brimonidine intravitreal device in normotensive rabbit eyes. *Acta Ophthalmol* 2012;90:e344-348.
180. De TK, Rodman DJ, Holm BA, Prasad PN, Bergey EJ. Brimonidine formulation in polyacrylic acid nanoparticles for ophthalmic delivery. *J Microencapsul* 2003;20:361-374.
181. Walters TR. Development and use of brimonidine in treating acute and chronic elevations of intraocular pressure: A review of safety, efficacy, dose response, and dosing studies. *Survey of Ophthalmology* 1996;41:S19-S26.
182. Yamamoto M, Okada H, Ogawa Y, Miyagawa T. Polymer, production and use thereof. *European Patent 86303417* Oct. 21, 1987.

183. Burke JA, Hughes PM, Zhang K-M, et al. Intraocular implants and methods for improving vision. *US Patent US8293741* 2012.
184. Matsuo T, Cynader MS. Localization of alpha-2 adrenergic receptors in the human eye. *Ophthalmic Res* 1992;24:213-219.
185. Chang J, Hughes P. Oil-in-water method for making alpha-2 agonist polymeric drug delivery systems. *US Patent 7589057* Sep. 15, 2009.
186. Huang X, Brazel CS. On the importance and mechanisms of burst release in matrix-controlled drug delivery systems. *Journal of Controlled Release* 2001;73:121-136.
187. Burke J, Kharlamb A, Shan T, et al. Adrenergic and imidazoline receptor-mediated responses to UK-14,304-18 (brimonidine) in rabbits and monkeys. A species difference. *Ann N Y Acad Sci* 1995;763:78-95.
188. Khan ZP, Ferguson CN, Jones RM. Alpha-2 and imidazoline receptor agonists: Their pharmacology and therapeutic role. *Anaesthesia* 1999;54:146-165.
189. Brubaker RF. Targeting outflow facility in glaucoma management. *Surv Ophthalmol* 2003;48 Suppl 1:S17-20.
190. Kaufman PL, Barany EH. Loss of acute pilocarpine effect on outflow facility following surgical disinsertion and retrodisplacement of the ciliary muscle from the scleral spur in the cynomolgus monkey. *Invest Ophthalmol* 1976;15:793-807.
191. Hikichi T, Yoshida A, Hasegawa T, Ohnishi M, Sato T, Muraoka S. Wound healing of scleral self-sealing incision: a comparison of ultrasound biomicroscopy and histology findings. *Graefes Arch Clin Exp Ophthalmol* 1998;236:775-778.
192. Anderson JM, Shive MS. Biodegradation and biocompatibility of PLA and PLGA microspheres. *Advanced Drug Delivery Reviews* 1997;28:5-24.
193. Lin SY, Chen KS, Teng HH, Li MJ. In vitro degradation and dissolution behaviours of microspheres prepared by three low molecular weight polyesters. *J Microencapsul* 2000;17:577-586.
194. Camras CB. Comparison of latanoprost and timolol in patients with ocular hypertension and glaucoma: a six-month masked, multicenter trial in the United States. The United States Latanoprost Study Group. *Ophthalmology* 1996;103:138-147.
195. Lee DA, Higginbotham EJ. Glaucoma and its treatment: a review. *American journal of health-system pharmacy : AJHP : official journal of the American Society of Health-System Pharmacists* 2005;62:691-699.
196. Reardon G, Kotak S, Schwartz GF. Objective assessment of compliance and persistence among patients treated for glaucoma and ocular hypertension: a systematic review. *Patient Preference and Adherence* 2011;5:441-463.
197. Jansen J, Koopmans SA, Los LI, et al. Intraocular degradation behavior of crosslinked and linear poly(trimethylene carbonate) and poly(d,l-lactic acid). *Biomaterials* 2011;32:4994-5002.
198. Pêgo AP, Van Luyn MJA, Brouwer LA, et al. In vivo behavior of poly(1,3-trimethylene carbonate) and copolymers of 1,3-trimethylene carbonate with D,L-lactide or ϵ-caprolactone: Degradation and tissue response. *Journal of Biomedical Materials Research Part A* 2003;67A:1044-1054.
199. Rai Udo J, Young SA, Thrimawithana TR, et al. The suprachoroidal pathway: a new drug delivery route to the back of the eye. *Drug Discov Today* 2015;20:491-495.

200. Mandelcorn ED, Kitchens JW, Fijalkowski N, Moshfeghi DM. Active aspiration of suprachoroidal hemorrhage using a guarded needle. *Ophthalmic Surg Lasers Imaging Retina* 2014;45:150-152.
201. Hoeh H, Ahmed, II, Grisanti S, et al. Early postoperative safety and surgical outcomes after implantation of a suprachoroidal micro-stent for the treatment of open-angle glaucoma concomitant with cataract surgery. *J Cataract Refract Surg* 2013;39:431-437.
202. Danylkova N, Gupta N, Jhaveri CD, Gill MK. Suprachoroidal silicone oil migration following retinal detachment repair. *Ophthalmic Surg Lasers Imaging Retina* 2013;44:284-286.
203. Klein R, Klein BE. The prevalence of age-related eye diseases and visual impairment in aging: current estimates. *Invest Ophthalmol Vis Sci* 2013;54:ORSF5-ORSF13.
204. Kempen GI, Ballemans J, Ranchor AV, van Rens GH, Zijlstra GA. The impact of low vision on activities of daily living, symptoms of depression, feelings of anxiety and social support in community-living older adults seeking vision rehabilitation services. *Qual Life Res* 2012;21:1405-1411.
205. Rein DB, Zhang P, Wirth KE, et al. The economic burden of major adult visual disorders in the United States. *Arch Ophthalmol* 2006;124:1754-1760.
206. Chia E-M, Wang JJ, Rochtchina E, Smith W, Cumming RR, Mitchell P. Impact of Bilateral Visual Impairment on Health-Related Quality of Life: the Blue Mountains Eye Study. *Investigative Opthalmology & Visual Science* 2004;45:71.
207. Fea AM, Belda JI, Rekas M, et al. Prospective unmasked randomized evaluation of the iStent inject ((R)) versus two ocular hypotensive agents in patients with primary open-angle glaucoma. *Clin Ophthalmol* 2014;8:875-882.
208. Schepens CL. The Scleral Buckling Procedures. *AMA Archives of Ophthalmology* 1957;58:797.
209. Mittl R, Tiwari R. Suprachoroidal injection of sodium hyaluronate as an internal buckling procedure. *Clin Ophthalmol* 1987;19:255-260.
210. Chang JH, Garg NK, Lunde E, Han KY, Jain S, Azar DT. Corneal neovascularization: an anti-VEGF therapy review. *Surv Ophthalmol* 2012;57:415-429.
211. Wang Y, Fei D, Vanderlaan M, Song A. Biological activity of bevacizumab, a humanized anti-VEGF antibody in vitro. *Angiogenesis* 2004;7:335-345.
212. Zhu G, Mallery SR, Schwendeman SP. Stabilization of proteins encapsulated in injectable poly (lactide- co-glycolide). *Nat Biotechnol* 2000;18:52-57.
213. Fu K, Klibanov AM, Langer R. Protein stability in controlled-release systems. *Nat Biotechnol* 2000;18:24-25.
214. Landsman ML, Kwant G, Mook GA, Zijlstra WG. Light-absorbing properties, stability, and spectral stabilization of indocyanine green. *J Appl Physiol* 1976;40:575-583.
215. Destro M, Puliafito CA. Indocyanine Green Videoangiography of Choroidal Neovascularization. *Ophthalmology* 1989;96:846-853.

VITA

BRYCE CHIANG

CHIANG was born in Baltimore, Maryland. He attended public schools in Freehold, New Jersey, received the B.S. and M.S.E. degrees in Biomedical Engineering from The Johns Hopkins University, Baltimore, Maryland in 2008 and in 2009, respectively, before coming to Atlanta, Georgia to pursue a dual M.D./Ph.D. degree at the Emory School of Medicine and a Ph.D. degree in Biomedical Engineering in the joint Georgia Tech-Emory Biomedical Engineering Department. When he is not working on his research, Mr. Chiang enjoys exploring cuisines and far-off destinations with his wife Pauline Che and newborn son Nathan.